LIQUEFACTION SUSCEPTIBILITY OF UNCEMENTED CALCAREOUS SANDS FROM PUERTO RICO BY CYCLIC TRIAXIAL TESTING

Todd Hunter LaVielle

Thesis submitted to the faculty of Virginia Polytechnic Institute and State University in partial fulfillment of the requirements for the degree of

MASTER OF SCIENCE

in

CIVIL ENGINEERING

C. Guney Olgun, Chair

James R. Martin II, Co-Chair

Thomas L. Brandon

September 9, 2008

Blacksburg, Virginia

Keywords:
Liquefaction, Cyclic Triaxial, Monotonic Triaxial, Triaxial, Calcareous

ABSTRACT

Title: Liquefaction Susceptibility of Uncemented Calcareous Sands From Puerto Rico by Cyclic Triaxial Testing

Author: Todd H. LaVielle

Laboratory tests were performed to investigate the liquefaction susceptibility of uncemented calcareous sands. A series of isotropically consolidated undrained monotonic and cyclic triaxial tests were performed using the Playa Santa sand from Porto Rico. Playa Santa sand is a poorly graded calcareous clean beach sand composed of angular particles with large intra-granular voids. A series of consolidated undrained triaxial tests were performed with the Playa Santa sand remolded to a variety of relative densities and consolidated under a range of confining pressures. In addition, cyclic triaxial tests were performed at a confining pressure of 100 kPa and three sets of relative densities (20%, 40% and 60%). Generation of excess pore pressure under different levels of cyclic loading was established. As a result, relationships were developed to relate the number of cycles required for triggering of liquefaction to cyclic stress ratio. It was seen that the Playa Santa sand was less susceptible liquefaction than quartzitic sands of the same relative density remolded and tested under similar conditions.

Dedicated to my parents for their never-ending love, support

and guidance down the river of life.

ACKNOWLEDGMENTS

I wish to thank my advisor Dr. C. Guney Olgun for his support and the freedom to pursue this study, for better or worse, in the manner that I thought best. I would also like to thank Dr. James R. Martin, II for this contributions and guidance to this work. I owe Dr. Thomas L. Brandon a great debt of gratitude. Without Dr. Brandon I would never have been able to perform this research. Thank you for putting up with me in your laboratory.

This study was funded by the United States Geological Survey under the research grant titled "Liquefaction Susceptibility of Uncemented Calcareous Sediments along the Coastal Plains of Puerto Rico." This financial support is greatly appreciated.

I would like to thank my companions and fellow students at the English Lab. Many hours were spent discussing the principles of soil mechanics and testing. These dear friends include Michael McGuire, Manuel Ochoa and Crysta Highfield. I owe a thank you to Matthew Sleep for all his harassment, backhanded encouragement and friendship. Matt also very kindly reviewed this thesis. I would like to thank my fellow classmates and friends, in Blacksburg, who have given me so much encouragement and whose friendship I will always cherish. This group includes, but is certainly not limited to, Alfredo Arenas, Kate Gunberg, Esther Ryan, Nathan Straub, Heather Hickerson, Letitia Valdes-Mcguire, Ivka Kolimbatovic and Miriam Parker.

A thank you that I can never say too much is one to my mother and father; Chrissy and Craig. They have given me the tools to be successful in life and the motivation to use them. I would like to thank my twin brother Ian LaVielle and my cousins Andrew, Susan, Becky and Nikos, for being such a big part of my life. Becky is due a special thanks for reviewing this thesis.

TABLE OF CONTENTS

LIST OF FIGURES

LIST OF TABLES

1 INTRODUCTION

1.1 Introduction

This research was performed in an effort to better understand the cyclic and monotonic behavior of uncemented calcareous sands from the coastal plains of Puerto Rico. Calcareous deposits are prevalent along the Puerto Rican coastal plains, where there are extensive commercial facilities such as hotels and ports and densely populated residential areas (Cataño 2006). There is a major gap in our understanding of the response of such deposits during earthquakes. An improved understanding of the dynamic behavior of calcareous sands is necessary to make a better assessment of the liquefaction susceptibility of the soils in these areas.

A series of laboratory tests was performed to investigate the dynamic behavior and the liquefaction susceptibility of uncemented calcareous sands. Monotonic and cyclic triaxial tests were performed for this purpose. The results from the laboratory tests were compared with the trends reported in the literature for quartzitic sands.

This study was funded by the United States Geological Survey under the research grant titled "Liquefaction Susceptibility of Uncemented Calcareous Sediments along the Coastal Plains of Puerto Rico." This research was a collaboration between Virginia Tech (VT) and the University of Puerto Rico at Mayaguez (UPRM). Each institution performed tests on different calcareous sands from the coastal plains of Puerto Rico. The laboratory tests at Virginia Tech were performed using sand from Playa Santa, Puerto Rico, and the tests at

University of Puerto Rico at Mayaguez were performed with sands from Cabo Rojo, Puerto Rico. Results of the tests performed at Virginia Tech are presented here.

1.2 Motivation

Current liquefaction evaluation procedures are based on liquefaction case histories at sites with predominantly quartzitic sands. Limited information is available on the performance of sites with calcareous sands during earthquakes (Mejia and Yeung 1995). The compressibility of calcareous sands is greater than quartzitic sands (Datta et al. 1982). Mineralogy, particle shape, soil skeleton and high void ratios of calcareous sands contribute to this high compressibility. Compared to quartzitic sands the particle crushing and rearrangement mechanisms are more significant in calcareous sands (Coop and Airey 2003). Of primary interest is how these mechanisms affect the pore-pressure generation during undrained monotonic and cyclic loading, and understanding the potential for liquefaction during an earthquake. This study utilizes the results of laboratory tests to evaluate the monotonic and cyclic behavior of these soils. The relationship of the field behavior during an earthquake to basic penetration tests is yet to be investigated. Even though liquefaction evaluation procedures exist, it is not clear if these procedures which were developed for quartzitic sands are directly applicable to calcareous sands. A continuation of this research is to address the current liquefaction evaluation procedures and their applicability to sites with calcareous sands.

An understanding of how these sands react to cyclic loading is necessary because a significant amount of port infrastructure and coastal development in Puerto Rico are founded on these soils (Cataño 2006). Ground damage associated with coastal deposits of

calcareous sands has been observed during the Guam Earthquake of 1993 (EERI 1995). This underlines the necessity for a better assessment of the response of calcareous soils during earthquakes.

1.3 Objectives

The main objective of performing this research is to understand how the cyclic behavior of uncemented calcareous sands differ from quartzitic sands. Most liquefaction research has been performed on quartzitic sands (Kramer 1996). It is not clear if the current liquefaction evaluation procedures, which are largely based on case histories from sites with quartzitic sands, are directly applicable to calcareous soils. This study investigates how the particle rearrangement and crushing mechanism in calcareous sand is manifested during cyclic loading. The specific objectives of performing this research are to:

1. Perform index testing on the calcareous sand. This included determining index densities and associated void ratios, specific gravity, grain-size distribution and particle shape classification.
2. Evaluate the undrained static stress-strain behavior of calcareous sand using monotonic triaxial testing. This provided preliminary insight into the pore-pressure generation during cyclic loading.
3. Evaluate the liquefaction susceptibility of calcareous sand using cyclic triaxial testing. Comparing these results with trends reported in the literature for quartzitic sands at similar relative densities provides a baseline for further research of in-situ test correlations.

2 BACKGROUND & CHARACTERIZATION

2.1 Introduction

Calcareous soils are the result of chemical deposition or physical weathering. During chemical deposition, calcium carbonate comes out of solution as a precipitate in sea water. Physical weathering breaks down the skeletal remains of marine organisms, such as mollusks, foraminifera, corals and algae into sand-sized particles (Coop and Airey 2003). The sands used for this research consist primarily of physically weathered mollusk shells and coral fragments. The marine organisms that create the source material for these sands are prevalent in warm, shallow tropical and subtropical shelves (Golightly and Hyde 1988). In the United States these areas include Guam, Hawaii, Puerto Rico, and parts of the Gulf Coast (Morioka and Nicholson 1999).

Due to the nature of their origin, calcareous sand particles have two attributes that cause their properties to differ from those of quarzitic soils. Calcareous sands have significant intra-particle void space (Coop and Airey 2003; Datta et al. 1982; Golightly and Hyde 1988; Hyodo et al. 1996; Hyodo et al. 1998; Nicholson 2006; Sharma and Ismail 2006). The intra-particle void space is created by the particles made of shells that have not been fully broken apart or by corals that have cavities within the particle or on the surface. Photographs of a variety of calcareous soil particles are shown in Figure 2-1. The second attribute that affects the behavior of these sands is the angular particle shape. There are a variety of particle shapes encountered in calcareous soils. Curved flat particles come from fragments of small shells. Hollow tube-shaped particles are the exoskeletons of other small mollusks. A loose, complex interlocking structure is created by these angular soil particles. This in combination

with the intra-particle pore space creates a very high void ratio. Void ratio in excess of 1.0 is commonly seen in calcareous soils. (Coop and Airey 2003; Datta et al. 1982; Golightly and Hyde 1988; Hyodo et al. 1996; Hyodo et al. 1998; Nicholson 2006; Sharma and Ismail 2006)

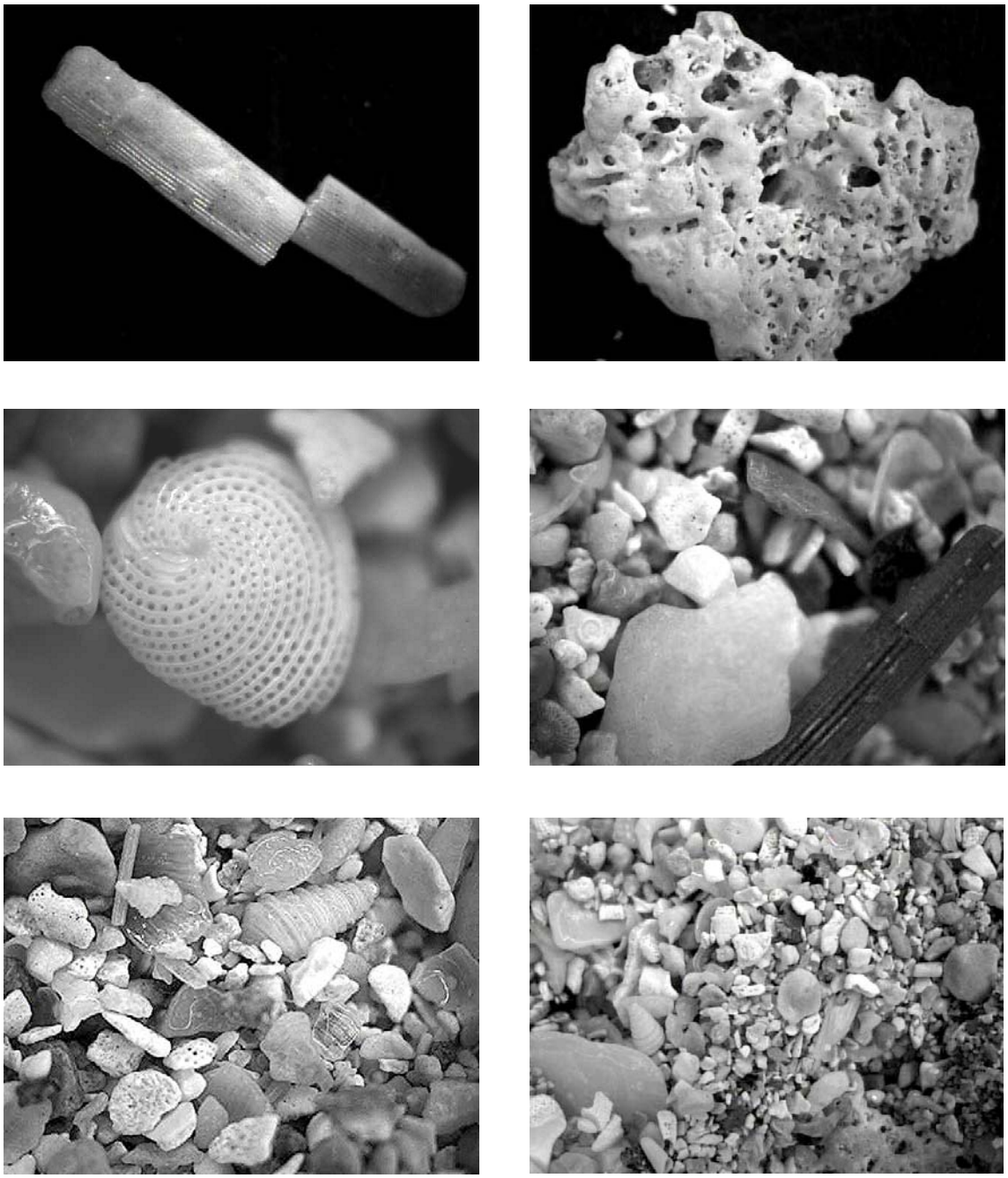

Figure 2-1. Calcareous Soil Particles (Playa Santa)

2.2 Engineering Properties

Engineering properties of calcareous sands vary significantly. In quartzitic sands most engineering properties can be related to the grain-size distribution and relative density (Mitchell 1993). This is not the case with calcareous sands. (Coop and Airey 2003) The most significant factors affecting engineering properties of calcareous sands are cementation and soil structure. The engineering properties of Playa Santa and other calcareous sands are discussed below.

2.3 Cementation

Cementation in calcareous soils occurs rapidly, and is a complicated physical and chemical process that is not fully understood (Coop and Airey 2003). Age, confining pressure, water temperature and chemistry are important factors in the cementation process (Demars and Chaney 1982). Laboratory tests for this study were conducted on remolded samples of uncemented Playa Santa sand.

2.4 Specific Gravity

In terrigenous soils the specific gravity does not vary significantly. Typical values range from 2.6 to 2.7, and are strongly dependant on the mineralogy of the soil particles. Clays typically have a higher specific gravity (approximately 2.70) than quartzitic sands (approximately 2.65) (Mitchell 1993). The specific gravity of the Playa Santa calcareous sand is 2.75 as determined by the ASTM standard specification D854 (2002). As shown in Table 2-1 the specific gravity of calcareous soil varies from 2.70 to 2.85. The specific gravity of the mineral

calcium carbonate ($CaCO_3$) is 2.70 (Mitchell 1993). Table 2-1 also includes grain-size distribution metrics and index void ratios.

Table 2-1. Index properties of Playa Santa sand and other calcareous and quartzitic soils. (Cataño Arango 2006; Golightly and Hyde 1988; Hyodo et al. 1996; Morioka and Nicholson 1999)

SAND	G_S [a]	D_{10} (mm) [b]	C_U [c]	e_{min} [d]	e_{max} [e]
Playa Santa	2.75	0.16	2.75	0.80	1.22
Cabo Rojo	2.86	0.20	1.05	1.34	1.71
Dogs Bay	2.75	0.24	2.06	0.98	1.83
Ballyconeely	2.72	1.00	1.11	1.62	1.98
Bombay Mix	2.80	0.17	2.23	0.75	1.07
Ewa Plains	2.72	0.20	5.05	0.66	1.30
Monterey[f]	2.63	0.20	4.5	0.33	0.71
Leighton Buzzard[f]	2.65	0.60	1.48	0.75	0.84

[a]Specific Gravity, [b]Sieve size with 10% passing, [c]Uniformity Coefficient, [d]Minimum Void Ratio, [e]Maximum Void Ratio, [f]Denotes quartzitic sands

2.5 Index Densities (Max/Min Void Ratio)

The maximum and minimum void ratios and densities have been established using the ASTM standard specifications D4253 and D4254 respectively (2006). Maximum and minimum void ratios (e_{max} and e_{min}) for Playa Santa sand are 1.22 and 0.80 respectively. Table 2-1 lists the maximum and minimum void ratios for other soils. As seen, calcareous sands have a much higher void ratio than quartzitic sands.

2.6 Grain-size Distribution

Grain-size distribution was established following ASTM standard specification D422 (2002). The sand tested in this study was initially run through a No. 4 (4.75 mm) sieve to remove the larger particles. The soil was washed through a No. 200 sieve to remove all fines and residual salts. Playa Santa sand has very low fines content, with less than 0.1% passing the No. 200 sieve. Grain-size distribution of Playa Santa sand is shown in Figure 2-2 with other calcareous sands reported in the literature. The uniformity coefficient for Playa Santa sand is 2.75. The Playa Santa sand classifies as a poorly graded sand (SP) according to the Unified Soil Classification System.

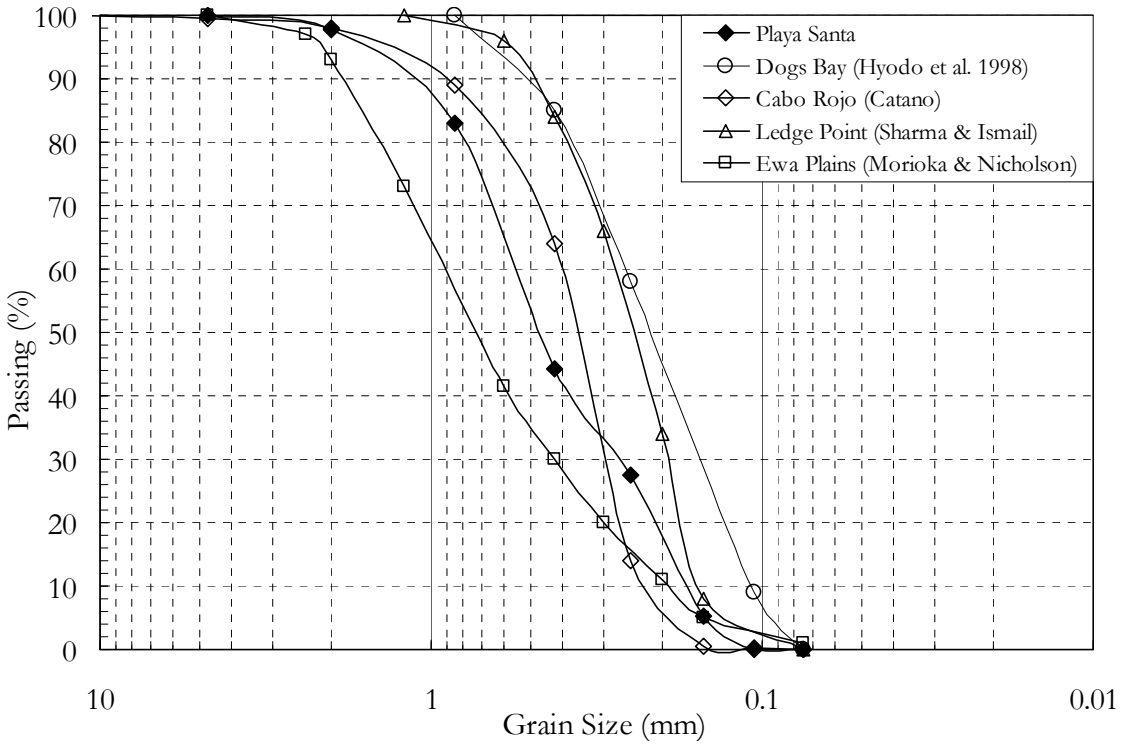

Figure 2-2. Grain-size distribution of Playa Santa and other calcareous sands. After (Hyodo et al. 1998) (Cataño Arango 2006) (Sharma and Ismail 2006) (Morioka and Nicholson 1999)

3 LITERATURE REVIEW

3.1 Compressibility

3.1.1 Introduction

High compressibility is a characteristic of uncemented calcareous soils. Under similar loading conditions and stress levels, calcareous sands can be 30 times more compressible than quartzitic sands (Morioka and Nicholson 2000). The petroleum industry encounters problems with offshore structures founded on piles in calcareous sands (Golightly and Hyde 1988; Semple 1988). Driven piles in calcareous sands often experience unexpected excessive settlements (Mitchell 1993). Pile driving causes increased compressive stresses at the pile tip. These stresses cause particle crushing in calcareous sands which usually does not occur in quartzitic sands. Particle crushing reduces the induced horizontal pressure around the pile shaft which reduces skin friction (Coop 1990; Golightly and Hyde 1988; Semple 1988).

3.1.2 Compression Index and Normal Consolidation Line (NCL)

The compressibility of sands is discussed in Lee and Seed's 1967 paper on the drained strength behavior of sands. Figure 3-1 shows a plot of an idealized compression (e-log p) curve where p' is the effective confining pressure. At low stresses the soil is very stiff with little volume change at increasing confining pressure. Yield stress, p_y, is reached with increased loading, and is defined by a distinct change in soil compressibility. This phenomenon is analogous to the preconsolidation pressure in clays. If a sand is subjected to stresses beyond the yield stress, it will undergo relatively significant volume change as a result of increased loading. This portion of the load curve defines the "normal consolidation

line", NCL and is characterized by the slope C_C, the Compression Index. The nomenclature used for clays is also used for sands.

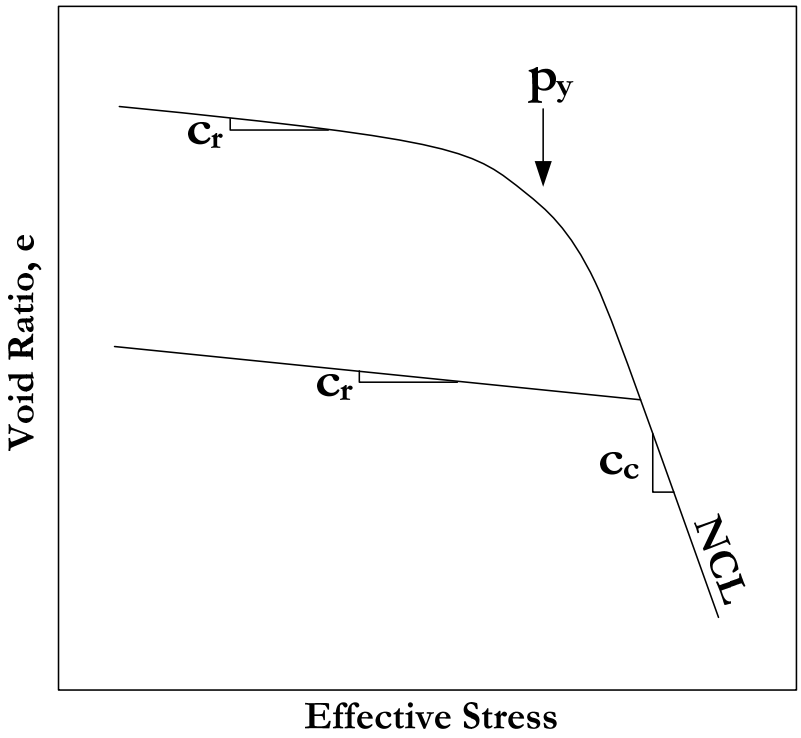

Figure 3-1. Idealized compression curve. Yield point (p_y) is the point of maximum curvature. Recompression/rebound (Cr) and compression (Cc) indices are the change in void ratio over one log cycle. (Lee and Seed 1967)

Elastic deformation in the soil skeleton accounts for most of the strain during the initial part of compression, and relatively little particle crushing and rearrangement occurs at this stage. As the confining stress is increased, the particle crushing and rearrangement mechanism becomes more significant. As Lee & Seed (1967) indicate, this component continues even after the excess pore pressures have dissipated. This mechanism causes secondary compression or creep and is discussed in detail in the following section.

Yield stress is a function of the NCL and the compacted void ratio (Lee and Seed 1967). Under compression the void ratio of a sand sample initially changes according the

recompression/rebound index, C_r. As the stress increases the stress-volume state approaches the NCL. This intersection defines the yield stress. For a given NCL, a sand sample prepared with a high void ratio has a lower yield stress than a sample prepared with a low void ratio. As also implied by Lee & Seed, the yield stress also serves as an indicator and memory of the load history.

Several researchers have proposed that within a compression framework there is a commonality of behavior among quartzitic sands and calcareous sands (Coop 1990; Hyodo et al. 1996; Semple 1988). Figure 3-2 shows the compression curves for Dogs Bay calcareous sand and Toyoura quartzitic sand. There are two significant hypotheses that researchers have made regarding the compression of calcareous sands. The first is that they have a similar NCL. The second is that the compression parameters (Compression Index and Recompression/Rebound Index) of these sands are similar. (Coop 1990; Semple 1988) Given these hypotheses the compressive behavior of calcareous sands can be related to the compression curve and the NCL of a common quartzitic sand.

The void ratio range of compacted sands is a function of particle shape and gradation. As indicated above, this range in calcareous sands is significantly different than quartzitic sands. As a result of the hypothesized commonality of the NCL of quartzitic and calcalreous sands and the higher void ratio, calcareous sands tend to have a lower yield stress compared to quartzitic sands. At typical working stresses the yield stress is exceeded and compression is defined by the C_c, rather than the C_r. If a quartzitic sand sample were constructed with a high void ratio, the compressive behavior would be similar under the e-log p' framework theory (Coop 1990; Semple 1988). This phenomenon is illustrated in Figure 3-2. As shown,

the yield stress for Dogs Bay calcareous sand, at a relative density of 60%, is at about 1 MPa or 10 TSF. Toyoura quartzitic sand has a yield point of about 10 MPa 100 TSF (Hyodo et al. 1996). While the yield stress of quartzitic sands would generally be above typical working stresses, the yield stress of calcareous sands can easily be exceeded at typical working stresses. As a result particle crushing can take place during loading of calcareous sands and can be a significant factor affecting the behavior.

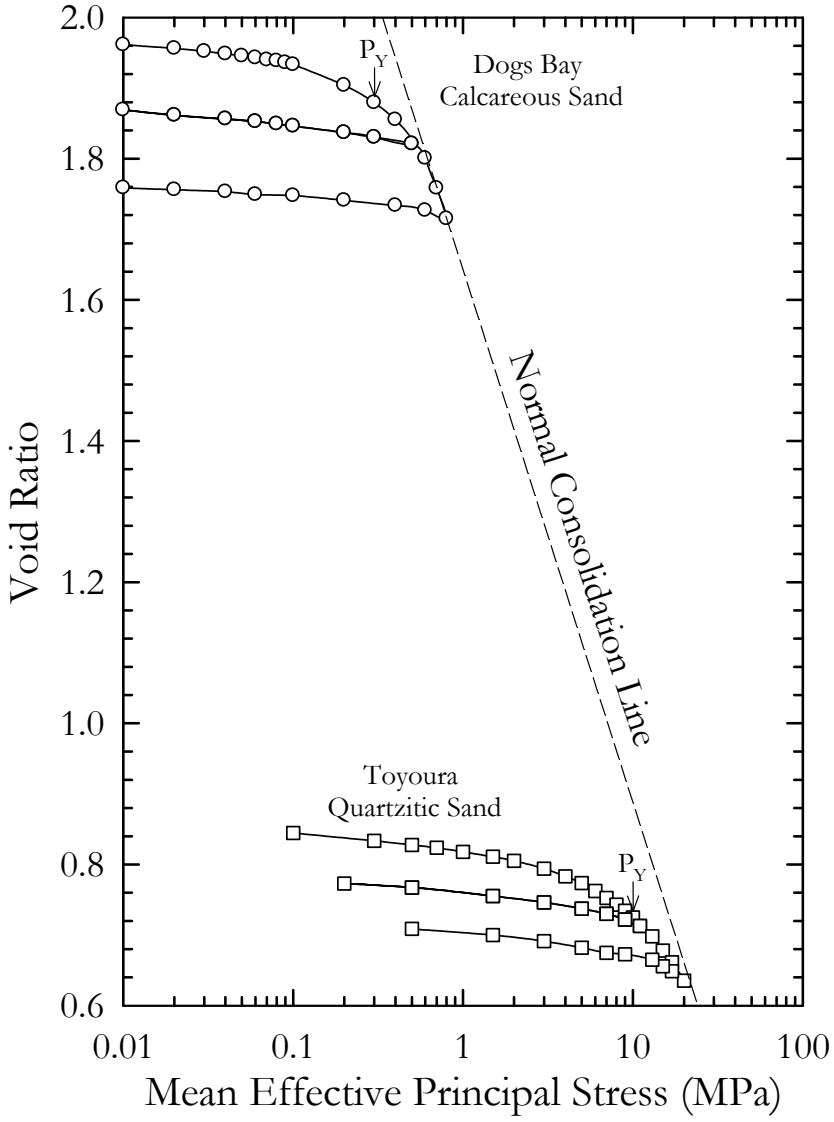

Figure 3-2. Isotropic compression of Dogs Bay Calcareous Sand and Toyoura Sand. After Hyodo et al. 1996

3.1.3 Secondary Compression & Creep

Secondary compression can be significant in calcareous soils when compared to terrigenous soils (Coop 1990; Coop and Airey 2003; Poulos et al. 1982). Secondary compression and creep of these soils are not well discussed in the literature, but this phenomenon plays an important role in their behavior. Creep is the time-dependent strain deformation of a material under a constant stress. Secondary compression is a special case of creep applied to the volumetric strain of soils. It is the continuous rearrangement and crushing of particles following primary consolidation (Mitchell 1993).

Secondary compression is observed to follow a linear trend when plotted versus the log of time. Poulos et al. (1982) performed several tests and determined the coefficient of secondary compression for a calcareous soil, and found it to be linear with the log of time for all tests. At load levels approaching and past the yield point, secondary compression becomes significant enough to obscure the end of primary consolidation.

3.1.4 Conclusion

Compressibility of calcareous sands is one of the most important factors affecting its monotonic behavior. The high compressibility of calcareous soils is attributed to its high void ratio. As the load increases asperities at the particle contacts break, resulting in soil particle rearrangement. At stresses below yield stress calcareous sand compression is similar to that of quartzitic sand at typical geotechnical working loads. It is important to know if the particle-crushing mechanism in a calcareous sand occurs at the working stresses for design, i.e., the working stresses exceed the yield stress.

3.2 Monotonic Shear Behavior of Sandy Soils

3.2.1 Introduction

This section provides a review of the monotonic behavior of terrigenous and calcareous soils. A general review of steady-state and stress-strain behavior is followed by a detailed discussion of the monotonic behavior of calcareous sands.

3.2.2 Background on Stress-Strain Behavior of Sands

Stress paths provide a useful tool for evaluating the behavior of a soil. Two conventions are typically defined and used. In stress path plots the x-axis represents the normal stress, p or p', of a soil element. The y-axis represents the shear stress, q, on a soil element. The conventions were named from the institution where they were first used. The MIT stress path convention defines p as the mean of the major and minor principle stresses, $(\sigma_1+\sigma_3)/2$, and the effective normal stress, p', is defined likewise, $(\sigma'_1+\sigma'_3)/2$. The y-axis, q, is the shear stress on the sample, $(\sigma'_1-\sigma'_3)/2$. The Cambridge stress path convention defines p as the mean of three principle stresses, $(\sigma_1+\sigma_2+\sigma_3)/3$ or $(\sigma_1+2\sigma_3)/3$, and the effective normal stress, p', is defined likewise, $(\sigma'_1+\sigma'_2+\sigma'_3)/3$ or $(\sigma'_1+2\sigma'_3)/3$. The y-axis, q, is the deviatoric stress on the sample, σ_d or $(\sigma'_1-\sigma'_3)$. This document uses the MIT stress path convention, but the Cambridge convention is used in several cited references.

Soils have a tendency for volume change when sheared. This tendency for volume change is explained by steady-state and critical state theories (Been et al. 1986; Been and Jefferies 1985; Been et al. 1987; Casagrande 1936; Poulos 1981; Roscoe et al. 1958). During shearing the effective stress or volume changes until the stress-volume state is at the critical or steady-

state. This is the point during shear at which the soil stresses and volume remain constant (Roscoe et al. 1958). The differences between steady-state theory and critical state theory are subtle. Generally, these titles are used interchangeably in current soil mechanics literature without significant emphasis on the differences (Rose 1993).

The steady-state of a saturated soil is defined by two parameters; void ratio and effective stress. Effective stress can be expressed in several different ways; vertical effective stress (p'), mean effective stress (I'), major principle stress (σ_1'), minor principle stress (σ_3'). Figure 3-3 shows a plot of a typical steady-state line for a sand. A straight line is not a requirement but is used for convenience. The plot shows four different stress paths for cases of drained and undrained loading. Two tests are conducted at different confining pressures (σ'_{CON}). The plot shows that the each test progresses towards the steady-state line under the applied shear load. The path taken depends on the drainage condition. Under drained shear Δu is maintained at zero as the volume of the sample changes due to shear. This results in a vertical path to the SSL, samples 1 and 2. Sample 1 dilated during shear, and sample 2 compressed during shear. Under undrained conditions sample volume is held constant. Tendency for volume change is expressed as change in pore-pressure. The change in pore-pressure results in negative change in effective confining stress. Under these conditions the path is horizontal, samples 3 and 4.

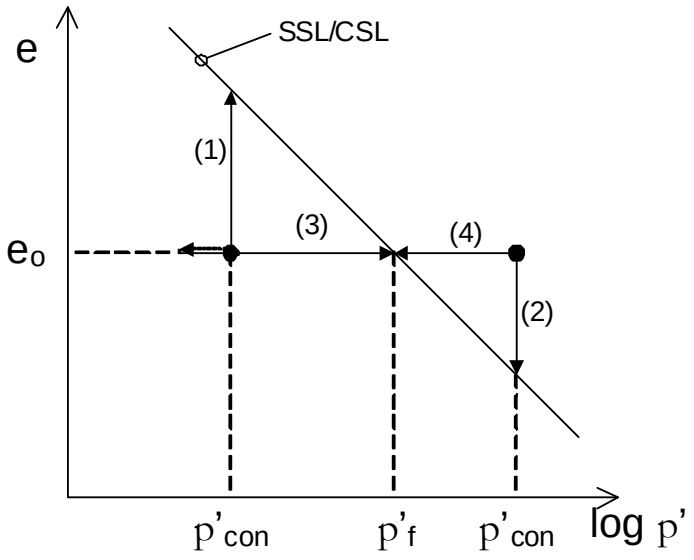

Figure 3-3. Steady-state/Critical State Line

Schematic stress paths for samples 3 and 4 are shown in Figure 3-4. The consolidated void ratios of these samples are the same. Under undrained conditions, constant volume, both samples shear to the same stress state. As shown in Figure 3-3 sample 3 has a tendency to dilate following an initial tendency for compression. Sample 4 has a tendency to compress. Each sample path proceeds toward the same point on the SSL because a constant sample volume is maintained.

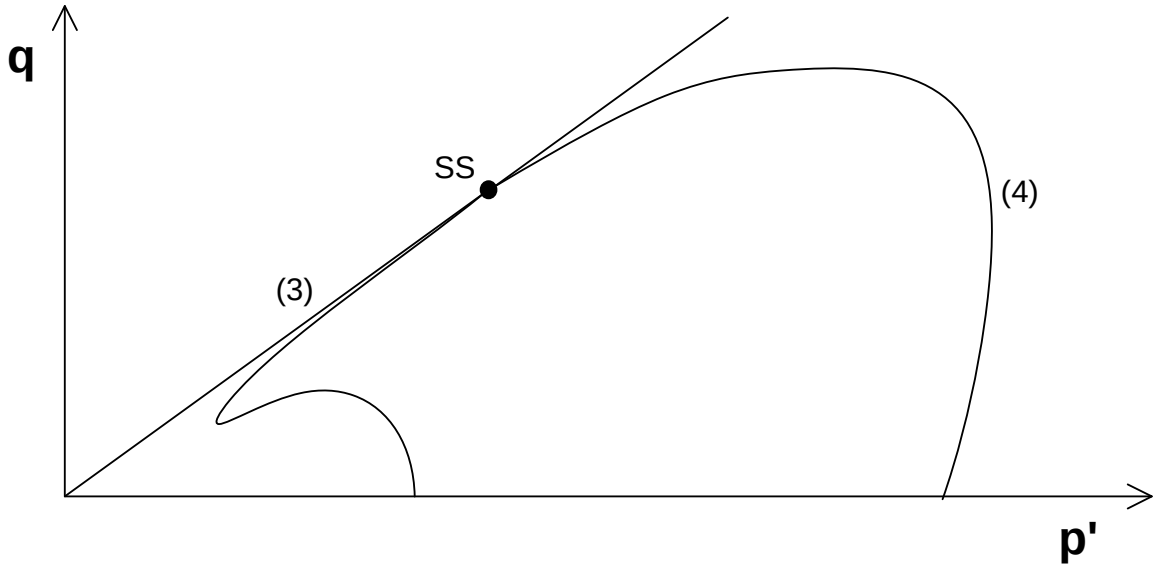

Figure 3-4. Stress paths for samples 3 and 4, prepared at equal void ratios and confined at different stress states. Each sample reached the same steady-state stress state.

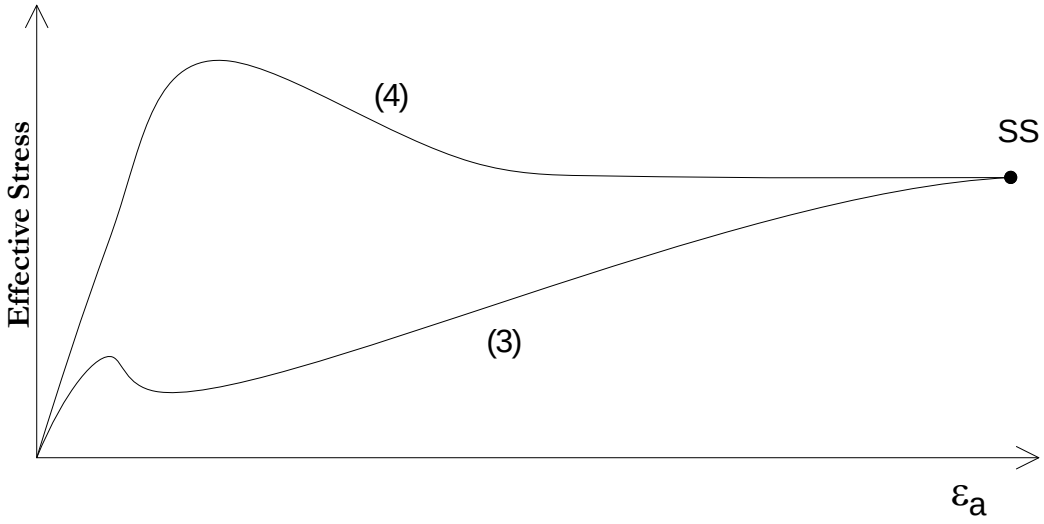

Figure 3-5. Stress-Strain plot for samples 3 and 4 undrained triaxial.

The stress-strain plots for the undrained samples, Figure 3-5, show that high strains are necessary to reach steady-state. The triaxial test is considered by many researchers to be unsatisfactory for establishing a steady-state (Coop et al. 2004; Finn 1990; Kramer 1989; Porter 1998; Seed et al. 1989). Because high strain is necessary to reach steady-state, it is

difficult to achieve with confidence using the triaxial test. These tests were developed and used to determine peak strengths which typically occur at low strain (Porter 1998). During undrained testing, as the sample is compressed it expands horizontally maintaining constant volume. This expansion is not constant throughout the sample, and the shape of the sample deformation is irregular. Cross-sectional sample area during loading is not known. Reasonably accurate sample stresses, as well as strains, cannot be calculated. (Porter 1998) Other more complex soil states are often defined to classify soil behavior. These include quasi-steady-state and phase transformation.

Phase transformation is a concept developed by Ishihara (1975). It defines the point during undrained shear at which the tendency for volume change of the soil changes from contractive to dilative behavior.

Working stresses and the depositional environment cause the typical behavior of a sand during shear to be similar to that of sample 3, i.e., an initial contractive tendency followed by a tendency for dilation. A schematic of the stress path for this idealized sample is shown in Figure 3-6. By definition the point at which the behavior changes from a tendency for contraction to a tendency for dilation is the maximum excess pore pressure. This is the stress state at which the difference between the effective stress and the total stress, p' and p, is greatest. From this point onward the tendency for volume change is dilative, manifested as decreasing pore-pressure.

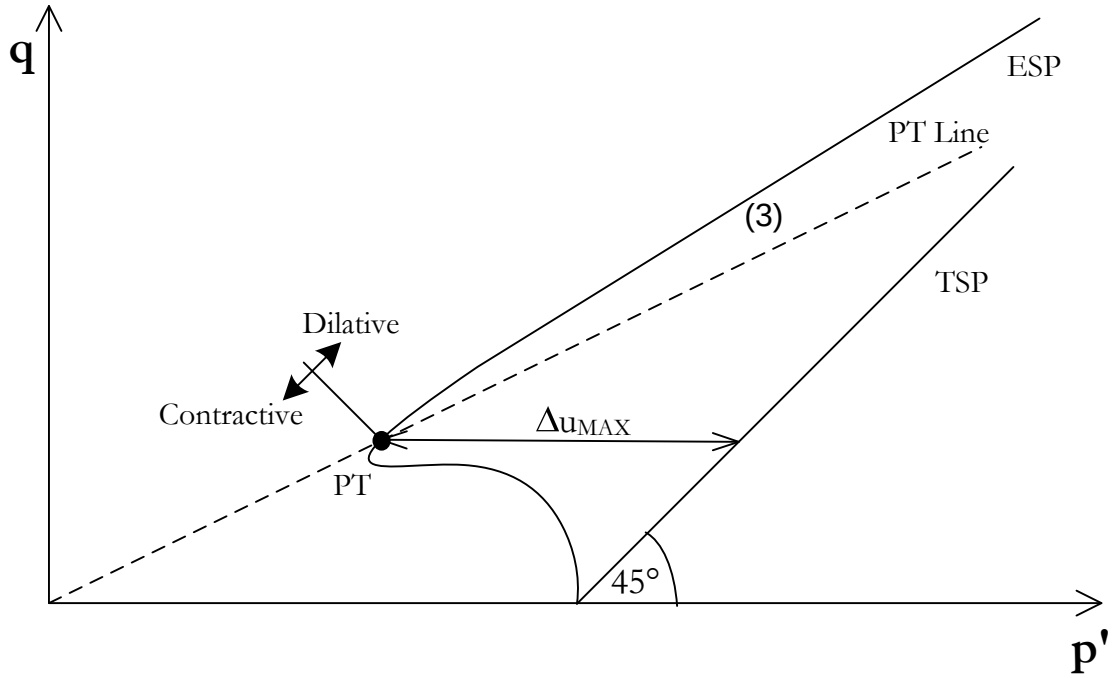

Figure 3-6. Phase Transformation of Sample 3

A line drawn through the PT point from the origin is the phase transformation line. Theoretically the slope of this line is the same for samples prepared at a common density. In other words, the PT line is independent of initial confining pressure. (Ishihara et al. 1975). This theory has great practical application to soil modeling. It can be said that if the effective stress path of a soil element crosses the PT line, forward or backward, the tendency for volume change will change regardless of the path taken.

Some definitions of phase transformation differ from the way it was originally introduced by Ishihara (1975). Many researchers define it as the point with lowest mean normal effective stress, $(\sigma_1'+2\sigma_3')/3$ (Hyodo et al. 1998; Kramer 1996; Sharma and Ismail 2006). This would be the point where the slope of the stress path becomes vertical, or the tip of the elbow in a Cambridge stress path. While inconsistent with Ishihara's original definition, it is often very close to the actual point of phase transformation, and may be just as significant as the true

point of phase transformation. Using he Cambridge convention the parameter p' is defined as the mean normal effective stress, $(\sigma_1'+2\sigma_3')/3$. Using this convention puts the phase transformation closer to the point of minimum mean normal effective stress, I', because the horizontal effective stress (σ_3') has greater weighting in the Cambridge convention. This minimizes the relative differences between the original (Ishihara's) and the alternative definition of phase transformation. While this might appear to be an inconsistency, this definition seems to be a standard, and is commonly used in the geotechnical earthquake engineering field. Ishihara's initial definition has been used to define the phase transformation.

3.2.3 Stress-strain Behavior of Calcareous Sands

Offshore petroleum platforms in shallow continental shelf areas are often founded on driven piles in calcareous materials (Coop 1990; Golightly and Hyde 1988; Hyodo et al. 1996; Semple 1988). In the late eighties during the construction of offshore platforms in the Bass Strait southeast of Australia it was found that the measured skin friction during driving was significantly lower than expected (Coop and Airey 2003). This encouraged research to develop a better understanding of the engineering properties of calcareous soils (Golightly and Hyde 1988). An international conference was held in Perth, Australia, in March of 1988 entitled *Engineering for Calcareous Sediments*. This conference contributed considerably to the understanding of the properties and behavior of calcareous sands.

The significant papers published, from the conference and other sources, on monotonic behavior of calcareous soils are summarized in Table 3-1. Several points are consistently made throughout the literature regarding the monotonic shearing behavior of calcareous

soils. Generally during drained shear, calcareous sands exhibit more contraction during loading than quartzitic sands prepared at similar relative densities (Coop 1990; Datta et al. 1982; Demars and Chaney 1982; Golightly and Hyde 1988; Semple 1988). They generally have greater peak strength friction angles, but this strength is not realized until significant strain has occurred. These soils are 1.5 to 2 times less stiff when compared to terrigenous soils (Morioka and Nicholson 2000). Some researchers have reported strains as high as 20% before peak strength is reached (Sharma and Ismail 2006).

During the 1988 Perth conference, a central theory about calcareous sands was discussed (Coop 1988; Golightly and Hyde 1988; Kaggwa et al. 1988; Semple 1988), and later formalized in more detail by Coop (1990). This theory corresponds directly with the compressive behavior of calcareous materials discussed previously. Calcareous soils behave exactly as terrigenous soil would if the terrigenous soil had the same loose structure. The nature of the calcareous particles creates a soil fabric with a large of void ratio. It is not the calcareous minerals that govern the behavior of calcareous sands. Rather, it is the bulky soil fabric that governs the behavior.

Coop uses critical state soil mechanics theory in the interpretation of the monotonic behavior of calcareous and terrigenous soils (Coop 1990; Coop and Airey 2003). He states that the location of the NCL and critical state line relative to the stress-volume state will control the compressibility of the soil (Coop 1990). Beyond the yield stress, the grain crushing and rearrangement mechanism overwhelmingly controls the compression behavior and development of volumetric strains. If the in-situ stress-volume state is close to the NCL, subsequent shear stress will bring the mean effective stress beyond the yield stress.

Compression theory of sands plays directly into further discussion of this concept. Initial compression of sand is small and almost entirely recoverable. The volumetric strain during the initial phase is sustained almost entirely by the soil skeleton, with relatively little particle crushing and rearrangement. As the confining stress is increased the particle crushing and rearrangement component of the strain gradually becomes more significant.

As stated previously, the yield stress of quartzitic sands is around 10 MPa or 100 TSF (Hyodo et al. 1996; Lee and Seed 1967). This is well beyond typical working stresses in geotechnical engineering. In calcareous sands the yield stress is significantly lower. Dogs Bay sand is around 1 MPa or 10 TSF (Coop 1988; Hyodo et al. 1996). A confining pressure of 1 MPa is within typical geotechnical working stresses. Because typical foundation stresses reach or approach the yield stress in calcareous soils the particle crushing and rearrangement mechanisms are significant. This results in a tendency for contraction during undrained shear. In quartzitic sand the yield stress is not approached and the roll of the crushing and rearrangement mechanism is not significant.

Table 3-1. Summary of static shear studies on calcareous soils

Year	Author(s)	Title	Motivation	Soil Type	Shear Tests	Significant Monotonic Shear Findings
1982	Poulos, H. G. Uesugi, M. & Young, G. S.	*Strength and deformation properties of Bass Strait carbonate sands*	Offshore Platforms in Bass Strait	- Soil A, a grey sand with some silt - Soil B, an orange-colored sand	CID triaxial comp.	- Increasing confining pressure reduced the friction angle and the dilative behavior.
1988	Airey, D. W. Randolph, M. F. & Hyden, A. M.	*The strength and stiffness of two calcareous sands*	Offshore Platforms in Bass Strait	- Kingfish, well graded sand - Halibut, medium to coarse grained sand	CID triaxial comp.	- Relatively high friction angles. Soils only dilate at low confining pressures. - Proposed an empirical relationship between the mean effective stress and Youngs Modulus (initial stiffness).
1988	Golightly, C. R. & Hyde, A. F. L.	*Some fundamental properties of carbonate sands*	Offshore Platforms	- Leighton Buzzard sand, quartzitic sand - Dog Bay sand, molluscan carbonate sand, Ireland - Ballyconneely sand, a coralline algal carbonate sand, Ireland - Bombay Mix, a marine siliceous carbonate sand, India	CID and CIU triaxial comp.	- Stress-strain curves for drained tests showed calcareous sand to be much less stiff than the quartzitic sand. Sands contract when sheared at relatively low effective confining pressures. - Found that friction angle of calcareous sands are greater. Increased mineral friction angle component, with some decrease in the sliding, crushing, rearrangement component. (As described by Rowe stress dilatancy theory.) - Significant early generation of high positive excess pore pressure was observed in undrained tests.
1988	Semple, R. M.	*The mechanical properties of carbonate soils*	Offshore Platforms in Bass Strait	- Several Bioclastic calcareous soils from the Bass Strait.	None	- Friction angles are greater in calcareous soils. Revisited Golightly's and Hyde's discussion of Rowe's stress dilatancy theory. Increased mineral friction with reduced dilatancy due to crushing. - Restated commonly accepted decreasing friction angle with increasing confining pressure. This change occurs at lower confining pressures in calcareous sands. - Suggests that it is the void ratio and particle angularity that govern the behavior not the carbonate minerals, i.e., if a quartzitic sand were tested with the same void ratio as calcareous sands the behavior would be comparable. Detailed discussion/argument for this by comparing very loose quartzitic sands to dense calcareous sands, equal void ratios. His argument is not well supported and makes no strong conclusions.

Year	Author(s)	Title	Motivation	Soil Type	Shear Tests	Significant Monotonic Shear Findings
1990	Coop, M. R.	*The mechanics of uncemented carbonate sands*	Offshore Platforms	- Dogs Bay calcareous sand	CID, CIU, CKoU triaxial comp.	- Higher friction angle in calcareous soils. Greater strains are needed to mobilize the frictional strength. - High compressibility reduces the horizontal loads negatively affecting skin friction in piles. - The significance of compressibility to soil strength is dependent on the location of the in-situ stress-volume relative to the normal compression line. Coop makes this is an extremely insightful and under appreciated point.
1996	Hyodo, M. Aramaki, N. Itoh, M. & Hyde, A. F. L.	*Cyclic strength and deformation of crushable carbonate sand*	Liquefaction susceptibility determination of crushable calcareous soils	- Dogs Bay calcareous sand	CIU and CAU triaxial comp. and exten.. Cyclic CU triaxial	- The analysis of the monotonic results is limited. A better review is included in their following paper. (Hyodo et al. 1998, See Below) - Identifies the phase transformation point and compares it at varied parameters. - Hyodo understands and conveys the behavior very well, but makes few useful big picture conclusions.
1998	Hyodo, M. Hyde, A. F. L. Aramaki, N. & Nakata, Y.	*Liquefaction of crushable soils*	Liquefaction susceptibility determination of crushable soils	- Ube & Hiroshima Masado, weathered granite, washed - Shirasu, weathered Volcanic soil, 35% Non-Plastic Fines - Dogs Bay, Calcareous Sand	CIU triaxial comp. and exten.. Cyclic CU triaxial	- When sheared in a dense state crushable soils have stress paths which are similar to those of loose sands of a less crushable nature. - Crushable soils are more dependent on the effective confining pressure because these stresses are often beyond the isotropic compression yield stress. - Identifies the phase transformation point and compares it at varied parameters.
1999	Morioka, B. T. & Nicholson, P. G.	*Evaluation of the static and cyclic properties of calcareous sand in a calibration chamber study*	Liquefaction susceptibility determination using penetration tests	- Ewa Plains Calcareous SP, Oahu, Hawaii - Monterey Sand (Scalped)	CU triaxial comp. and cyclic CU triaxial	- Found significantly higher friction angle of calcareous sand at several relative densities compared to Monterey Sand. - It required twice the strain to mobilize the peak strength in the calcareous sand. This is due to significant contractive tendencies of calcareous sands. - Found significant fluctuations in deviator and volume change data. Suggests that this is due to particle rearrangement and crushing. (M&N are the first to make a speculation like this.)

Year	Author(s)	Title	Motivation	Soil Type	Shear Tests	Significant Monotonic Shear Findings
2003	Coop, M. R. & Airey, D. W.	*Carbonate sands*	General Review	- Several Sands referenced (Mostly Dogs Bay calcareous sand)	None	- Main focus with regard to monotonic shear testing is on critical state theory. States that the CS is not typically reached in triaxial testing because tests are usually terminated at 20%. The true CSL is in fact straight and is not curved as frequently assumed. - Performs an excellent review of research on calcareous soils, with special attention on their basic properties. - Limited analysis of monotonic shear of uncemented calcareous sands
2006	Sharma, S. S. & Ismail, M. A.	*Monotonic and cyclic behavior of two calcareous soils of different origins*	Offshore Platforms (Monotonic & Cyclic)	- Goodwyn (GW) Fine-grained, offshore calcareous soil. - Ledge Point (LP) Coastal aeolian calcareous sand	CIU triaxial comp., and cyclic CU triaxial	- Tested two calcareous soils. Showed that the soil with weaker soil particles, also at a greater void ratio, had significantly more excess pore pressure generation. - Higher strains are needed to reach the PT in calcareous sands. - The friction angle is greater, but high strains are required, more than 20%.
2006	Cataño Arango, J.	*Stress strain behavior and dynamic properties of Cabo Rojo calcareous sands*	General study of Puerto Rican calcareous sand.	- Cabo Rojo, fine to medium calcareous poorly graded sand - South Bend, fine to medium silica poorly grades sand	Direct shear and CU Triaxial comp.	- Calcareous sand is more ductile, higher strains are needed to reach peak strength. - Calcareous sands are weaker, have a lower deviator stress at failure. - More compressive, greater development of positive excess pore pressure during shear
References: (Airey et al. 1988; Cataño Arango 2006; Coop 1990; Coop and Airey 2003; Golightly and Hyde 1988; Hyodo et al. 1996; Hyodo et al. 1998; Morioka and Nicholson 1999; Poulos et al. 1982; Semple 1988; Sharma and Ismail 2006)						

3.3 Cyclic Shear Behavior of Sandy Soils

3.3.1 Introduction

The following section summarizes the current state of the art on the cyclic/dynamic behavior of calcareous sands. A review is presented with a specific focus on the research conducted using cyclic triaxial testing. A tabulated summary of studies on the dynamic behavior of calcareous sands is provided at the end of this section, Table 3-2.

3.3.2 Cyclic Stress States Under Laboratory and Field Conditions

When discussing the use of cyclic triaxial testing to determine the susceptibility of a soil to liquefaction, it is important to understand the differences in how the stresses are applied in an actual seismic event versus in a cyclic triaxial test. The way in which dynamic stresses are applied to an in-situ soil element have to do with how seismic energy propagates within soil and rock. Seismic energy travels more slowly and dissipates more quickly through soils than when traveling though hard rock. Due to this stiffness contrast, path of the waves traveling through the stiffer deeper layers is bent to near vertical as they approach the softer near surface deposits.

Seismic energy travels in two forms; compression waves and shear waves. Shear waves are significantly more destructive to soil and structures than compression waves. As a result, the seismic energy that earthquake engineers are most interested in is the result of vertically propagating, horizontally polarized shear waves, i.e., shear waves traveling up though the soil column shearing parallel to the ground surface. This energy puts a pure shear stress on the soil column, which is commonly modeled as a shear beam.

At a level site underlain by a uniform normally consolidated material, k_0 conditions would apply. Initial stress conditions of a soil element are shown in stress path space in Figure 3-7, circle (a). During a seismic event a pure shear stress is applied. This changes the diameter of the Mohr's circle. Constant vertical and horizontal stresses are maintained. A rotation of the principle stresses occurs.

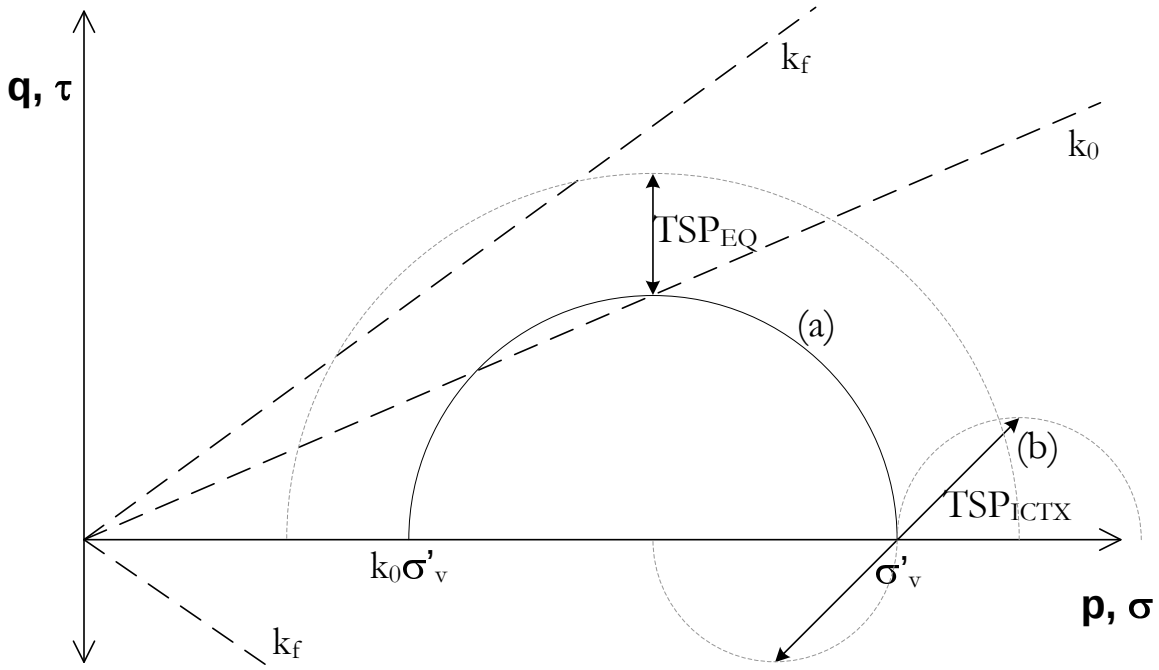

Figure 3-7. Cyclic total stress paths under earthquake and cyclic triaxial loading conditions.

Stress path (b) in Figure 3-7 shows the stress conditions of an isotropic cyclic triaxial test run at the same confining pressure and the Cyclic Stress Ratio, CSR. It is defined as the ratio of the cyclic shear stress and the initial effective confining pressure. Because stress conditions in a triaxial element are controlled solely by changes in vertical and horizontal normal stresses, zero shear stress occurs on the vertical and horizontal planes. This creates a change in stress conditions with no change in the orientation in the principle axes except in the case of principle stress reversal.

Because of these critical differences in stress behavior, the cyclic triaxial test should be considered an index test and not a representation of the actual stress conditions within the soil during a seismic event. Anisotropic cyclic triaxial testing is sometimes used to better model seismic energy than the isotropic cyclic triaxial test. It should be noted that while the loading in stress path space may look similar, the stress path fails to represent the location and rotation in principle stresses that occur with seismic loading. In a triaxial test the maximum shear occurs along the 45° plane during compression and the opposing plane during extension.

The cyclic simple shear test can model seismic loading more realistically than the triaxial test. For this test a sample is consolidated at true k_0 conditions and cyclically loaded in shear on the horizontal plane. This creates similar stress conditions to the in-situ loading during a seismic event.

In cyclic triaxial testing studies shear loading scheme is described as one-way loading or two-way loading. The difference lies in whether there is a reversal of the principle stresses (negative shear) within each cycle. If the stress path crosses the horizontal axis there is a reversal in principle stresses and is considered a two-way test. In a one-way test the orientation of principle stresses within the sample does not change. These terms are not just applied to anisotropically consolidated samples. Some researchers consolidate samples isotropically then load the samples so that maximum and minimum shear stresses remain positive (Sharma and Ismail 2006). By reversing the principle stresses there is a significant reduction in the cyclic strength (Hyodo et al. 1998; Sharma and Ismail 2006).

3.3.3 Idealized Cyclic Behavior

The cyclic behavior of soils and their susceptibility to liquefaction remains a topic still to be investigated. The concept of liquefaction was first introduced by Casagrande in 1936. The pioneering research to investigate liquefaction during earthquakes and to develop a method to predict the onset of liquefaction was performed by Seed and Lee (1966) following the 1964 earthquakes in Alaska and Niigata. Further research focused on distinguishing between and predicting two different types of behavior; liquefaction (flow liquefaction) and cyclic mobility (Kramer 1996). In both cases there is buildup in excess pore water pressure due to contractive tendencies of the soil structure when sheared as a result of static or dynamic loading. Increased pore pressure reduces the effective stress and further results in strength loss.

Steady-state or critical state theory is used widely in geotechnical engineering to predict soil behavior as outlined above. Steady-state theory suggests that under constant volume conditions a sample will tend towards a steady-state effective stress independent of initial effective confining pressure. Loose clean sands under high confining pressure typically will have a tendency for contraction coupled with pore pressure increase, under steady-state theory, and may liquefy. Thus loose sands, when loaded cyclically, experience pore pressure increases and lose strength. However, dense sands that have a tendency for dilation can also experience increased pore pressures during cyclic loading. Pore pressures in such soils can increase due to the initial contractive behavior of such soils at small strains. Under these conditions of pore pressure generation in medium to dense sands, the term cyclic mobility is used. The practical differences of liquefaction and cyclic mobility are explained by Kramer (1996). One major difference is the limited deformations expected during cyclic mobility in

contrast to the unlimited flow and deformation potential during liquefaction of fully contractive loose sands. During cyclic mobility pore pressures can steadily increase in response to cyclic loading but when large deformations start taking place the dense sand transforms from its small strain contractive behavior to dilative behavior resulting in reduced excess pore pressures and recovered strength.

The stress path is a useful tool in interpreting the loading conditions and soil behavior. As discussed previously, analyzing the stress path of a sample monotonically loaded at the same consolidation pressure provides further insight into the cyclic behavior. The state points defined using monotonic testing are theoretically identical to those in observed cyclic testing. Figure 3-8 is a schematic of ideal cyclic and monotonic behavior. Two stress paths are shown. The monotonic stress path follows typical behavior, initial tendency for compression is followed by a tendency for dilation. This behavior creates an elbow in the stress path. A more pronounced elbow signifies a greater contractive tendency. The point at which the tendency for volume change shifts from contractive to dilative is defined as phase transformation. As discussed previously, the phase transformation is dependent on the void ratio and soil type and is independent of confining pressure. After the phase transformation, the monotonic stress path follows the K_f line in the strain-hardening phase of the test. As the soil is strained, it approaches steady-state. The steady-state line in this p'-q space is very close to the K_f line.

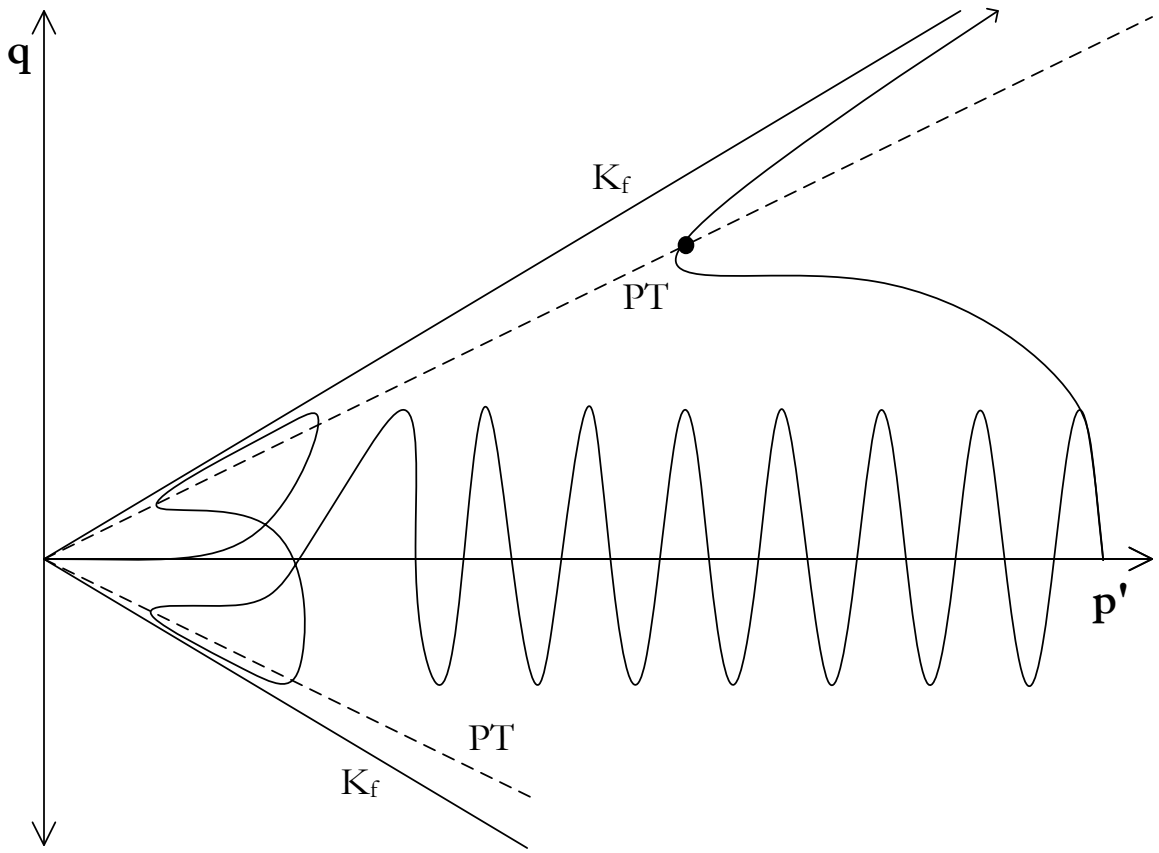

Figure 3-8. Schematic of cyclic and monotonic stress paths

The idealized cyclic stress path is shown in Figure 3-8. The cyclic sample is initially consolidated to the same point as the monotonic sample and then cyclically loaded under stress-controlled conditions. With each cycle, excess pore pressure develops reducing the effective stress. This is expressed as a migration of the stress path from right to left. Equal shear stress, independent of pore-pressure, is applied with each cycle. Similar to monotonic testing at very low confining pressures, the soil initially contracts. Within a cycle as shear stress increases the phase transformation line is crossed. As indicated earlier, the sample dilates creating an increased effective stress state. The soil follows the failure line up and to the right until the end of the compression cycle. This behavior continues through many cycles producing the 'butterfly' pattern. Eventually significant disturbance will occur, and

the contact pressure between soil particles is significantly reduced. As the sample goes into compression, a collapse in the soil skeleton occurs. The collapse pushes the excess pore pressure up causing the effective stress to drop to zero (Alarcon-Guzman et al. 1988). Seed and Lee (1966) define this point where the effective stress first reaches zero as "initial liquefaction". As described above, medium to dense sands can also experience significant pore pressure increases and cyclic mobility. In these soils, when the stress path approaches the failure envelope the sample dilates, inhibiting full liquefaction with unlimited flow potential.

3.3.4 CSR vs. Number of Cycles to Failure

Results of liquefaction evaluation studies are presented in different ways. The most common is with a Number of Cycles to Failure versus CSR plot. CSR is the cyclic stress ratio. This is the ratio of the applied cyclic shear stress to the initial effective confining pressure. At least three tests are run at a range of cyclic stress amplitudes. Curves can be constructed for each condition; density, confining pressure, one-way/two-way shear, an/isotropic consolidation, failure criteria and soil type.

The number of cycles to failure is defined in a number of ways. Failure is defined in this study as initial liquefaction. The cycle in which the pore pressure ratio equals 100% is defined as failure. Failure can also be defined as the cycle in which a double amplitude strain of 5% is reached. Soils that slowly accumulate residual strain during cyclic loading, i.e., dense sands, may never reach a pore pressure ratio of 100%.

3.3.5 Cyclic Behavior of Calcareous Sands

Past studies on the cyclic behavior of calcareous sands are limited. The cyclic behavior of calcareous soils was first researched by the petroleum industry for offshore oil platforms. During large storms the force of waves impacting the platforms creates a cyclic load. Researchers were interested in how foundations in calcareous sands would be affected. When compared to earthquake engineering, the shear stresses on these soils are relatively small. The number of cycles can be significant, in the range of several thousands (Airey et al. 1988; Fahey 1988; Kaggwa et al. 1988; Sharma and Ismail 2006). There are few studies on calcareous sands with a focus on earthquake loading. The most significant earthquake work on calcareous soils was performed by Japanese researchers Hyodo et al. (1996; 1998). Morioka and Nicholson (1999; 2000) also performed a series of cyclic and monotonic triaxial tests and CPT calibration chamber testing. Table 3-2 is a detailed summary of cyclic studies on calcareous soils. Information is provided on the types of tests perform and the variables tested.

In all cases, studies that have compared the cyclic strength of calcareous sands to quartzitic sands have found calcareous sands to be stronger (Hyodo et al. 1996; Hyodo et al. 1998; Kaggwa et al. 1988; Morioka and Nicholson 1999). Authors have attributed this to the highly angular nature of calcareous sand particles. This angularity creates a more stable interlocking soil fabric, resistant to liquefaction.

Table 3-2. Summary of cyclic studies on calcareous soils

Year	Authors	Title	Motivation	Soil Type	Cementation	No. of Tests	Loading	σ_{CON} (kPa)	D_R (%)	CSR
1988	Fahey	*The response of calcareous soil in static and cyclic triaxial tests*	Offshore platforms in Bass Strait (Monotonic & Cyclic)	- See Carter et al. (1988) and Currie et al. (1988) (fine grained material)	Limited	5	Two-Way	unknown	n/a	0.05-0.3
1988	Semple	*The mechanical properties of carbonate soils*	Offshore platforms in Bass Strait (Monotonic & Cyclic)	- Several Bioclastic calcareous soils from the Bass Strait.	None	n/a	n/a	n/a	n/a	n/a
1991	Airey & Fahey	*Cyclic response of calcareous soil from the North-West Shelf of Australia*	Offshore platforms in Bass Strait (Cyclic)	-Silts and Sands with essentially no cementing (same as tested in Fahey 1988) (undisturbed samples were tested) - moderately cemented calcarenite with sand-sized particles. (undisturbed samples were tested)	Naturally cemented & uncemented	12 (C) 11 (UC)	20 Two-Way 3 One-Way	500 to 725 (C) 50 to 215 (UC)	n/a	0.05-0.44 (UC)
1996	Hyodo, Aramaki, Itoh & Hyde	*Cyclic strength and deformation of crushable carbonate sand*	Liquefaction susceptibility determination of crushable calcareous soils	- Dogs Bay Calcareous Sand	None	13 (I) 20 (A)	Two-Way	100, 300 & 500	80	0.17-0.37 (I) 0.24-0.50 (A)
1998	Hyodo, Hyde & Aramaki	*Liquefaction of crushable soils*	Liquefaction susceptibility determination of crushable soils	- Ube & Hiroshima Masado, weathered granite, washed - Shirasu, weathered Volcanic soil, 35% Non-Plastic Fines - Dogs Bay, Calcareous Sand	None	~25 (M) ~25 (S) 25 (DB)	Two-Way	100, 300 & 500 (Dogs Bay)	60 & 80 (Dogs Bay)	0.15-0.23 (60%) 0.18-0.37 (80%) (Dogs Bay)
1999	Morioka & Nicholson	*Evaluation of the liquefaction potential of calcareous sand*	Liquefaction susceptibility determination using CPTs	- Ewa Plains Calcareous SP, Oahu, Hawaii - Monterey Sand (Scalped)	Artificially aged and uncemented	~20 (A, NA)	Two-Way	100	40, 50 & 65	0.14 to 0.27 0.36 to 0.44 (A)
2006	Sharma & Ismail	*Monotonic and cyclic behavior of two calcareous soils from different origins*	Offshore platforms (Monotonic & Cyclic)	- Goodwyn (GW) Fine-grained, offshore calcareous soil. - Ledge Point (LP) Coastal aeolian calcareous sand	None	10 (GW) 21 (LP)	One-Way & Two-Way	200 & 600 (GW) 50, 200 & 600 (LP)	75 (GW) 30 & 75 (LP)	0.38 to 0.1 (GW) 1.2 to 0.1 (LP)
References: (Airey and Fahey 1991; Fahey 1988; Hyodo et al. 1996; Hyodo et al. 1998; Morioka and Nicholson 1999; Semple 1988; Sharma and Ismail 2006)										

3.4 Case History of In-Situ Liquefaction of Calcareous Sands

3.4.1 Introduction

There are a few documented cases where calcareous sands have shown signs of liquefaction due to seismic loading. One case is the Guam Earthquake of 1993. This large earthquake occurred in August 1993 and caused significant damage attributed to liquefaction throughout the island. The damage was most extensive at the U.S. Navy and commercial port facilities where hydraulically placed fill was used for construction of wharfs and piers. There are many other highly seismic areas with calcareous soils. In the United States, these areas include Puerto Rico and Hawaii. (EERI 1995)

3.4.2 Guam Earthquake Details

The Guam earthquake of August 8th, 1993 was of magnitude 8.1 (moment magnitude, M_W 7.7). The earthquake occurred in the Marianas subduction zone about 60 km south of Agana, Guam, at a depth of about 50 km. The Mariana subduction zone is between the Pacific Plate and the Marianas Plate. The Marianas Plate is a microplate on the eastern edge of the Philippine Plate. (Mejia and Yeung 1995) Both plates are moving in a northwestern direction. The Pacific Plate is traveling faster creating the subduction fault (Vahdani et al. 1994). Subduction faults have associated volcanic features due to the plunging plate. Guam and the other Mariana Islands are these volcanic features (Mejia and Yeung 1995).

3.4.3 Guam Geology

The low-lying waterfront areas most damaged by liquefaction consisted of a coralline fills of silty sands and gravels. These are underlain by loose lagoonal and estuarine deposits of soft clay and loose coralline silts, sands and gravels (Mejia and Yeung 1995). These deposits are

underlain by limestone. Guam has a considerable amount of volcanic soils. There is little evidence of liquefaction or lateral spreading in these soils.

3.4.4 Earthquake Details

No ground motion records exist from this earthquake. The peak ground acceleration, PGA, can be estimated using attenuation models. Mejia and Yeung (1995) performed an attenuation analysis using two subduction-zone relationships. Their estimate for the PGA on hard rock at Apra Harbor is between 0.15 and 0.20 g. There are up to 80 feet of soft clays and loose coral sands at this site. Mejia and Yeung used a PGA of 0.25 g at the ground surface for their analysis of Apra Harbor. Based on the limited damage to "low-rise structures and significant damage to some high-rise buildings" Vahdani et al. (1994) estimate the predominate period of the earthquake to be between 0.5 and 1.5 seconds.

3.4.5 Damage

There was considerable damage to both the naval and commercial port facilities within Apra Harbor in Guam. Liquefaction of hydraulically placed fill and lagoonal deposits below the water line caused most of the damage. These facilities all have similar designs. The wharfs consist of an anchored sheet pile bulkhead wall. The anchors are either deadmen or sheet piles, and are attached to the wall about 8 feet below the ground surface. A local coralline soil, silty sand and gravels, is hydraulically placed behind the wall up to the waterline. Above the waterline the soil is mechanically compacted. (Mejia and Yeung 1995)

A Navy personnel bar called Andy's Hut was completely destroyed. This was the result of lateral spreading of over 15 feet. The Mejia & Yeung (1995) report states that the movement

started after the shaking had stopped. This delay allowed the estimated 100 people in the structure to escape safely.

Damage to wharfs within Apra Harbor consisted of lateral movement of the bulkhead wall. In some cases this movement was as much as 3 feet. This lateral movement caused cracks parallel to the wall. These cracks were as much as 6 inches wide extending 200 feet from the wall. Significant settlement also occurred as a result of liquefaction. This settlement was 24 inches in some places. A passive failure bulge was also observed in front of some of the deadman anchors. (Mejia and Yeung 1995)

Settlements of several inches were observed at the two electric power plants in Piti. Both structures are supported on piles. The site consisted of 5 to 8 feet of fill over a "medium-dense, relatively clean, coral sand layer about 6 feet thick." (Vahdani et al. 1994)

3.4.6 SPT Results

Mejia and Yeung (1995) were the only researchers to publish an evaluation of Standard Penetration Test (SPT) results. This provided the data to evaluate the applicability of the SPT to estimate liquefaction susceptibility of calcareous sands. There are no other available SPT or CPT data on calcareous soil following an earthquake. Their paper includes the results of evaluations of two sets of SPT data. The first was performed at one of the commercial wharfs following the earthquake. The second was performed at Navy wharfs M and N prior to the earthquake. At wharfs M and N tests were performed in two areas, one at an area of significant damage and the other at an area of minimal damage.

Mejia and Yeung's results are presented in the Figure 3-9 and Figure 3-10 taken from their paper. These figures show a threshold required for no liquefaction. This threshold is determined using the SPT-based liquefaction evaluation procedure presented by Seed et al. (1985) for a clean quartzitic sand. As is shown in the figures, for the area where minimal damage occurred a majority of the test results lie to the right of the threshold. For the area with significant damage occurred a majority of the test results lie below the threshold.

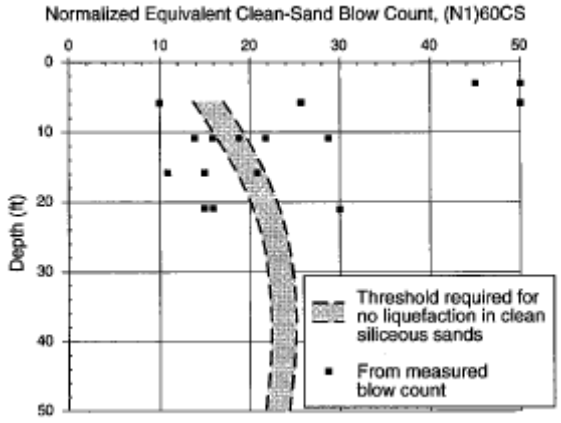

Figure 3-9. SPT Blow Counts at Wharves M and N – Damaged area. From Mejia & Yeung (1995)

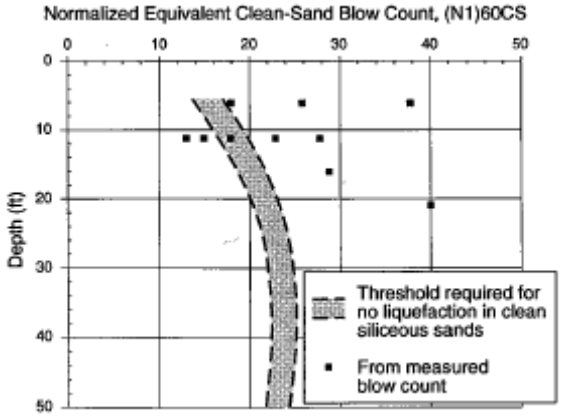

Figure 3-10. SPT Blow Counts at Wharves M and N – Area of minimal damage. From Mejia & Yeung (1995)

3.4.7 Conclusion

These results are significant to the study of liquefaction in calcareous sands. This study provided SPT results in calcareous sands that have shown to experience liquefaction and no-liquefaction during the 1993 Guam Earthquake. The results provide some evidence that the current practice of liquefaction susceptibility evaluation can be used in calcareous sands. Even though it cannot be conclusively justified, the results show that the current liquefaction potential evaluation procedure developed for quartzitic sands may be applicable for these calcareous soils. There is a critical need to verify this with further studies as there are significant port facilities constructed of calcareous sands in Hawaii and Puerto Rico both of which are in seismically active areas (EERI 1995).

4 TESTING PROGRAM & PROCEDURES

4.1 Introduction

Geocomp triaxial testing apparatuses were used for the monotonic and cyclic testing of Playa Santa calcareous sand. A description of the testing program performed and a detailed description of the laboratory testing procedures are summarized in the subsequent sections.

4.2 Triaxial Testing Program

4.2.1 Monotonic Testing Program

A total of 17 isotropically consolidated undrained monotonic triaxial tests were performed on Playa Santa calcareous sand from Puerto Rico. The tests are summarized in Table 5-1. For each test, the point of phase transformation is defined from the pore pressure generation behavior. In an effort to understand how the tendency for volume change varies due to changes in relative density, a series of tests were performed at a constant confining pressure of 100 kPa with varying relative densities; 20%, 30%, 40% and 60%. Additionally, a series of tests were performed at a constant relative density of 20% with varying confining pressures; 75 kPa, 100 kPa, 150 kPa, 200 kPa, and 300 kPa.

4.2.2 Cyclic Testing Program

A total of 13 isotropically consolidated undrained cyclic triaxial tests were performed on Playa Santa calcareous sand. The three significant variables in cyclic triaxial testing are the sample density, effective confining pressure, and the applied cyclic shear stress. The cyclic shear stress is normalized by the initial effective confining pressure and expressed as a Cyclic Stress Ratio (CSR).

The intent of the testing program is to develop a relationship between the number of cycles to liquefaction with respect to the applied CSR. All tests were performed at a common confining pressure of 100 kPa. Samples were tested at three different relative densities; 20%, 40% and 60%. The intent is to show the variation in cyclic strength and pore-pressure generation at various relative densities. Cyclic tests performed for this study are summarized in Table 5-2.

4.3 Triaxial Sample Preparation Procedure

4.3.1 Introduction

The sample preparation and saturation procedures are the same for the monotonic triaxial and cyclic triaxial tests. All samples were prepared using the preparation method commonly known as moist tamping. When using this method each sample is prepared at a specific water content. A predetermined mass of moist sand is compacted to a set volume. The sand mass is calculated based on the desired density. This method eliminates compactive effort from the equation and creates a more consistent density from sample to sample. A technique called undercompaction was used for all tests. Developed by Ladd (1978) and modified by Chan (1985), this technique assumes that with the addition and compaction of subsequent lifts the preceding lifts become denser. To account for this, Ladd proposed that each additional lift be placed at a higher density. Chan proposed that each lift be placed at a relative density one percentage point higher. Following Chan's recommendation, if a final relative density of 20% is desired and seven lifts are to be used, the first lift would be placed at 17%, followed by lifts at 18%, 19%, 20%, 21%, 22% and 23%. This sequence would produce in a uniform final density of 20%.

4.3.2 Compaction

The procedure for sample preparation begins with applying vacuum grease to the bottom platen and placing the membrane over it. A split vacuum mold and membrane, with o-rings placed at the top and bottom, is positioned over the bottom platen. Filter paper is used to distribute the vacuum throughout the interior surface of the mold. Once the filter paper is in place, the top of the membrane is flipped over the top edge of the mold and a vacuum is applied. The membrane lies smoothly and tightly against the surface of the mold. Each lift is placed and compacted using gauge blocks to measure lift height and a 1.4 inch diameter foot tamper. The top of the final lift is even with the top of the mold. The top platen is then positioned. The membrane and o-rings are pulled up over the top platen. The vacuum is taken off the mold and applied to the sample via the top platen; the house vacuum is typically at about 15 inHg (-50 kPa). The mold is removed and the sample height and diameter are measured. Thee height measurements are taken using a machinist scale to the nearest 64^{th} of an inch. The diameter is measured in three places using a pi-tape to the nearest 1000^{th} of an inch. The diameter is corrected to account for the thickness of the membrane, 0.025 inches total. All samples were prepared with approximate height and diameter dimensions of 6" x 2.8" (152 x 71 mm).

4.3.3 Sample Flushing

Because calcareous sand has a large void space, the sample pre-saturation and saturation phases are critical. Some researchers take an additional step to ensure saturation in calcareous soils (Golightly and Hyde 1988; Hyodo et al. 1996). This includes leaving the uncompacted soil in water under a vacuum overnight. Satisfactory results have been achieved without taking this step. Pre-saturation consists of three steps; flushing the sample

with CO_2, flushing with deaired water and then flushing all water lines. After the cell is filled and pressurized to 30 kPa, the sample is flushed with CO_2. The regulator on the CO_2 tank is opened and pressure adjusted. The hose is then attached to the bottom platen and the valve opened. The vacuum is removed leaving the valve open to the atmosphere. CO_2 is allowed to freely flow through the sample for 5 minutes. The vacuum line is reattached and the CO_2 line is removed. A deaired water supply line is attached to the bottom platen with about 1.5 meters of water head. Water is allowed to flow/sucked through the sample using the house vacuum. After roughly a liter of water is collected the vacuum and deaired water supply are removed. A sample pressure of 15 kPa is applied and all lines are flushed. The saturation phase is then started.

4.3.4 Saturation

Because sands have high permeability, the saturation phase can be quick. However, it has been the author's experience that the saturation of calcareous sand is not as easy as the saturation of quartzitic sands. More time and attention is necessary, most likely due to the large intra-particle void structure in this type of sand. The Geocomp system uses a stair step procedure for saturation. The cell pressure is increased every 10 min by 50 kPa. A minimum back pressure of 500 kPa was used for most tests. Skempton's pore-pressure parameter B of 0.97 was targeted as a minimum limit to ensure saturation for all the tests (Skempton 1954).

4.4 Monotonic Shear Procedures

4.4.1 Description of Monotonic Apparatus

Monotonic triaxial testing was performed using the Geocomp LoadTrac II/FlowTrac II system. This is a fully automatic apparatus used for performing all types of monotonic triaxial tests. This same equipment can be used to run an array of geotechnical tests. The system consists of a loading frame, two flow pumps and a computer with a system card. Vertical loading is controlled by a high speed, microstepper motor within the loading frame. The pressure and volume control of the cell and sample are controlled by two FlowTrac II piston pumps. The pump is controlled by a high speed, mircostepper motor. Sample volume change is determined by tracking the step count for the piston pumps. The cell that was used for all tests is manufactured by Geotac. The top and bottom end platens have two drain lines. During all phases of testing a hose connects the top and bottom platens to maintain a consistent pressure. (Geocomp 2002a; Geocomp 2002b)

4.4.2 Monotonic Shear Procedures

Following the saturation phase, a confining pressure is placed on the sample; typically 100 kPa. The consolidation phase of a triaxial test in calcareous sands is very quick due the high permeability of the material. The consolidation time varied from sample to sample. All samples were allowed to consolidate for at least one hour, while some were left for more than 24 hours.

After the sample is allowed to consolidate, the shear phase of the test is started. All tests were performed undrained. Cell pressure is continually measured and maintained. All monotonic testing is strain-controlled. The ASTM D4767 for consolidated undrained (CU)

triaxial testing recommends that the rate of strain used in CU triaxial testing be determined based on the permeability or rate of consolidation of the material being tested (2004). The calcareous sand investigated in this study has trace amount of fines and has a high permeability. All tests were run at the highest recommended rate of strain of 0.1 %/min. The shearing was terminated at 25% strain or when the maximum load was reached on the load cell.

4.4.3 Monotonic Data Reduction

An area correction was made for all tests. The correction is made by dividing the initial area by the axial strain plus one. This correction is recommended by ASTM D4767, and assumes the sample maintains a cylindrical shape (2004). One pound of frictional resistance is also assumed in all vertical loads, this corresponds to about 1.1 kPa of stress on the sample. The following plots have been prepared for each test and are included in Appendix I**;** deviator stress vs. strain, excess pore-pressure vs. strain, effective vertical and effect horizontal stress vs. strain, and MIT style total and effective stress paths. Detailed data reduction calculations can be found in the ASTM D4767 specification (2004).

4.5 Cyclic Test Procedures

4.5.1 Description of the Cyclic Triaxial Testing Apparatus

The cyclic triaxial testing system is manufactured by Geocomp. The system is based on the Geocomp monotonic triaxial system with additional components for cyclic loading. The system consists of the LoadTrac II load frame and two piston pumps to apply and measure cell and sample pressures. All static vertical loading is applied by the stepper motor at the base of the load frame. Cyclic loading is performed by a hydraulic cylinder coupled with a

servo control valve and a hydraulic actuator driven by a 2.5 gpm/3000 psi hydraulic pump. The hydraulic cylinder applies the load from above of the cell. The cylinder is attached to the top of the loading frame. A second set of sample and cell pressure transducers that connect directly to the cell are used during the cyclic phase of testing. (Geocomp 2007)

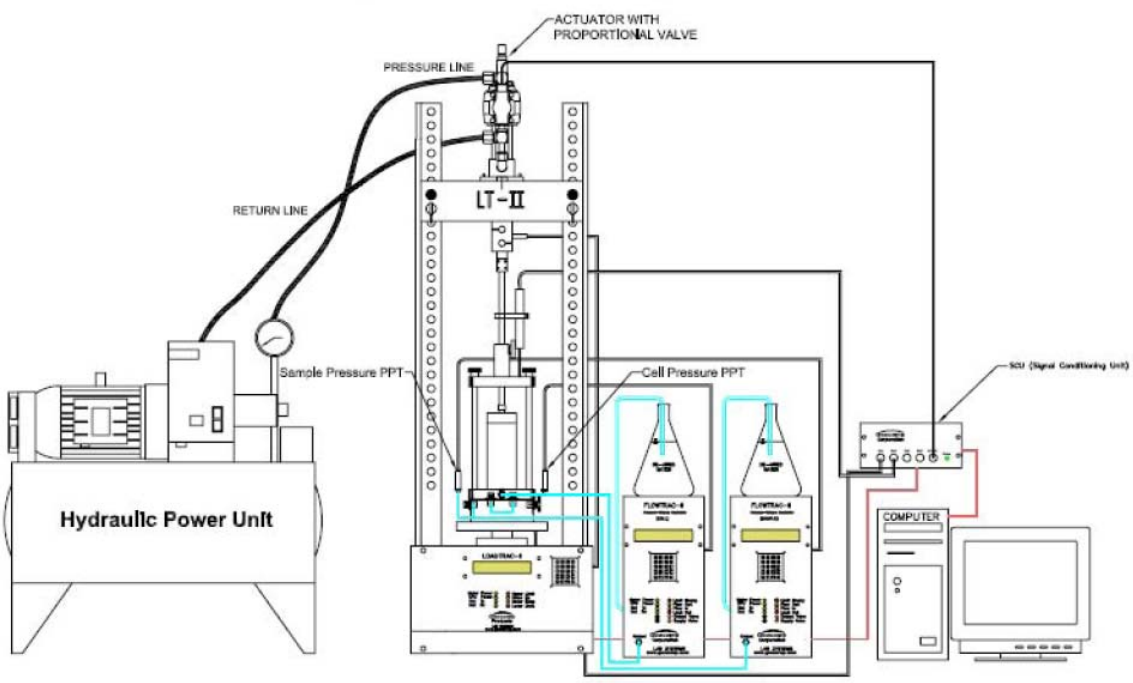

Figure 4-1. Cyclic Triaxial System. From Geocomp

4.5.2 Cyclic Shearing Procedure

The test procedures for the cyclic test are identical to the monotonic test through the end of the consolidation phase. Following consolidation a cyclic stress is applied under stress controlled conditions. The cyclic phase is started by first powering the hydraulic pump. The initial position of the hydraulic cylinder is fully retracted. Because the sample is loaded in compression and extension during the cyclic phase of testing the cylinder must be able to act in both directions. The system centers the cylinder by lowering the base as the servo

controls the hydraulic cylinder to maintain a constant load on the sample. After the hydraulic cylinder is centered, cyclic loading commences. After a minimum of 5% accumulated axial strain is achieved the test is terminated.

4.5.3 Cyclic Data Reduction

The basic reduction of the cyclic data is exactly the same as the reduction of the monotonic data. Because strains are very small no area correction has been made. A deviator stress is determined, excess pore-pressure and effective stress is calculated. An additional step in data reduction is necessary for the cyclic test data. This step consists of several refinements to make the data presentable for interpretation, and include; (1) filtering, (2) applying a phase shift to the cell and sample pressures, and (3) adjusting the offsets or zeros for the sample pressure, cell pressures, and vertical load. A detailed description of this data reduction and refinement is included in APPENDIX III.

5 RESULTS AND ANALYSIS

5.1 Monotonic Triaxial Testing

5.1.1 Typical Monotonic Test

A total of 17 monotonic isotropically consolidated undrained triaxial tests were performed at varied densities and confining pressures. These tests are summarized in Table 5-1. For each test two plots were prepared to present the results. The figures for Test MCU07 are provided in this section for discussion, Figure 5-1 and Figure 5-2. The figures for the other tests are provided in Appendix I.

Table 5-1. Summary of Monotonic Triaxial tests performed

Test No.	D_r (%)	σ_{CON} (kPa)	e	Δu_{MAX} (kPa)	r_{UMAX}*	Phase Transformation			PSR+
						p' (kPa)	q (kPa)	ε (%)	
MCU01	0 (-3.2)†	150	1.234	155	1.03	n/a	n/a	n/a	n/a
MCU02	0 (4.1)	150	1.203	155	1.03	n/a	n/a	n/a	n/a
MCU03	0 (5.0)	150	1.199	153	1.02	n/a	n/a	n/a	n/a
MCU04	10 (12.8)	150	1.167	109	0.73	109	68	5.35	4.36
MCU05	20 (21.6)	75	1.130	45	0.60	77	47	1.96	4.10
MCU06	20 (18.6)	100	1.143	60	0.60	100	62	2.21	4.19
MCU07	20 (17.9)	200	1.145	117	0.59	185	112	2.82	4.04
MCU08	20 (21.7)	300	1.129	194	0.65	271	166	3.05	4.17
MCU09	30 (33.7)	75	1.079	44	0.59	78	47	1.59	4.01
MCU10	30 (26.8)	100	1.108	55	0.55	109	64	1.30	3.84
MCU11	40 (43.2)	100	1.039	45	0.45	128	76	0.66	3.96
MCU12	40 (40.5)	100	1.051	43	0.43	139	83	1.14	3.95
MCU13	40 (35.4)	150	1.072	88	0.59	155	94	1.99	4.03
MCU14	40 (42.2)	200	1.044	103	0.51	241	148	1.35	4.21
MCU15	50 (53.4)	300	0.997	185	0.62	315	195	1.90	4.27
MCU16	50 (46.9)	300	1.024	179	0.60	322	201	1.75	4.33
MCU17	60 (58.3)	100	0.976	39	0.39	142	83	0.53	3.85

† Rounded final relative density (actual final relative density)
* Maximun Pore-Pressure Ratio
+ Principal Stress Ratio at phase transformation

The test MCU07 was performed on a sample with a target relative density of 20%. Initial relative density or initial void ratio is determined from height and diameter measurements following compaction. The final sample volume, as determined from the measured volume change during consolidation, is used to calculate the final relative density. The final relative density of sample MCU07 is 17.9%. For categorization and referencing, the relative density has been rounded to the nearest 20 percent for this sample. In this report the actual final relative density will often follow the rounded final relative density in parentheses. This sample was consolidated to an effective confining pressure of 200 kPa. The first figure, Figure 5-1, is the monotonic stress path using the MIT convention for the stress invariants (p' and q). The value of p' is equal to $(\sigma'_1+\sigma'_3)/2$. The value of q is equal to the maximum shear stress, $\sigma_d/2$ or $(\sigma'_1-\sigma'_3)/2$. Both the effective stress path and total stress path are shown. The point of phase transformation and corresponding phase transformation line are referenced. Additionally, in Figure 5-2, three plots have been provided in a combined figure. It shows the behavior of four parameters with respect to strain; deviator stress (σ_d), vertical effective stress (σ_v'), horizontal effective stress (σ_h') and excess pore-pressure (Δu). The rounded final relative density and confining pressure are also shown in the figure. These figures show the typical behavior of these sands. An initial tendency for contraction is followed by dilative behavior as indicated by the point of phase transformation.

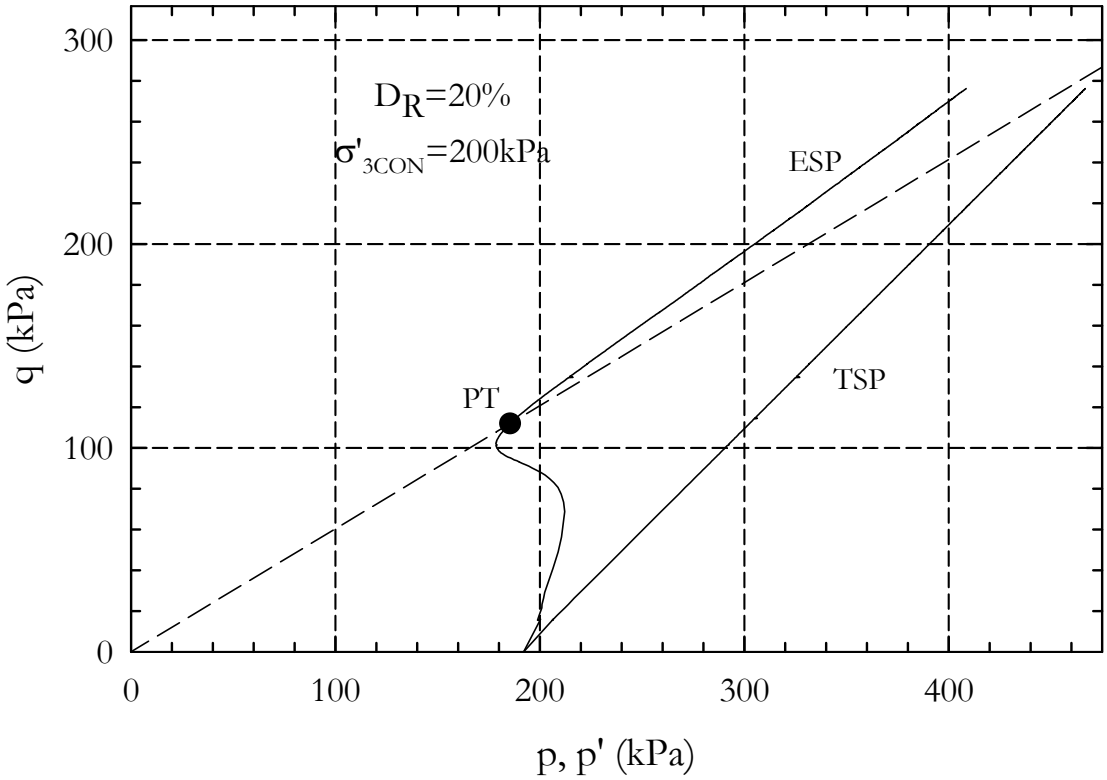

Figure 5-1. Stress Path - Test MCU07

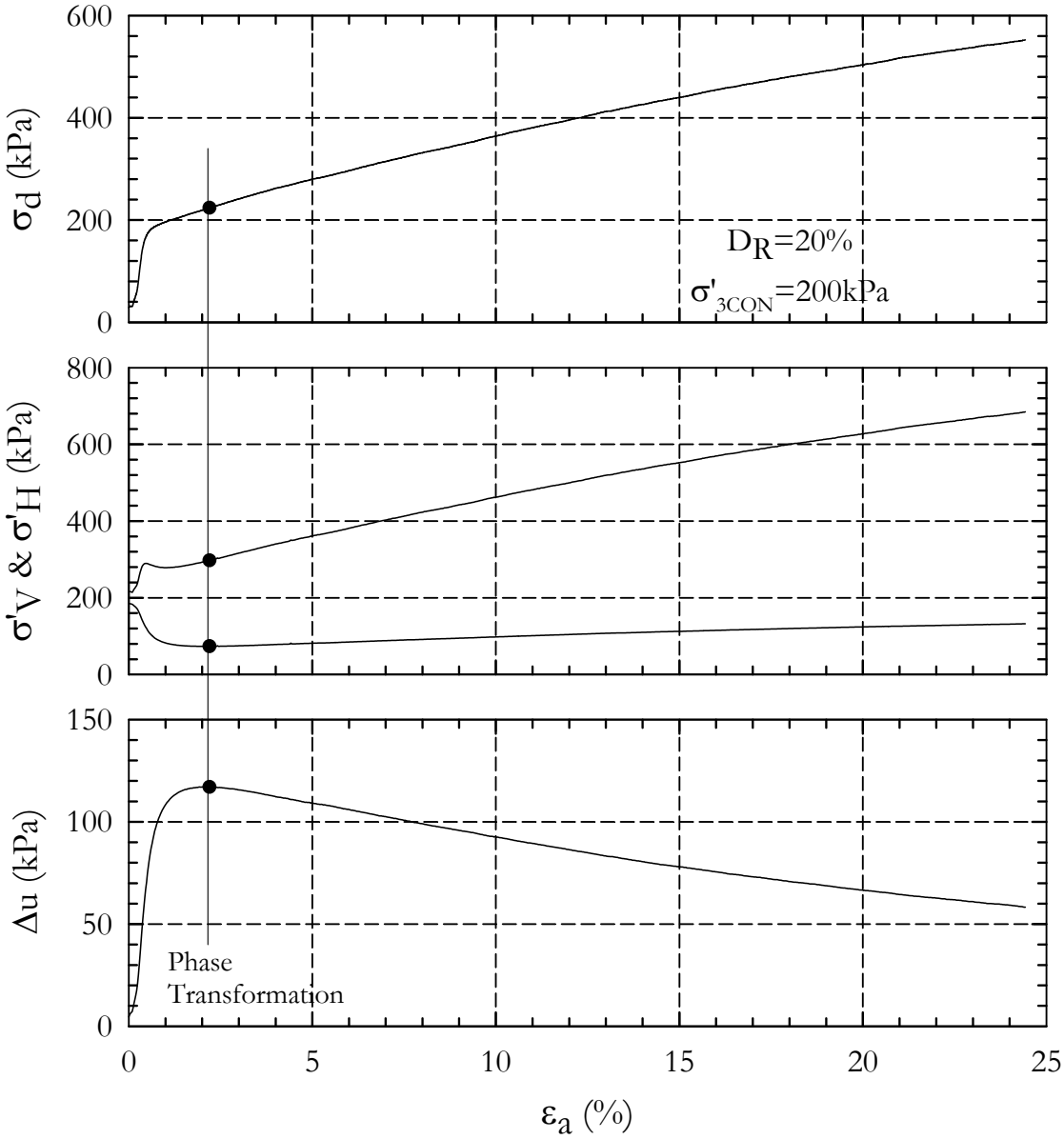

Figure 5-2. Strain Plot - Test MCU07

5.1.2 Significance of Relative Density

As discussed in Section 3.2 the density or void ratio is the major factor determining how a sand will behave during shear. In the following a series tests are presented to show how the void ratio affects the soil behavior of Playa Santa calcareous sand during shear. This series

consists of four tests (MCU06, MCU10, MCU11 and MCU17) all consolidated under an initial confining pressure of 100 kPa. The relative density of the samples following consolidation are as follows; 19%, 27%, 43% and 58%.

Three figures have been prepared to present the soil behavior under shear at varied densities. Figure 5-3 is the deviatoric stress (σ_d) plotted versus the axial strain (ε_a). Figure 5-4 is the excess pore pressure (Δu) plotted versus the axial strain and Figure 5-5 is the effective stress paths for each test. The sample's initial stiffness and the contractive tendency during shear are significant. As Figure 5-3 shows, at low strains the soil is very stiff followed by a softening a higher strains. For the 19%, 27%, 43% and 58% samples a modulus of initial stiffness of 32.6, 30.1, 61.1 and 59.5 MPa, are measured. As expected, initial stiffness generally increases with sample density. These values correspond well with other published values for calcareous sands (Cataño Arango 2006). This residual stiffness is maintained through the end of the test.

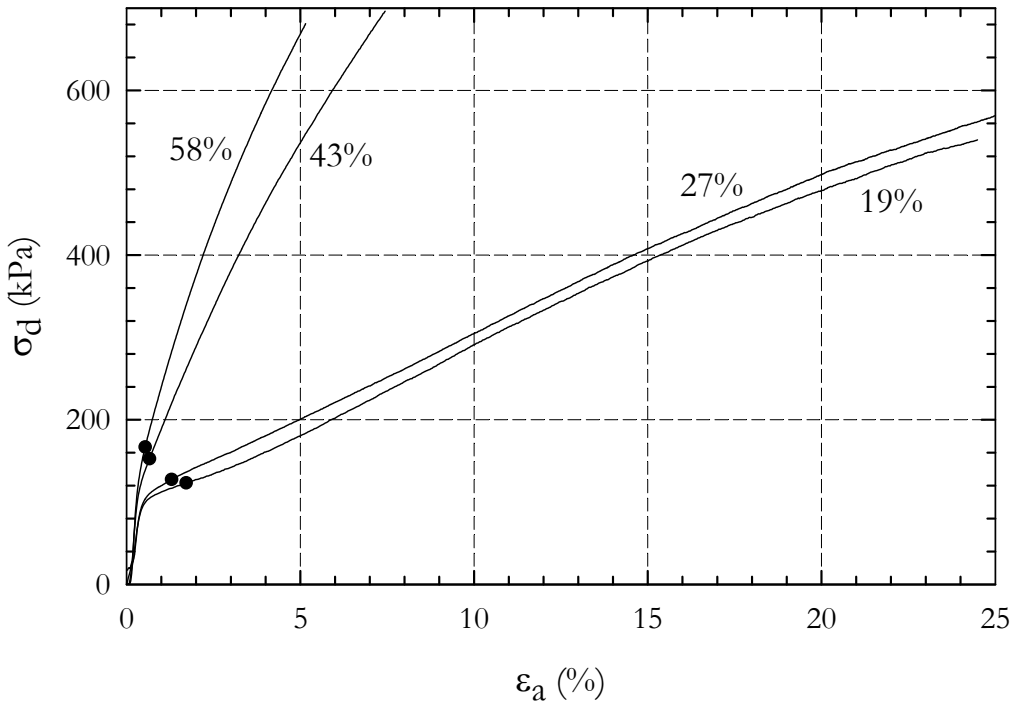

Figure 5-3. Deviator stress versus axial strain at varied relative densities – Test No. MCU06, MCU10, MCU11 & MCU17

The excess pore-pressure is plotted versus axial strain in Figure 5-4. An increase in pore-pressure shows a contractive tendency. In all cases an initial tendency for contraction is followed by a partial tendency for dilation then subsequent full dilation. Contractive behavior can be quantified using several metrics. These include maximum excess pore pressure, strain at the point of phase transformation and strain at zero excess pore-pressure. All metrics show that with decreasing density, Playa Santa calcareous sand has a greater tendency for contraction. As seen in the figure, more strain is necessary to reach the phase transformation point in looser samples. This behavior can also be observed in the stress paths for each test, Figure 5-5. Contractive behavior is expressed in a stress path, independent of strain, through a more defined elbow. Additionally, these tests have shown that the angle of phase transformation, principle stress ratio of PT, is independent of density.

Hyodo et al. also reported that these values are independent (1998). Phase transformation data is presented in Table 5-1.

Sands at higher void ratios exhibit a larger contractive tendency. This behavior is explained by the steady-state theory. At a high void ratio the soil structure is loose and fragile. Shearing disturbs the soil structure and the soil grains tend to rearrange to a denser state of packing. At greater densities the initial state of packing is efficient. Initially there is a contractive tendency driving the pore-pressure up. Under additional strain the particles are forced to roll over one another. This rolling induces a tendency for dilation reducing the pore pressure.

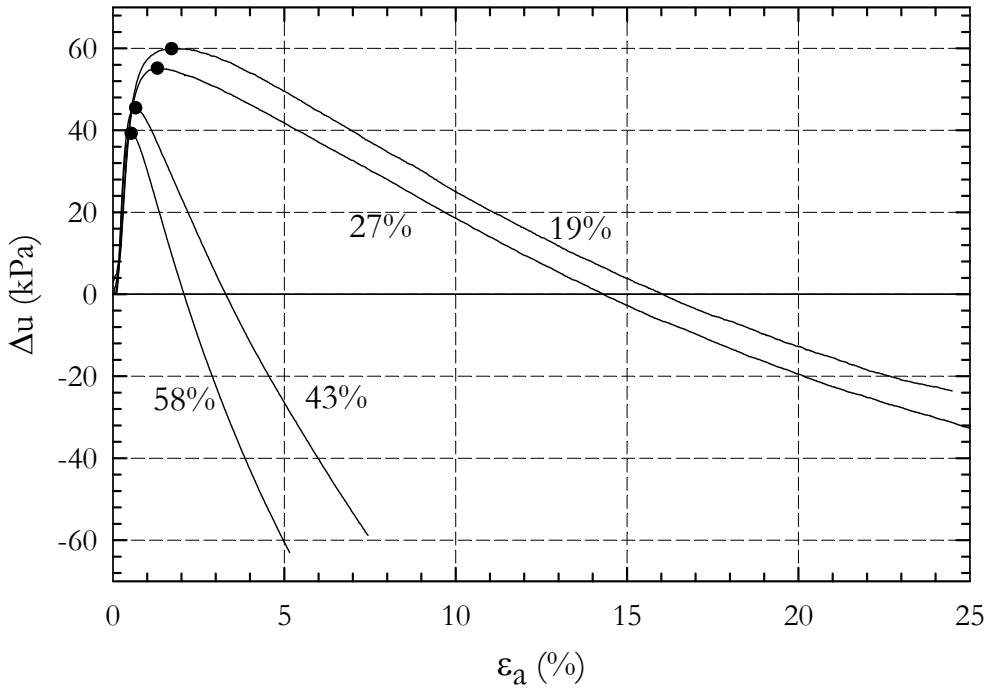

Figure 5-4. Excess pore-pressure versus axial strain at varied relative – Test No. MCU06, MCU10, MCU11 & MCU17

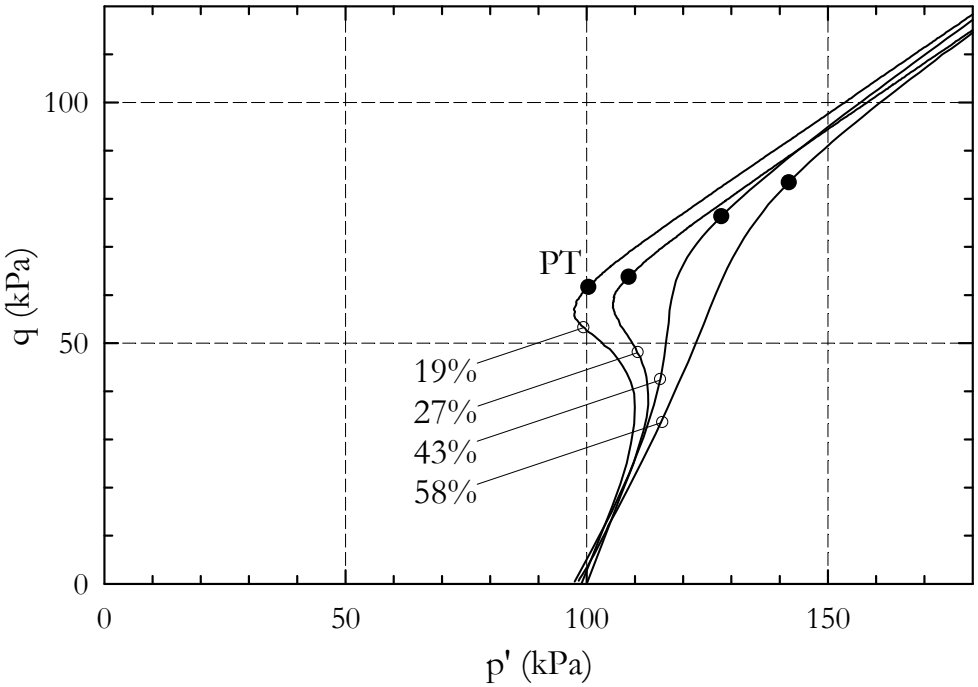

Figure 5-5. Stress Path at varied relative densities – Test No. MCU06, MCU10, MCU11 & MCU17

5.1.3 Significance of Confining Pressure

One factor affecting the behavior of a soil under shear is the initial effective confining pressure. A series of tests were completed to identify how altering the confining pressure and maintaining a constant void ratio affects the behavior. Four tests were performed at a relative density of about 20%; MCU05, MCU06, MCU07 & MCU08. The tests are run at different confining pressures; 75kPa, 100kPa, 200kPa & 300kPa, respectively.

The effective stress path for each test is presented in Figure 5-6. Each sample is initially isotropically consolidated and then sheared under undrained conditions. All samples have an initial contractive tendency followed by a tendency for dilation. Two of the four samples fully dilated with negative excess pore-pressure by the end of the test. This figure shows that

the principle stress ratio at phase transformation is about equal in all tests. A phase transformation line through the four points is very well defined. The behavior of these four samples show typical behavior for sands sheared under undrained conditions. Initial contractive tendency is followed by a phase transformation. As the sample approaches the K_f line, further tendency for dilation occurs.

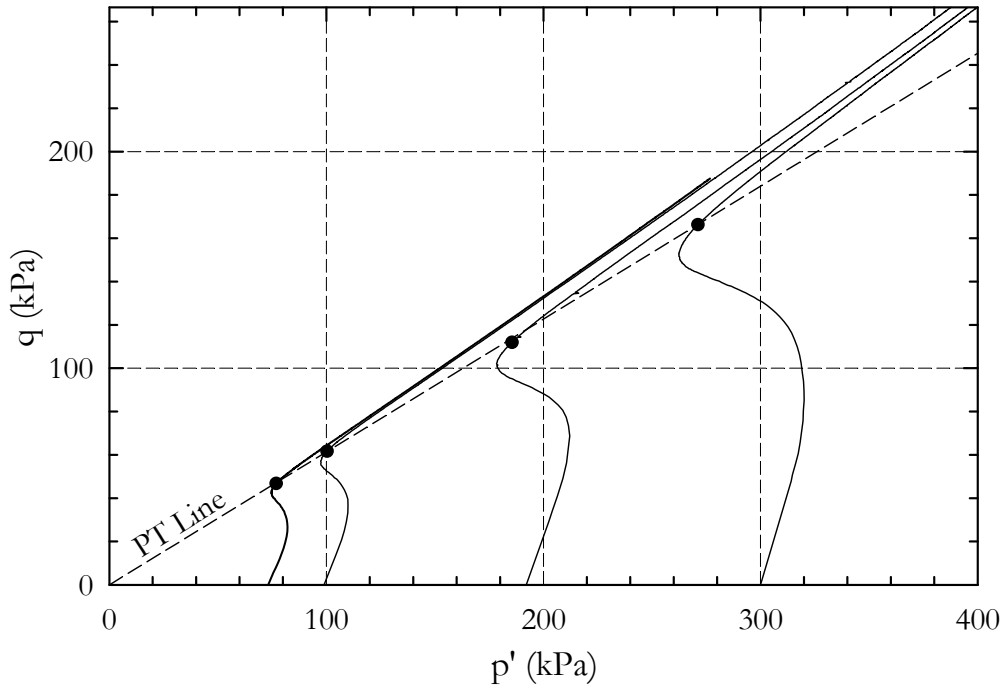

Figure 5-6. Stress Paths at varyied confining pressure – MCU05, MCU06, MCU07 & MCU08

The deviator stress is plotted versus the axial strain in Figure 5-7, below. With increased confining pressure the calcareous soil is capable of sustaining increased shear stress. An initial stiff portion of the stress-strain curve is followed by a relatively softer response. The initial stiffness modulus for the 75kPa, 100kPa, 200kPa and 300kPa test is equal to 28.0MPa, 30.2MPa, 38.0MPa and 57.1MPa, respectively. These tests show an increased stiffness with increasing confining pressure. More tests are necessary to define a trend.

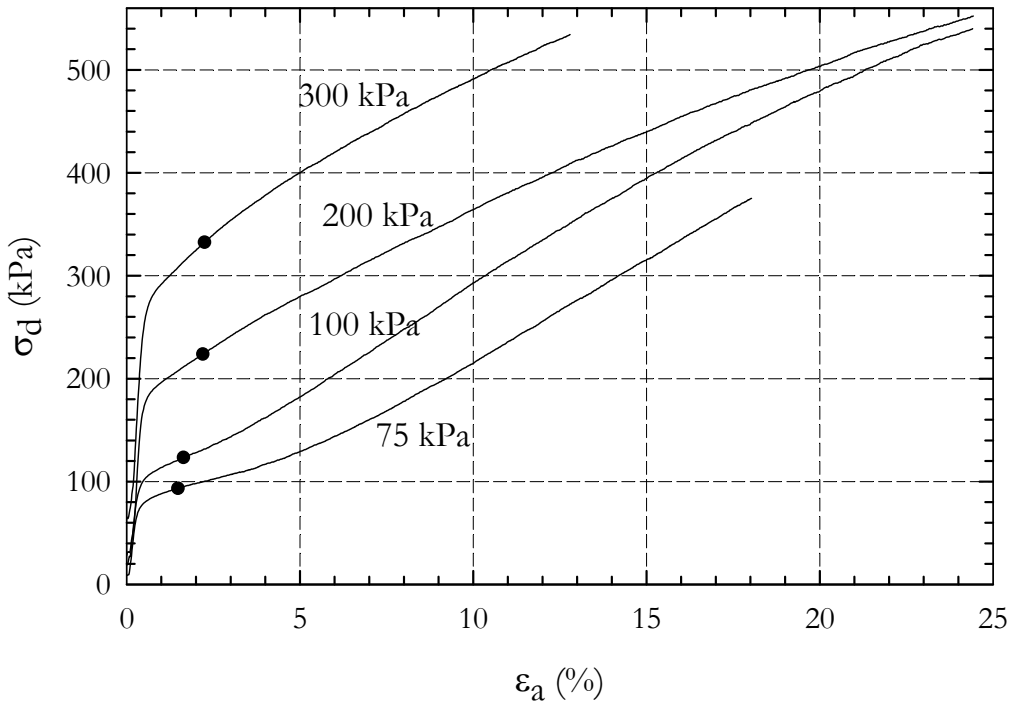

Figure 5-7. Deviator stress versus axial strain at varied confining pressure – MCU05, MCU06, MCU07 & MCU08

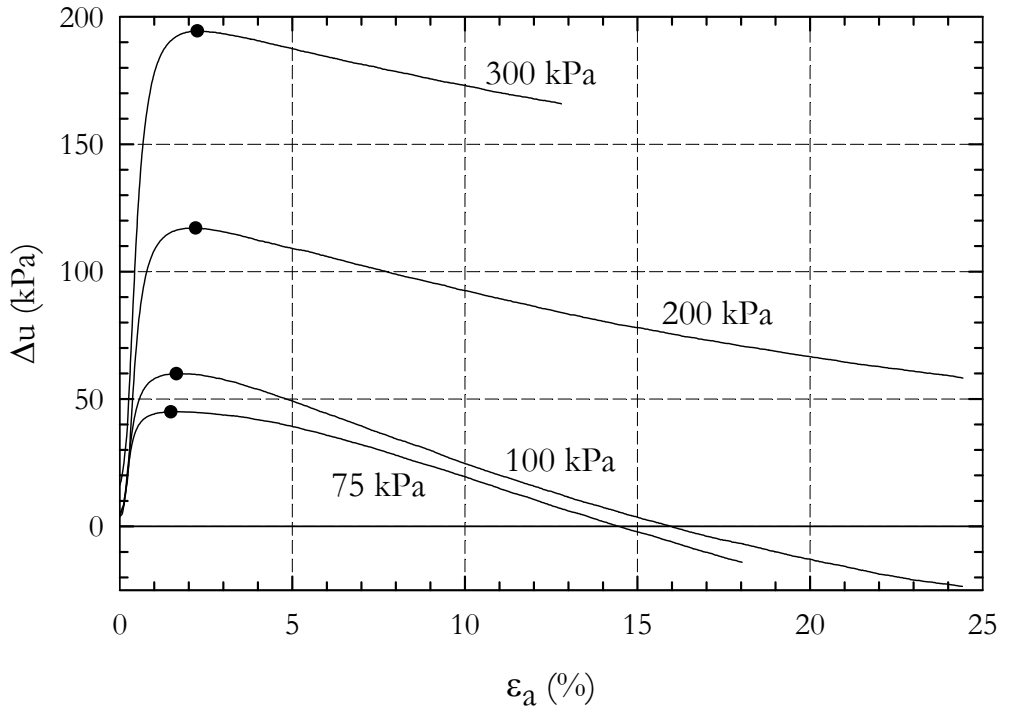

Figure 5-8. Excess pore-pressure versus axial strain at varied confining pressures – MCU05, MCU06, MCU07 & MCU08

An increase in contractive tendency is observed by normalizing the data with respect to the confining pressure. The normalized stress paths are presented in Figure 5-9. With increased confining pressure the elbow in the stress path becomes more exaggerated. Figure 5-10 and Figure 5-11 are normalized deviator stress and excess pore-pressure plots. Increased confining pressure increases the contractive tendency in sands. This behavior is explained in steady-state theory. Under these conditions both samples have the same volume and the soil structure. At higher confining pressures the propensity for the grains to slip into a more dense packing is greater. At lower confining pressures instead of slipping into a more dense packing the soil particles will roll over one another causing a tendency for dilation. These mechanisms are not mutually exclusive. The soil particles will, under shear, roll over one another while at the same time slip and settle into a denser packing (Coop et al. 2004).

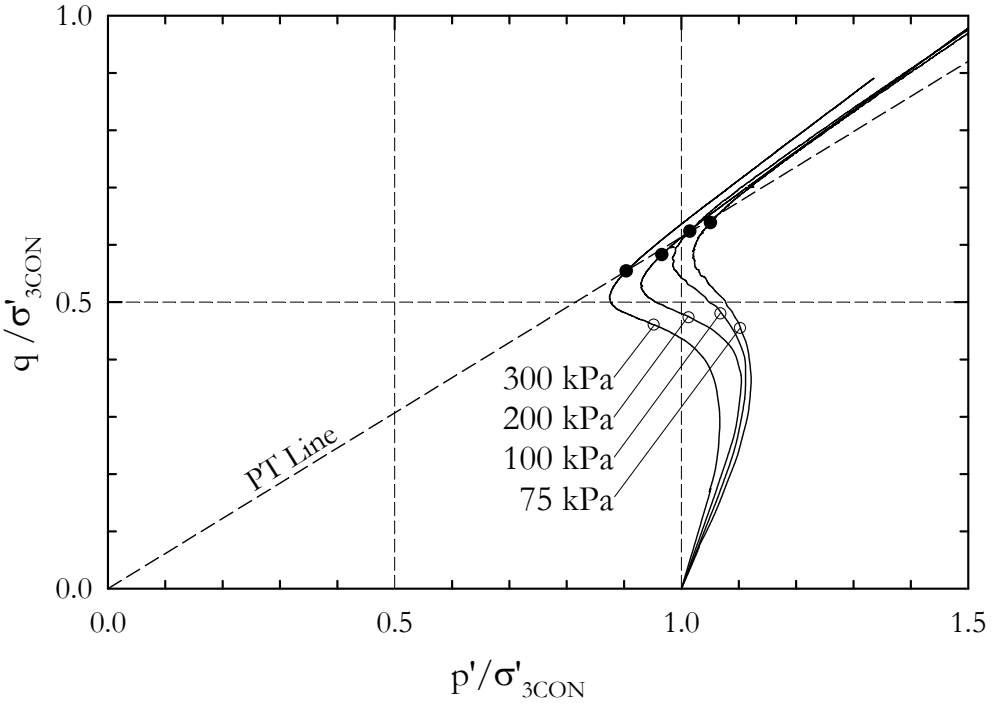

Figure 5-9. Normalized Stress Paths at varied confining pressures – MCU05, MCU06, MCU07 & MCU08

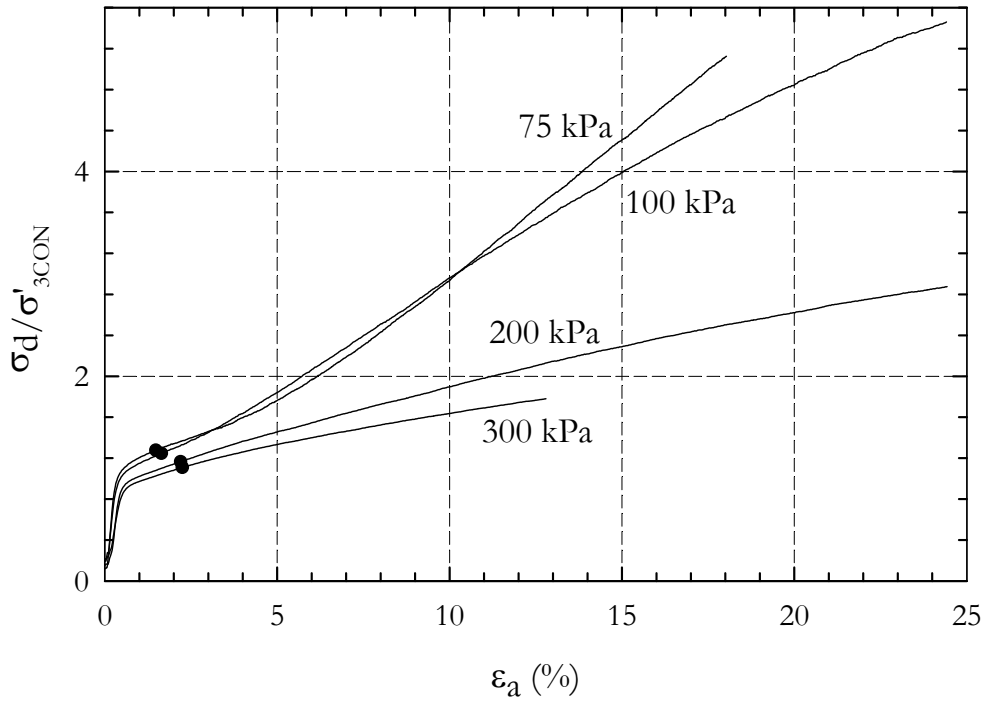

Figure 5-10. Normalized deviator stress versus strain at varied confining pressures – MCU05, MCU06, MCU07 & MCU08

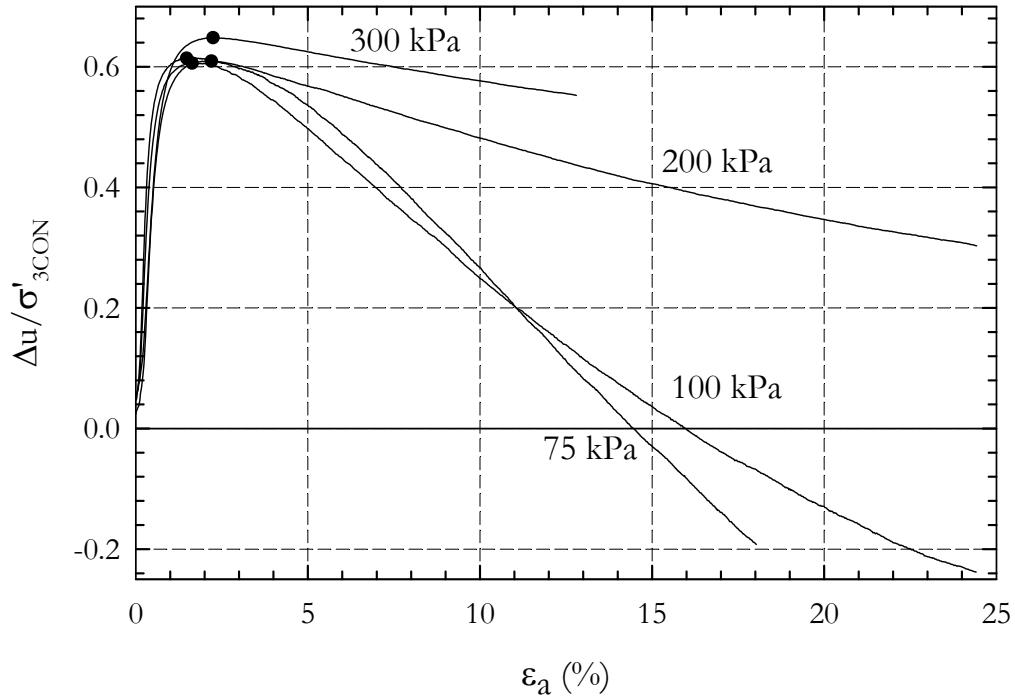

Figure 5-11. Normalized excess pore-pressure vs. strain at varied confining pressures – MCU05, MCU06, MCU07 & MCU08

5.1.4 Flow Liquefaction under Monotonic Loading

In some cases full dilation is achieved (negative Δu), in others only partial dilation is achieved. Of the 17 tests preformed, all but three had an initial tendency for contraction followed by a tendency for dilation. Three tests did not have any dilative tendency and were completely contractive throughout the test. These samples exhibited a flow-type liquefaction failure. All three tests were performed at a relative density of about 0% and confining pressure of 150kPa. The results of Test MCU02 are provided below; Figure 5-12 and Figure 5-13. Once the effective stress reaches zero the soil is essentially a liquid and cannot sustain any shear stress.

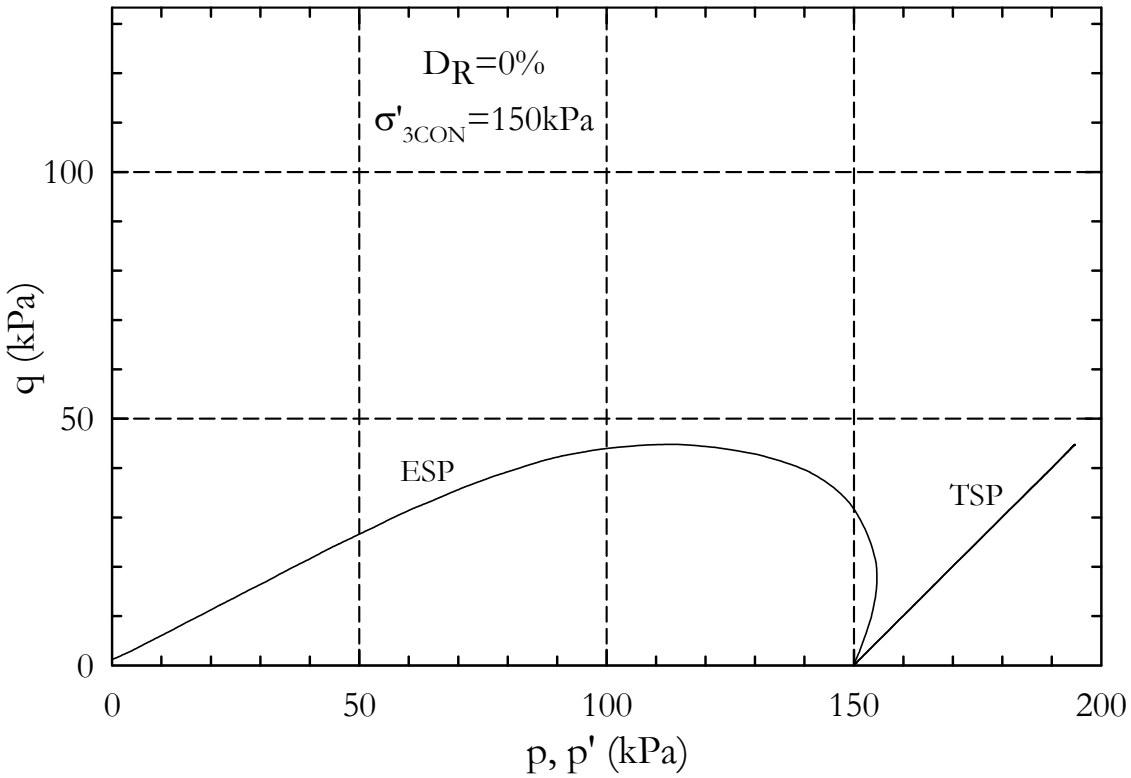

Figure 5-12 Stress Path - Test MCU02

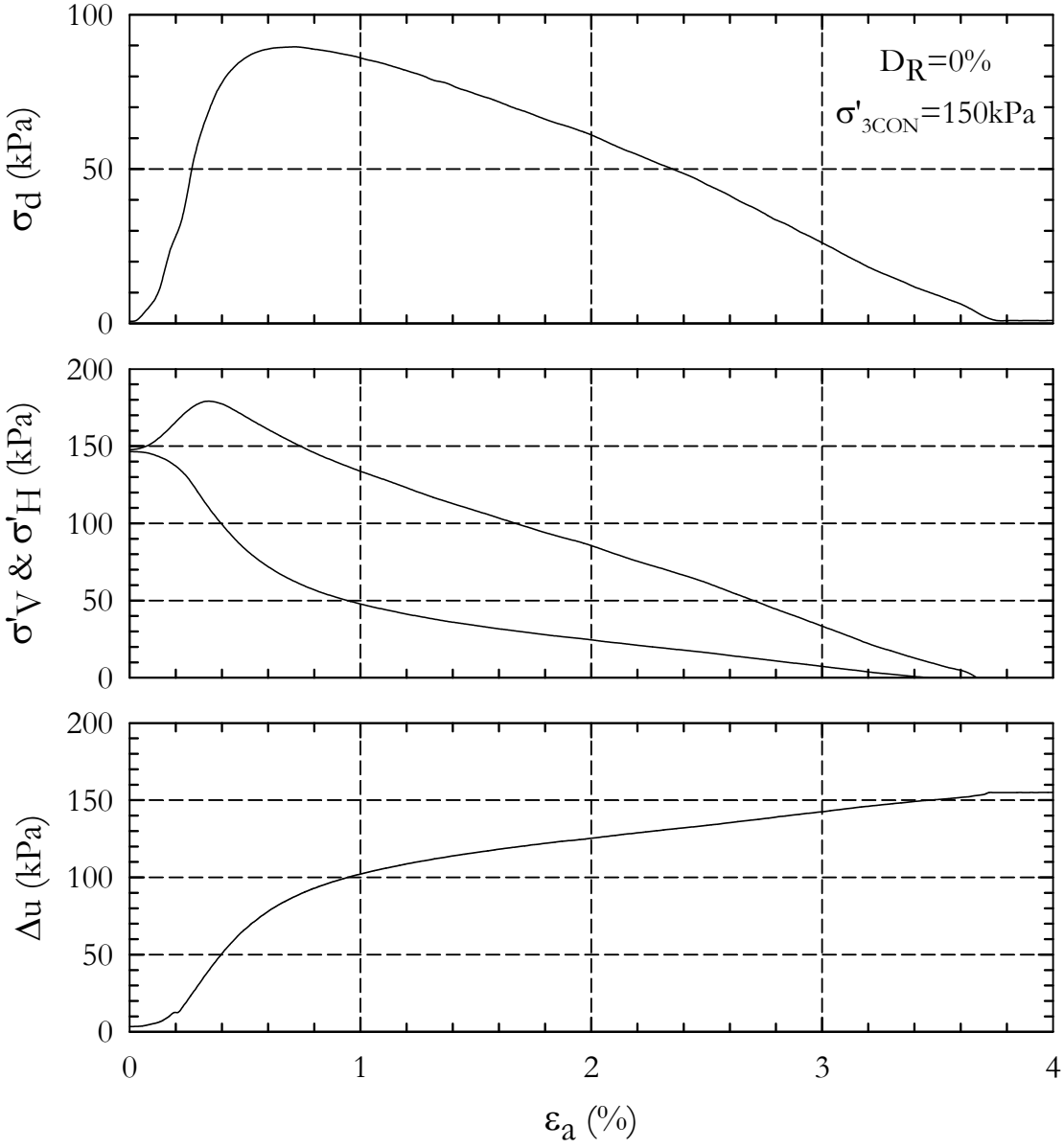

Figure 5-13. Strain Plot - Test MCU02

5.2 Cyclic Triaxial Tests

5.2.1 Typical Cyclic Test Results

A total of 13 isotropically consolidated undrained cyclic triaxial tests were performed at varying densities at a confining pressure of 100 kPa. These tests are summarized in Table 5-2. CSR is defined as one half the applied maximum deviatoric stress divided by the initial confining pressure (CSR = $\sigma_d/(2\ \sigma_{CON})$). Every cyclic test performed for this study is initially isotropically consolidated and vertically loaded under stress controlled conditions at a period of 2 sec (frequency of 0.5 Hz). An equal load is applied with each cycle. For each test 4 figures are prepared to present the results. The figures for Test CTX07 are provided in this section for discussion; Figure 5-14, Figure 5-15, Figure 5-16 and Figure 5-17. The rest of the figures for all tests are provided in APPENDIX II.

Table 5-2. Summary of Cyclic Triaxial tests performed

Test No.	D_r (%)	σ_{CON} (kPa)	e	CSR	No. of Cycles to Failure ($r_U = 1$)*	No. of Cycles to Failure ($\varepsilon > 5\%$)$^+$
CTX01	20 (21.7)†	100	1.129	0.10	36	40
CTX02	20 (22.0)	100	1.128	0.15	8	11
CTX03	20 (23.6)	100	1.126	0.20	5	7
CTX04	20 (23.1)	100	1.123	0.15	29	31
CTX05	20 (23.2)	100	1.123	0.13	13	17
CTX06	40 (38.4)	100	1.059	0.25	3	4
CTX07	40 (41.3)	100	1.047	0.20	11	13
CTX08	40 (42.6)	100	1.042	0.15	23	26
CTX09	60 (55.4)	100	0.988	0.30	8	9
CTX10	60 (56.6)	100	0.983	0.35	7	9
CTX11	60 (56.8)	100	0.982	0.32	7	9
CTX12	60 (57.8)	100	0.978	0.30	11	14
CTX13	60 (58.9)	100	0.974	0.25	38	42

† Rounded final relative density (actual final relative density)
* Pore-pressure ratio equal to 1 (initial liquefaction)
$^+$ 5% Accumulated axial strain

Test sample CTX07 had a target relative density of 40%. The actual final relative density after consolidation was 41.3%. The sample was isotropically consolidated to an effective confining pressure of 100 kPa. The first figure, Figure 5-14, is the effective stress path in response to cyclic loading. The phase transformation line, as determined from the monotonic tests of the same density, is shown for reference. The second figure, Figure 5-15, is a plot of the axial strain versus the applied deviator stress showing the hysteresis loops during cyclic loading. The cyclic strain increases with increased number of cycles. The third figure is the pore-pressure ratio (r_U) plot, Figure 5-16. Pore-pressure ratio is defined as the ratio of excess pore-pressure to initial effective confining pressure ($r_U=\Delta u/\sigma'_{CON}$). Included in this plot is the residual pore-pressure, defined as the pore-pressure at zero deviator stress. A distinction has been made for the points of zero deviatoric stress. The first is the pore-pressure at the transition from compression to extension (End of Compression, i.e., the point of zero deviatoric stress at the end of the compression cycle when the compressive load is totally removed). The second is the transition from extension to compression (End of Extension). Therefore two separate lines have been plotted to connect each set of points. Additionally, five plots have been provided in a combined figure, Figure 5-17. These plots show the behavior of several parameters with respect to the number of cycles. Five parameters are plotted: deviator stress (σ_d), vertical effective stress (σ_V'), horizontal effective stress (σ_h'), excess pore-pressure (Δu) and axial strain (ε_a).

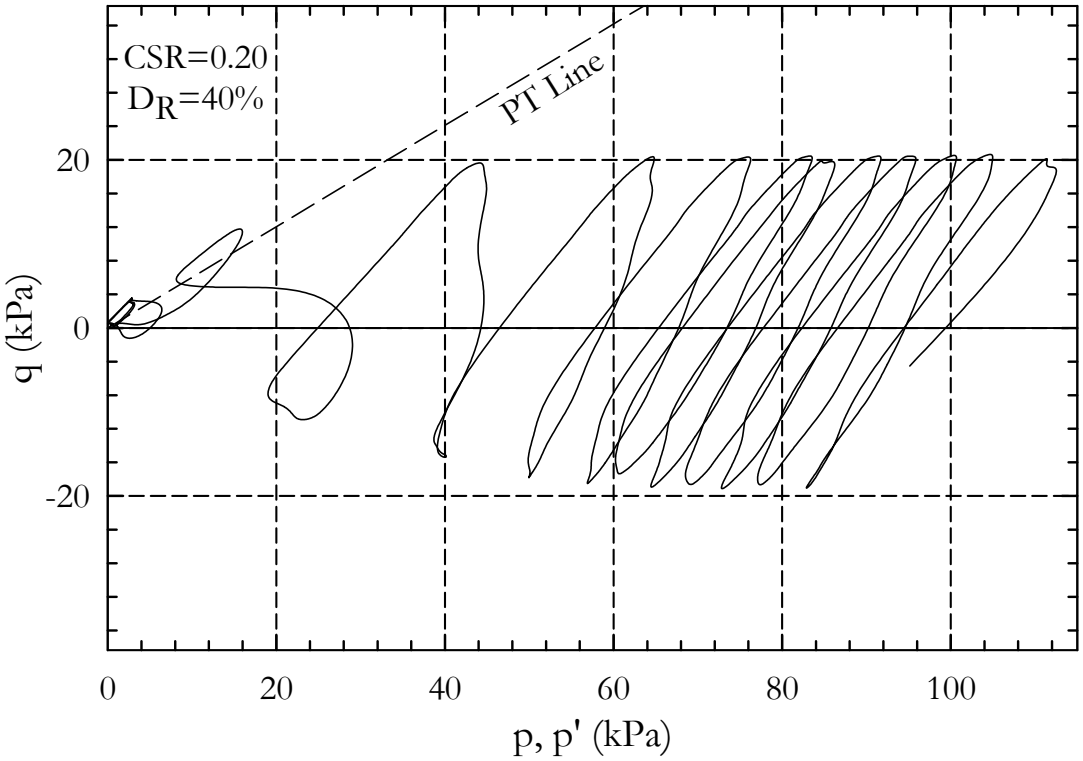

Figure 5-14. Stress Path – CTX07

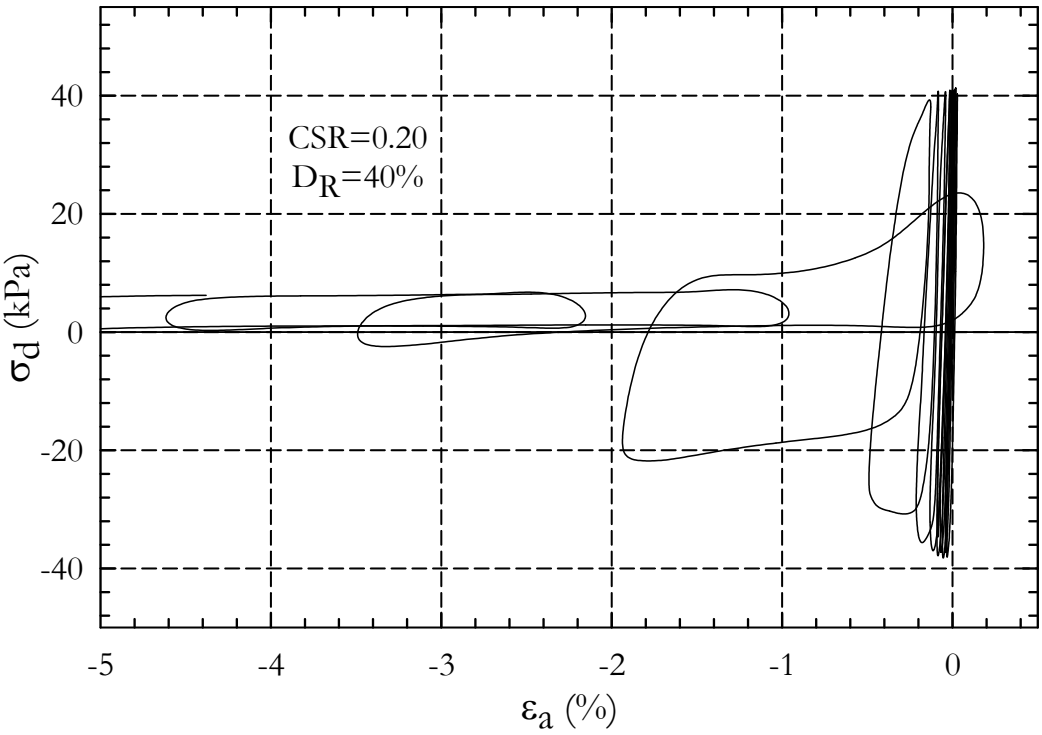

Figure 5-15 Strain vs. Deviator stress– Test CTX07

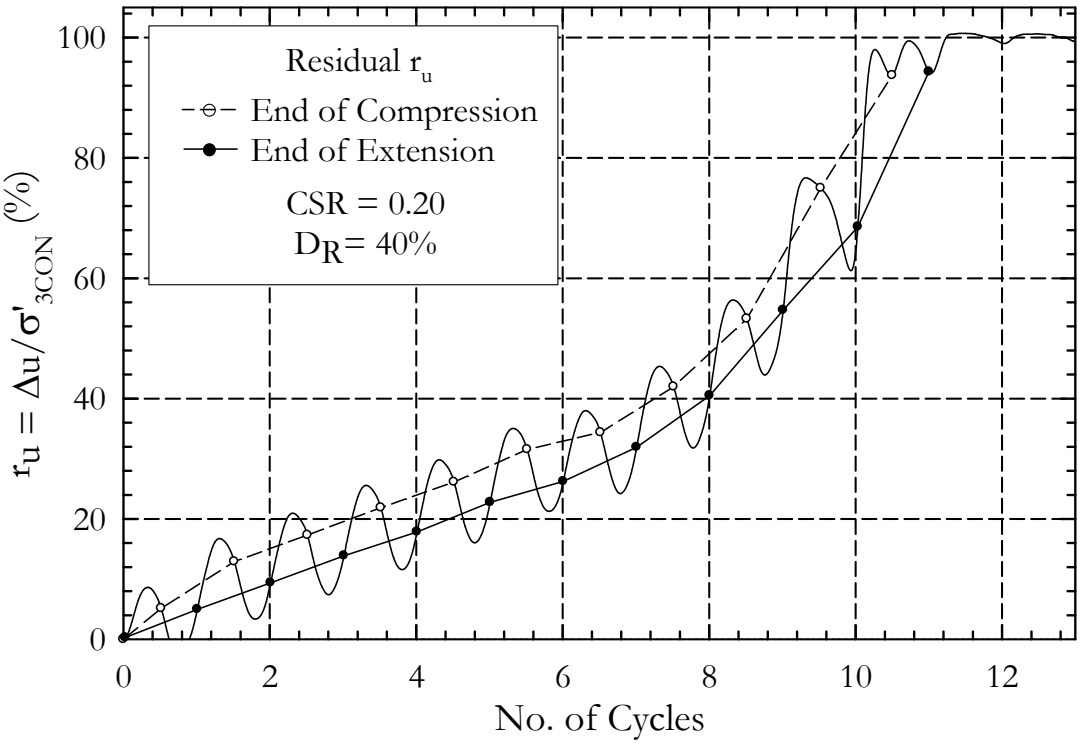

Figure 5-16. Pore-pressure ratio with residual pore-pressure – Test CTX07

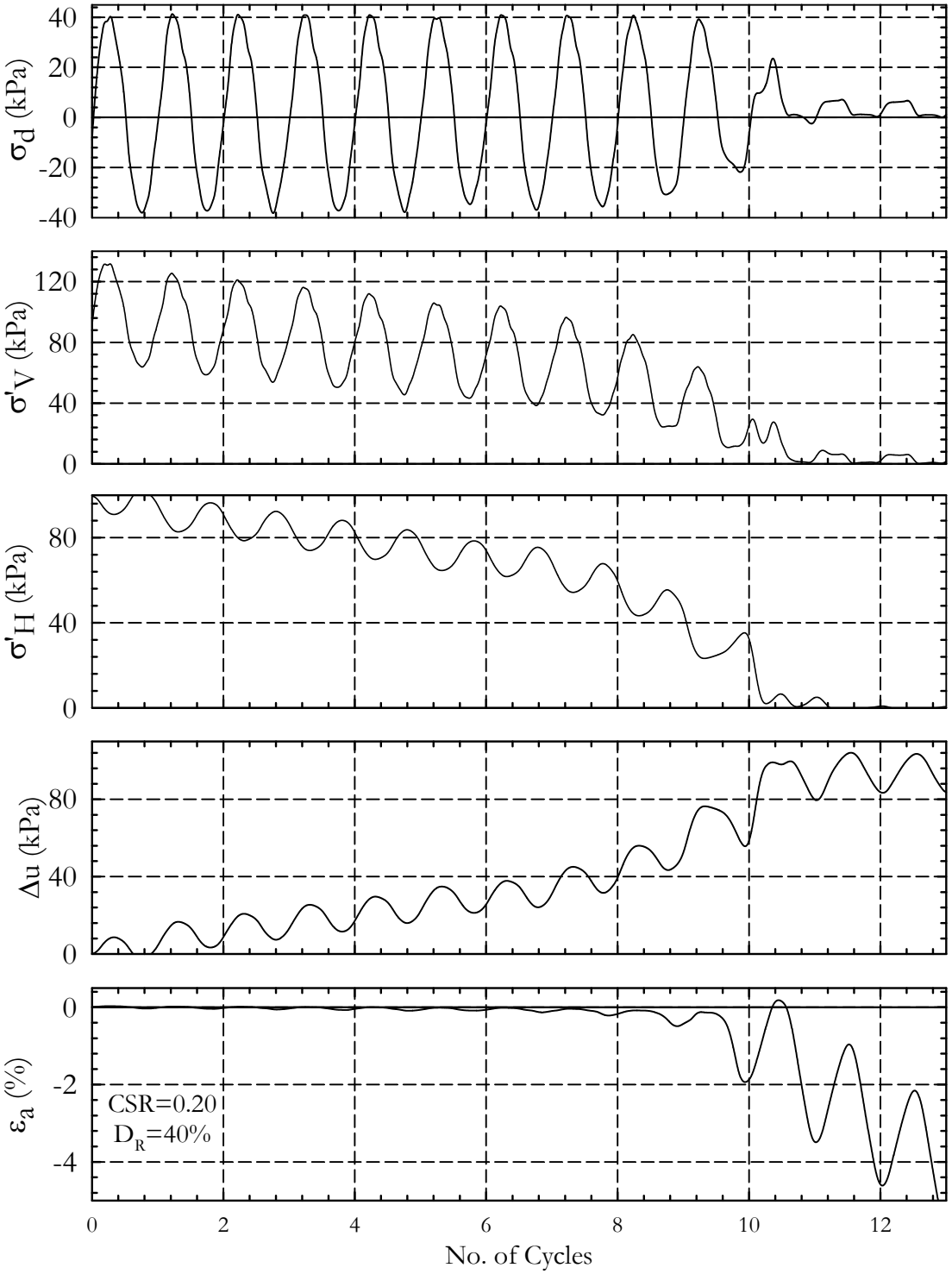

Figure 5-17. Cyclic Parameters – Test CTX07

Every cyclic test performed for this study is initially isotropically consolidated and vertically loaded under stress controlled conditions at a period of 2 sec (frequency of 0.5 Hz). An equal load is applied with each cycle. As the sample is cyclically loaded residual excess pore-pressure is accumulated until the pore-pressure ratio is equal to unity. In the case of flow liquefaction there will be a final large increased in the pore-pressure ratio. At this point the soil has lost shear strength and strained significantly.

5.2.2 Contractive vs. Dilative Behavior

A phase transformation line has been determined for each relative density using the corresponding monotonic triaxial tests. As shown in Figure 5-18 by plotting the PT line for this density along with the cyclic stress path, it is evident that a similar behavior is occurring during cyclic loading as is occurring during monotonic loading. The behavior of the sample when the stress path crosses the PT line is of significance in terms of dynamic behavior. The stress path will either move up the line (dilative tendency) or down the line (contractive tendency). The extent to which this behavior occurs defines the difference between flow liquefaction (total strength loss) and cyclic mobility (some strength gain). The cyclic stress path for tests CTX02 (D_R=20%) and CTX12 (D_R=60%) are shown below, Figure 5-18 and Figure 5-19. In test CTX12 when the stress path approaches the K_f line, which is not shown, there is a significant tendency for dilation, reducing pore-pressure. The shear strength of the soil is increased with increased effective confining pressure. In test CTX02 as the stress path approaches the K_f line there is a contractive tendency. This forces the stress path down the K_f line towards liquefaction. Comparison of these tests and their respective behaviors near phase transformation line (PT) indicates the difference between cyclic mobility and flow liquefaction. In flow liquefaction there is an associated jump in the pore-pressure ratio as the stress path plunges towards the origin. In cyclic mobility the pore-

pressure builds steadily until a pore-pressure ratio of unity is achieved. The residual and cyclic strains build steadily causing liquefaction. Test CTX02 fails due to flow liquefaction and test CTX12 experiences cyclic mobility. As a result of this behavior, the denser sample is able to sustain a relatively larger load. A portion of the generated excess pore-pressure is recovered at each cycle. The pore pressure in the looser sample continually increases. The sample with relative density of 60% makes several crossings with the PT line each resulting in an upward bend of the stress path indicating the dilative tendency.

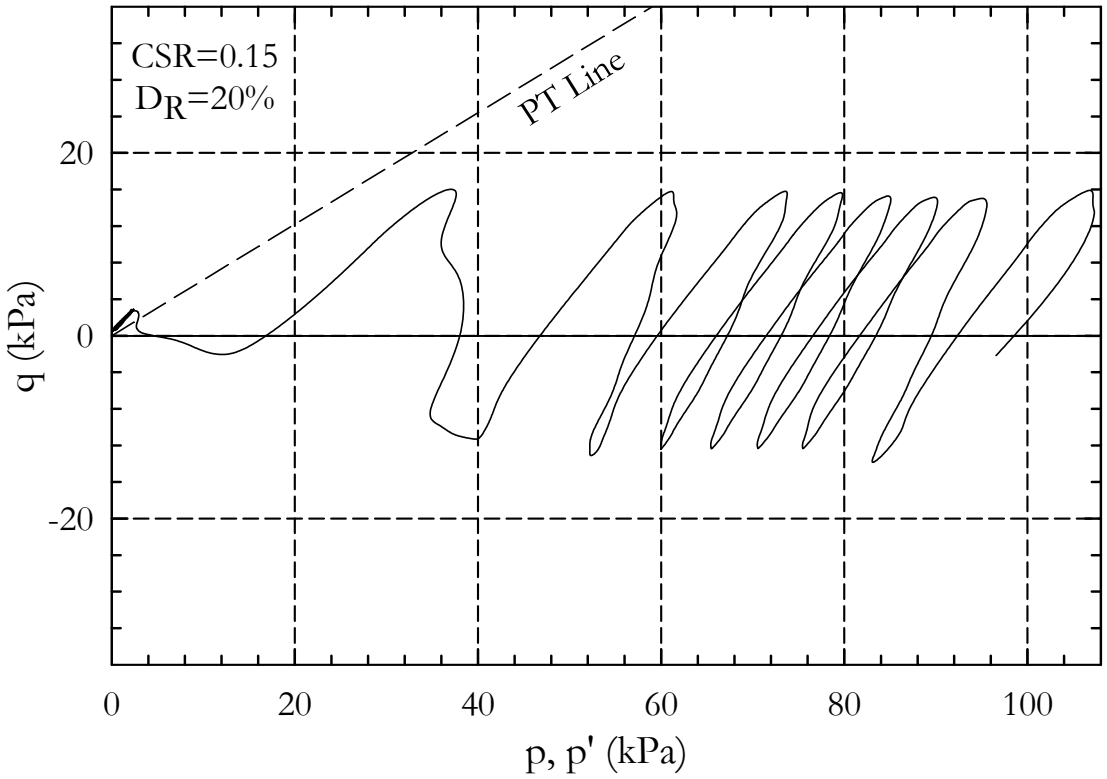

Figure 5-18. Stress Path – CTX02

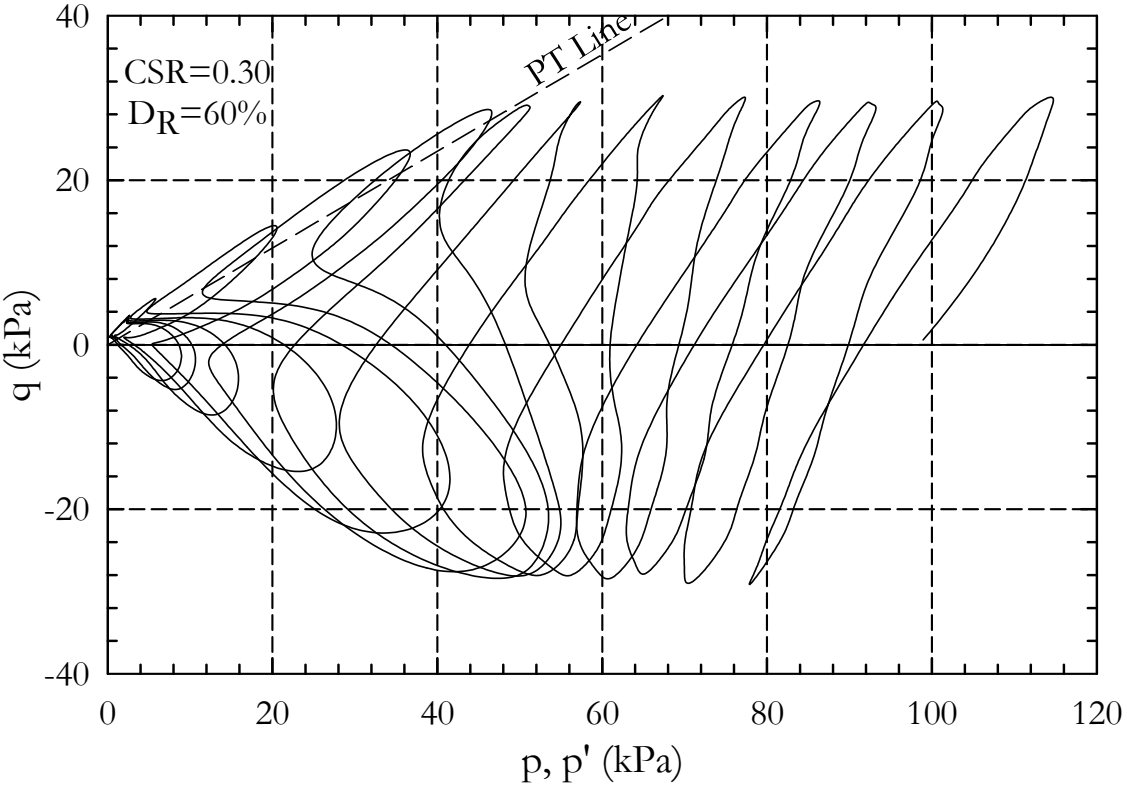

Figure 5-19. Stress Path – CTX12

5.2.3 Pore-Pressure Generation

As discussed in the previous section pore-pressure generation is very important when evaluating liquefaction susceptibility. The pore-pressure generation response during cyclic loading is indicative of the liquefaction susceptibility. Contractive or loose soils will steadily gain pore-pressure which brings the stress path to the left. As the stress path approaches the K_f line the sample will have contractive tendencies. This contraction forces the stress path down towards the origin, creating a jump in pore-pressure at failure. In dilative or dense soils the pore-pressure steadily builds throughout loading. As the K_f line is approached the soil dilates drawing the stress path up the K_f line. This behavior hinders liquefaction.

This study indicates that there is a distinct difference in the dynamic behavior at each relative density tested. In the 20% samples as the stress path approaches the K_f line, the sample contracts and experiences liquefaction. The 60% samples have more of a dilative tendency. When the stress path reaches the K_f line the sample dilates preventing liquefaction. The tests prepared at 40% have a behavior somewhere in between. These differences are very well represented by looking at the stress paths from tests CTX02 (20%), CTX07 (40%) and CTX12 (60%); Figure 5-18, Figure 5-20 and Figure 5-19.

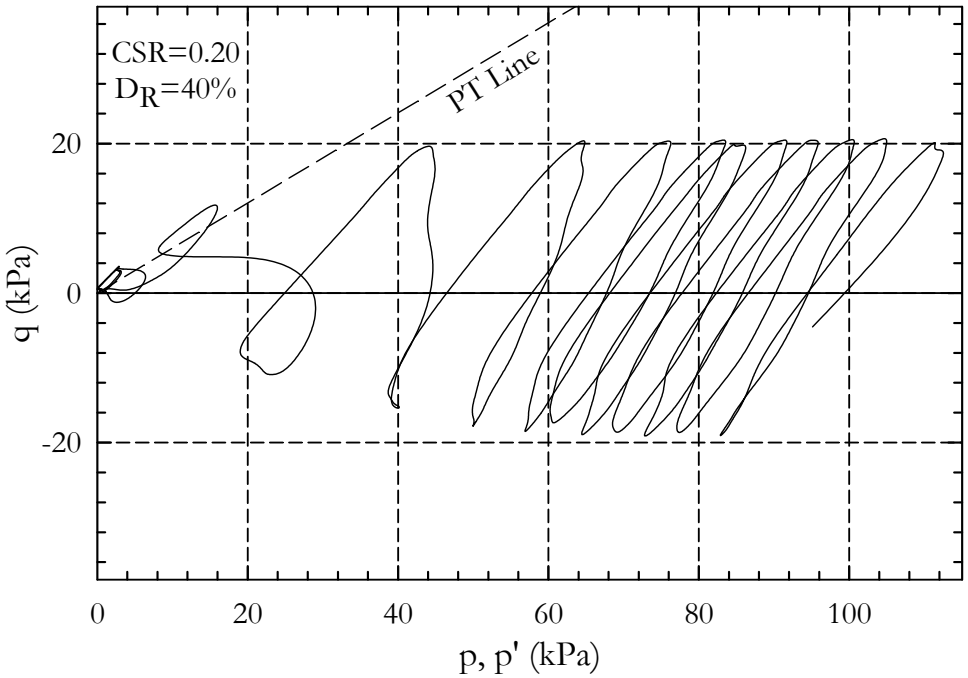

Figure 5-20. Stress Path – CTX07

This behavior can also be observed by looking at the pore-pressure generation with a normalized number of cycles. In Figure 5-21 the residual pore-pressure ratio for three tests has been plotted versus a normalized number of cycles. The CSR for the 20%, 40% and 60% tests shown are 0.15, 0.15 and 0.30, respectively. For simplification only the residual pore-pressure ratio at the end of compression has been presented. The number of cycles are

normalized with respect to the number of cycles to failure, r_U=100%. The samples at relative densities of 20% and 40% fail in flow liquefaction. Steady increase in pore-pressure followed by a jump to a pore-pressure ratio equal to 100%. The 60% relative density sample has a steadily building pore-pressure ratio throughout the test. This behavior is an example of cyclic mobility.

Lee and Albeisa (1974) created a standard pore-pressure generation curve for cyclic testing of soils. The upper and lower bounds are shown in Figure 5-21. The pore-pressure generation of the calcareous soils is very similar to the behavior of the quartzitic soils. Figure 5-22, Figure 5-23 and Figure 5-24 are all the residual pore-pressure curves for the tests run at 20%, 40% and 60% relative density. Lee and Albeisa's curves for upper and lower ranges are provided for reference.

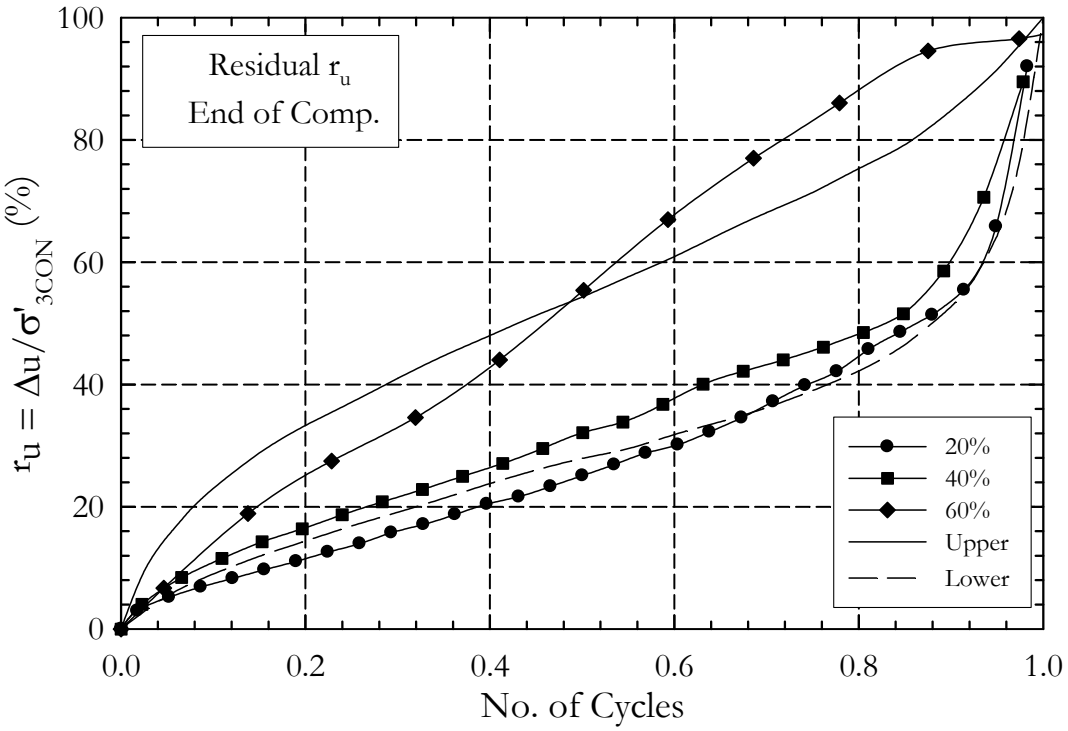

Figure 5-21. Typical D_r = 20%, 40% and 60% normalized residual pore-pressure generation curves with upper and lower bounds shown (Lee and Albeisa 1974) – CTX04, CTX08 & CTX12

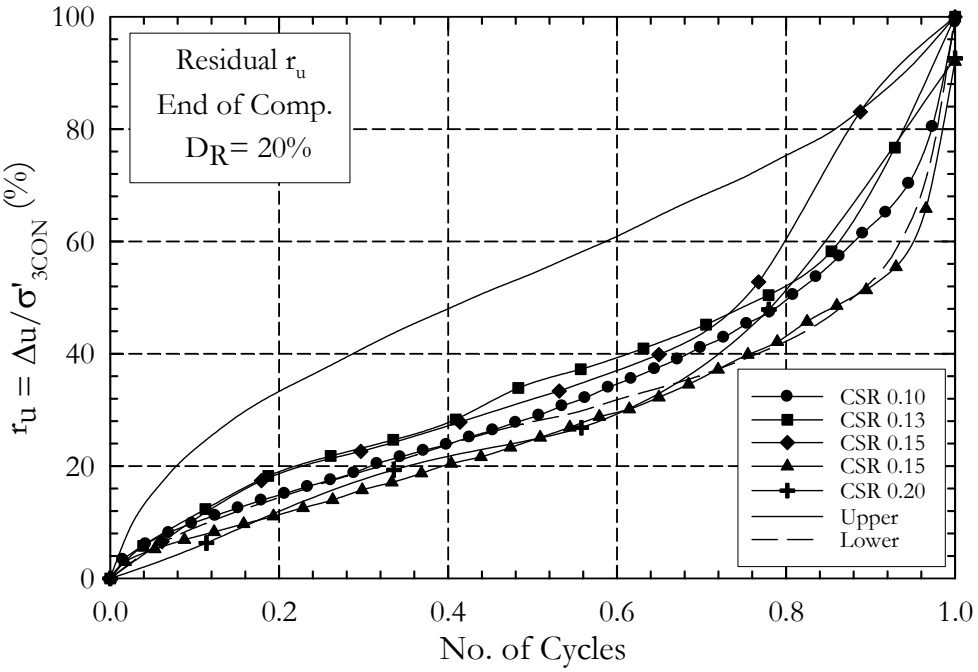

Figure 5-22. Normalized residual pore-pressure generation curves for samples at 20% relative density with upper and lower bounds shown (Lee and Albeisa 1974)

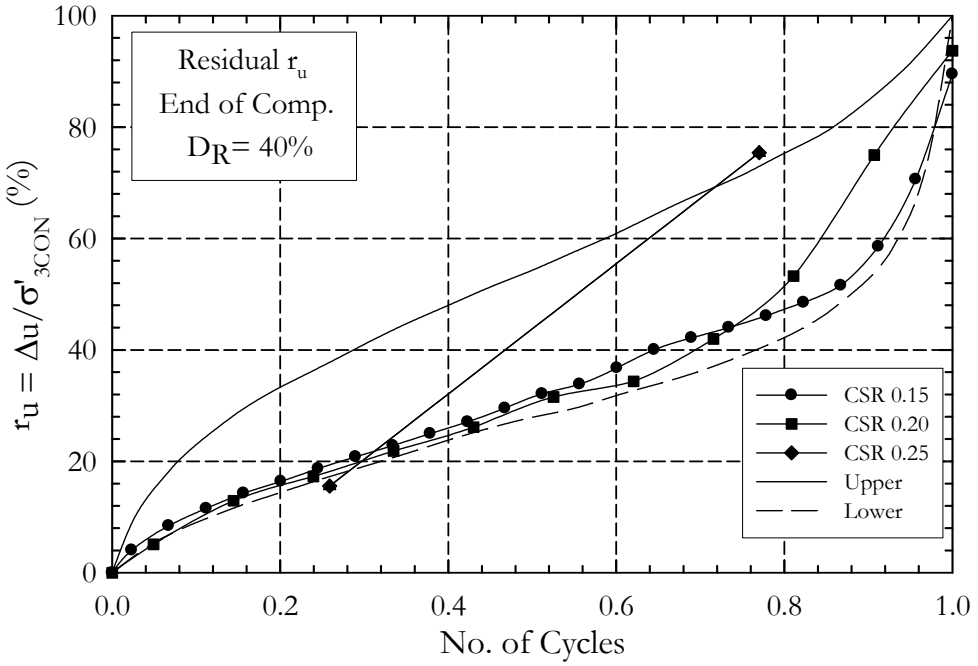

Figure 5-23. Normalized residual pore-pressure generation curves for samples at 40% relative density with upper and lower bounds shown (Lee and Albeisa 1974)

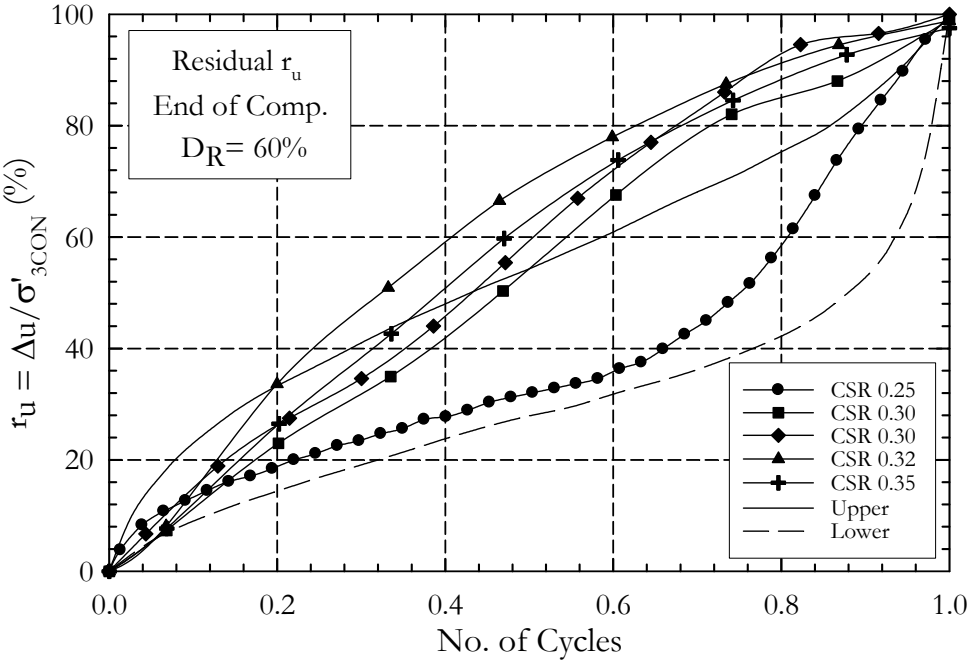

Figure 5-24. Normalized residual pore-pressure generation curves for samples at 60% relative density with upper and lower bounds shown (Lee and Albeisa 1974)

5.2.4 No. of Cycles to Failure vs. CSR Plot

Of particular interest is the number of cycles to failure versus the applied cyclic stress ratio (CSR). This provides a standard for comparison with other studies. While the triaxial test does not model actual dynamic earthquake stress states, it does provide an index for comparison. Typically a curve is produced for each set of variables. These include relative density, confining pressure, isotropic/anisotropic consolidation, and one-way/two-way cyclic shear. While the applied cyclic stress is normalized by the confining pressure it cannot necessarily be assumed that the behavior would be similar as the confining pressure is varied. In this study all cyclic tests have been performed at the same confining pressure, are isotropically consolidated and are run with two-way cyclic shear. A total of three curves, one at each relative density, are produced from these results.

Several CSR plots were prepared from the results of this study. Failure is defined as being the cycle during which the sample reaches a pore-pressure ratio of 100%. CSR is defined as one half the applied maximum deviatoric stress divided by the initial confining pressure. Between 3 and 5 tests are run at each relative density over a range of CSRs. A logarithmic best fit line has been added with each data set to show the general trend. Figure 5-25, Figure 5-26 and Figure 5-27 are the plots of 20%, 40% and 60%, respectively. These figures are shown with an arithmetic scale. Figure 5-28 is all the data shown together on a logarithmic scale.

These results show the expected trend of increased resistance to liquefaction with increased density. The difference in CSR necessary to fail a 40% and 20% sample is small compared with the difference in CSR between a 60% and 40%. Both the 20% and 40% tests failed due to flow liquefaction; where the 60% samples all failed exhibiting to cyclic mobility. Generally the results are consistent and form a line. Test CTX04, D_R=20% and CSR=0.15, is uncharacteristic of the trend in the results. It has been shown on the figures, but is not used to from the best fit line. Presented additionally are results for Monterey Sand by Morioka and Nicholson (1999). This quartzitic sand was compacted to a relative density of 65%. It can be seen that the liquefaction resistance curve (number of cycles to liquefaction vs. CSR) for this sand at relative density of 65% is about the same as the D_r = 20% curve of Playa Santa sand that was used in this study. As a comparison the liquefaction resistance curve for the D_r = 60% Playa Santa sand lies well above the 65% curve for Monterey sand.

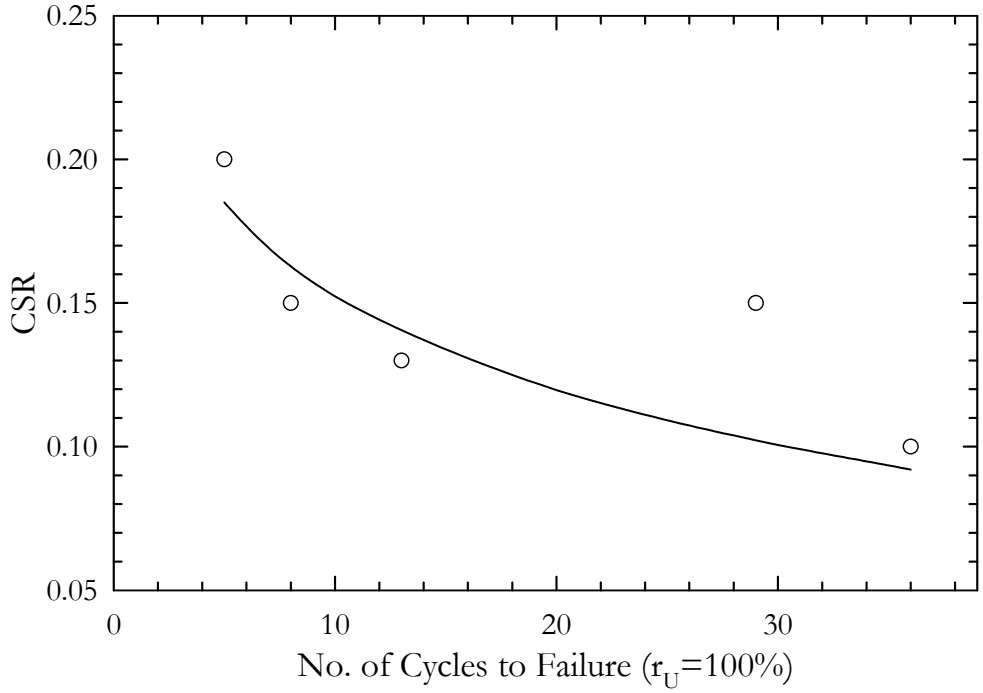

Figure 5-25. 20% Relative Density – Arithmetic CSR Plot

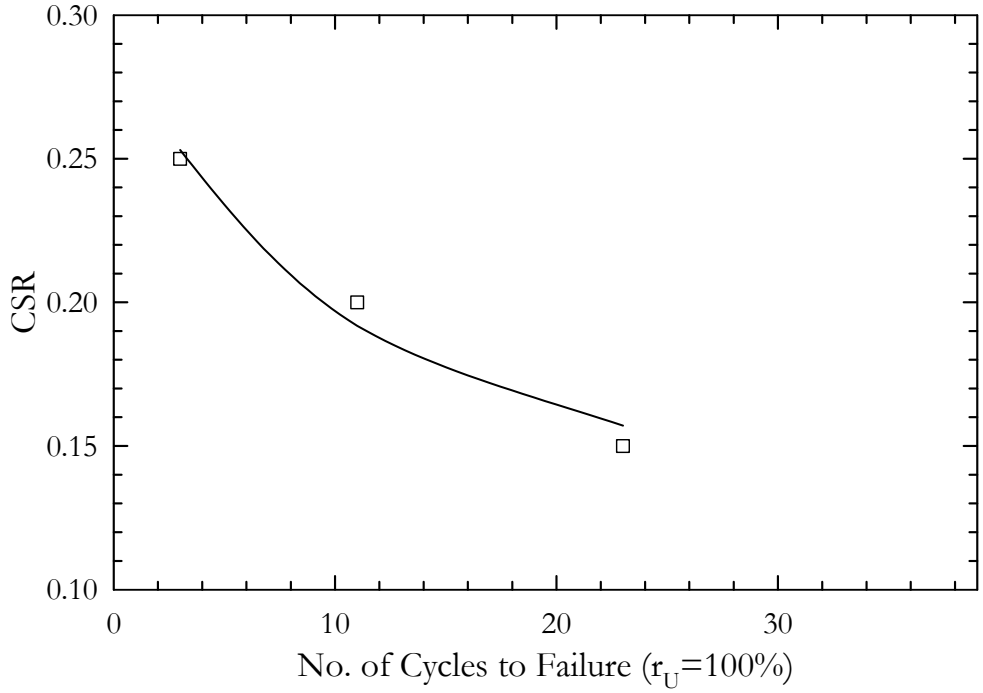

Figure 5-26. 40% Relative Density – Arithmetic CSR Plot

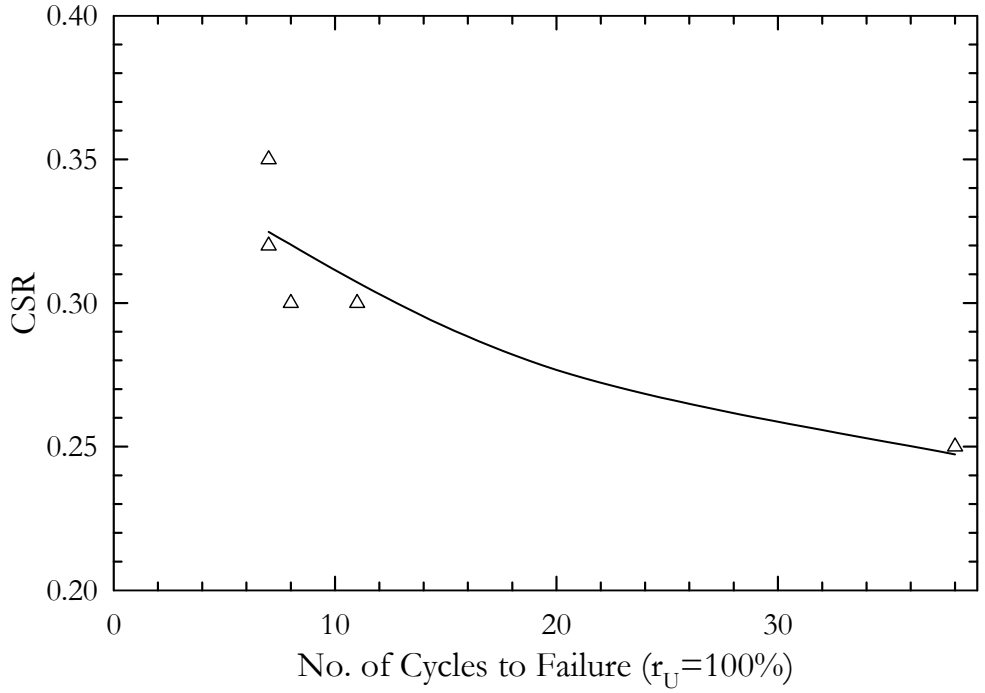

Figure 5-27. 60% Relative Density – Arithmetic CSR Plot

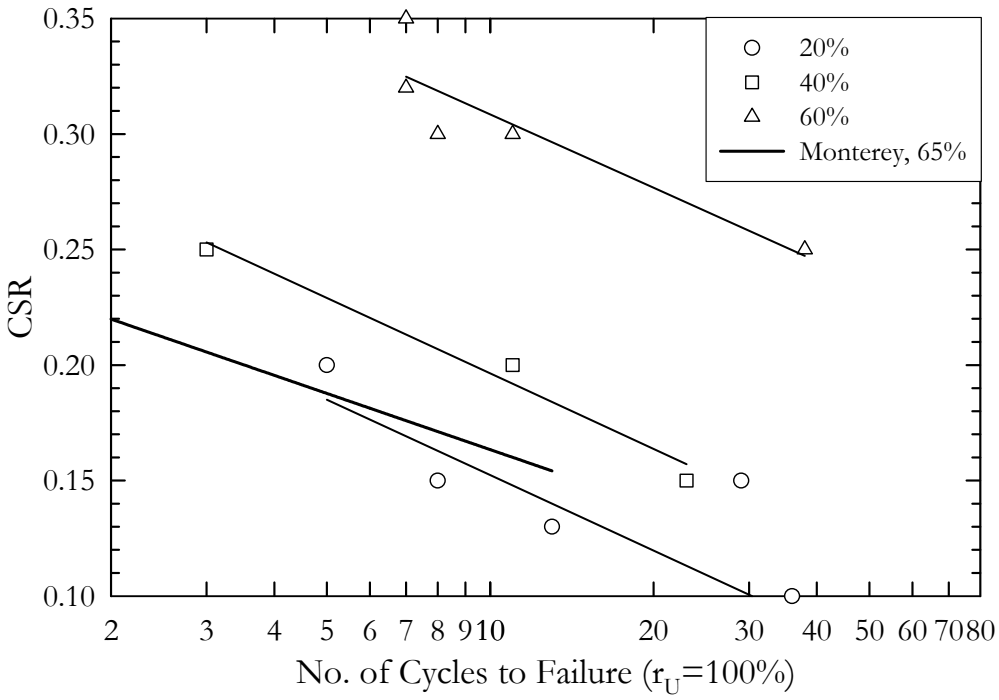

Figure 5-28. CSR Plot (20%, 40%, 60%) (Monterey 65% data from Morioka and Nicholson 1999)

6 SUMMARY & CONCLUSIONS

6.1 Introduction

A series of monotonic and cyclic triaxial tests were performed to investigate the behavior of Playa Santa calcareous sand under undrained loading conditions. These tests were performed with remolded samples prepared at a variety of relative densities. Of particular interest were the pore pressure generation behavior and the subsequent liquefaction resistance curves for the Playa Santa calcareous sand.

In general, sands that have greater tendency for contraction are more susceptible to liquefaction. Calcareous soils have a large void ratio due to the intra-granular voids within the particles and are well known for being more compressible than terrigenous soil. Therefore, we had initially thought that this compressible soil skeleton of calcareous soils would result in a more contractive soil matrix and thus result in calcareous sands being more susceptible to liquefaction than quartzitic soils. This research and others has found that this is not the case.

The test results summarized above indicate that Playa Santa calcareous sand has greater cyclic strength and is less susceptible to liquefaction when compared to quartzitic sands. This has also been the conclusion of many other studies on calcareous soils. Increased cyclic strength is likely the result of the angular calcareous sand particle shape (Hyodo et al. 1996;

Hyodo et al. 1998; Kaggwa and Poulos 1990; Morioka and Nicholson 1999; Sharma and Ismail 2006).

6.2 Implications for Design Practice

More research is necessary for a definitive statement regarding the appropriate design practice for the assessment of the liquefaction susceptibility of calcareous sands. Current state of practice for the assessment of the liquefaction susceptibility of soils is based on correlations from penetration tests. These correlations based on field tests and case histories of earthquake performance are from sites that are predominantly composed of quartzitic sands. Due to excessive particle crushing in calcareous sands, penetration tests can be unreliable and it is likely that these empirical correlations would estimate a lower relative density than actual. If this relative density were assumed to be correct any subsequent design would be conservative. Furthermore, at a given relative density calcareous sands tend to have greater cyclic strength than quartzitic sands adding more conservatism to the design. These two features create the situation that when penetration tests are used for design in calcareous sands the result will be, in general, highly conservative.

6.3 Further Research

It is of practical significance to better correlate the penetration test results, i.e., SPT and CPT, to potential for liquefaction of calcareous soils. Correlations currently used, are for quartzitic sands and may not be applicable to calcareous soils. Better correlations would enable practicing engineers to create more realistic and economically feasible designs with regard to predicting a soil's liquefaction potential. While more case histories of earthquake

performance at calcareous sand sites will enhance our understanding of the liquefaction potential of these soils, it may be necessary to perform calibration chamber tests to further study the penetration resistance correlations of these soils. Such tests coupled with full scale dynamic load tests, i.e., VibroSeis, or dynamic centrifuge testing can reveal important information on in-situ behavior and help us develop unique correlations before a comprehensive case history database is developed.

All cyclic tests were performed at a confining pressure of 100 kPa. While CSR is a normalized parameter, there is no reason to assume a curve constructed from a series of tests run at 200 kPa would be equivalent. Therefore it is of interest to see the effect of confining pressure on the liquefaction resistance curve by performing additional test on a variety of confining pressure.

As reviewed previously the cyclic triaxial is only an index test. It poorly duplicates the stress states associated with true field earthquake conditions. Most significant is that there is no change in the orientation of the principle stresses. Cyclic simple shear testing creates a better reproduction of field conditions. Cyclic simple shear studies on calcareous sand are considerably more limited than cyclic triaxial studies. Therefore laboratory tests using the cyclic simple shear testing device would also be of interest to better simulate the field behavior.

REFFERENCES

Airey, D. W., and Fahey, M. (1991). "Cyclic response of calcareous soil from the North-West Shelf of Australia." *Geotechnique*, 41(1), 101-121.

Airey, D. W., Randolph, M. F., and Hyden, A. M. (1988). "The strength and stiffness of two calcareous sands." Engineering for Calcareous Sediments, Proc. Int. Conf. on Calcareous Sediments, Jewell and Andrews, eds., Balkema, Rotterdam, Perth, Australia, 42-51.

Alarcon-Guzman, A., Leonards, G. A., and Chameau, J. L. (1988). "Undrained monotonic and cyclic strength of sands." *Journal of the Geotechnical Engineering Division, ASCE*, 114(10), 1089-1109.

ASTM D422. (2002). "Standard Test Method for Particle-Size Analysis of Soils." ASTM International.

ASTM D854-02. (2002). "Standard test method for specific gravity of soil solids by water pycnometer." ASTM International.

ASTM D4253-00. (2006). "Standard test methods for maximum index density and unit weight of soils using a vibratory table." ASTM International.

ASTM D4254-00. (2006). "Standard test methods for minimum index density and unit weight of soils and calculation of relative density." ASTM International.

ASTM D4767. (2004). "Standard Test Method for Consolidated Undrained Triaxial Compression Test for Cohesive Soils." ASTM International.

Been, K., Crooks, J. H. A., Becker, D. E., and Jefferies, M. G. (1986). "Cone penetration test in sands: Part I, State parameter interpretation." *Geotechnique*, 36(2), 239-249.

Been, K., and Jefferies, M. G. (1985). "State parameter for sands." *Geotechnique*, 35(2), 99-112.

Been, K., Jefferies, M. G., Crooks, J. H. A., and Rothenburg, L. (1987). "Cone penetration test in sands: Part II, General inference of state." *Geotechnique*, 37(3), 285-299.

Casagrande, A. (1936). "Characteristics of cohesionless soils affecting the stability of slopes and earth fills." *Journal of the Boston Society of Civil Engineers, Society of Civil Engineers*, 257-276.

Cataño Arango, J. (2006). "Stress strain behavior and dynamic properties of Cabo Rojo calcareous sands," University of Puerto Rico, Mayaguez.

Chan, C. K. (1985). "Instruction Manual, CKC E/P Cyclic Loading Triaxial System Users Manual." Soil Engineering Equipment Company. San Francisco, CA.

Coop, M. R. (1988). "Particle crushing of carbonate sand." Engineering for Calcareouse Sediments, Proc. Int. Conf. on Calcareous Sediments, Jewell and Andrews, eds., Balkema, Rotterdam, Perth, Australia, 875-876.

Coop, M. R. (1990). "The mechanics of uncemented carbonate sands." *Geotechnique*, 40(4), 607-626.

Coop, M. R., and Airey, D. W. (2003). "Carbonate sands " Characterisation and engineering properties of natural soils, T. S. Tan, K. K. Phoon, D. W. Hight, and S. Leroueil, eds., A.A. Balkema, Publishers, 1049-1086.

Coop, M. R., Sorensen, K. K., Freitas, T. B., and Georgoutsos, G. (2004). "Particle breakage during shearing of a carbonate sand." *Geotechnique*, 54(3), 157-163.

Datta, M., Gulhati, S. K., and Rao, G. V. "Engineering behavior of carbonate soils of India and some observations on classification of such soils." *Geotechnical Properties, Behavior and Performance of Calcareous Soils, ASTM Special Technical Publication 777*, 113-140.

Demars, K. R., and Chaney, R. C. (1982). "Symposium Summary." Geotechnical Properties, Behavior and Performance of Calcareous Soils, ASTM Special Technical Publication 777, 395-404.

EERI. (1995). "Guam earthquake of August 8, 1993 reconnaissance report." *Earthquake Engineering Research Institue, Earthquake Spectra, Supplement to Volume 11, April*, 1-175.

Fahey, M. (1988). "The response of calcareouse soil in static and cyclic triaxial tests." Engineering for Calcareouse Sediments, Proc. Int. Conf. on Calcareous Sediments, Jewell and Andrews, eds., Perth Australia, 61-68.

Finn, W. D. (1990). "Analysis of post-liquefaction deformations in soil structures." Proceedings of the H. Bolton Seed Memorial Symposium, 291-312.

Geocomp. (2002a). "FlowTrac II User's Manual." Geocomp Corporation, Boxborough, Massachusetts.

Geocomp. (2002b). "LoadTrac II User's Manual." Geocomp Corporation, Boxborough, Massachusetts.

Geocomp. (2007). "Cyclic Stress Path User's Manual Version 5.0." Geocomp Corporation, Boxborough, Massachusetts.

Golightly, C. R., and Hyde, A. F. L. (1988). "Some fundamental properties of carbonate sands." Engineering for Calcareous Sediments, Proc. Int. Conf. on Calcareous Sediments, Jewell and Andrews, eds., Balkema, Rotterdam, Perth, Australia, 69-78.

Hyodo, M., Aramaki, N., Itoh, M., and Hyde, A. F. L. (1996). "Cyclic strength and deformation of crushable carbonate sand." *Soil Dynamics and Earthquake Engineering*, 15(5), 331-336.

Hyodo, M., Hyde, A. F. L., and Aramaki, N. (1998). "Liquefaction of crushable soils." *Geotechnique*, 48(4), 527-543.

Ishihara, K., Tatsuoka, F., and Yasuda, S. (1975). "Undrained deformation and liquefaction of sand under cyclic stresses." *Soils and Foundations*, 15(1), 29-44.

Kaggwa, W. S., and Poulos, H. G. (1990). "Comparison of the behaviour of dense carbonate sediments and silica sand in cyclic triaxial tests." University of Sydney, School of Civil and Mining Engineering.

Kaggwa, W. S., Poulos, H. G., and Carter, J. P. (1988). "Response of carbonate sediments under cyclic triaxial test conditions." Engineering for Calcareous Sediments, Proc. Int. Conf. on Calcareous Sediments, Jewell and Andrews, eds., Balkema, Rotterdam, Perth, Australia, 97-107.

Kramer, S. L. (1989). "Uncertainty in steady-state liquefaction evaluation procedures." *Journal of the Geotechnical Engineering Division, ASCE*, 115(10), 1402-1419.

Kramer, S. L. (1996). *Geotechnical earthquake engineering*, Prentice Hall, Upper Saddle River, N.J. :.

Ladd, R. S. (1978). "Preparing test specimens using undercompaction." *Geotechnical Testing Journal*, 1(1), 16-23.

Lee, K. L., and Albeisa, A. (1974). "Earthquake induced settlements in saturated sands." *Journal of the Geotechnical Engineering Division, ASCE*, 100(4), 387-406.

Lee, K. L., and Seed, H. B. (1967). "Drained strength characteristics of sands." *Journal of the Soil Mechanics and Foundations Division, ASCE*, 93(SM6), 117-141.

Mejia, L. H., and Yeung, R. "Liquefaction of coralline soils during the 1993 Guam earthquake." *Earthquake-induced movements and seismic remediation of existing foundations and abutments, Geotechnical Special Publication No. 55, ASCE*, 33-48.

Mitchell, J. K. (1993). *Fundamentals of soil behavior*, Wiley, New York :.

Morioka, B. T., and Nicholson, P. G. (1999). "Evaluation of the Static and Cyclic Properties of Calcareous Sand in a Calibration Chamber Study." United States.

Morioka, B. T., and Nicholson, P. G. "Evaluation of the liquefaction potential of calcareous sand." *Proceedings of the International Offshore and Polar Engineering Conference*, Seattle, WA, USA, 494-500.

Nicholson, P. G. (2006). "Liquefaction evaluation discrepancies in tropical lagoonal soils." *Geotechnical and Geological Engineering*, 24(5), 1259-1269.

Porter, J. R. (1998). "An examination of the validity of steady state shear strength determination using isotropically consolidated undrained triaxial tests," Dissertation, Virginia Polytechnic Institute & State University, Blacksburg.

Poulos, H. G., Uesugi, M., and Young, G. S. (1982). "Strength and deformation properties of Bass Strait carbonate sands." *Geotechnical Engineering*, 13(2), 189-211.

Poulos, S. J. (1981). "The steady state of deformation." *Journal of the Geotechnical Engineering Division, ASCE*, 107, 553-562.

Roscoe, K. H., Schofield, A. N., and Wroth, C. P. (1958). "On yielding of soils." *Geotechnique*, 8(1), 22-53.

Rose, A. T. (1993). "A comparison of steady state and critical state concepts." T. L. Brandon, ed., Virginia Polytechnic Institute and State University Blacksburg, VA.

Seed, H. B., and Lee, K. L. (1966). "Liquefaction of saturated sands during cyclic loading." *Journal of the Soil Mechanics and Foundations Division, ASCE*, 92(SM6), 105-134.

Seed, H. B., Seed, R. B., Harder, L. F., and Jong, H. L. (1989). "Re-evaluation of the slide in the lower San Fernando Dam in the 1971 San Fernando Earthquake." Report No. UCB/EERC-88/04, University of California, Berkeley.

Seed, H. B., Tokimatsu, K., Harder, L. F., and Chung, R. M. (1985). "Influence of SPT Procedures in Soil Liquefaction Resistance Evaluations." *Journal of the Geotechnical Engineering Division, ASCE*, 111(12), 1425-1445.

Semple, R. M. (1988). "The mechanical properties of carbonate soils." International Conference on Calcareous Sediments, Jewell and Andrews, eds., Balkema, Rotterdam, Perth, W.A., 807-836.

Sharma, S. S., and Ismail, M. A. (2006). "Monotonic and Cyclic Behavior of Two Calcareous Soils of Different Origins." *Journal of Geotechnical and Geoenvironmental Engineering, ASCE*, 132(12), 1581-1591.

Skempton. (1954). "The pore-pressure coefficients A and B." *Geotechnique*, 4(4), 143-147.

Vahdani, S., Pyke, R., and Siriprusanen, U. "Liquefaction of calcareous sands and lateral spreading experienced in Guam as a result of the 1993 Guam Earthquake." *5th U.S.-Japan workshop on Earthquake resistant design of lifeline facilities and countermeasures against soil liquefaction*, Snowbird, UT, United States, pp.117-134.

APPENDIX I MONOTONIC TRIAXIAL RESULTS

Test No.: MCU01
Test Ref.: 20070718_Test01_D0_C2174
$D_{R(FINAL)}$: 0% (-3.2%)*
e: 1.234
σ'_{3CON}: 150 kPa

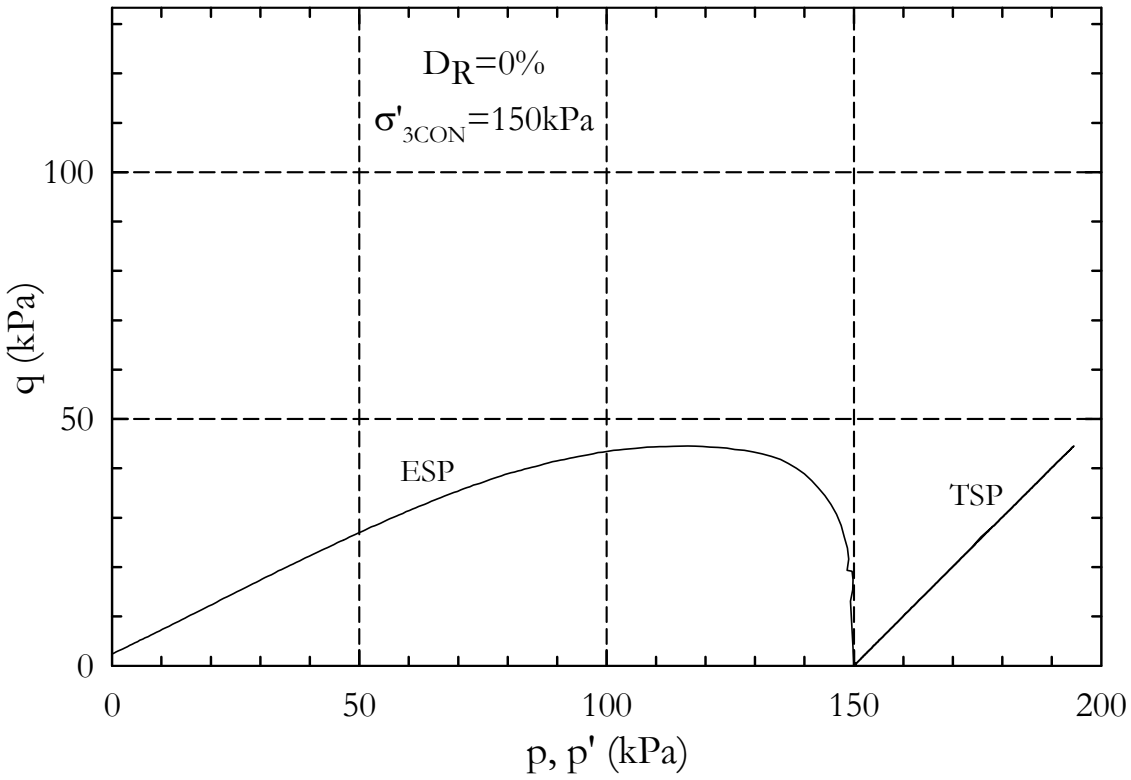

Figure I-1. Stress Path - Test MCU01

* Rounded (Actual)

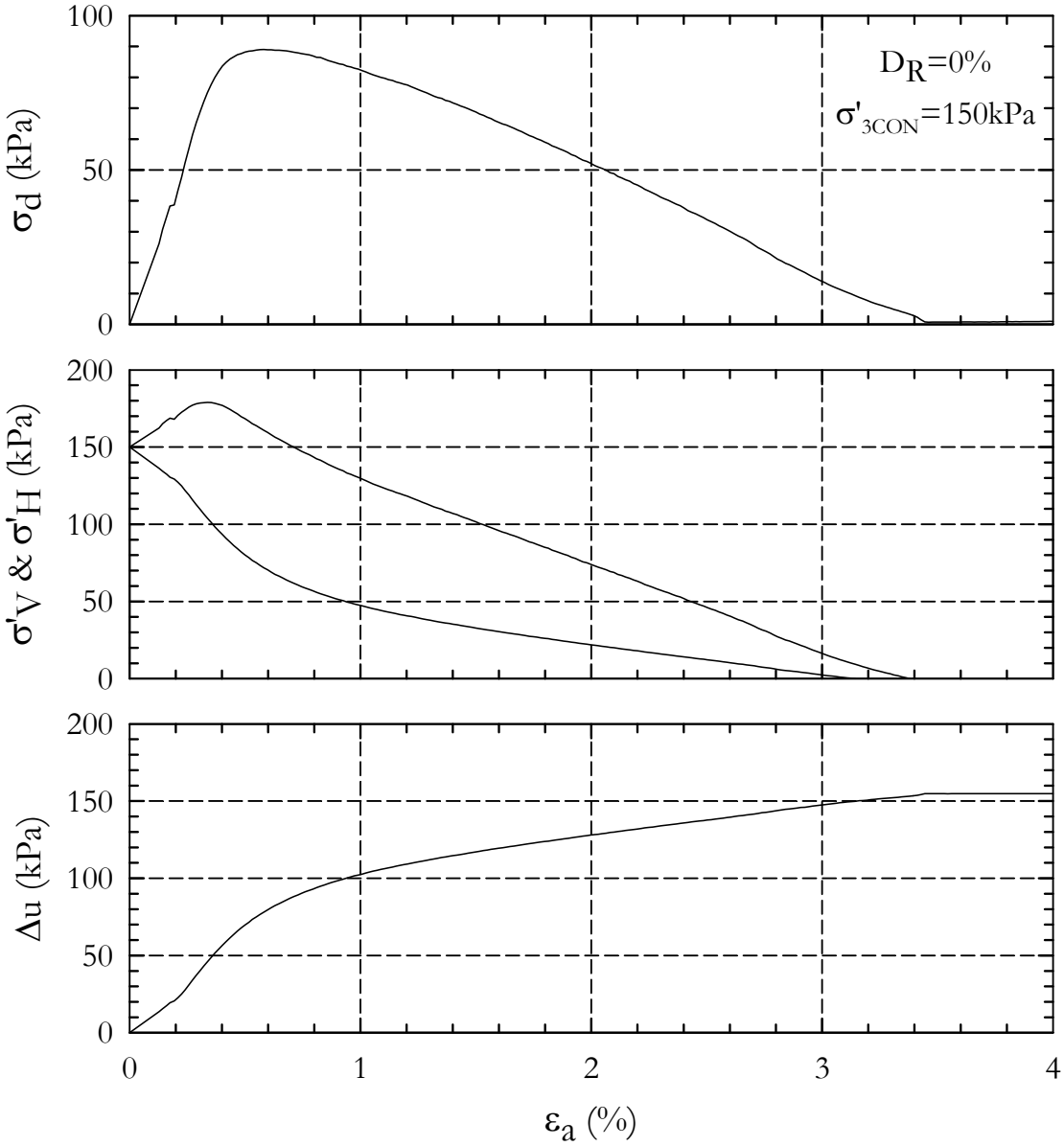

Figure I-2. Strain Plot - Test MCU01

Test No.: MCU02
Test Ref.: 20070719_Test01_D0_C2174
$D_{R(FINAL)}$: 0% (4.1%)
e: 1.203
σ'_{3CON}: 150 kPa

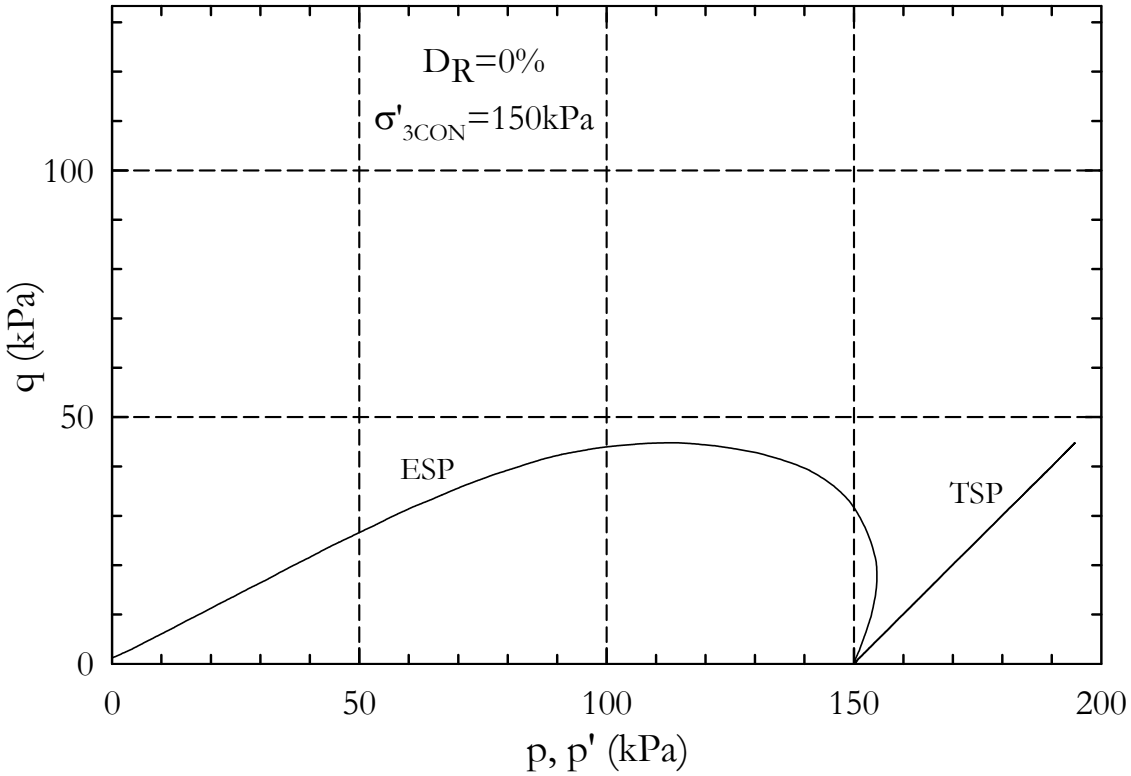

Figure I-3 Stress Path - Test MCU02

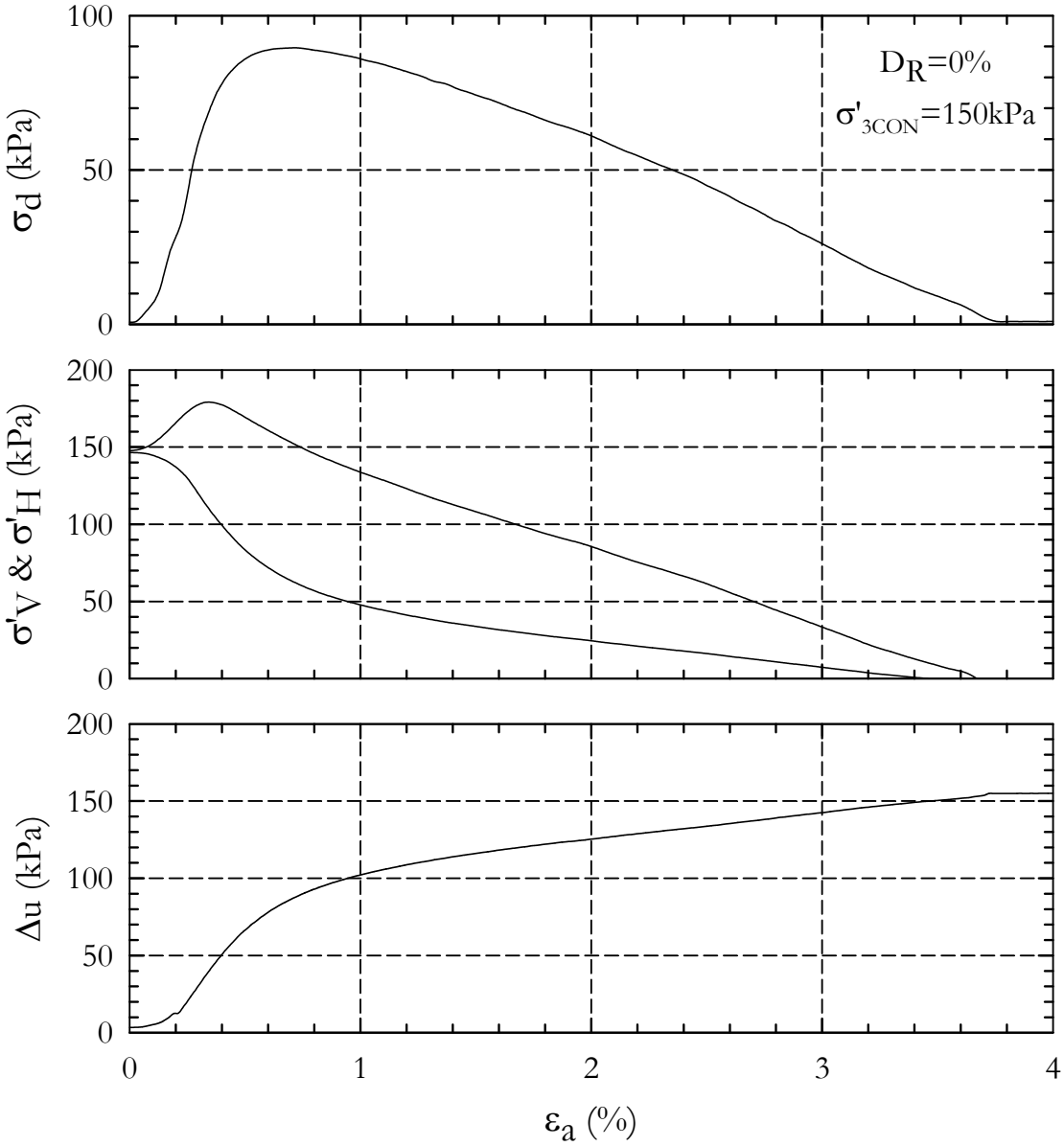

Figure I-4. Strain Plot - Test MCU02

Test No.: MCU03
Test Ref.: 20070719_Test02_D0_C2174
$D_{R(FINAL)}$: 0% (5.0%)
e: 1.199
σ'_{3CON}: 150 kPa

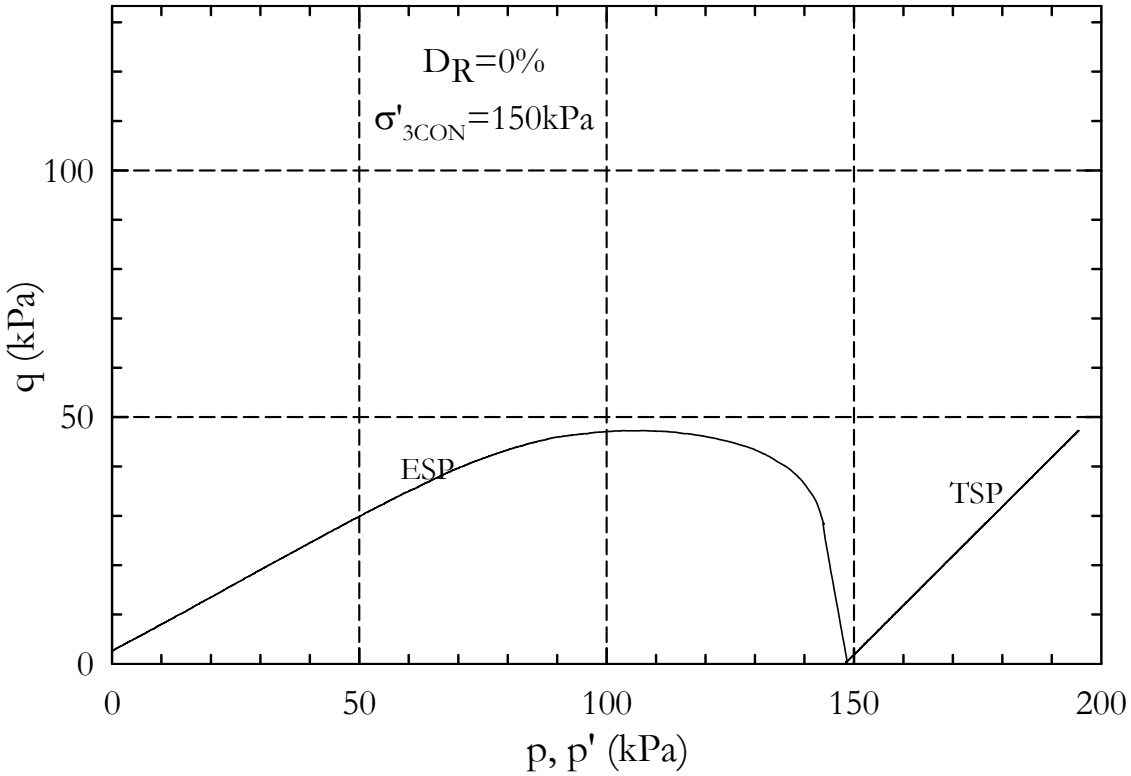

Figure I-5. Stress Path - Test MCU03

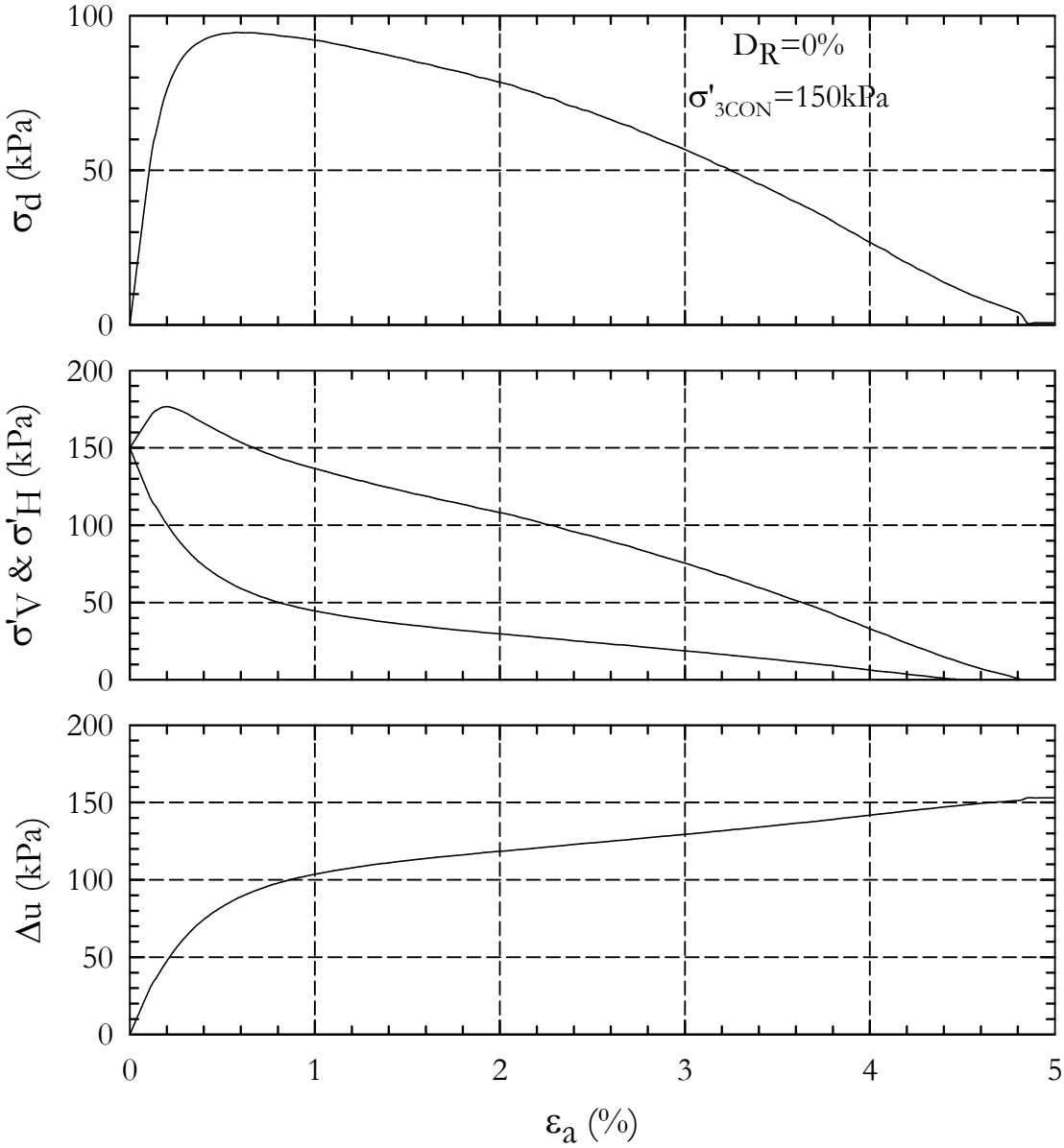

Figure I-6. Strain Plot - Test MCU03

Test No.: MCU04
Test Ref.: 20070723_Test01_D10_C2175
$D_{R(FINAL)}$: 10% (12.8%)
e: 1.167
σ'_{3CON}: 150 kPa

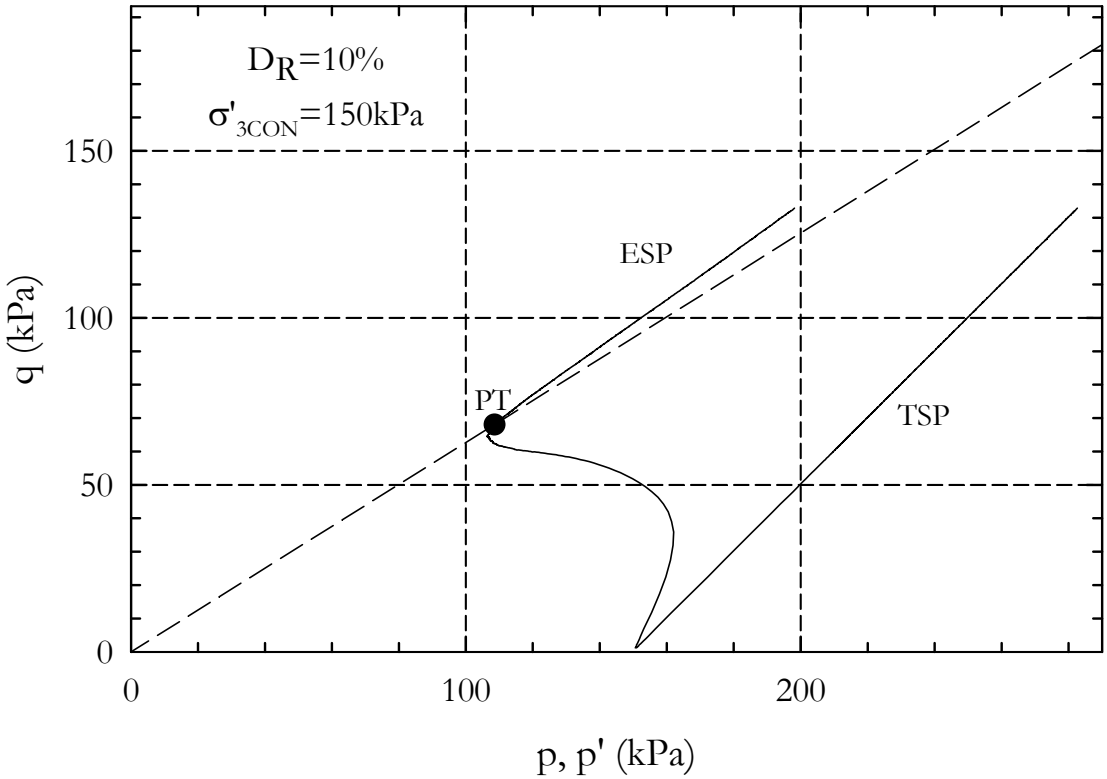

Figure I-7. Stress Path - Test MCU04

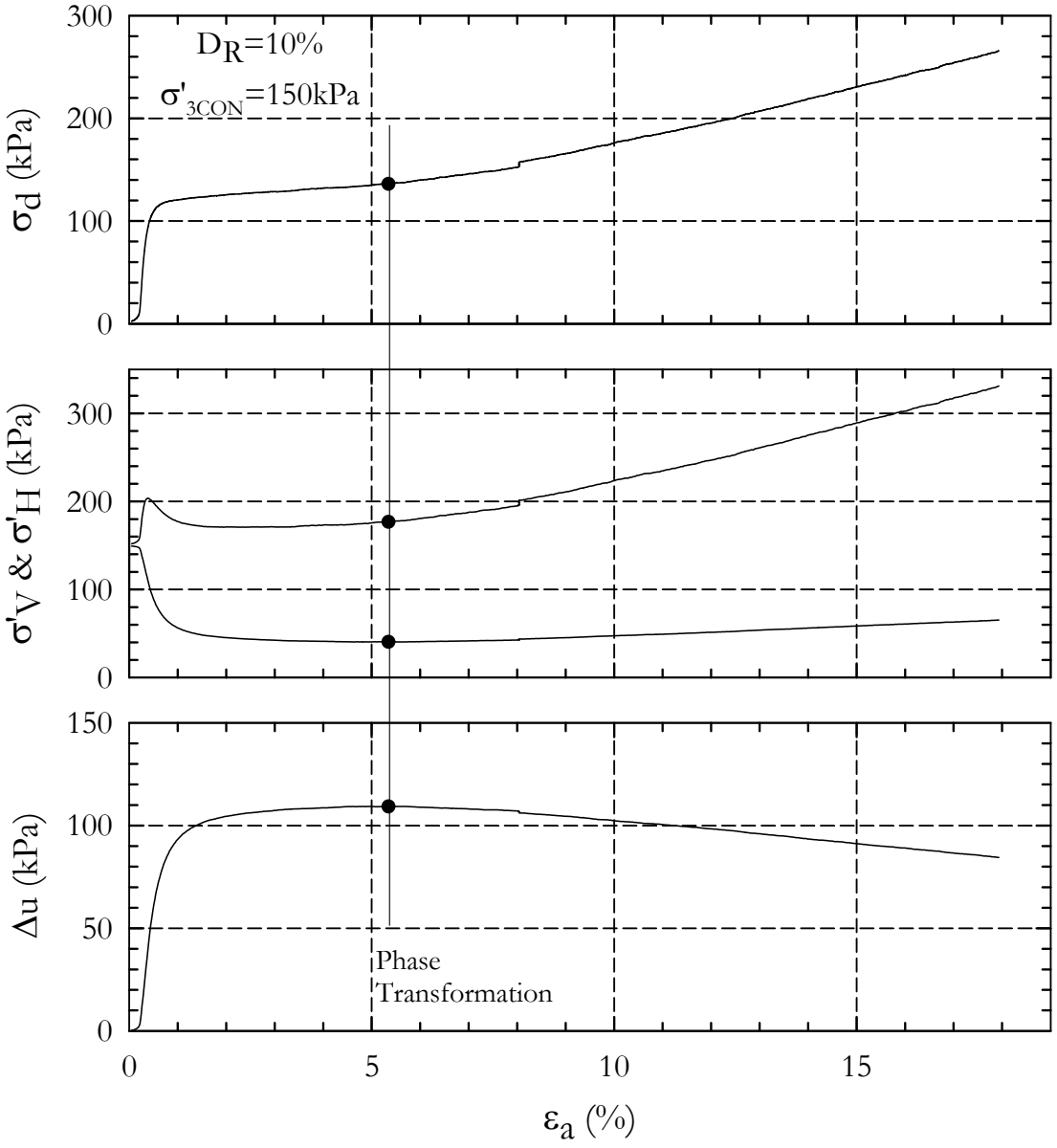

Figure I-8. Strain Plot - Test MCU04

Test No.: MCU05
Test Ref.: 20070724_Test01_D20_C1087
$D_{R(FINAL)}$: 20% (21.6%)
e: 1.130
σ'_{3CON}: 75 kPa

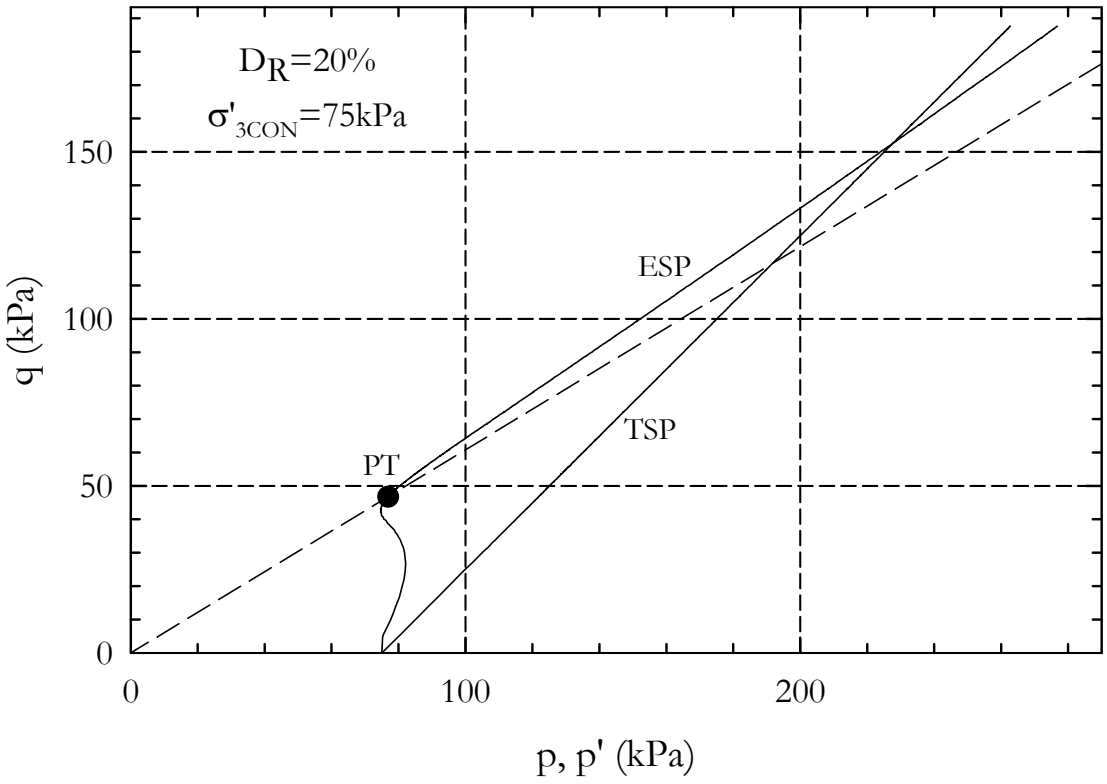

Figure I-9. Stress Path - Test MCU05

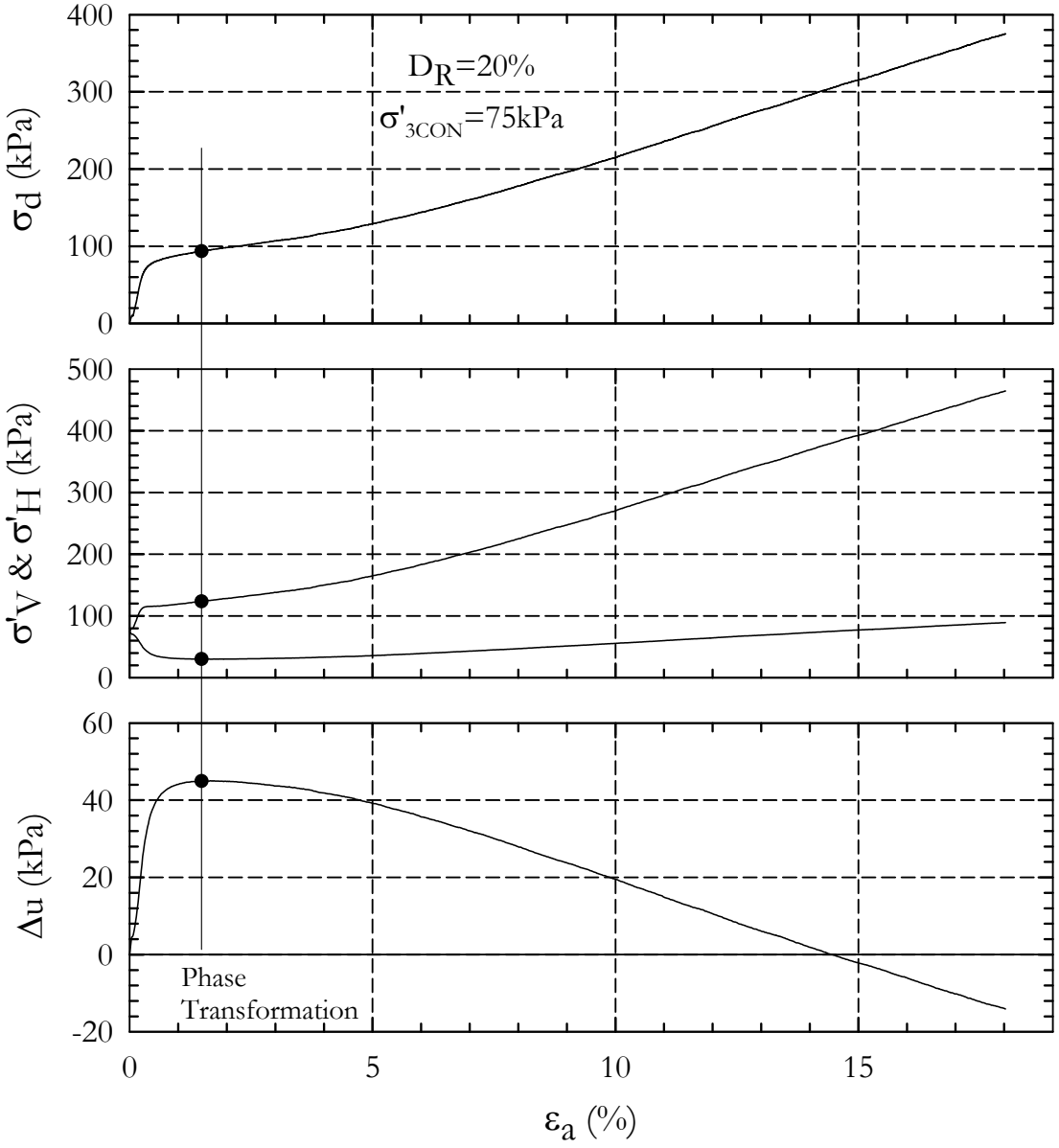

Figure I-10. Strain Plot - Test MCU05

Test No.: MCU06
Test Ref.: 20070923_Test01_D20_C100
$D_{R(FINAL)}$: 20% (18.6%)
e: 1.143
σ'_{3CON}: 100 kPa

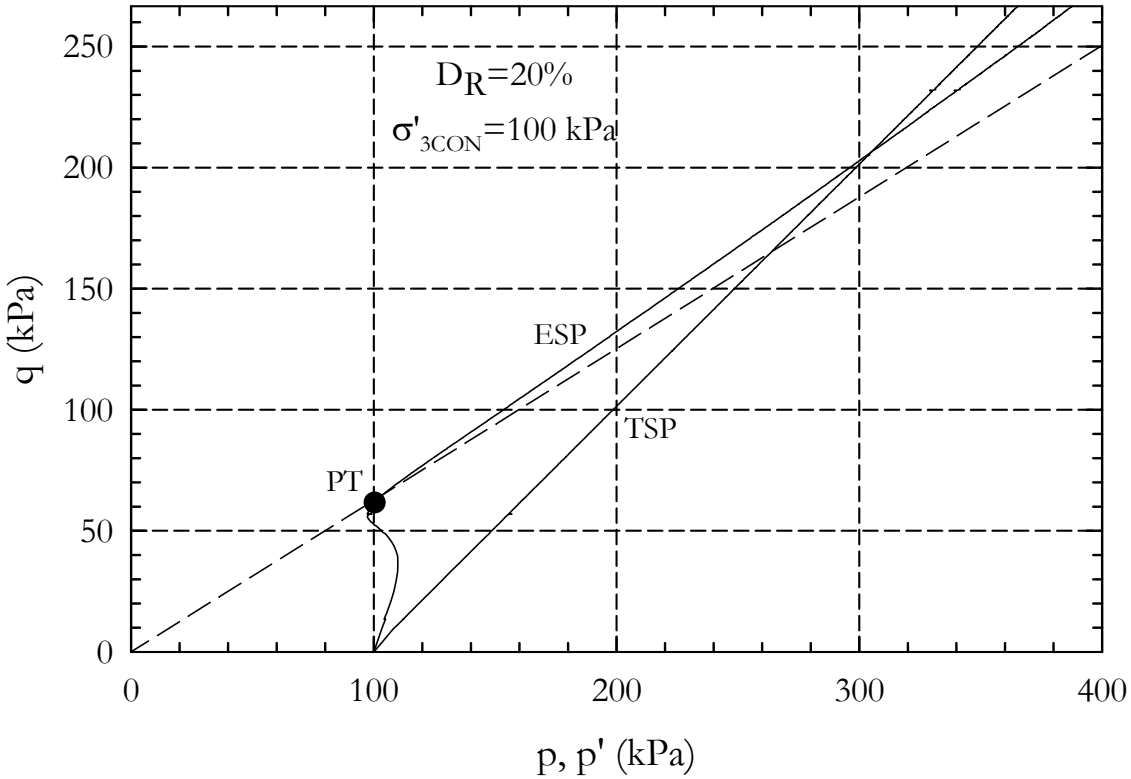

Figure I-11. Stress Path - Test MCU06

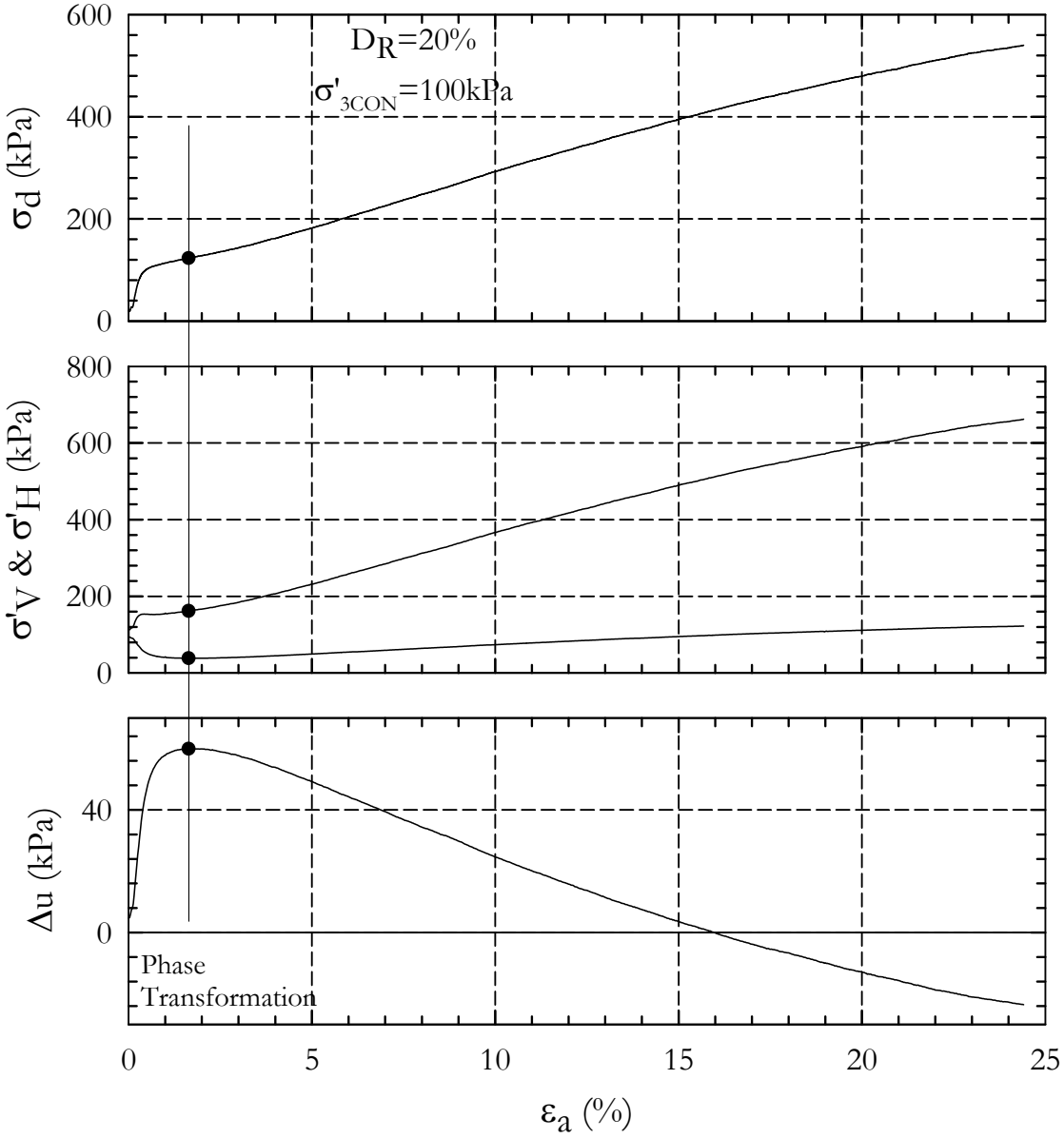

Figure I-12. Strain Plot - Test MCU06

Test No.: MCU07
Test Ref.: 20070925_Test01_D20_C200
$D_{R(FINAL)}$: 20% (17.9%)
e: 1.145
σ'_{3CON}: 200 kPa

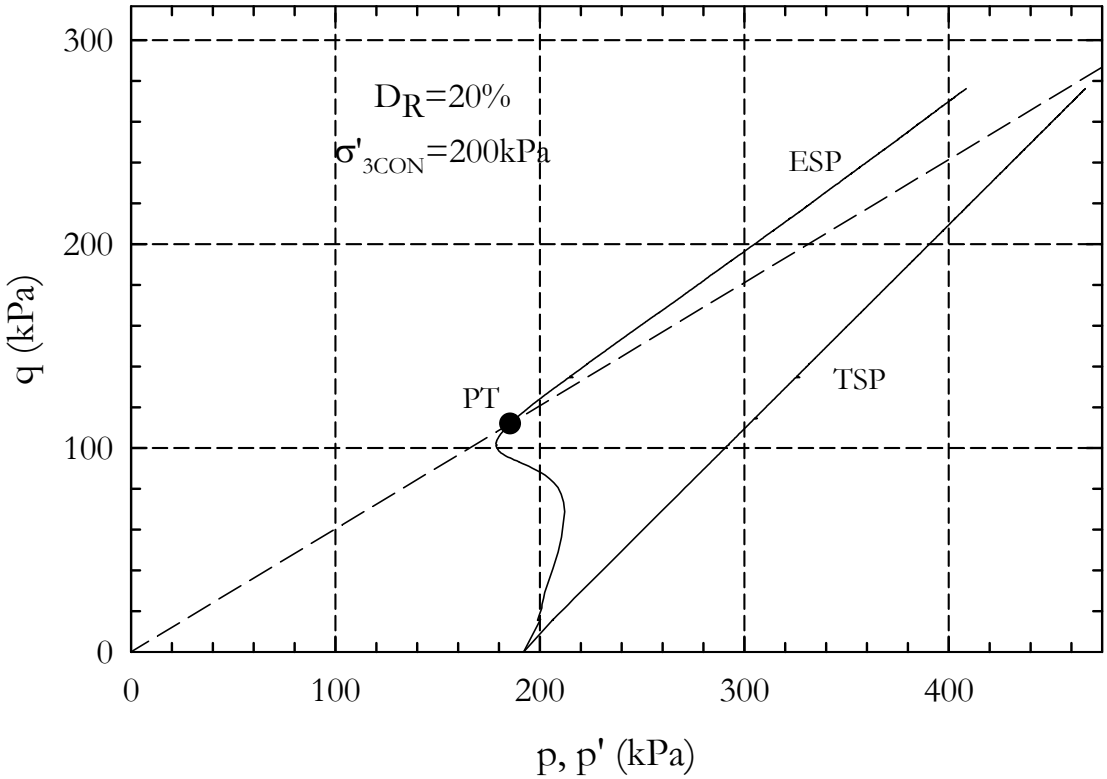

Figure I-13. Stress Path - Test MCU07

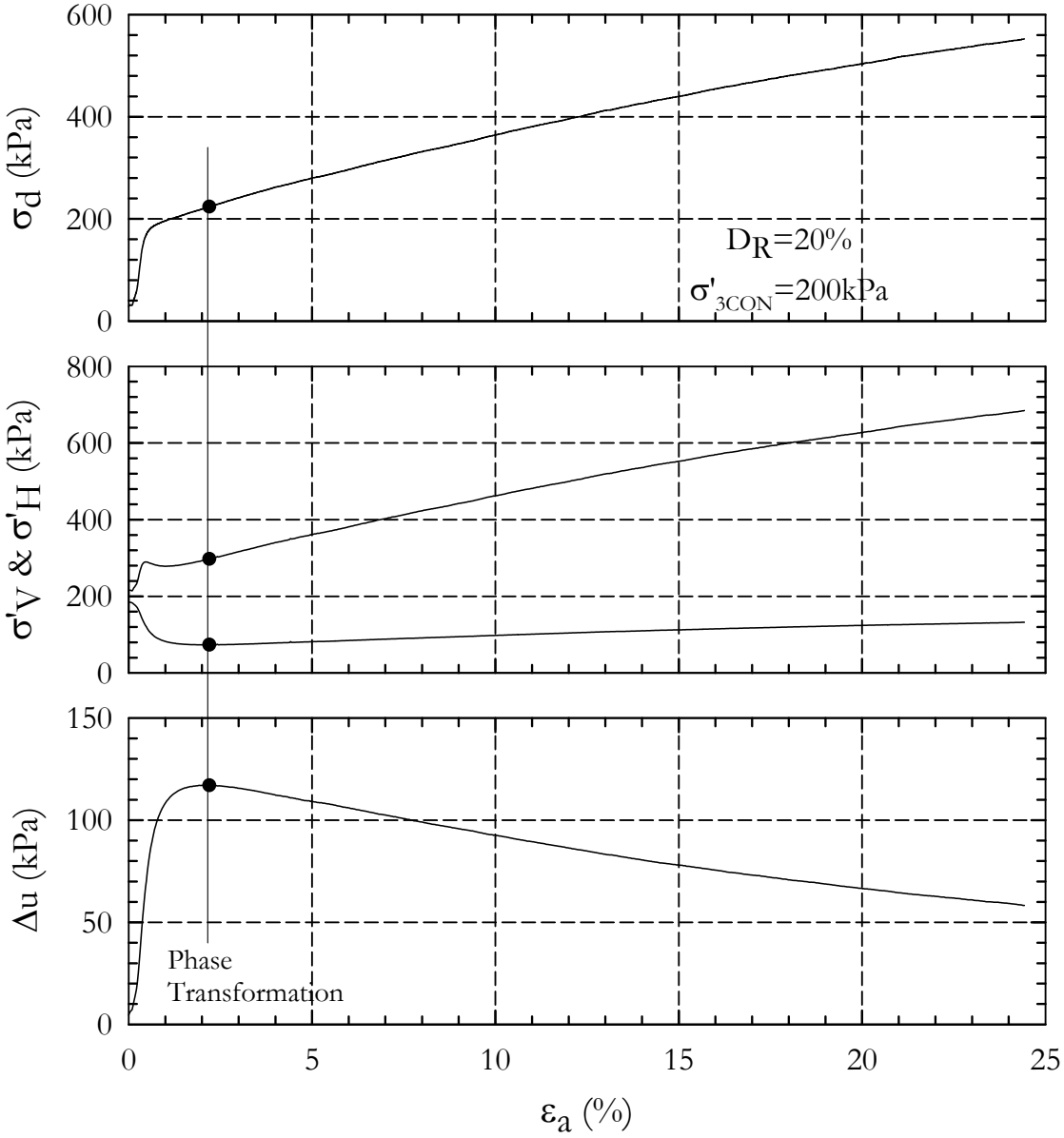

Figure I-14. Strain Plot - Test MCU07

Test No.: MCU08
Test Ref.: 20071002_Test01_D20_C300
$D_{R(FINAL)}$: 20% (21.7%)
e: 1.129
σ'_{3CON}: 300 kPa

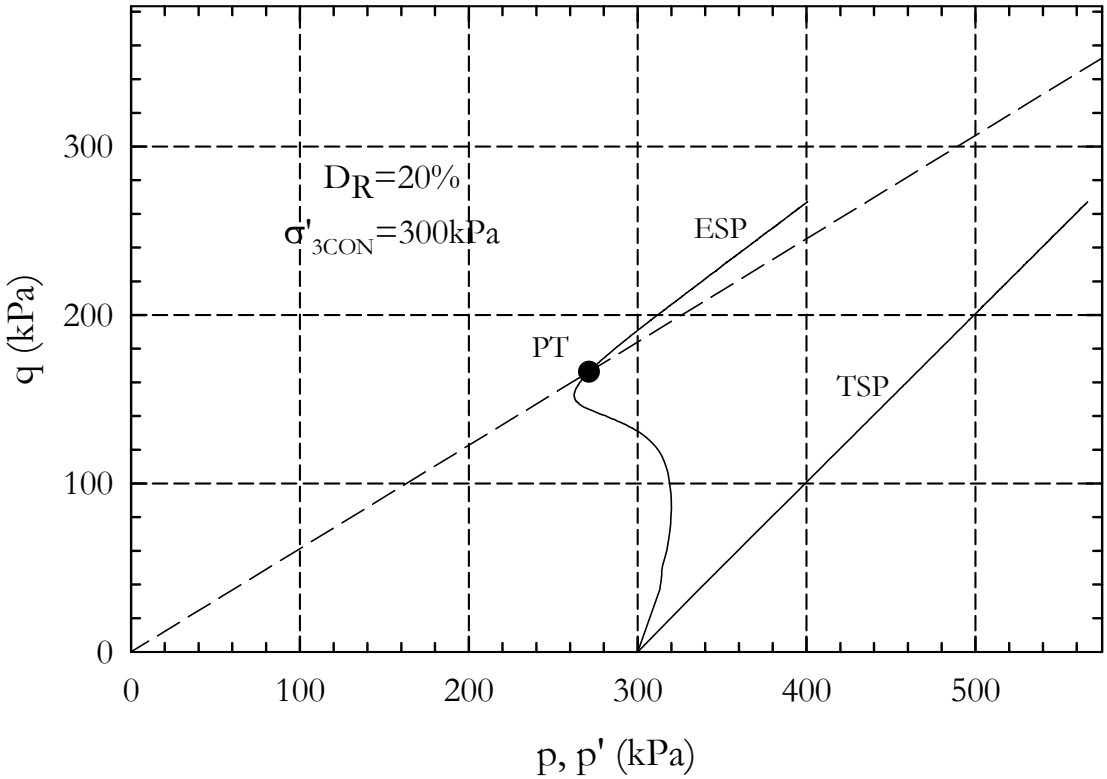

Figure I-15. Stress Path - Test MCU08

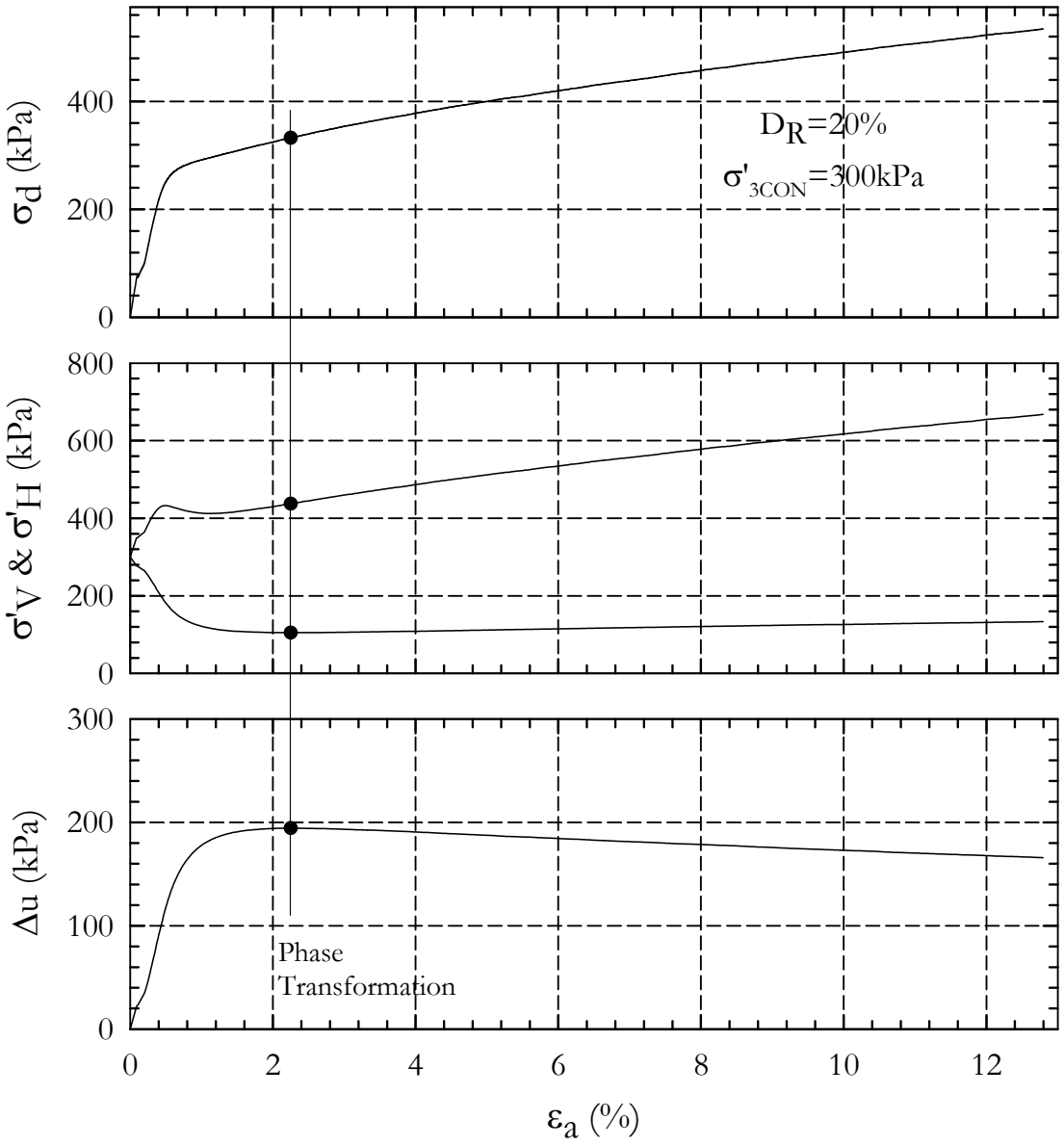

Figure I-16. Strain Plot - Test MCU08

Test No.: MCU09
Test Ref.: 20070717_Test01_D40_C1087
$D_{R(FINAL)}$: 30% (33.7%)
e: 1.079
σ'_{3CON}: 75 kPa

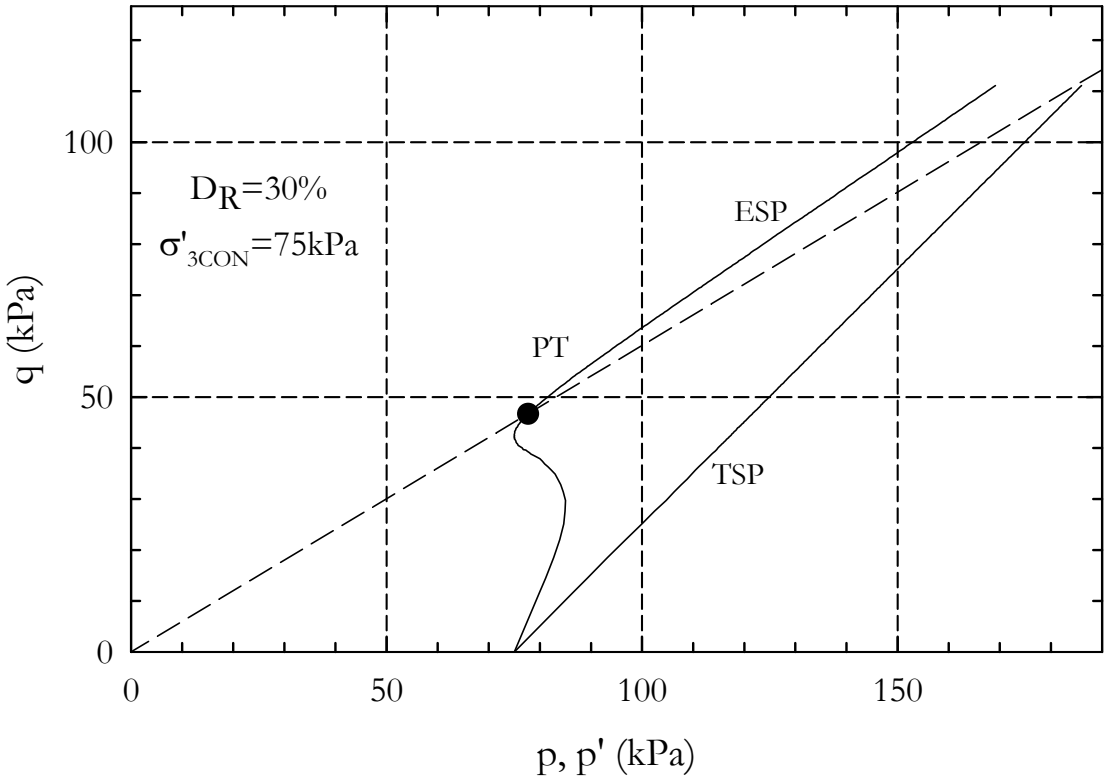

Figure I-17. Stress Path - Test MCU09

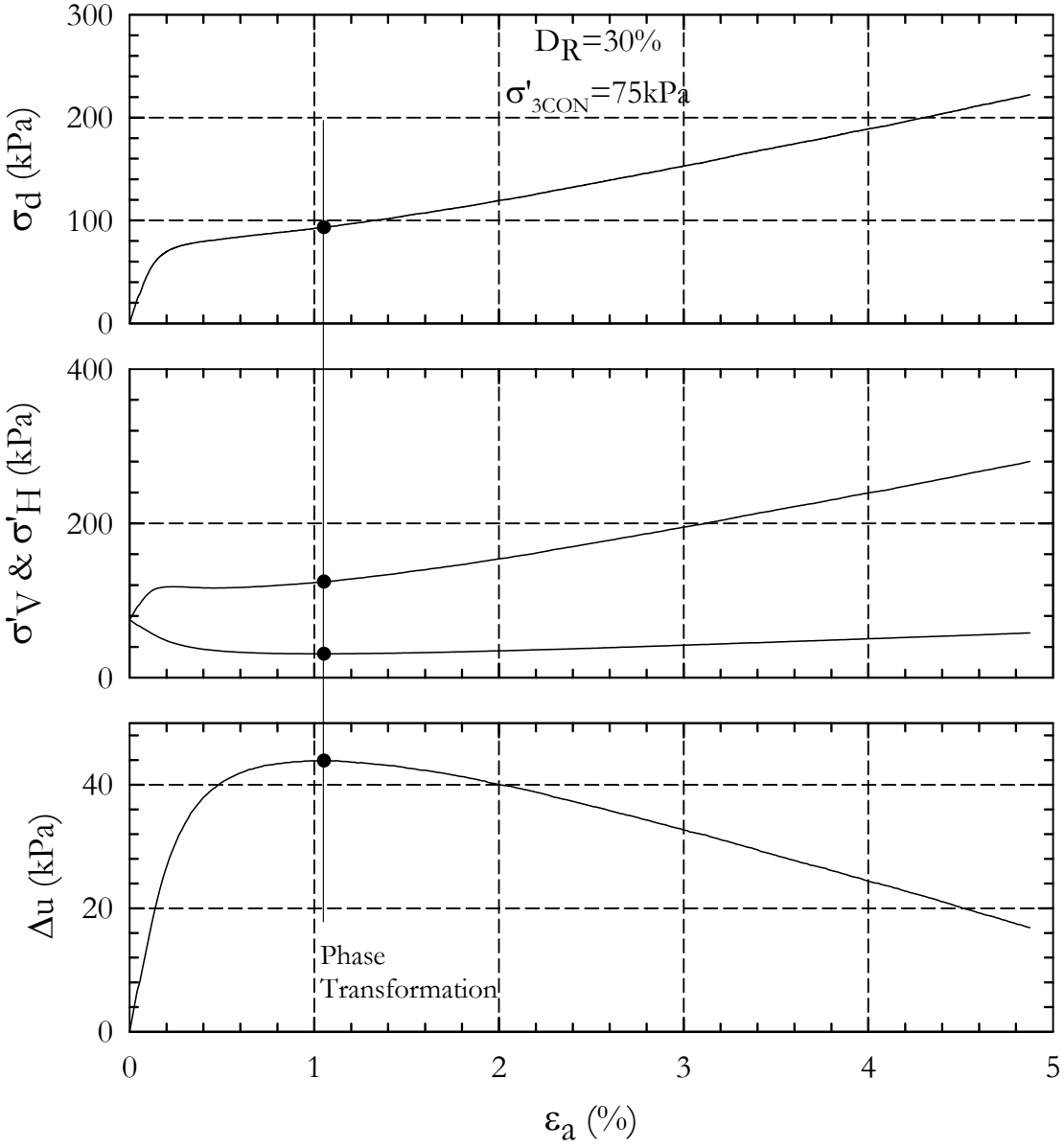

Figure I-18. Strain Plot - Test MCU09

Test No.: MCU10
Test Ref.: 20071208_Test01_D20_C100
$D_{R(FINAL)}$: 30% (26.8%)
e: 1.108
σ'_{3CON}: 100 kPa

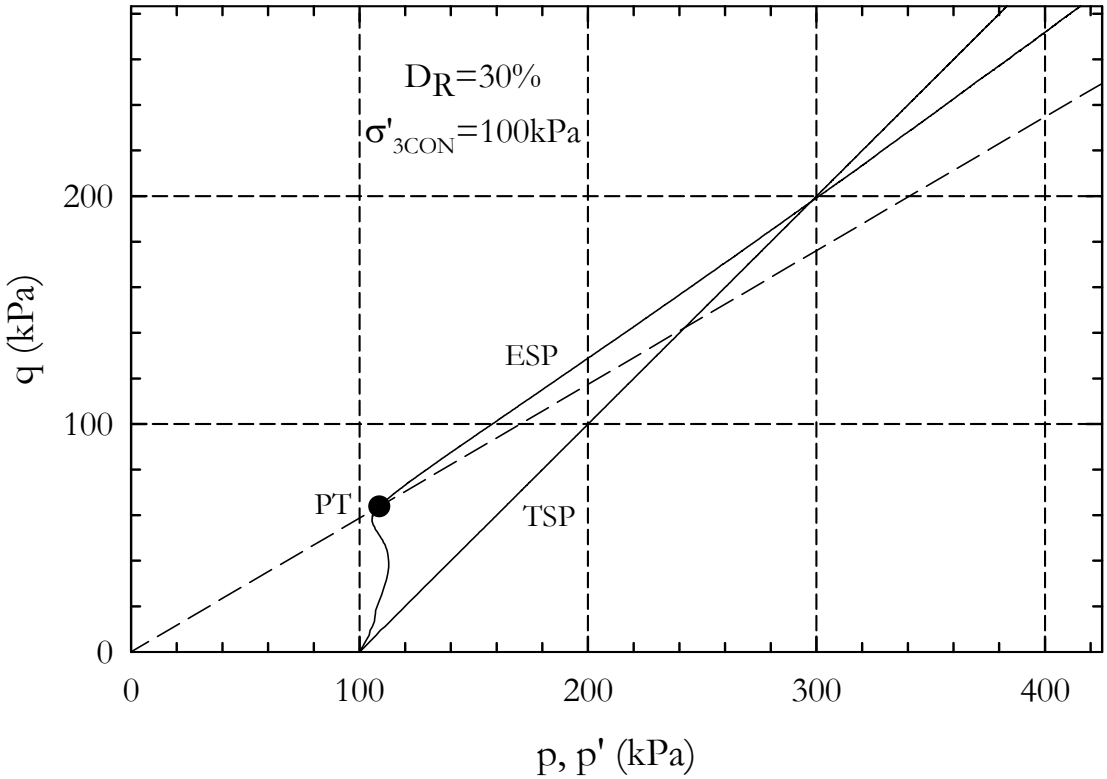

Figure I-19. Stress Path - Test MCU10

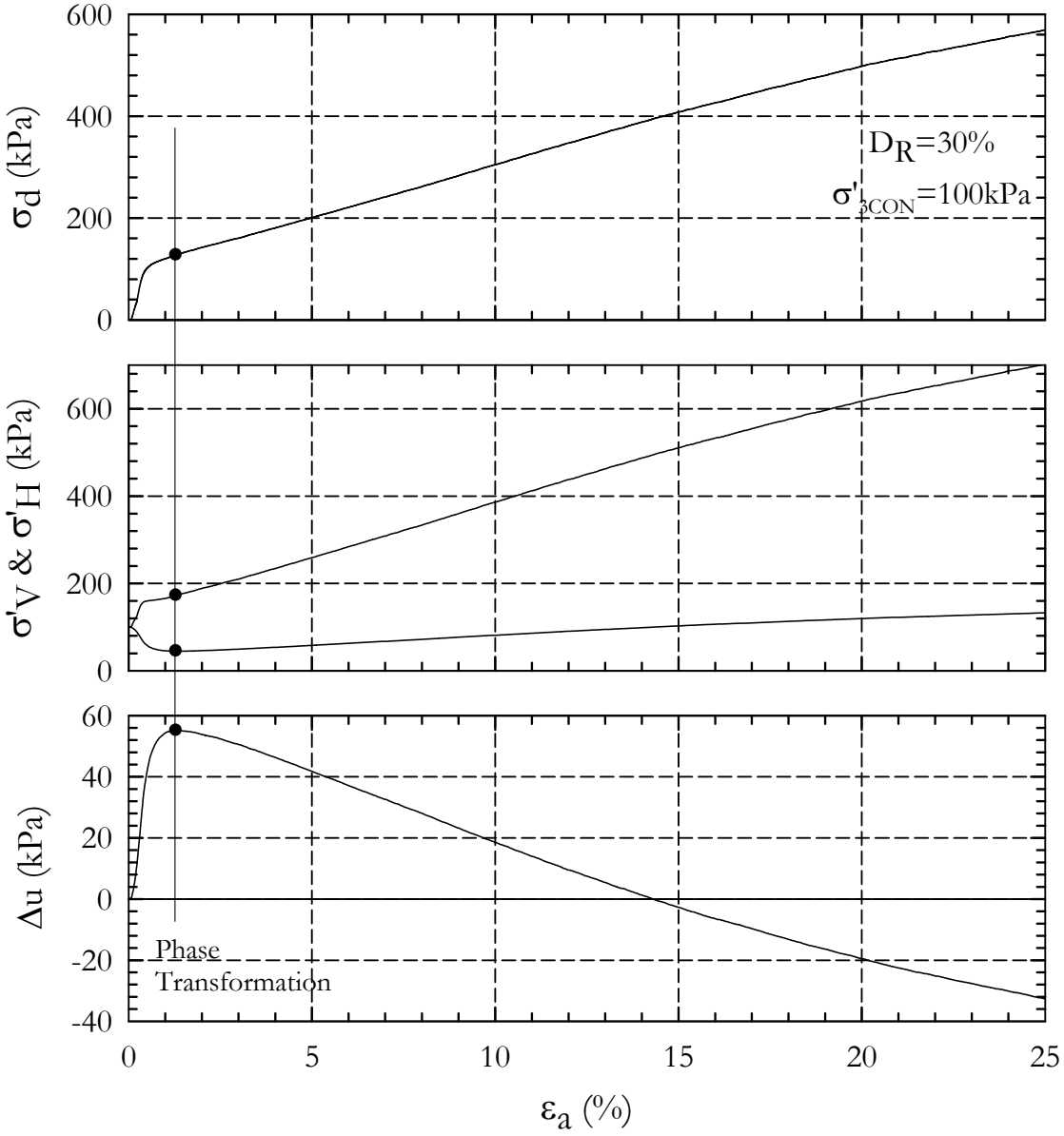

Figure I-20. Strain Plot - Test MCU10

Test No.: MCU11
Test Ref.: 20070927_Test02_D50_C100
$D_{R(FINAL)}$: 40% (43.2%)
e: 1.039
σ'_{3CON}: 100 kPa

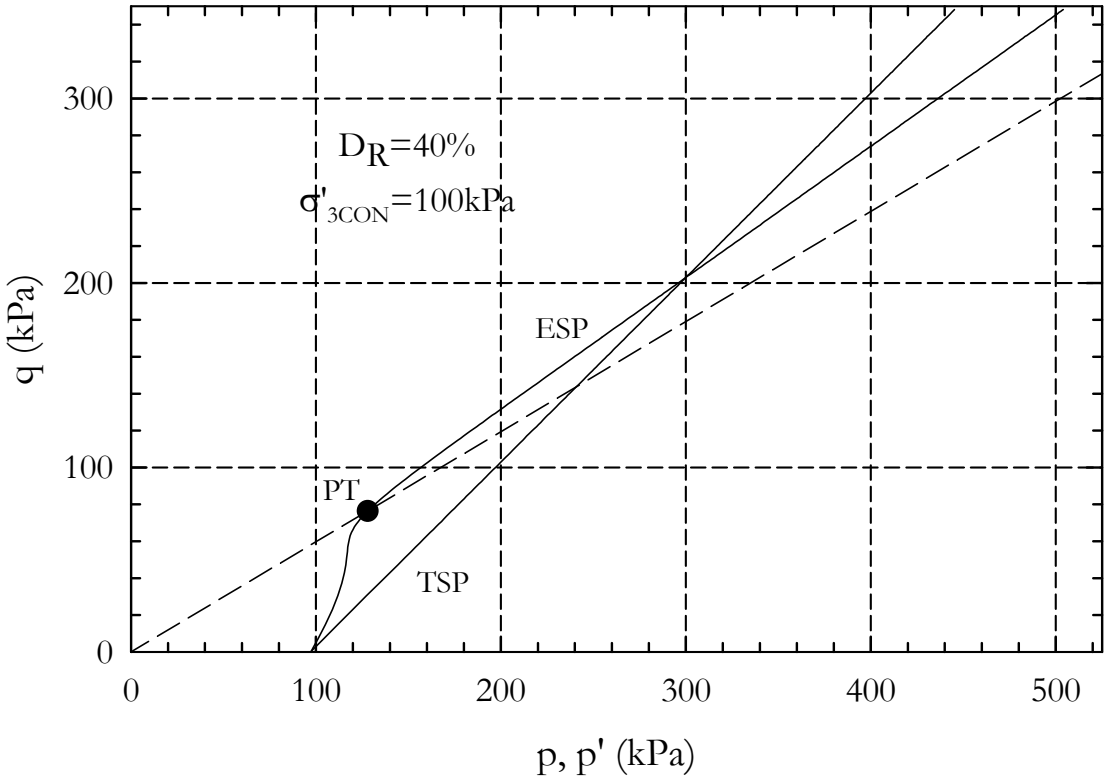

Figure I-21. Stress Path - Test MCU11

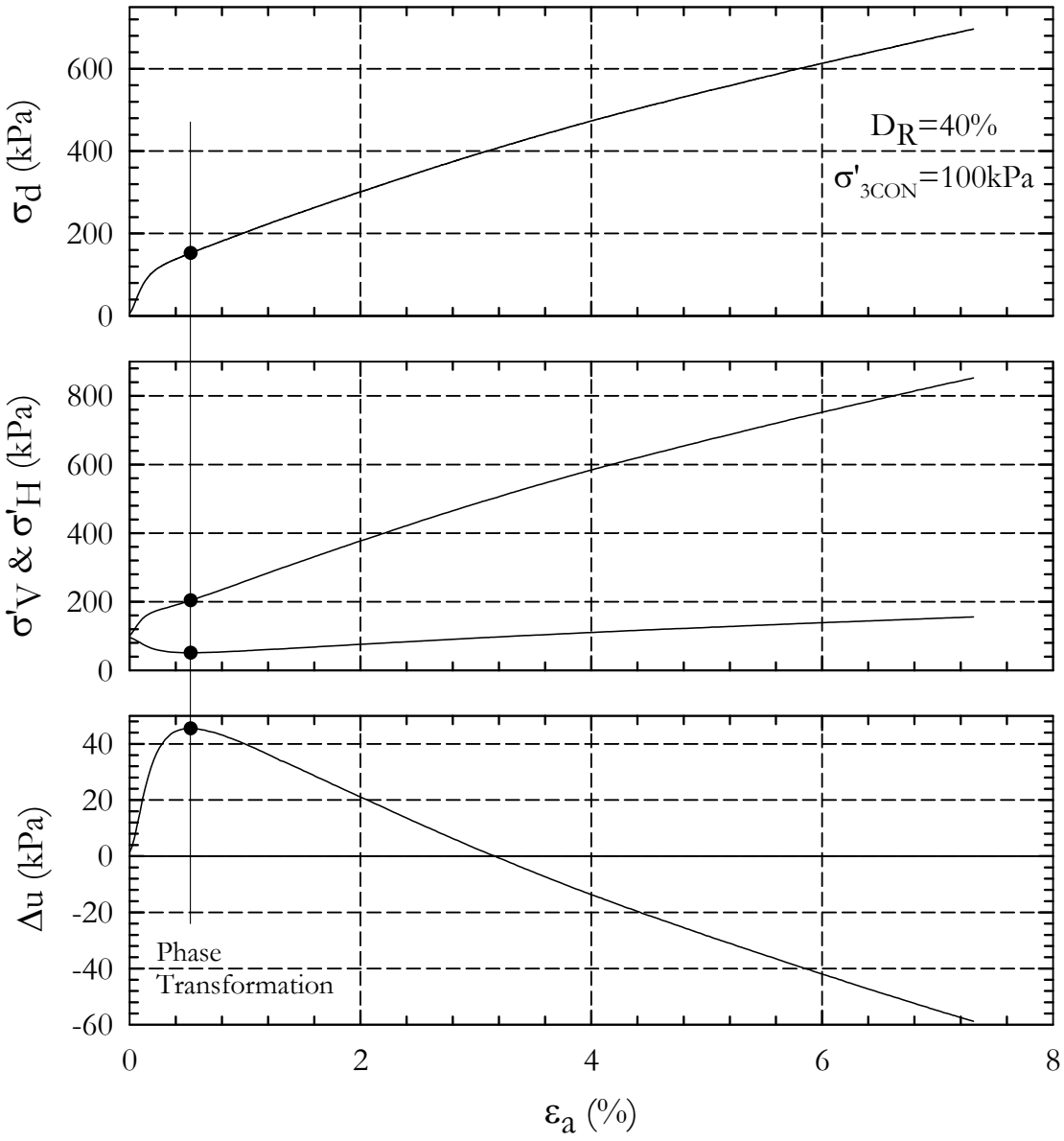

Figure I-22. Strain Plot - Test MCU11

Test No.: MCU12
Test Ref.: 20071001_Test01_D50_C100
$D_{R(FINAL)}$: 40% (40.5%)
e: 1.051
σ'_{3CON}: 100 kPa

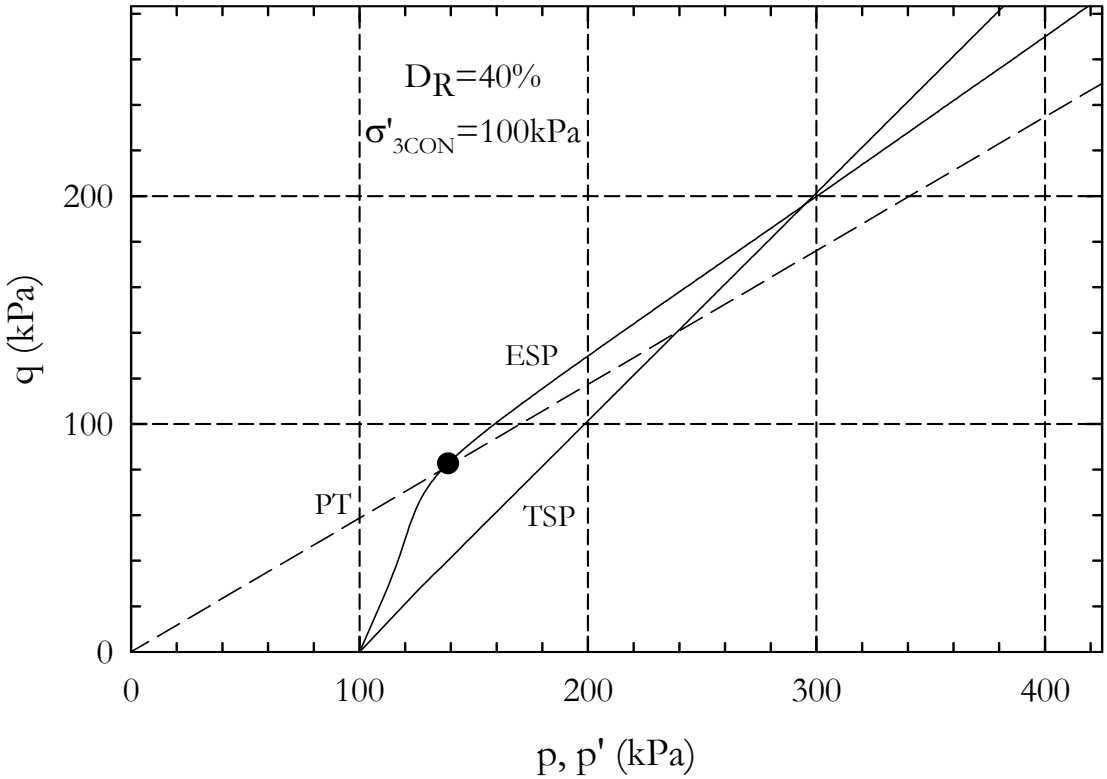

Figure I-23. Stress Path - Test MCU12

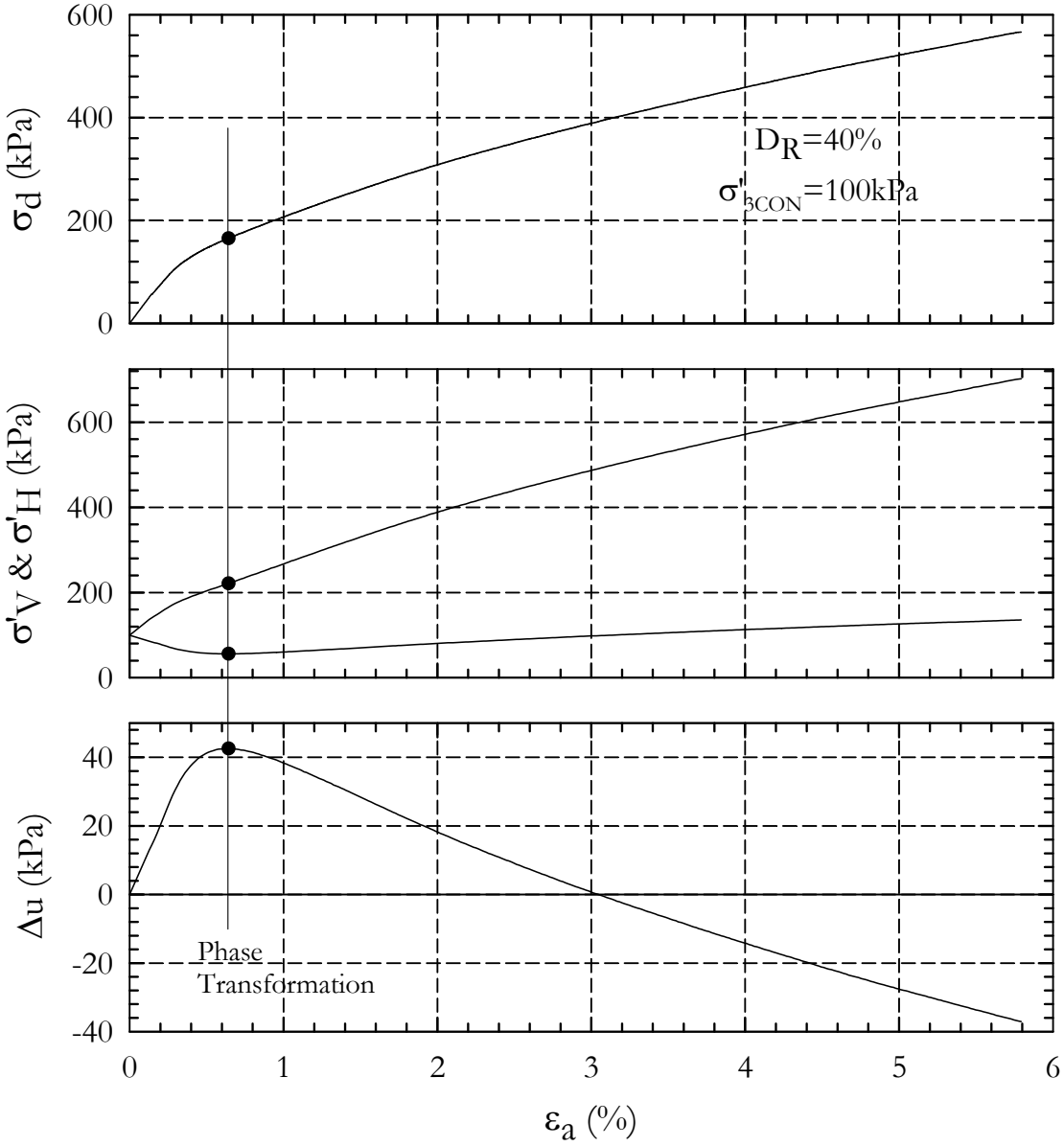

Figure I-24. Strain Plot - Test MCU12

Test No.: MCU13
Test Ref.: 20070716_Test01_D40_C2174
$D_{R(FINAL)}$: 40% (35.4%)
e: 1.072
σ'_{3CON}: 150 kPa

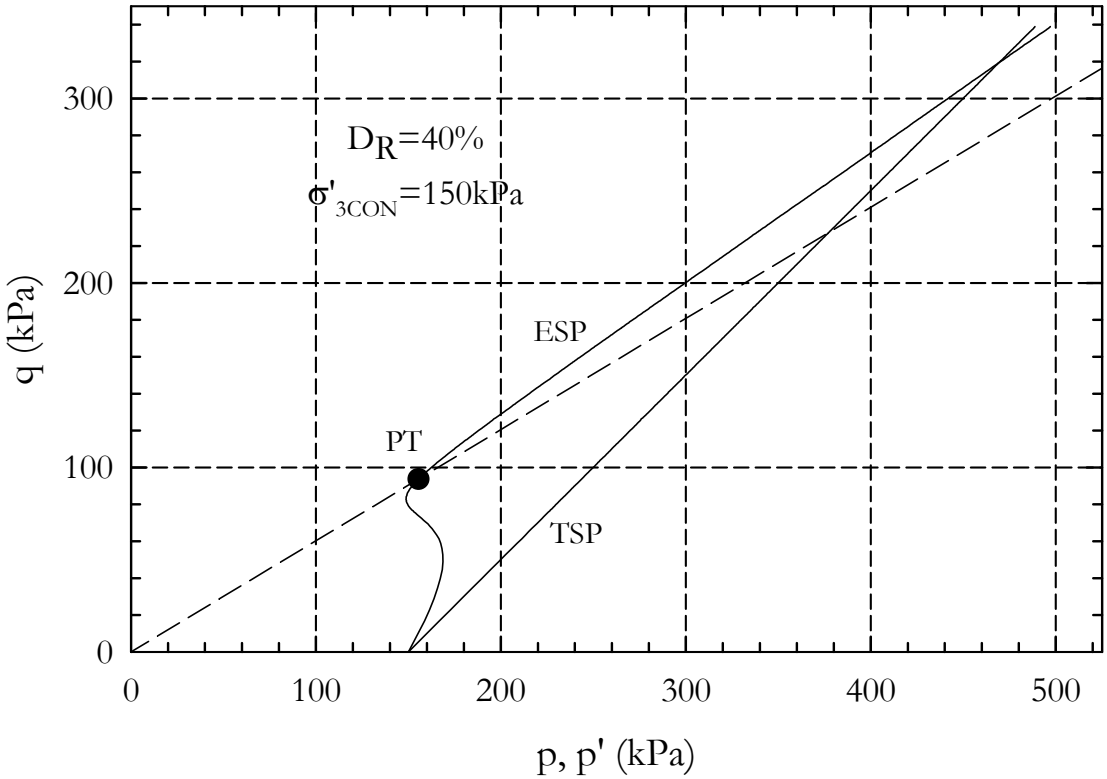

Figure I-25. Stress Path - Test MCU13

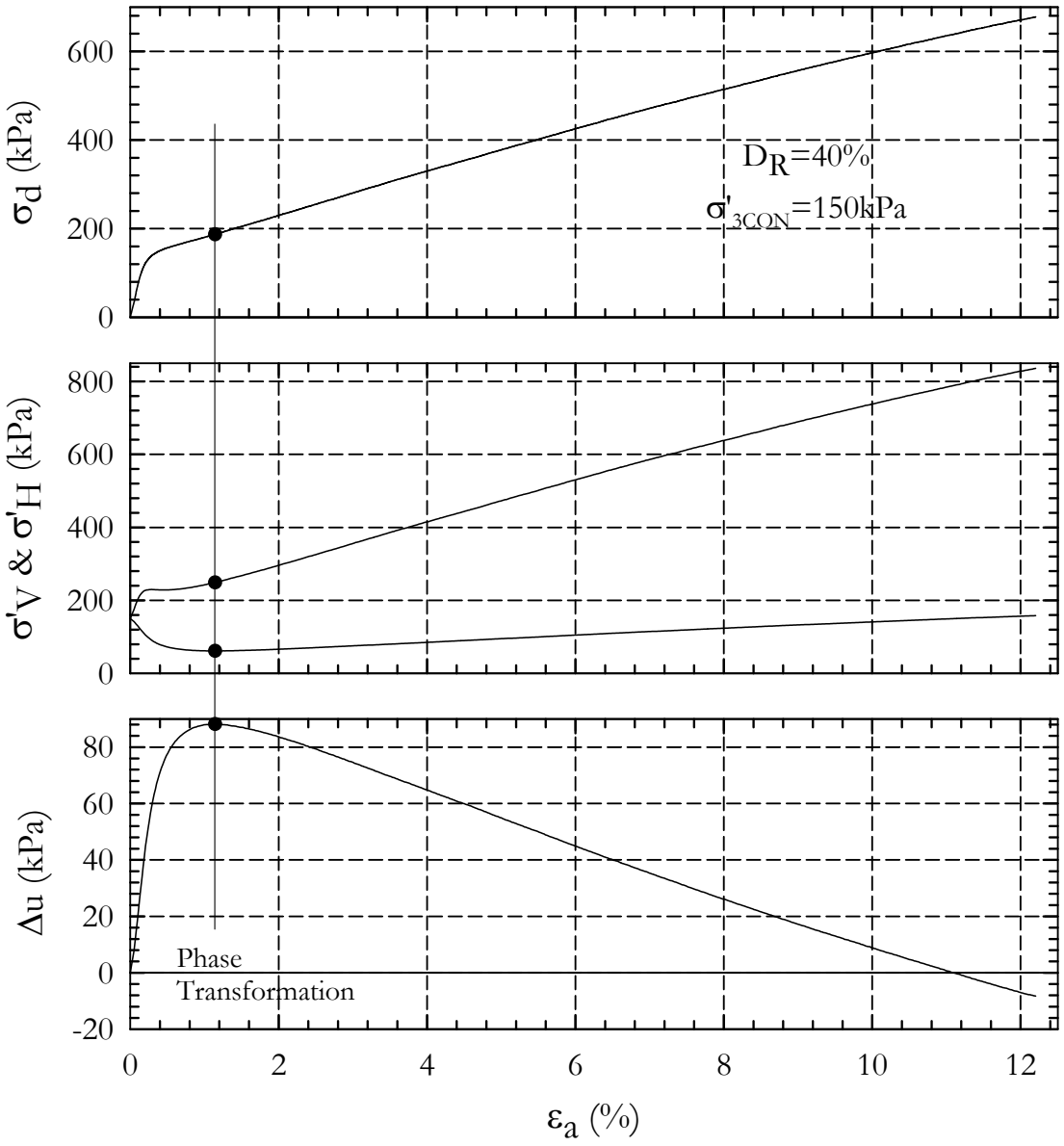

Figure I-26. Strain Plot - Test MCU13

Test No.: MCU14
Test Ref.: 20071004_Test01_D50_C200
$D_{R(FINAL)}$: 40% (42.2%)
e: 1.044
σ'_{3CON}: 200 kPa

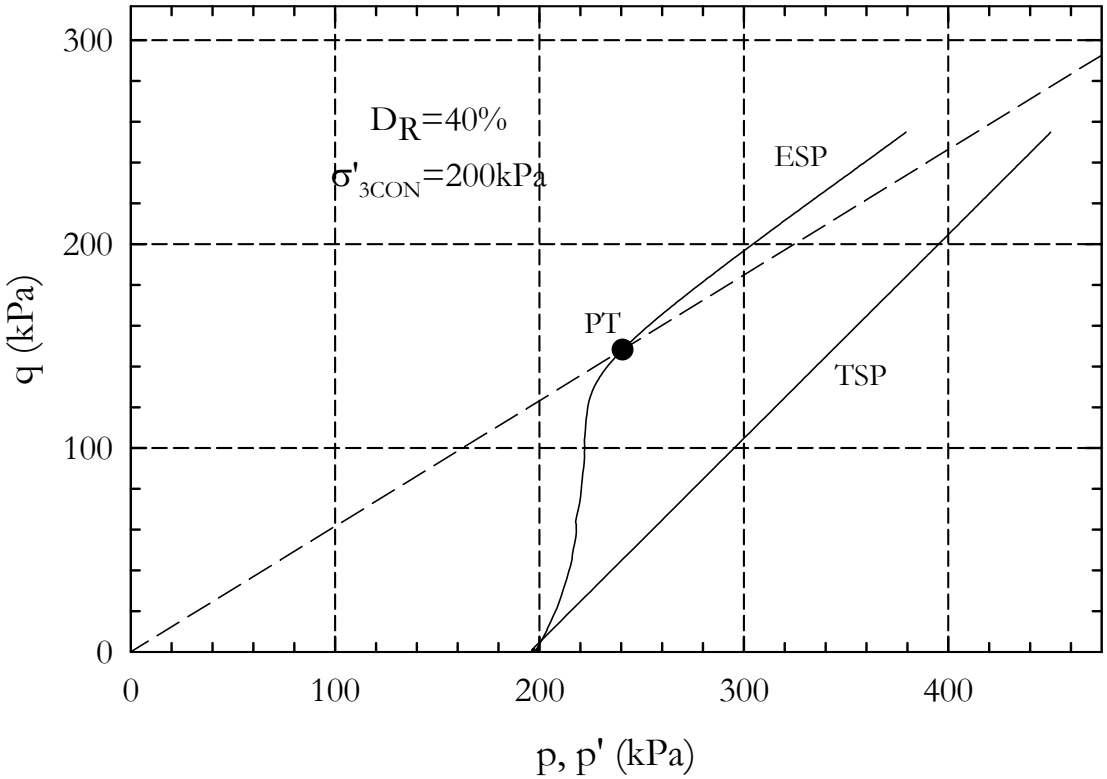

Figure I-27. Stress Path - Test MCU14

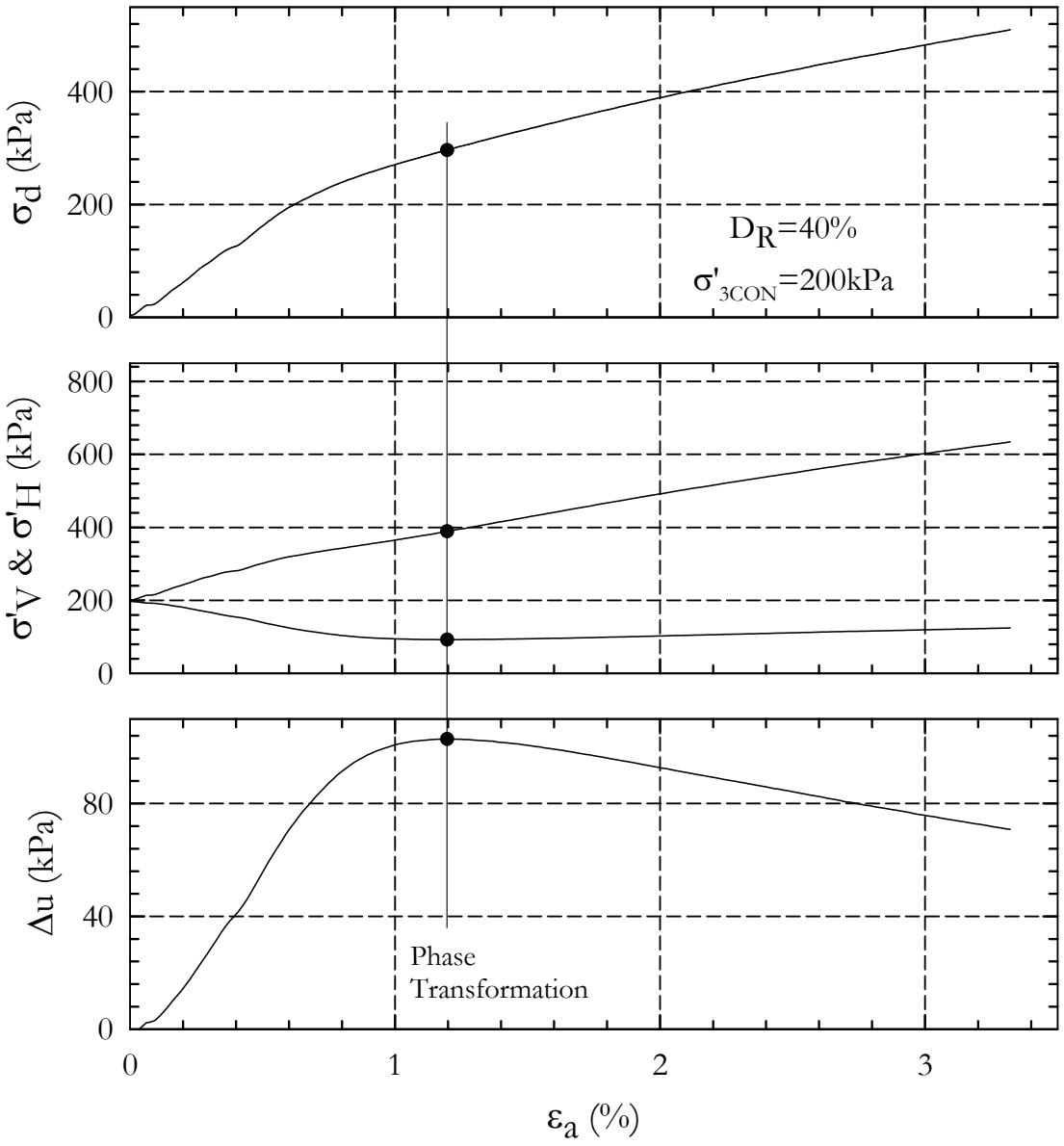

Figure I-28. Strain Plot - Test MCU14

Test No.: MCU15
Test Ref.: 20071009_Test01_D50_C300
$D_{R(FINAL)}$: 50% (53.4%)
e: 0.997
σ'_{3CON}: 300 kPa

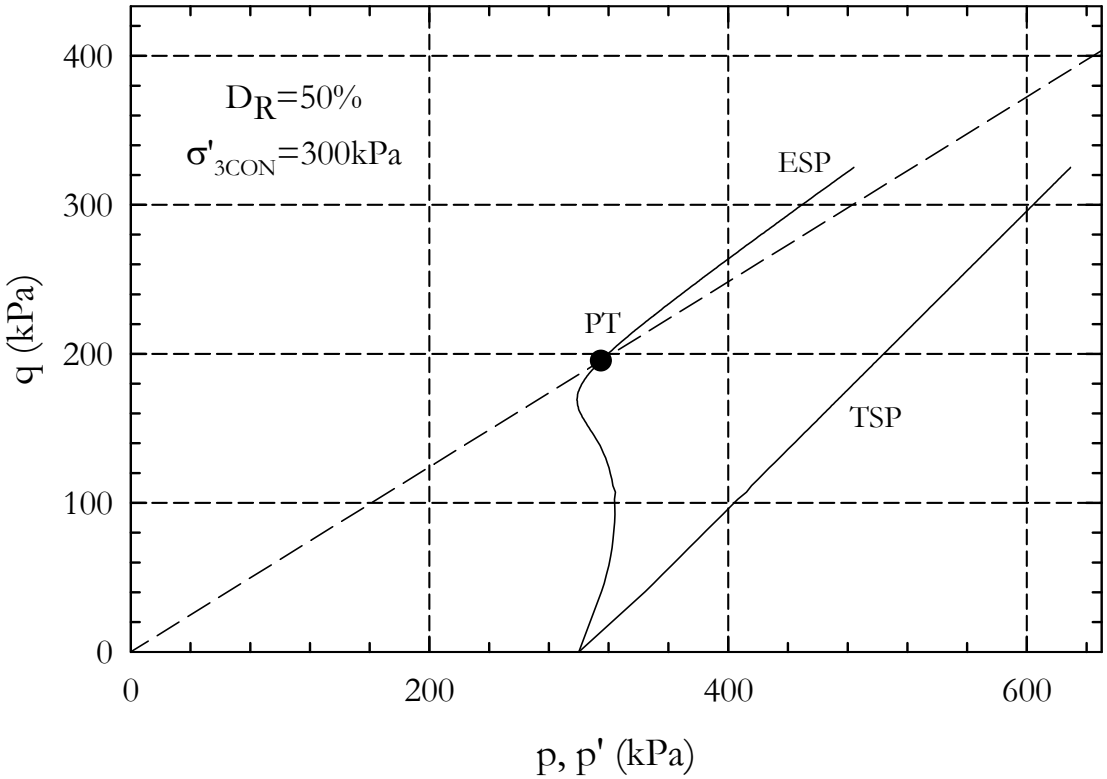

Figure I-29. Stress Path - Test MCU15

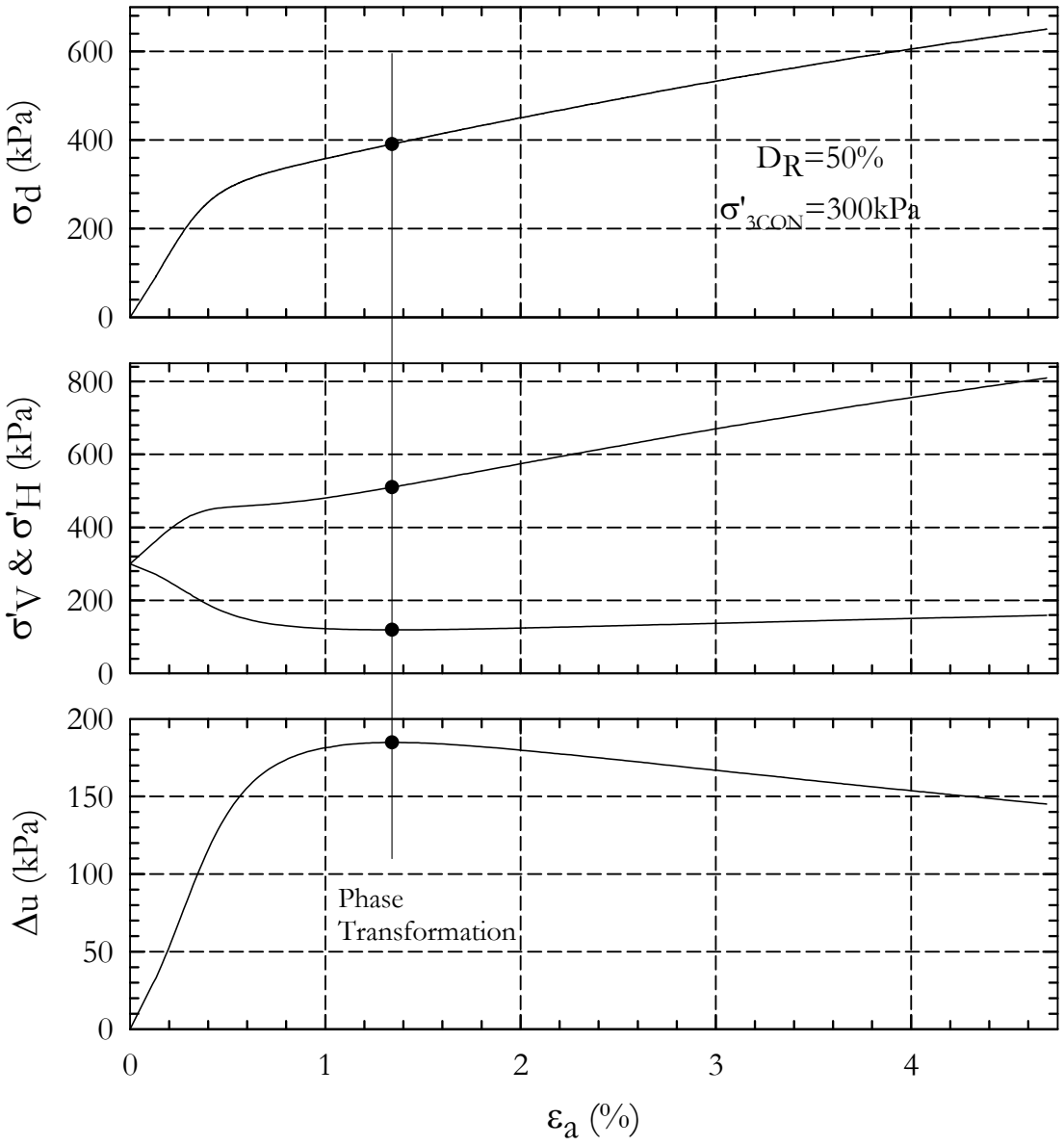

Figure I-30. Strain Plot - Test MCU15

Test No.: MCU16
Test Ref.: 20071009_Test02_D50_C300
$D_{R(FINAL)}$: 50% (46.9%)
e: 1.024
σ'_{3CON}: 300 kPa

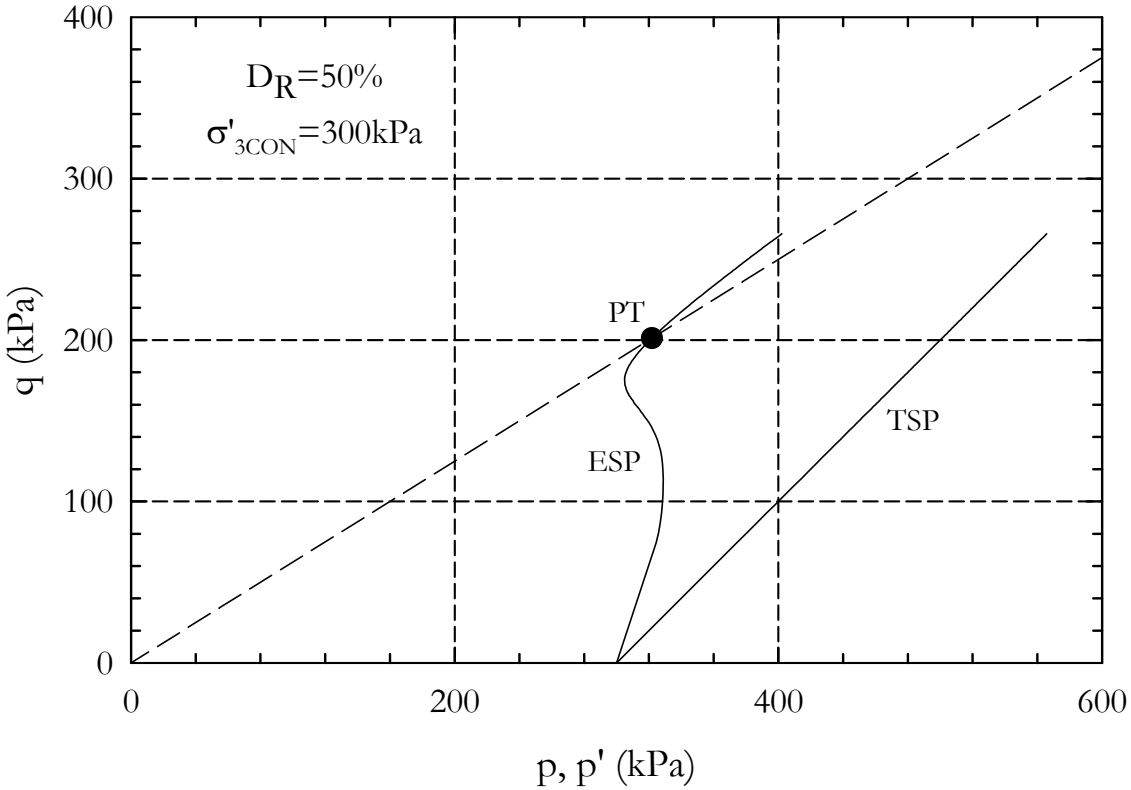

Figure I-31. Stress Path - Test MCU16

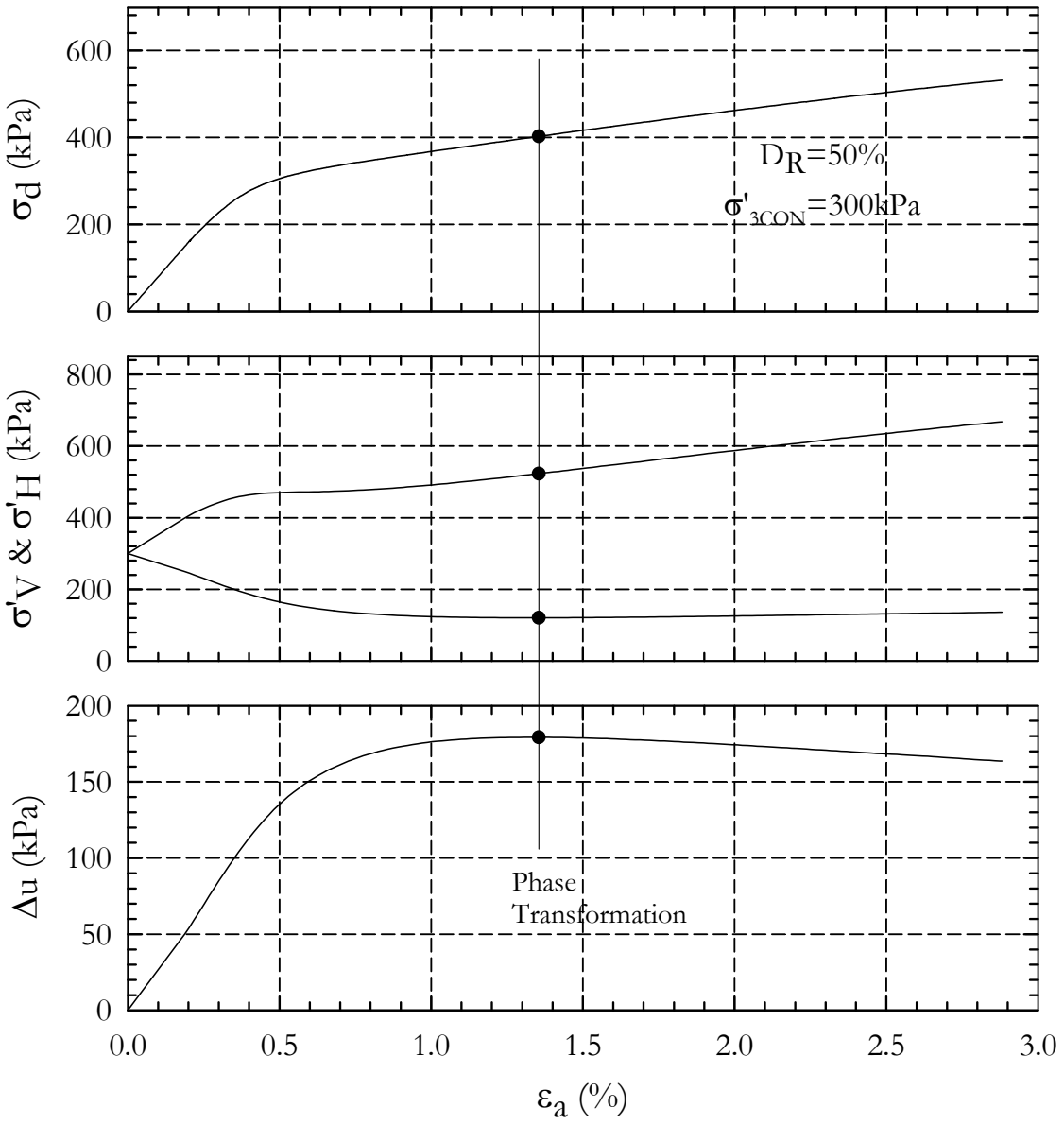

Figure I-32. Strain Plot - Test MCU16

Test No.: MCU17
Test Ref.: 20080201_Test01_D60_C100
$D_{R(FINAL)}$: 60% (58.3%)
e: 0.976
σ'_{3CON}: 100 kPa

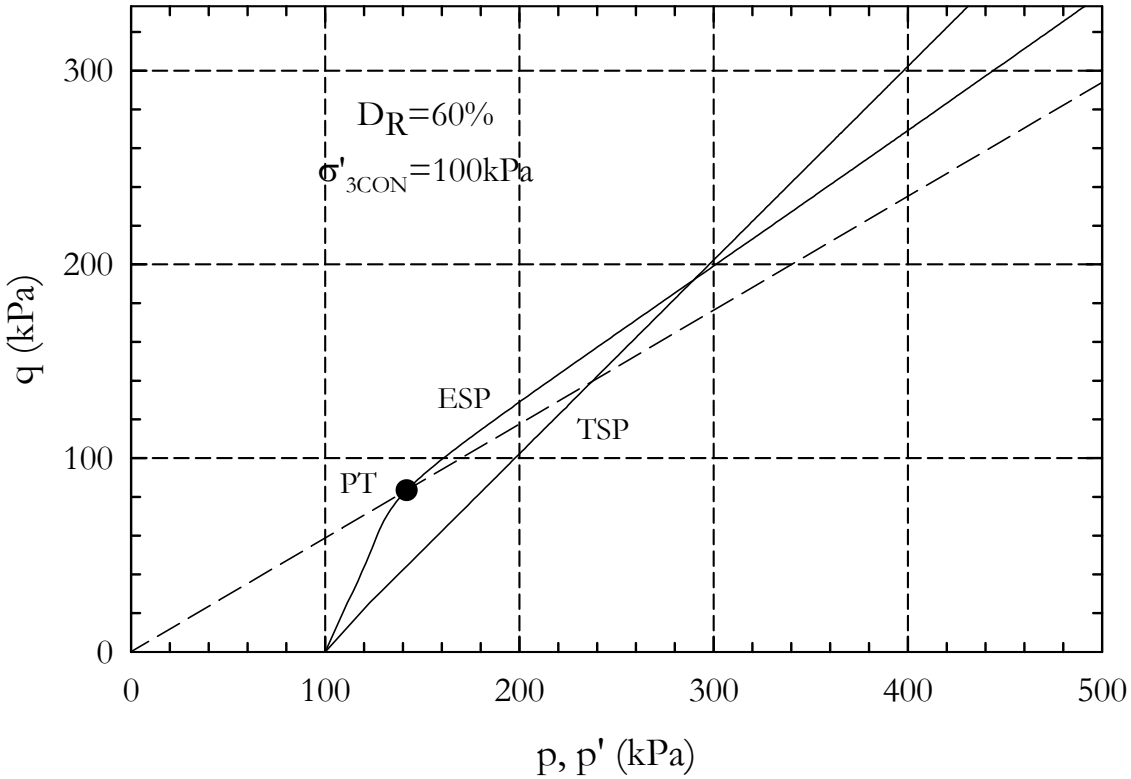

Figure I-33. Stress Path - Test MCU17

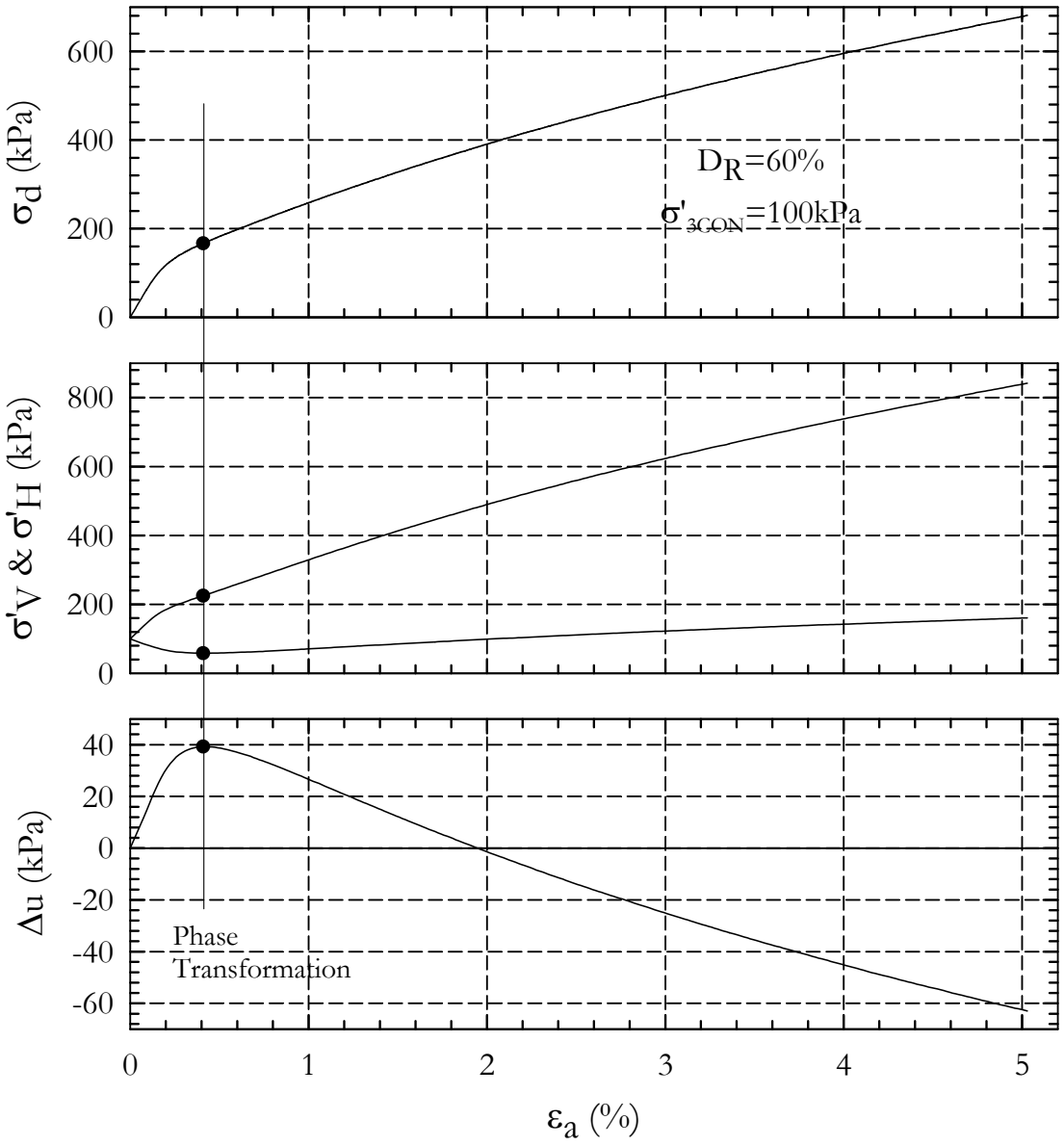

Figure I-34. Strain Plot - Test MCU17

APPENDIX II CYCLIC TRIAXIAL RESULTS

Test No.: CTX01
Test Ref.: 20080128_Cyclic01_D20_CSR10
$D_{R(FINAL)}$: 20% (21.7%)‡
e: 1.129
σ'_{3CON}: 100 kPa
CSR: 0.10

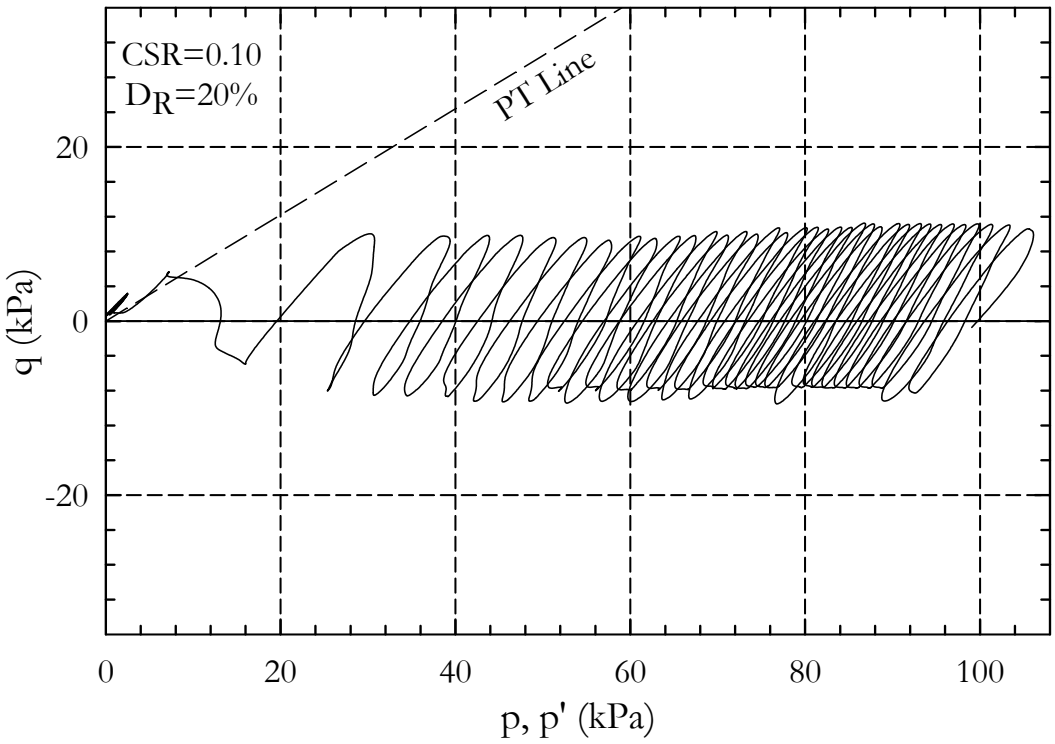

Figure II-1. Stress Path – CTX01

‡ Rounded (Actual)

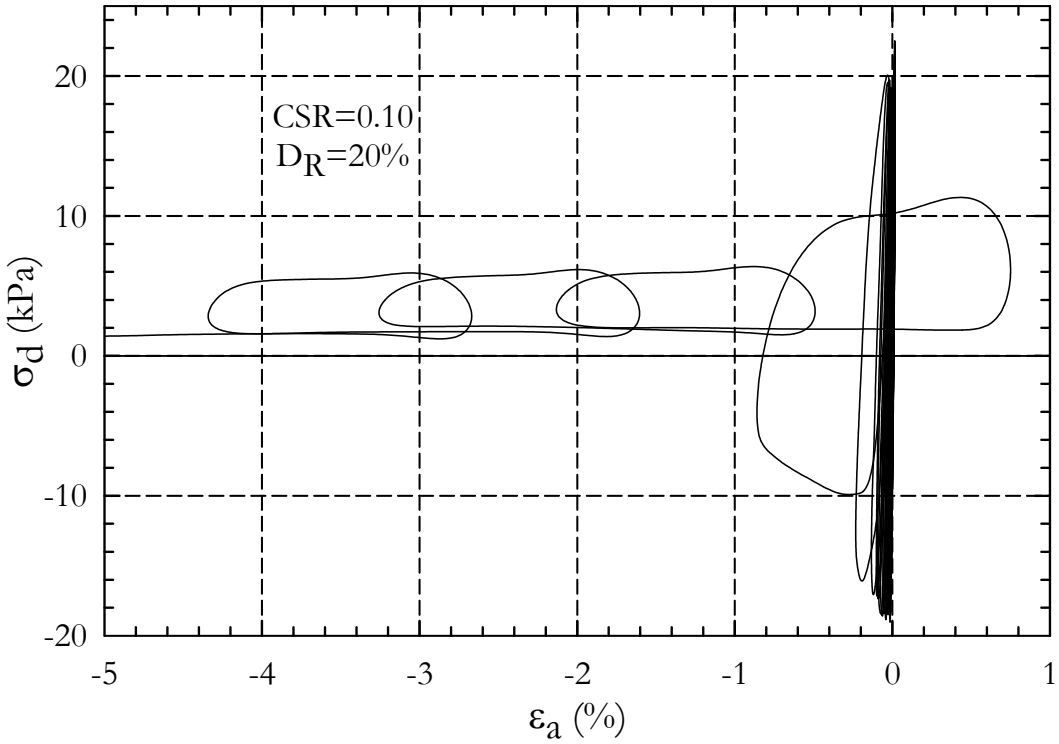

Figure II-2. Strain vs. Deviator stress– Test CTX01

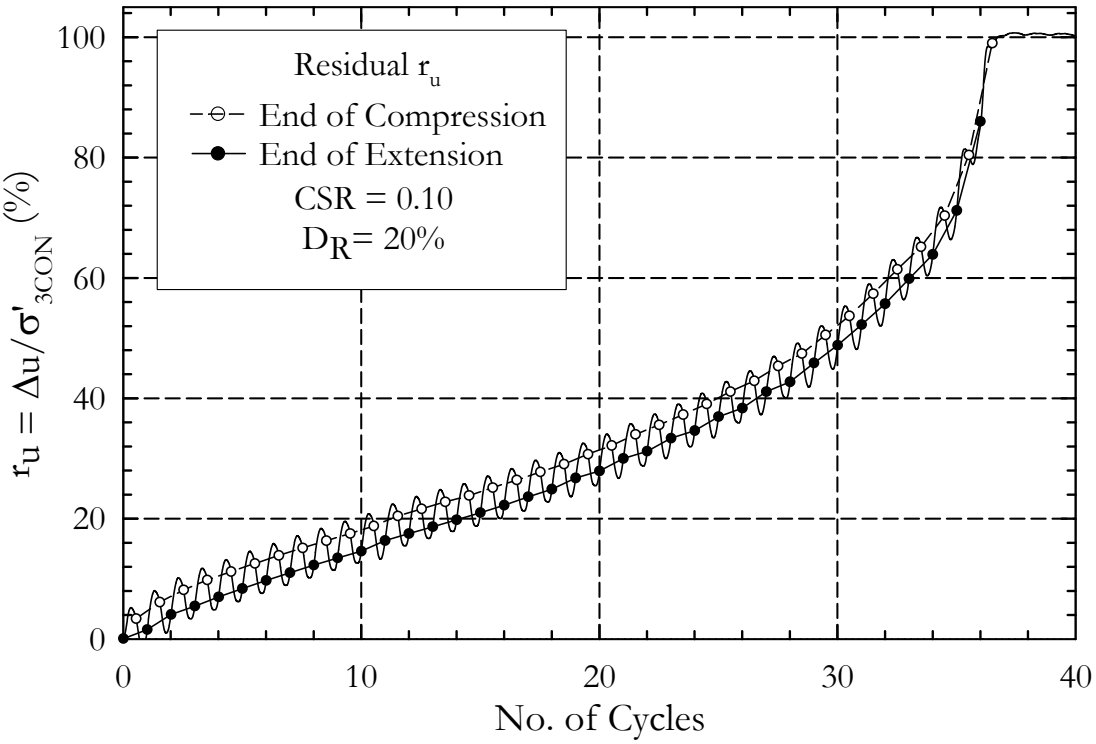

Figure II-3. Pore Pressure Ratio with Residual Pore Pressure – Test CTX01

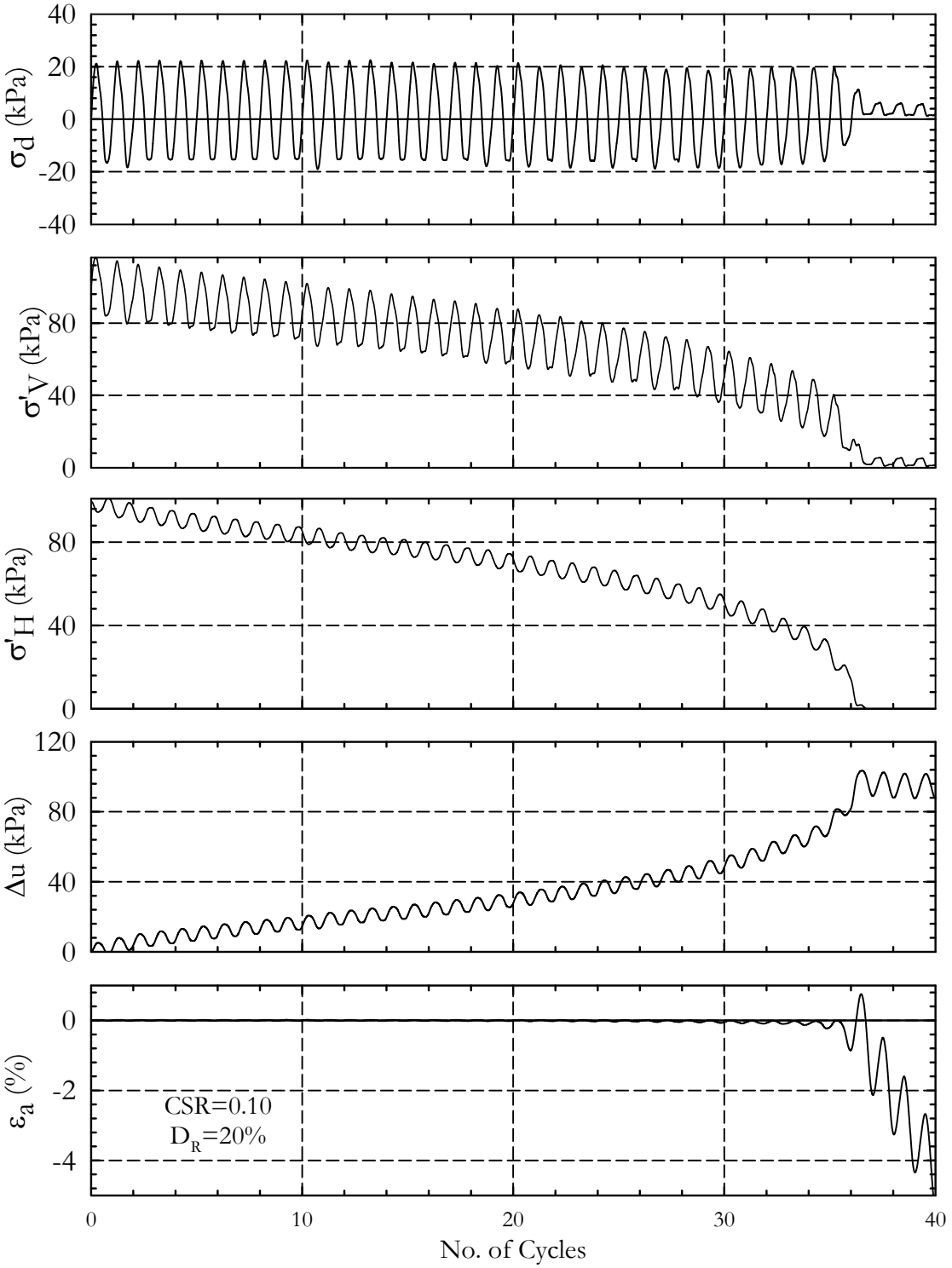

Figure II-4. Cyclic Parameters – Test CTX01

Test No.: CTX02
Test Ref.: 20080124_Cyclic01_D20_CSR
$D_{R(FINAL)}$: 20% (22.0%)
e: 1.128
σ'_{3CON}: 100 kPa
CSR: 0.15

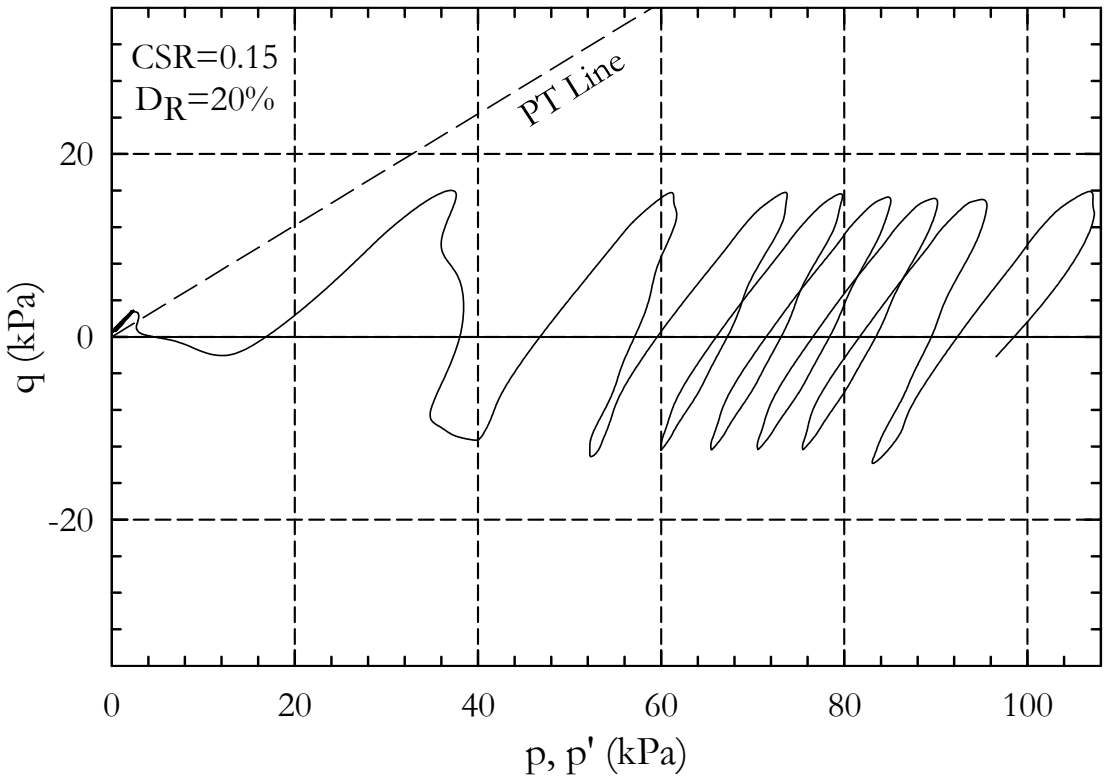

Figure II-5. Stress Path – CTX02

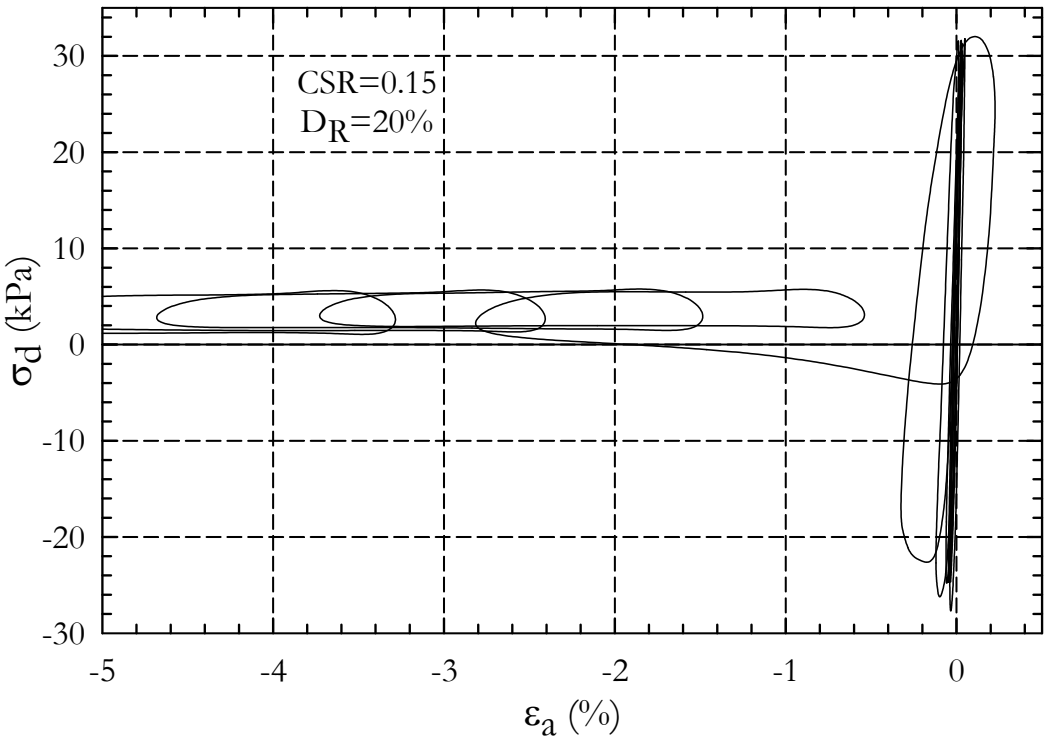

Figure II-6. Strain vs. Deviator stress– Test CTX02

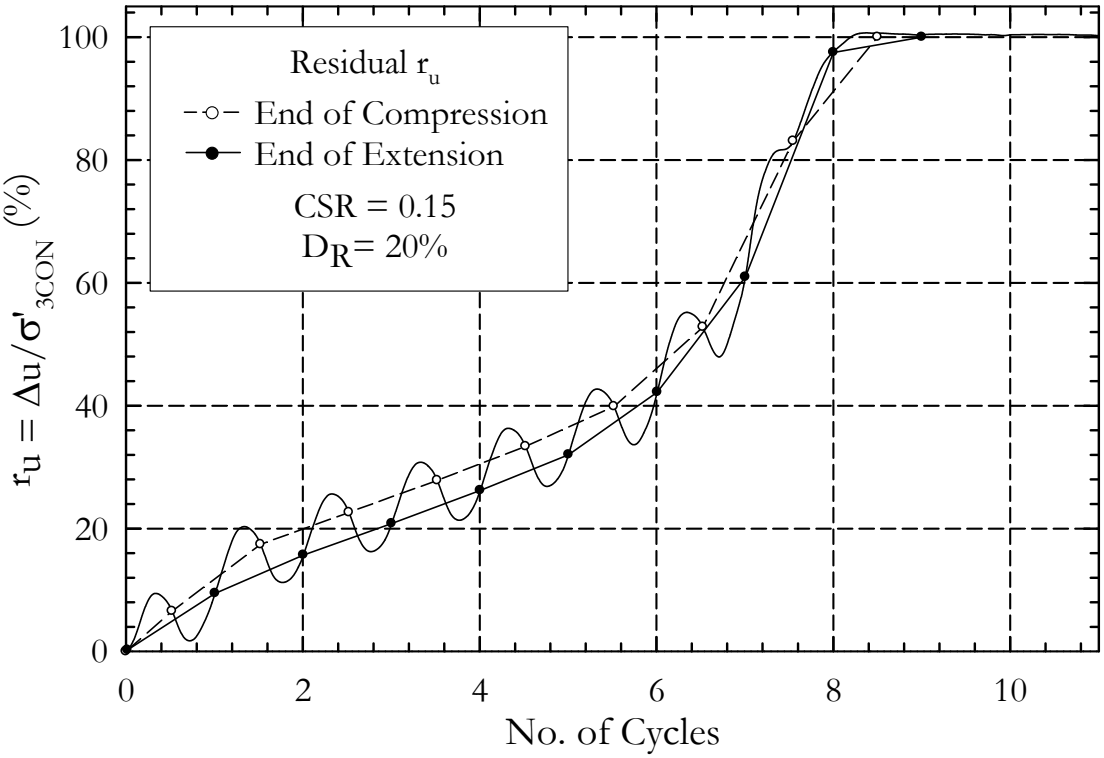

Figure II-7. Pore Pressure Ratio with Residual Pore Pressure – Test CTX02

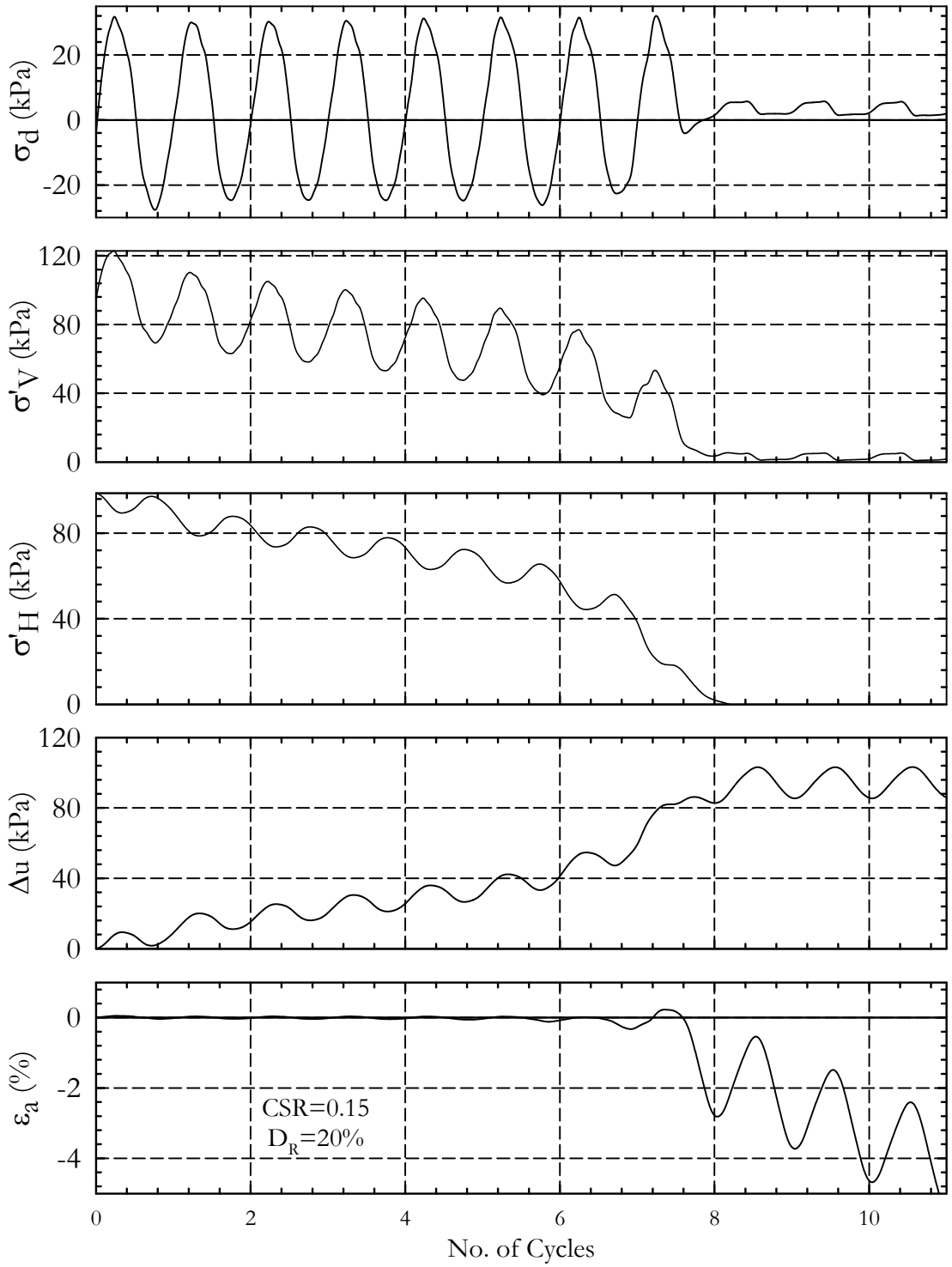

Figure II-8. Cyclic Parameters – Test CTX02

Test No.: CTX03
Test Ref.: 20071210_Cyclic01_D20_CSR2
$D_{R(FINAL)}$: 20% (23.6%)
e: 1.126
σ'_{3CON}: 100 kPa
CSR: 0.20

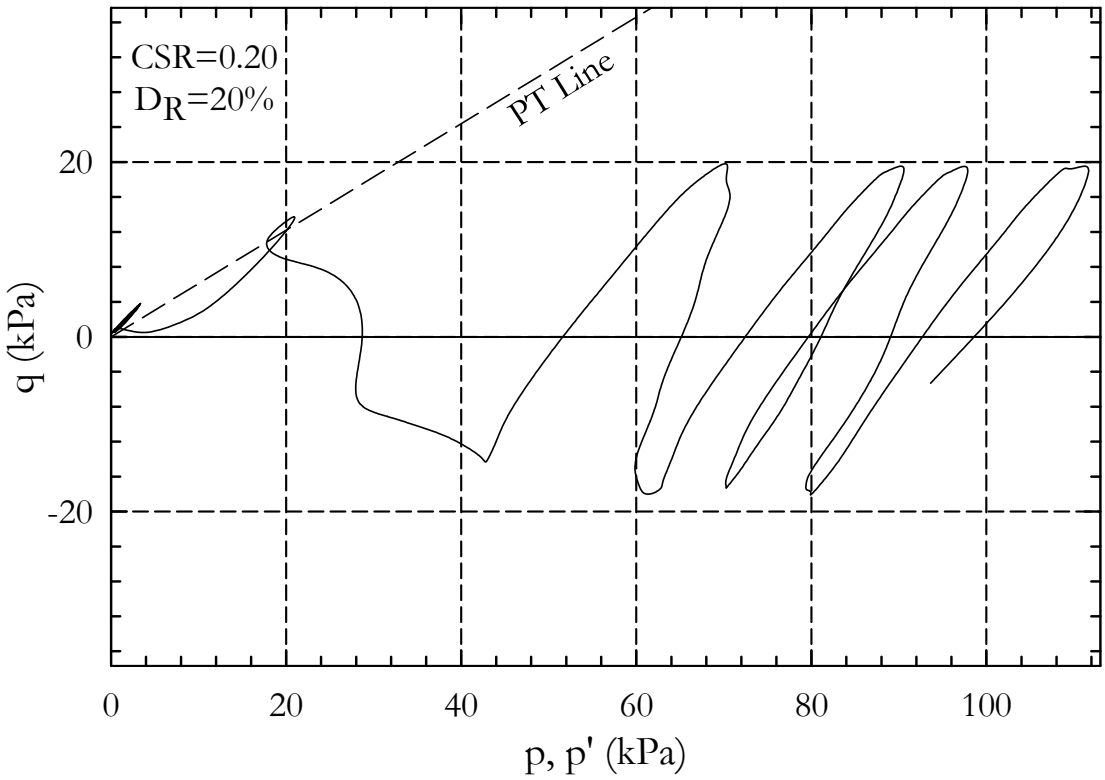

Figure II-9. Stress Path – CTX03

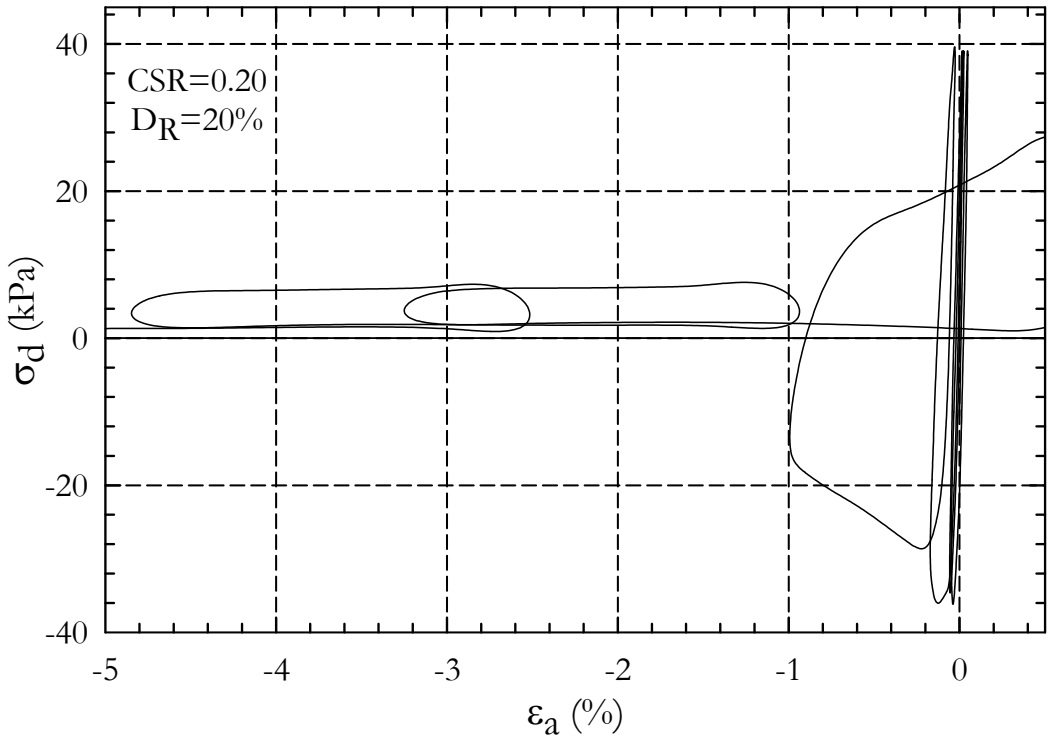

Figure II-10. Strain vs. Deviator stress– Test CTX03

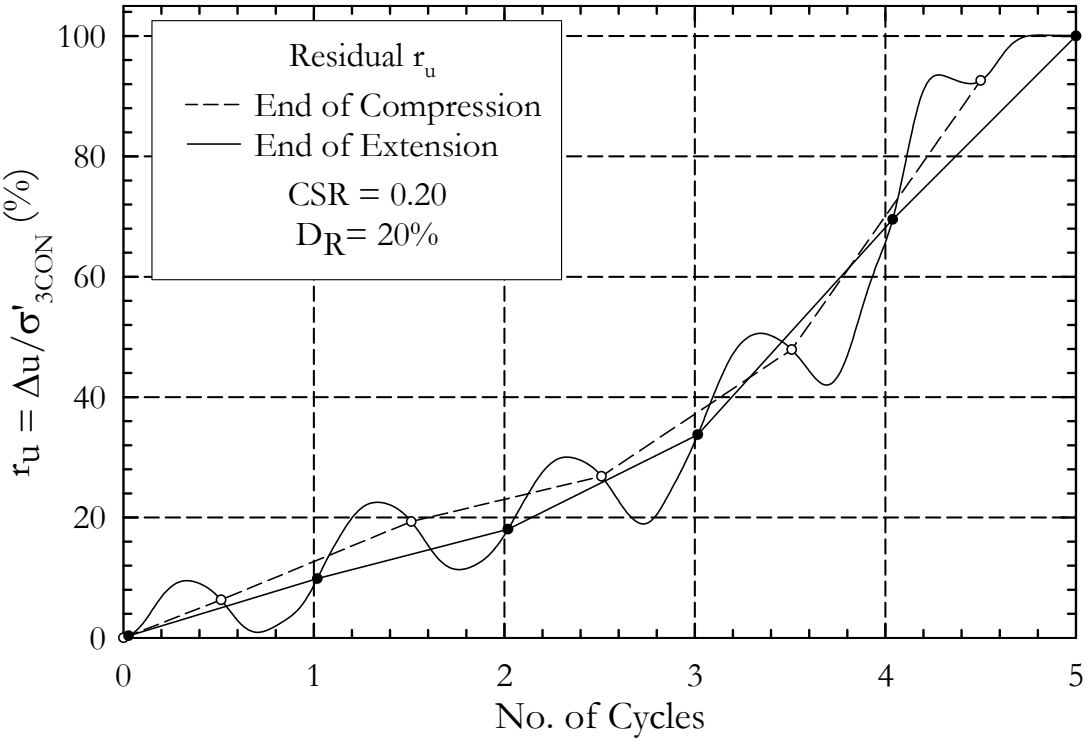

Figure II-11. Pore Pressure Ratio with Residual Pore Pressure – Test CTX03

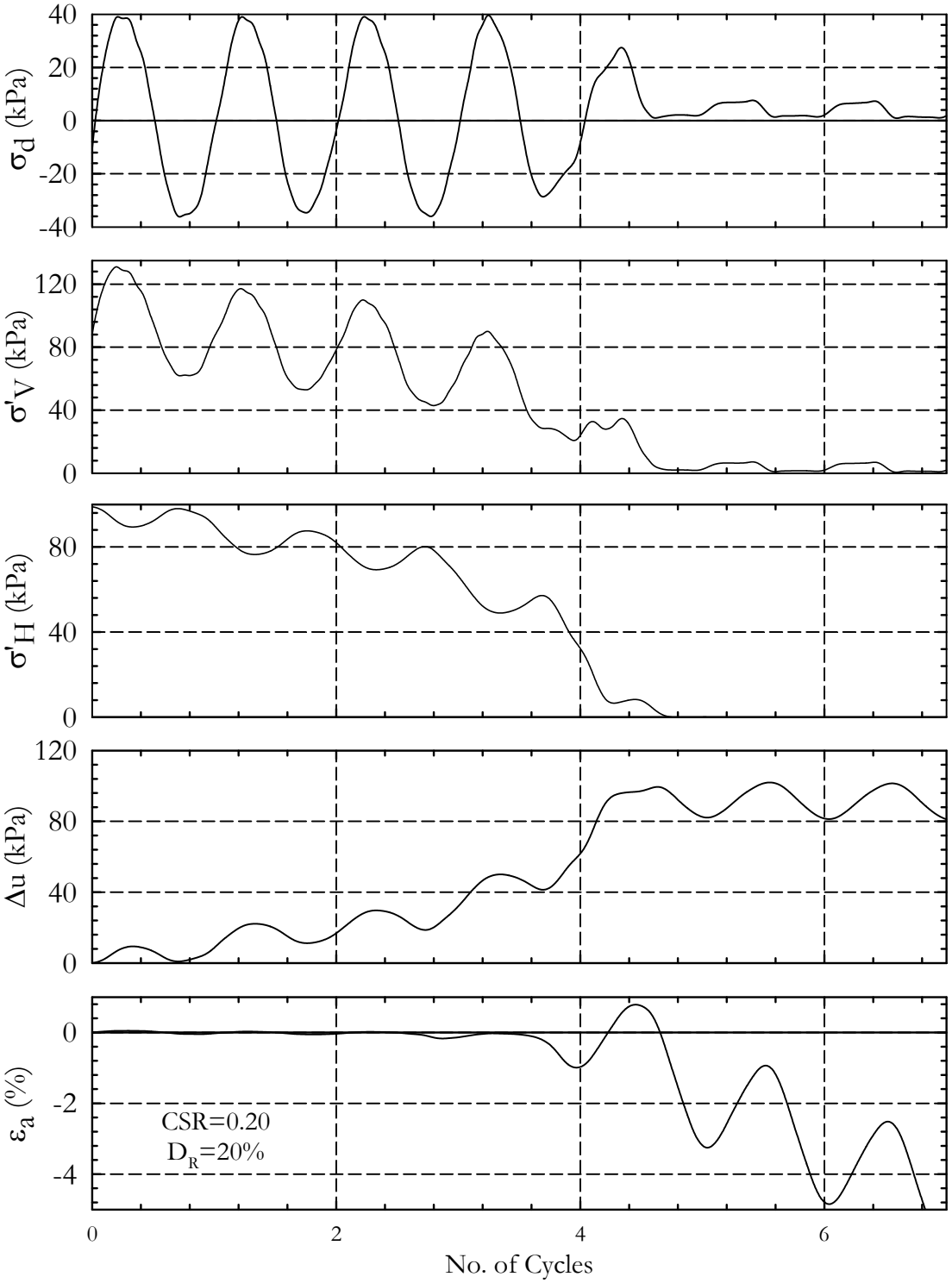

Figure II-12. Cyclic Parameters – Test CTX03

Test No.: CTX04
Test Ref.: 20071211_Cyclic01_D20_CSR15
$D_{R(FINAL)}$: 20% (23.1%)
e: 1.123
σ'_{3CON}: 100 kPa
CSR: 0.15

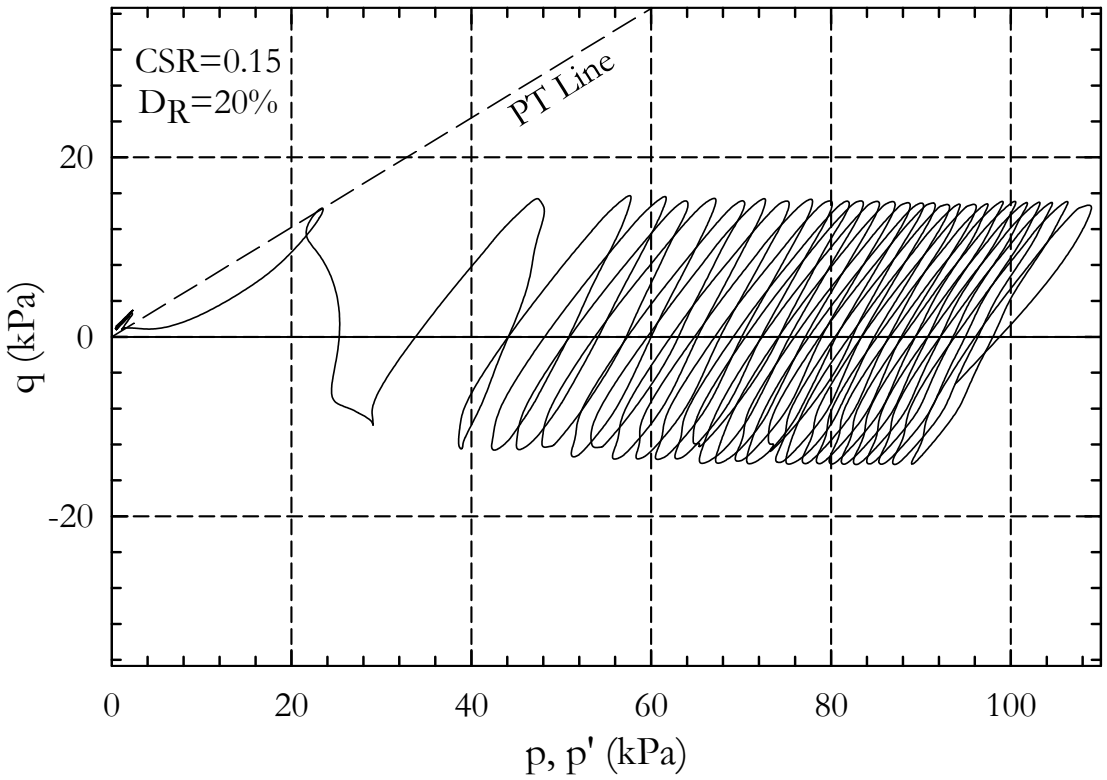

Figure II-13. Stress Path – CTX04

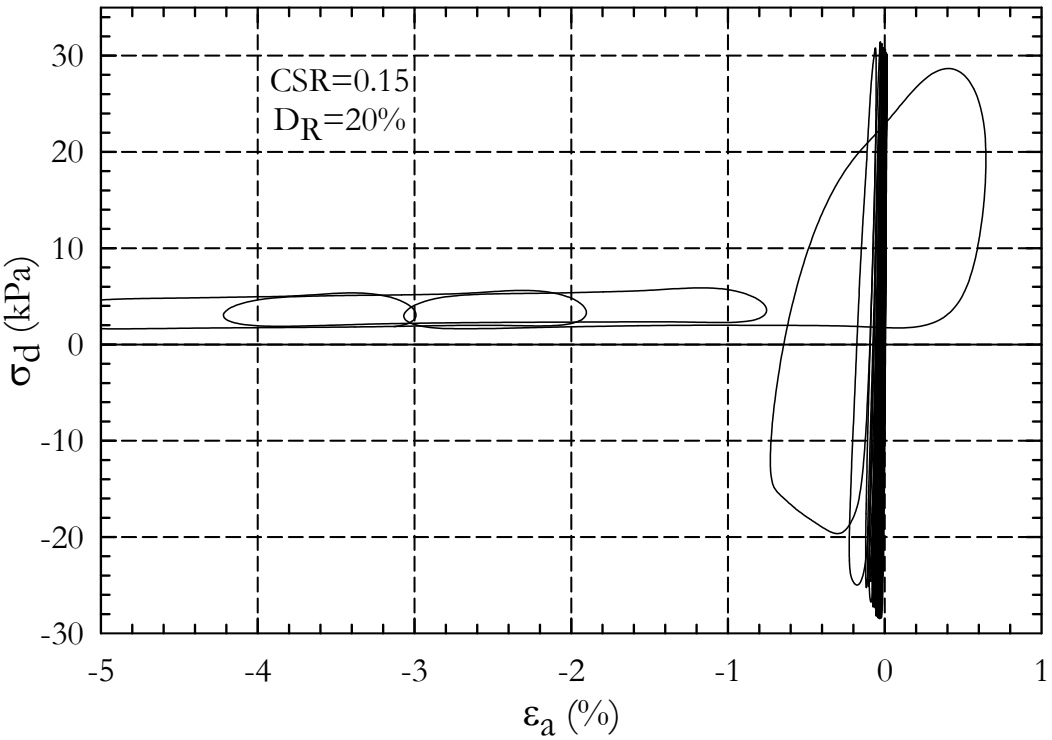

Figure II-14. Strain vs. Deviator stress– Test CTX04

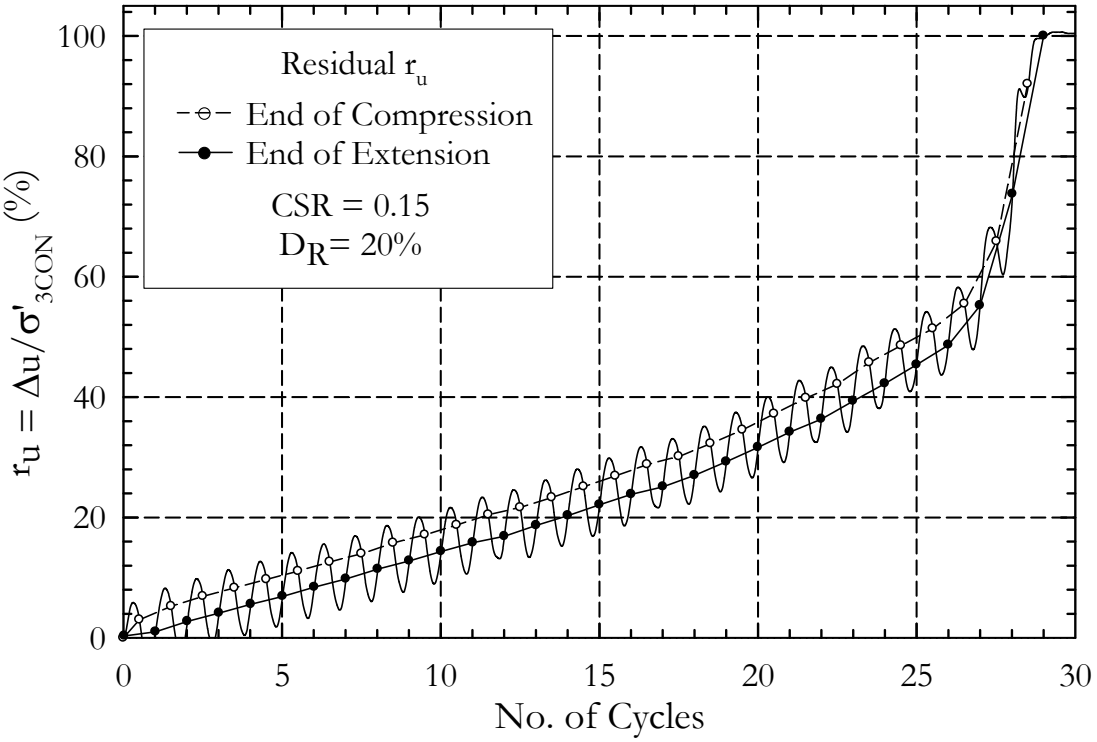

Figure II-15. Pore Pressure Ratio with Residual Pore Pressure – Test CTX04

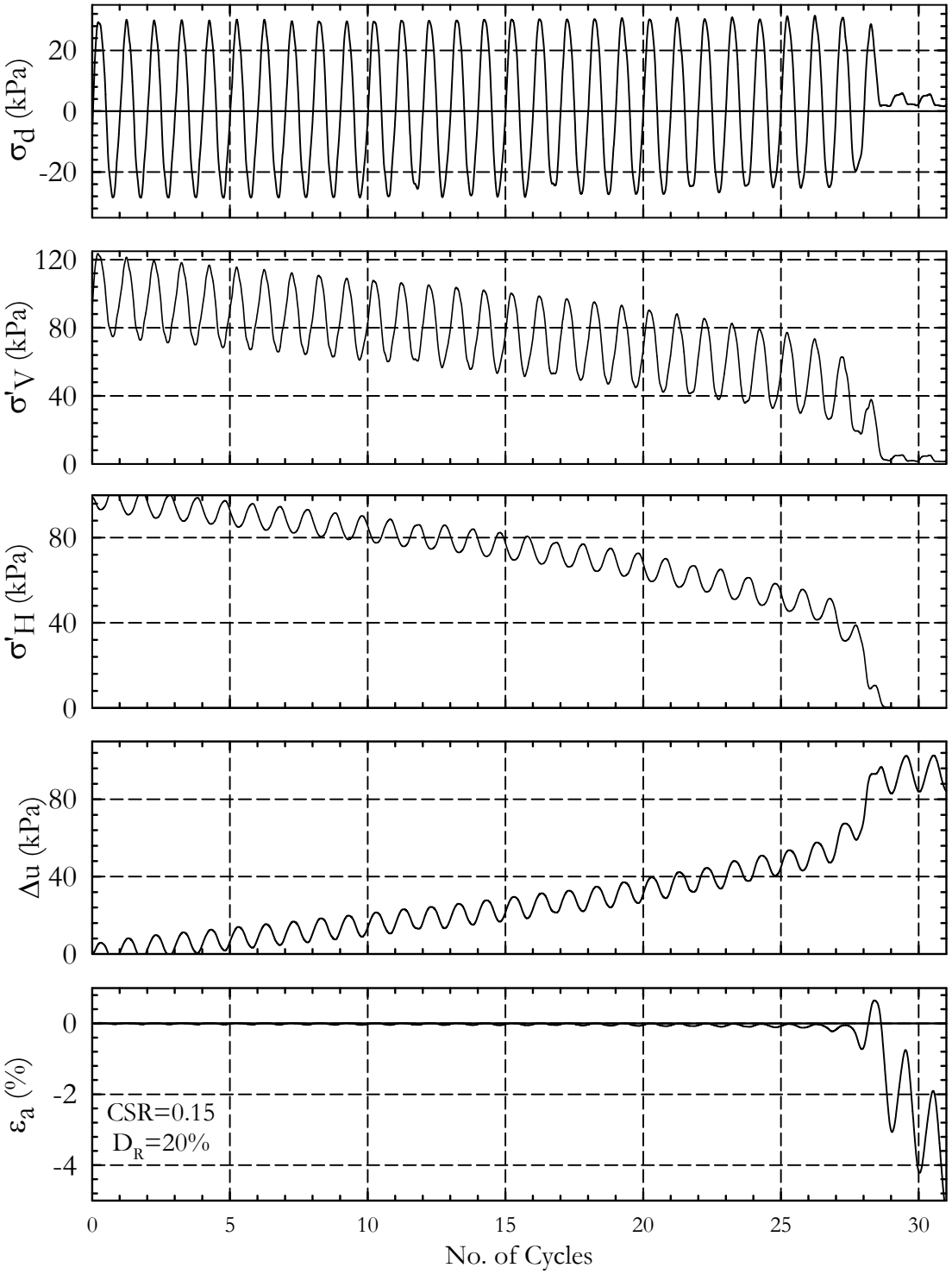

Figure II-16. Cyclic Parameters – Test CTX04

Test No.: CTX05
Test Ref.: 20080125_Cyclic01_D20_CSR
$D_{R(FINAL)}$: 20% (23.2%)
e: 1.123
σ'_{3CON}: 100 kPa
CSR: 0.13

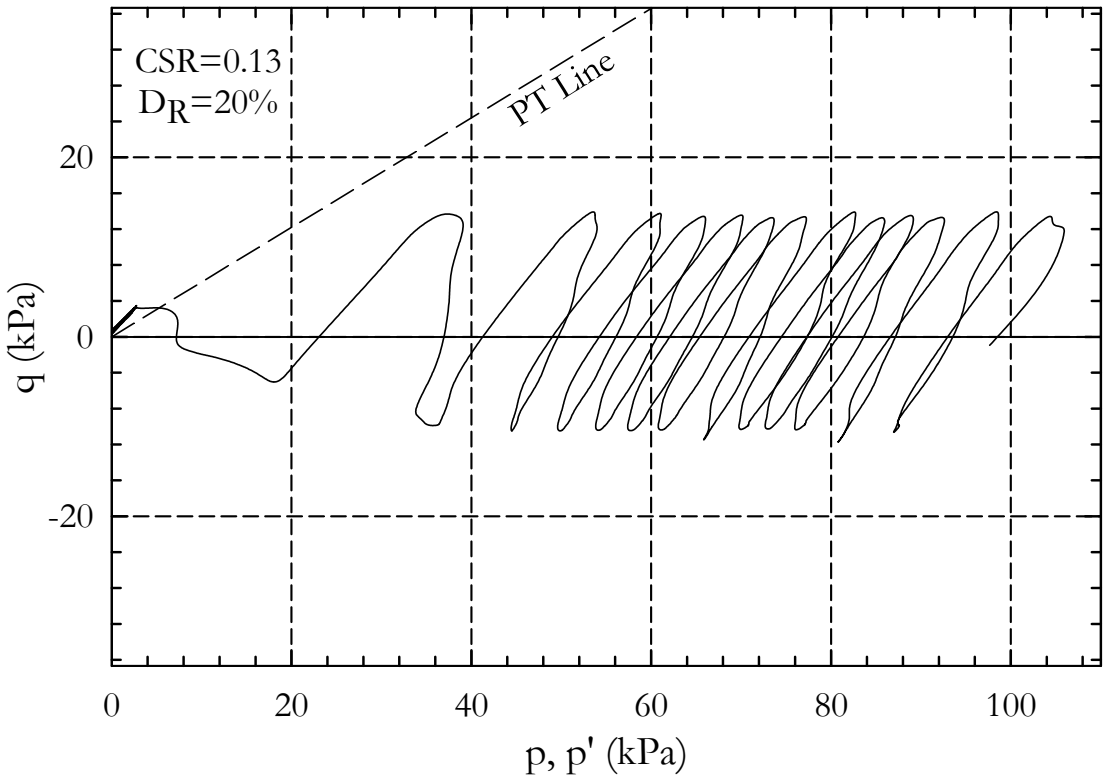

Figure II-17. Stress Path – CTX05

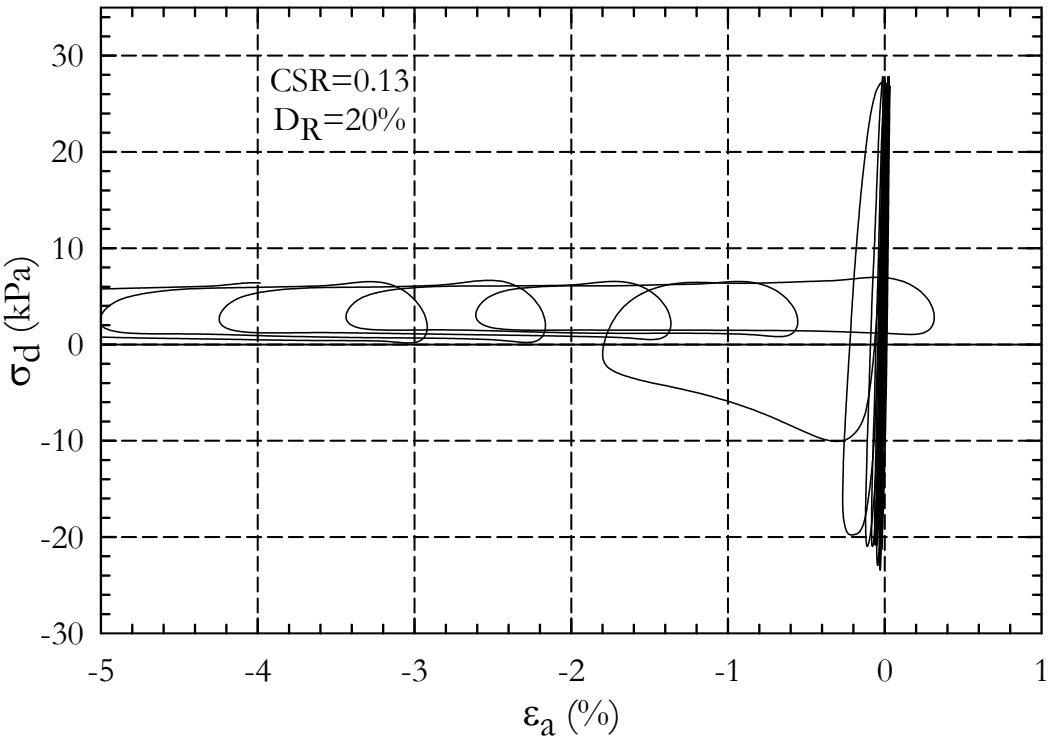

Figure II-18. Strain vs. Deviator stress– Test CTX05

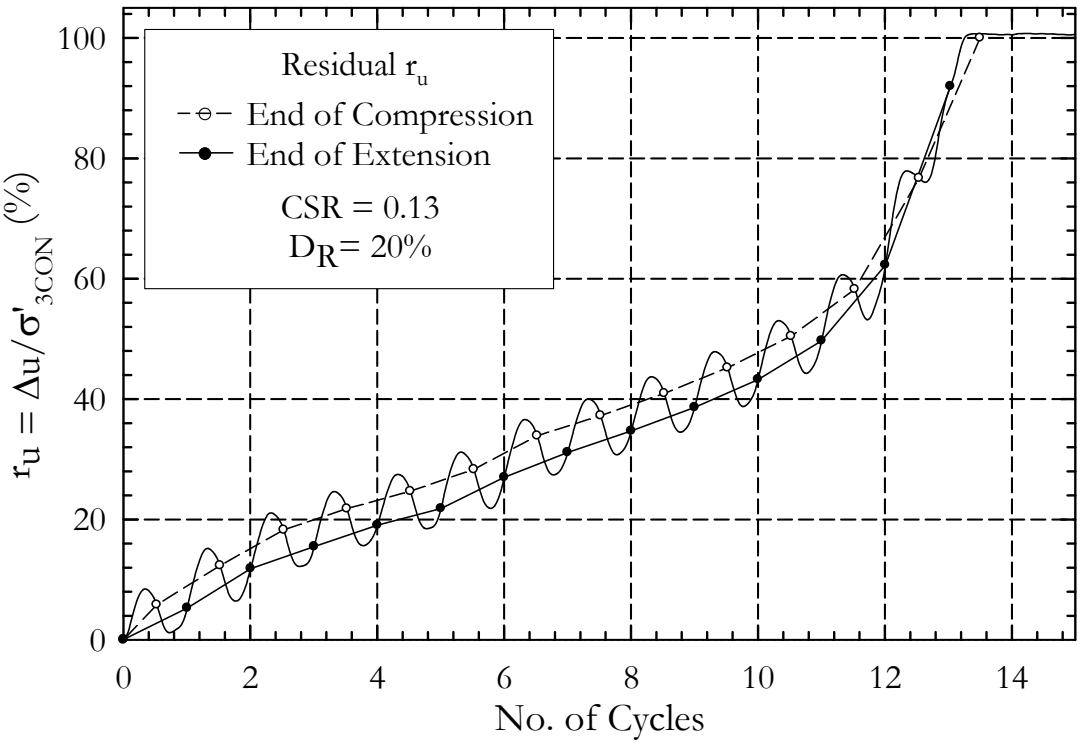

Figure II-19. Pore Pressure Ratio with Residual Pore Pressure – Test CTX05

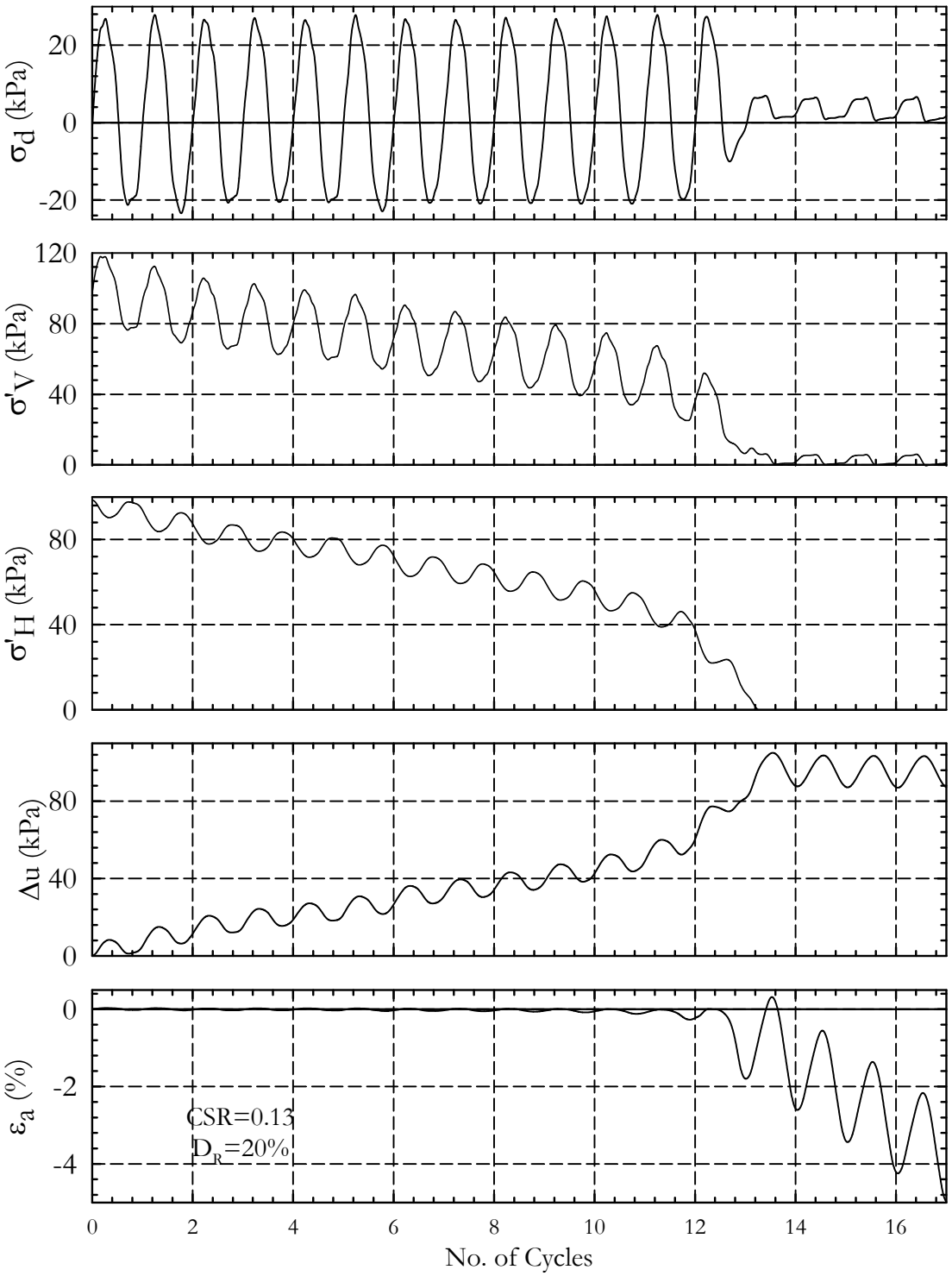

Figure II-20. Cyclic Parameters – Test CTX05

Test No.: CTX06
Test Ref.: 20071206_Cyclic01_D40_CSR25
$D_{R(FINAL)}$: 40% (38.4%)
e: 1.059
σ'_{3CON}: 100 kPa
CSR: 0.25

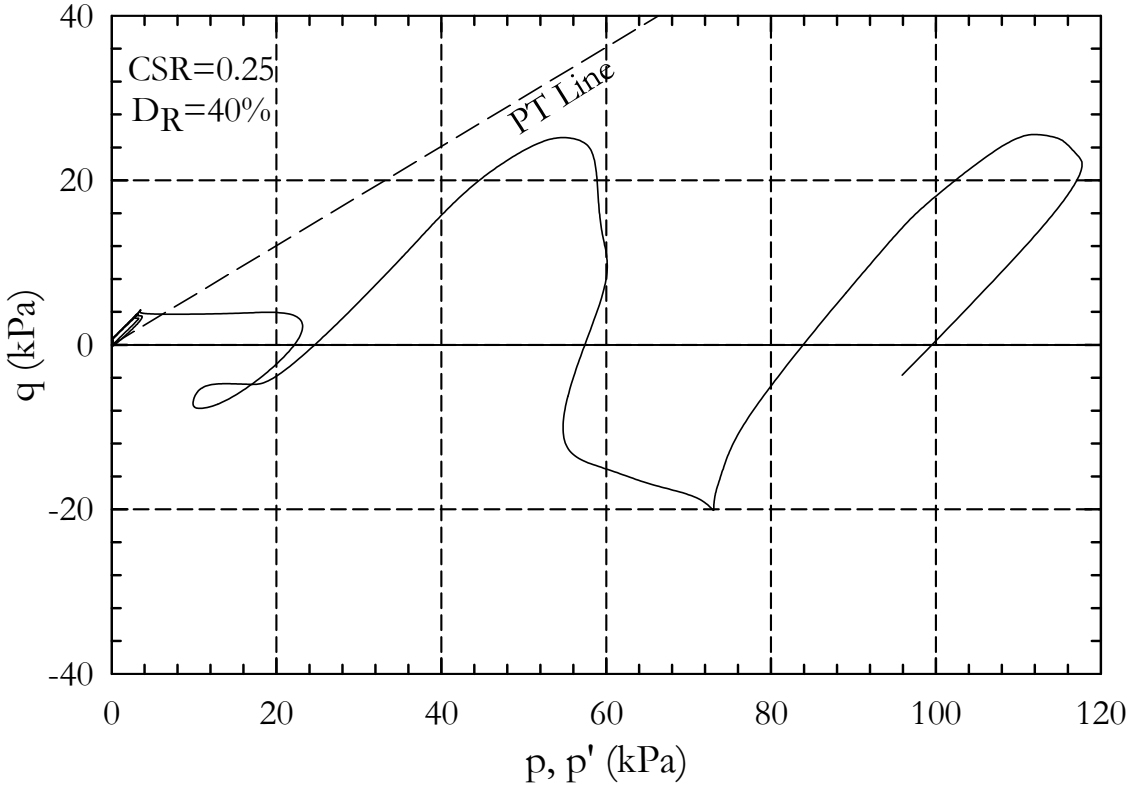

Figure II-21. Stress Path – CTX06

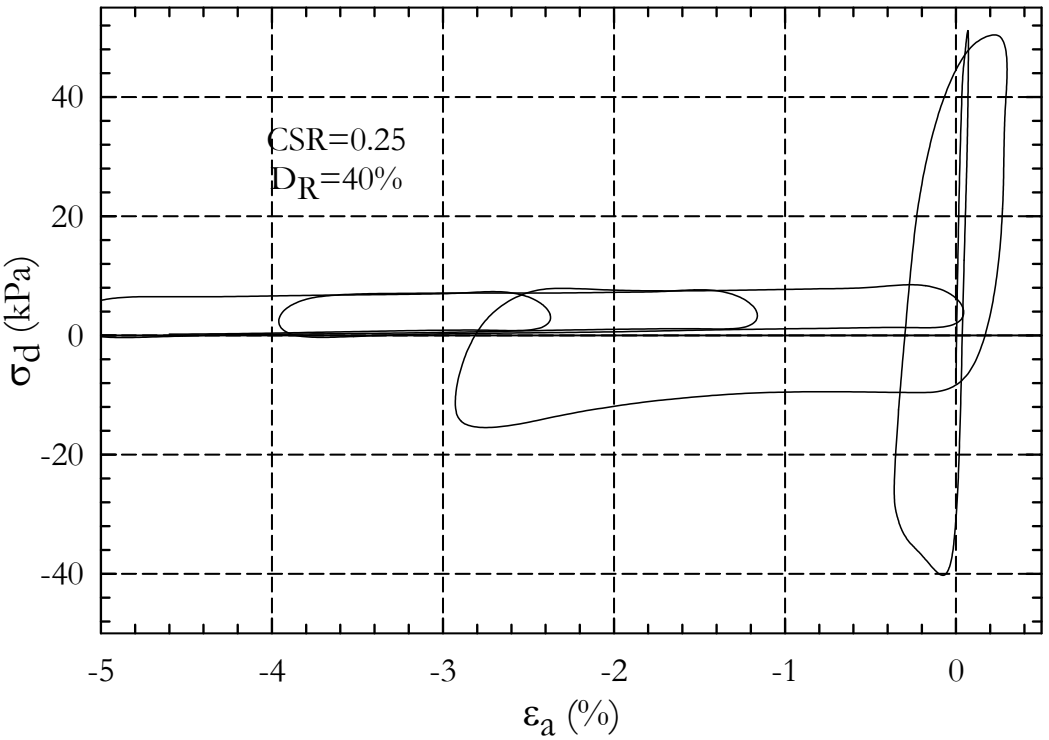

Figure II-22. Strain vs. Deviator stress– Test CTX06

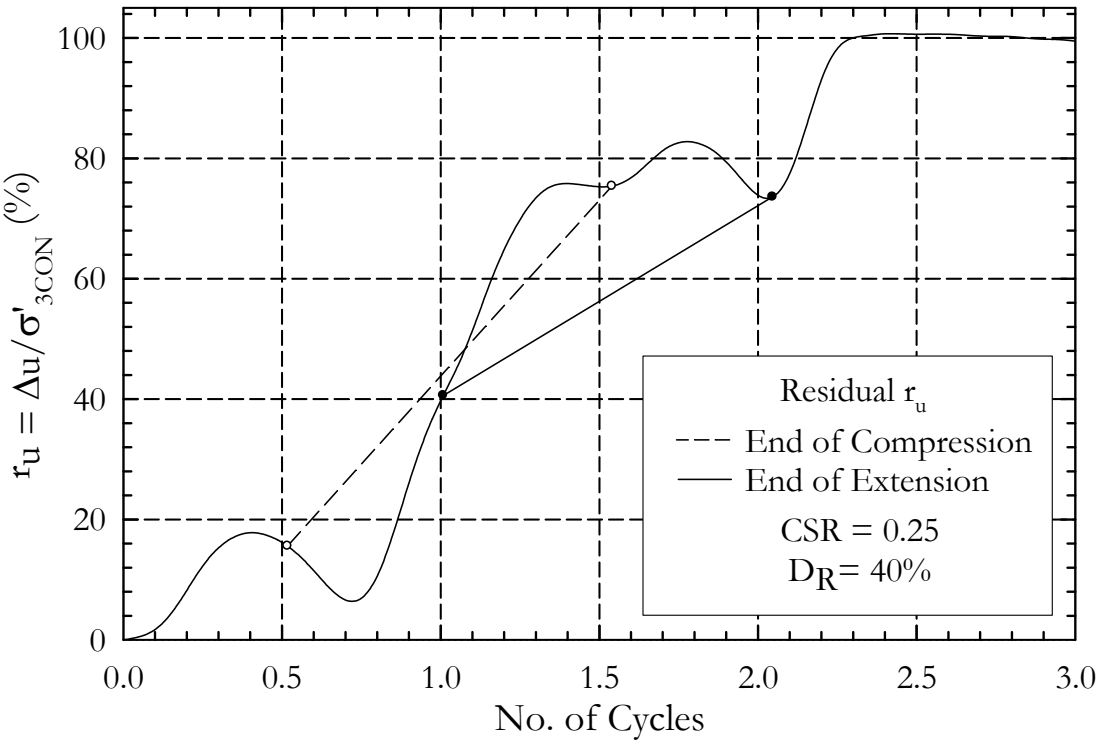

Figure II-23. Pore Pressure Ratio with Residual Pore Pressure – Test CTX06

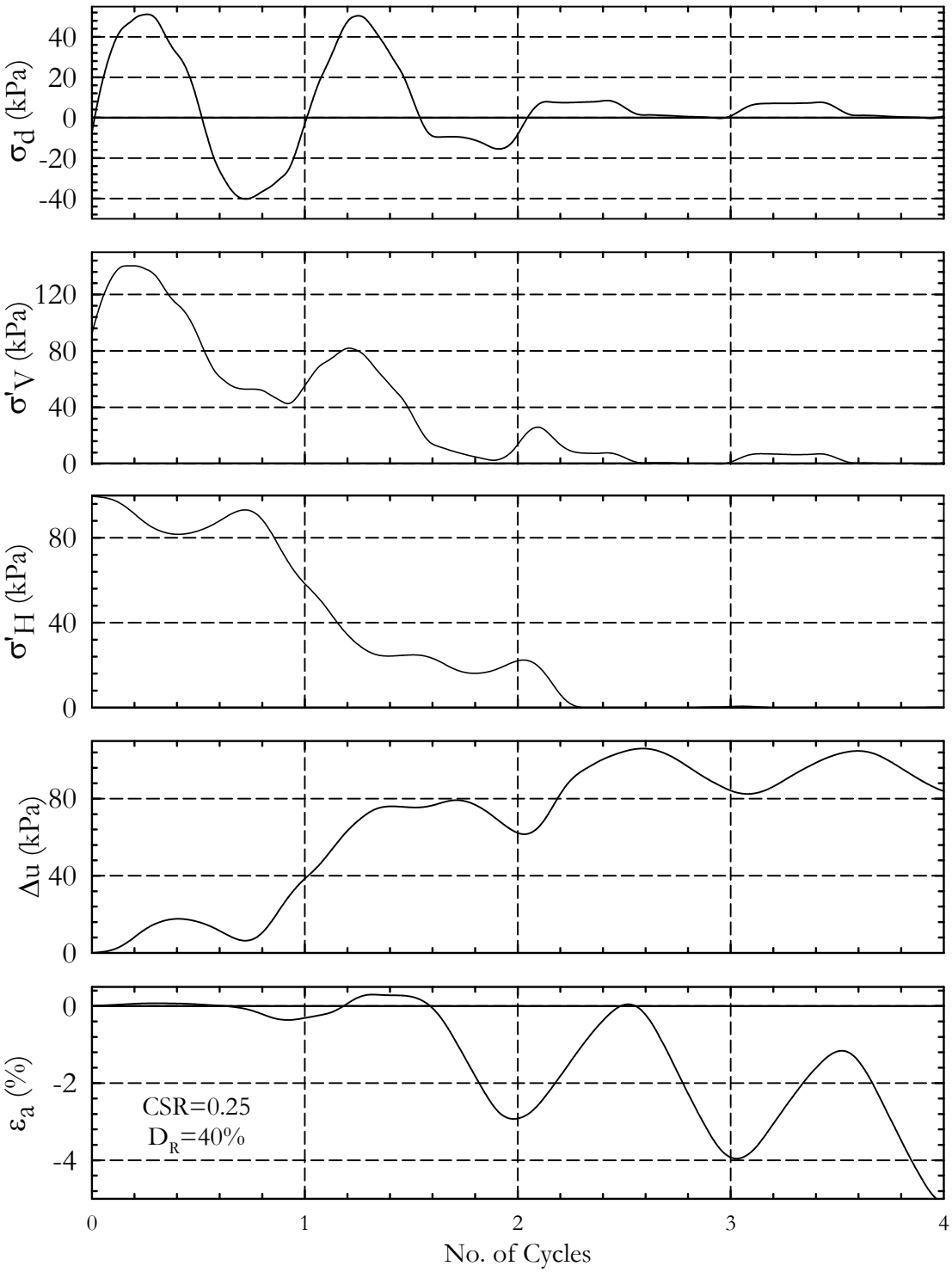

Figure II-24. Cyclic Parameters – Test CTX06

Test No.: CTX07
Test Ref.: 20071206_Cyclic02_D40_CSR2
$D_{R(FINAL)}$: 40% (41.3%)
e: 1.047
σ'_{3CON}: 100 kPa
CSR: 0.20

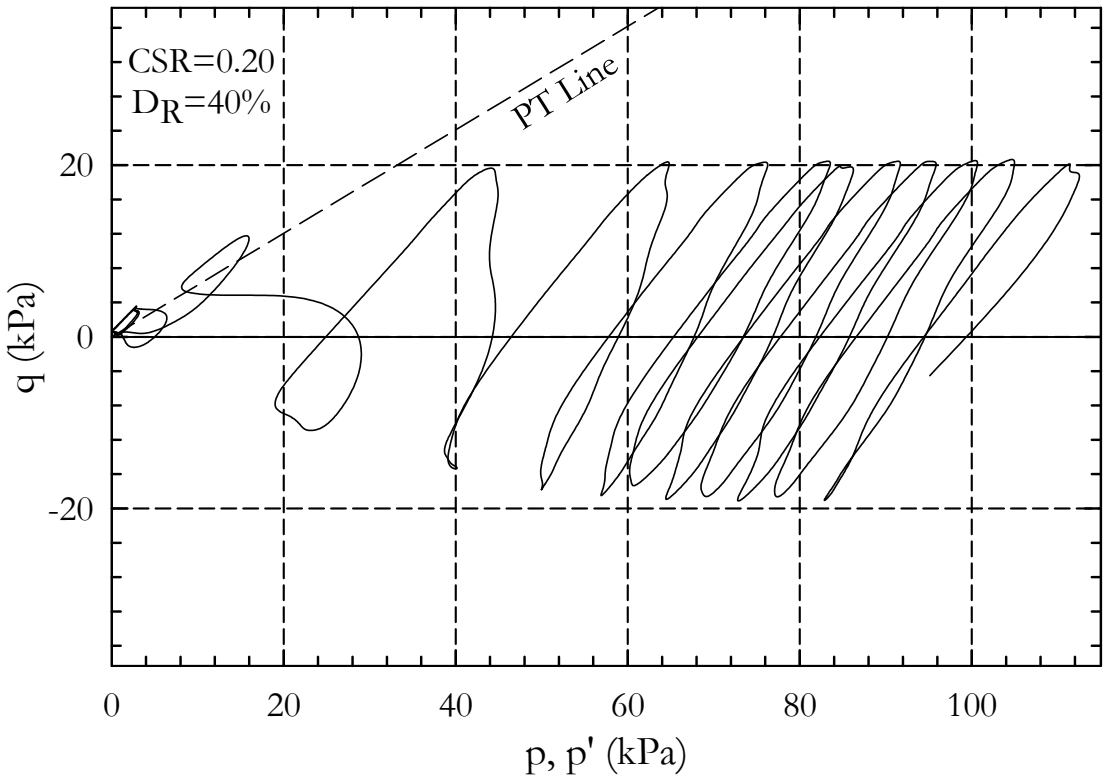

Figure II-25. Stress Path – CTX07

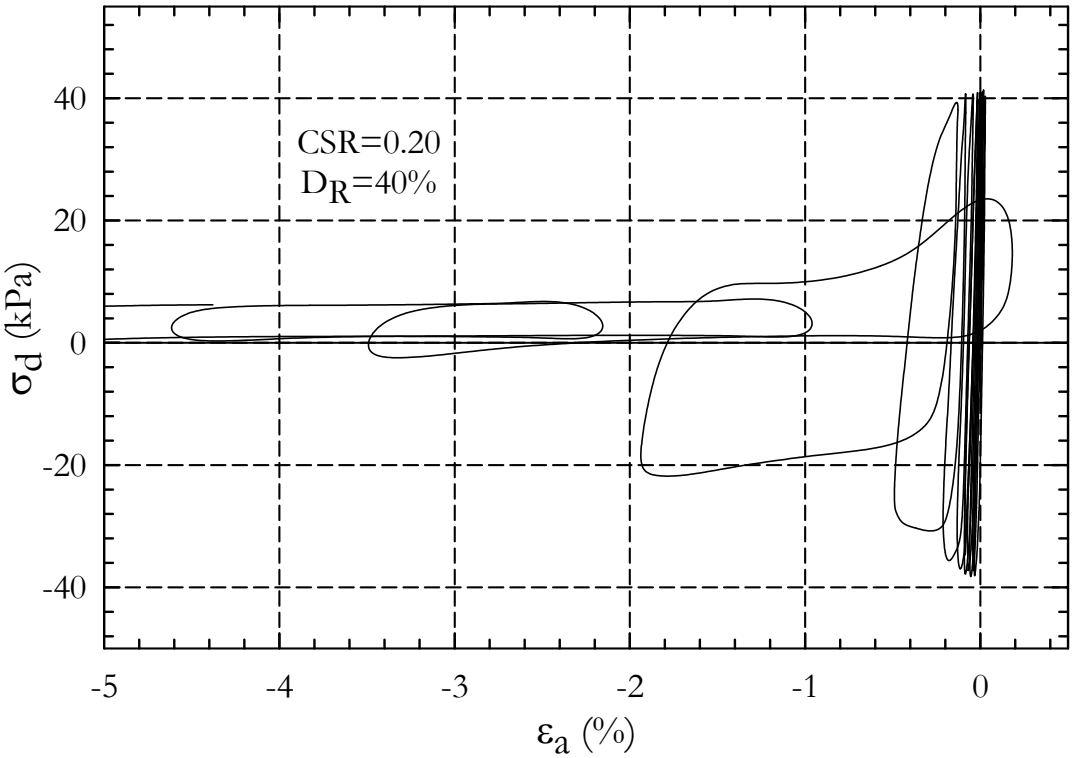

Figure II-26. Strain vs. Deviator stress– Test CTX07

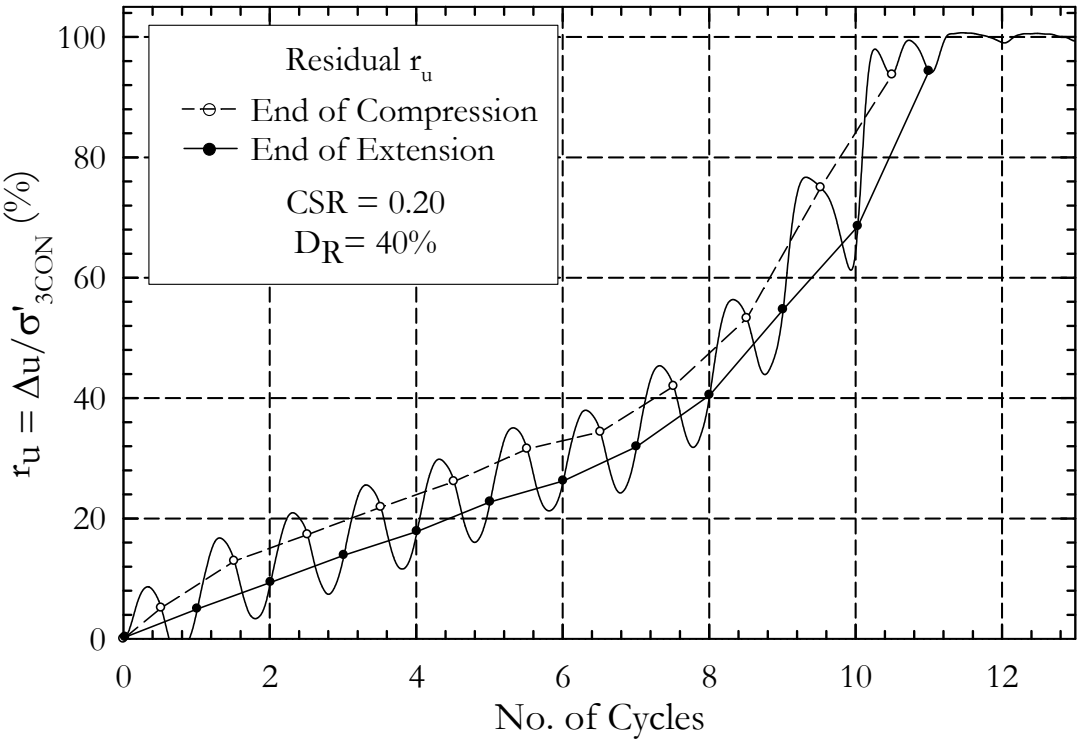

Figure II-27. Pore Pressure Ratio with Residual Pore Pressure – Test CTX07

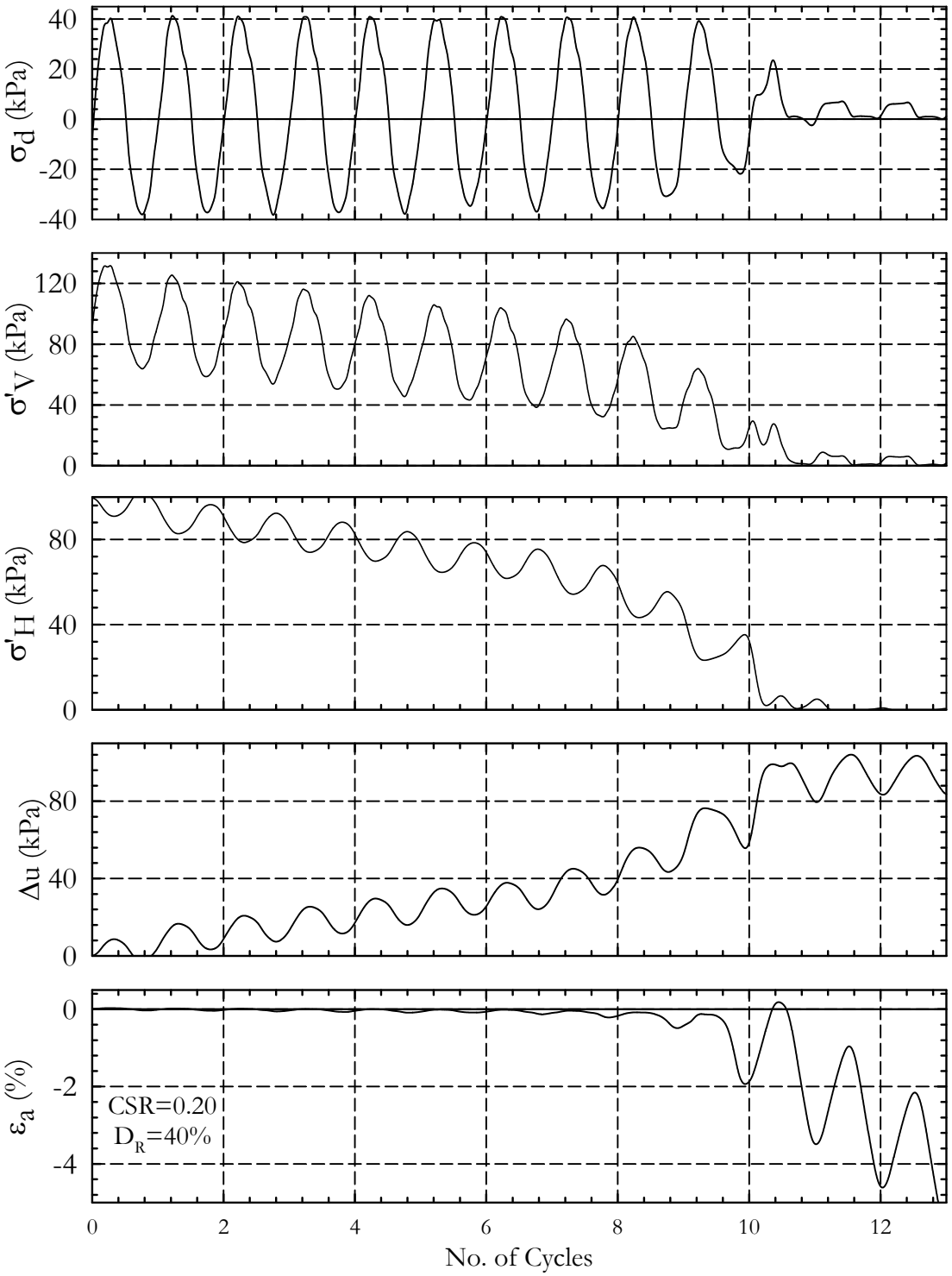

Figure II-28. Cyclic Parameters – Test CTX07

Test No.: CTX08
Test Ref.: 20071207_Cyclic01_D40_CSR15
$D_{R(FINAL)}$: 40% (42.6%)
e: 1.042
σ'_{3CON}: 100 kPa
CSR: 0.15

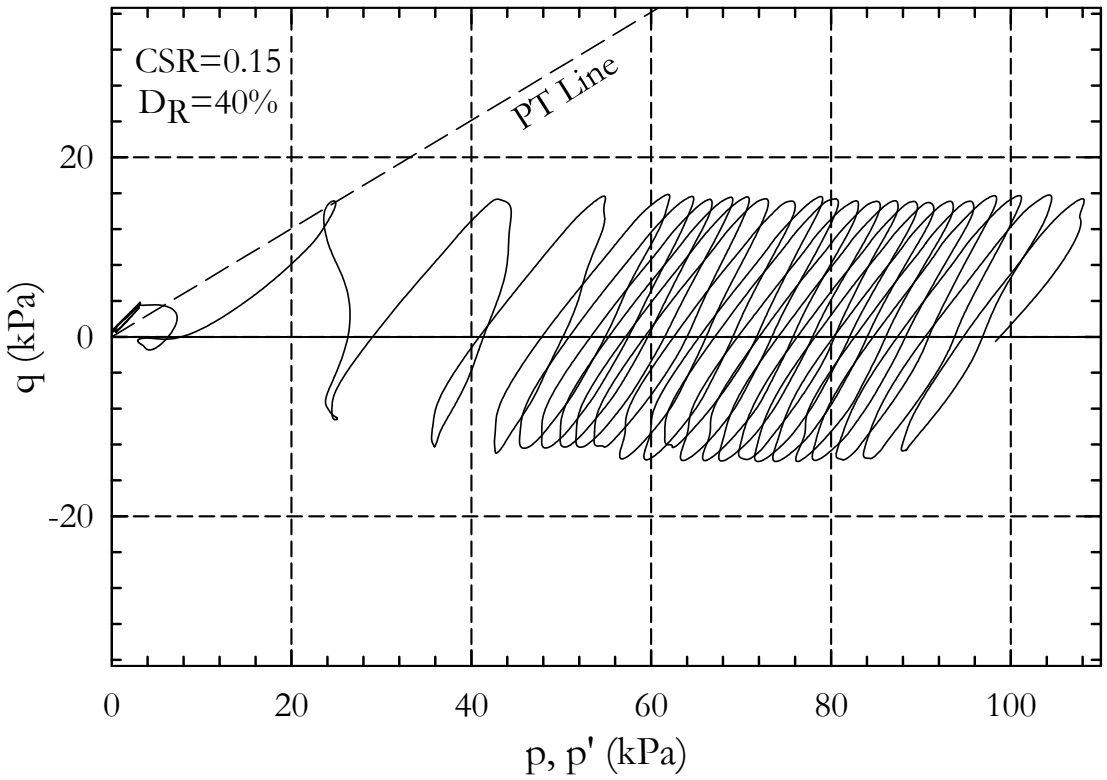

Figure II-29. Stress Path – CTX08

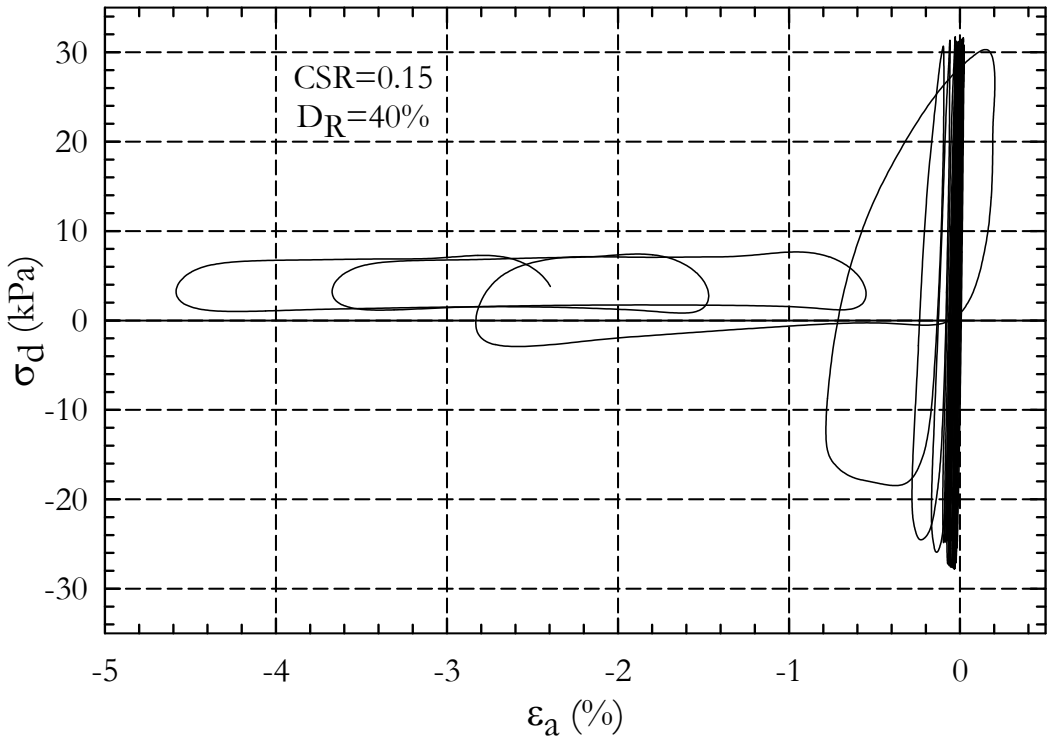

Figure II-30. Strain vs. Deviator stress– Test CTX08

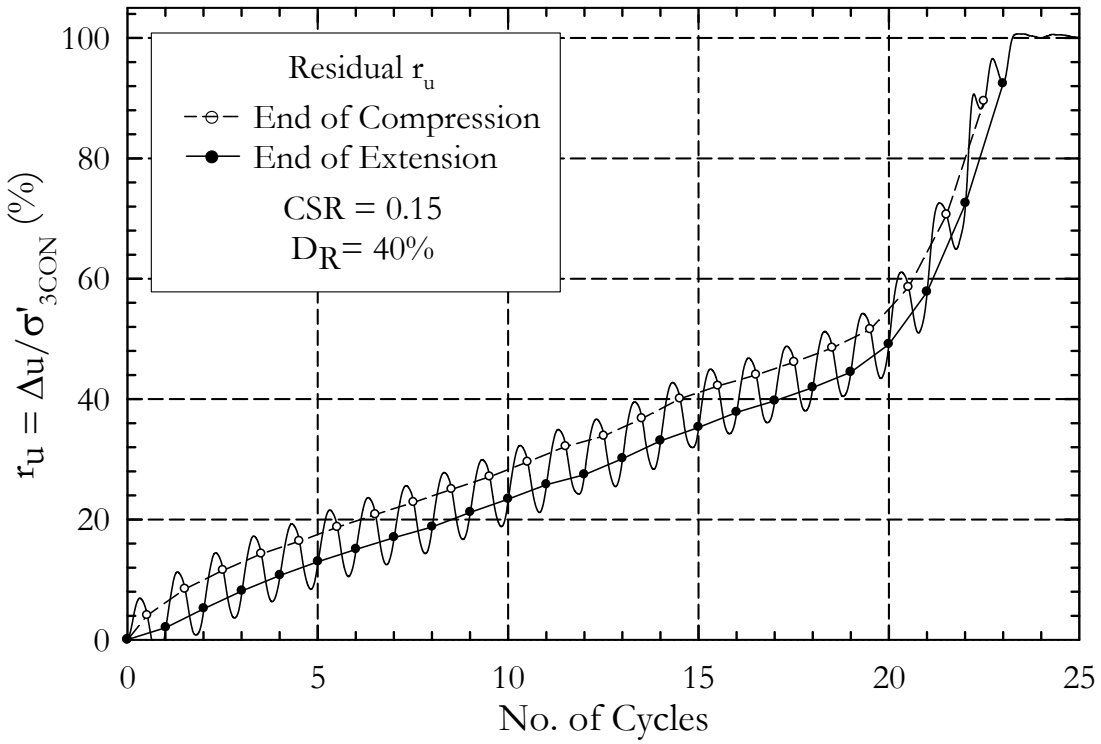

Figure II-31. Pore Pressure Ratio with Residual Pore Pressure – Test CTX08

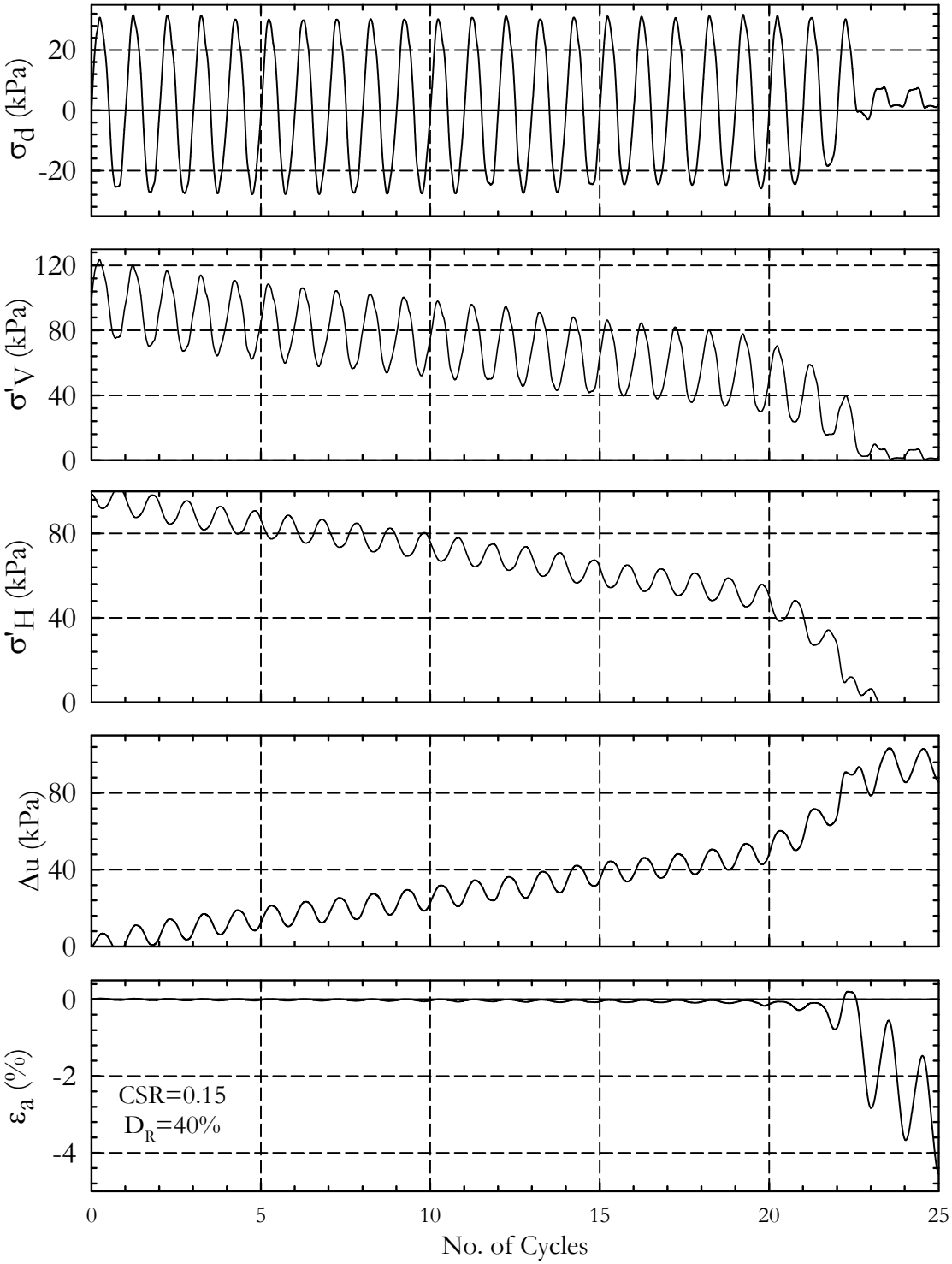

Figure II-32. Cyclic Parameters – Test CTX08

Test No.: CTX09
Test Ref.: 20080217_Cyclic01_D60_CSR
$D_{R(FINAL)}$: 60% (55.4%)
e: 0.988
σ'_{3CON}: 100 kPa
CSR: 0.30

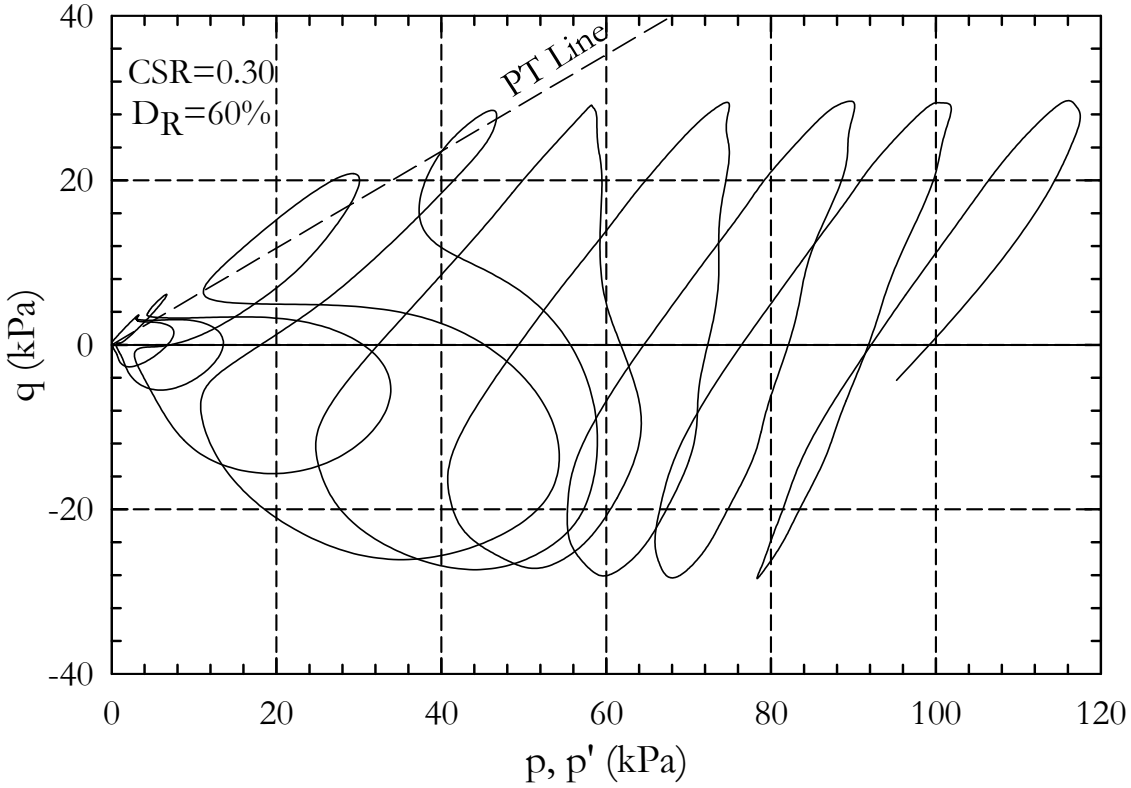

Figure II-33. Stress Path – CTX09

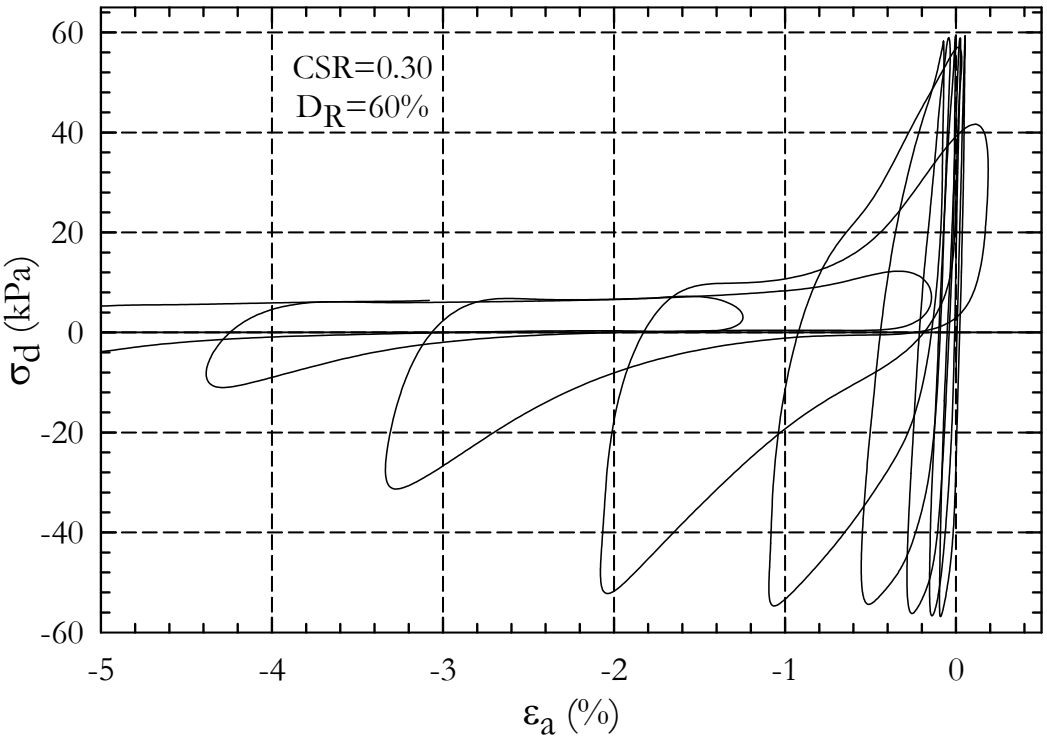

Figure II-34. Strain vs. Deviator stress– Test CTX09

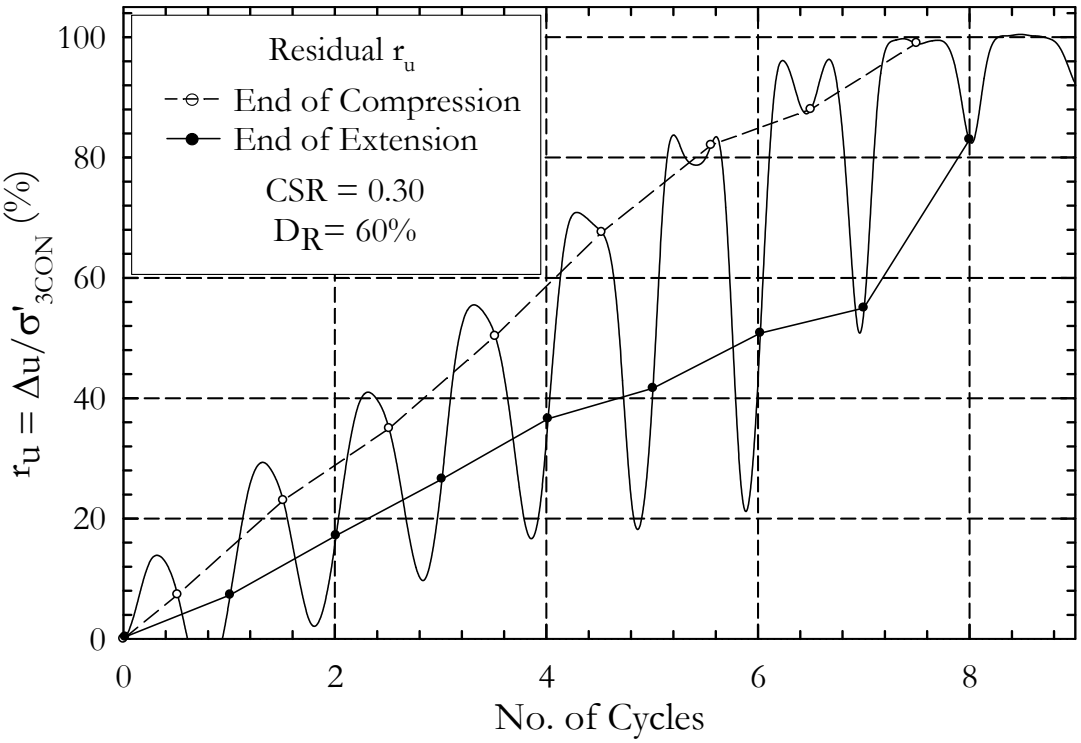

Figure II-35. Pore Pressure Ratio with Residual Pore Pressure – Test CTX09

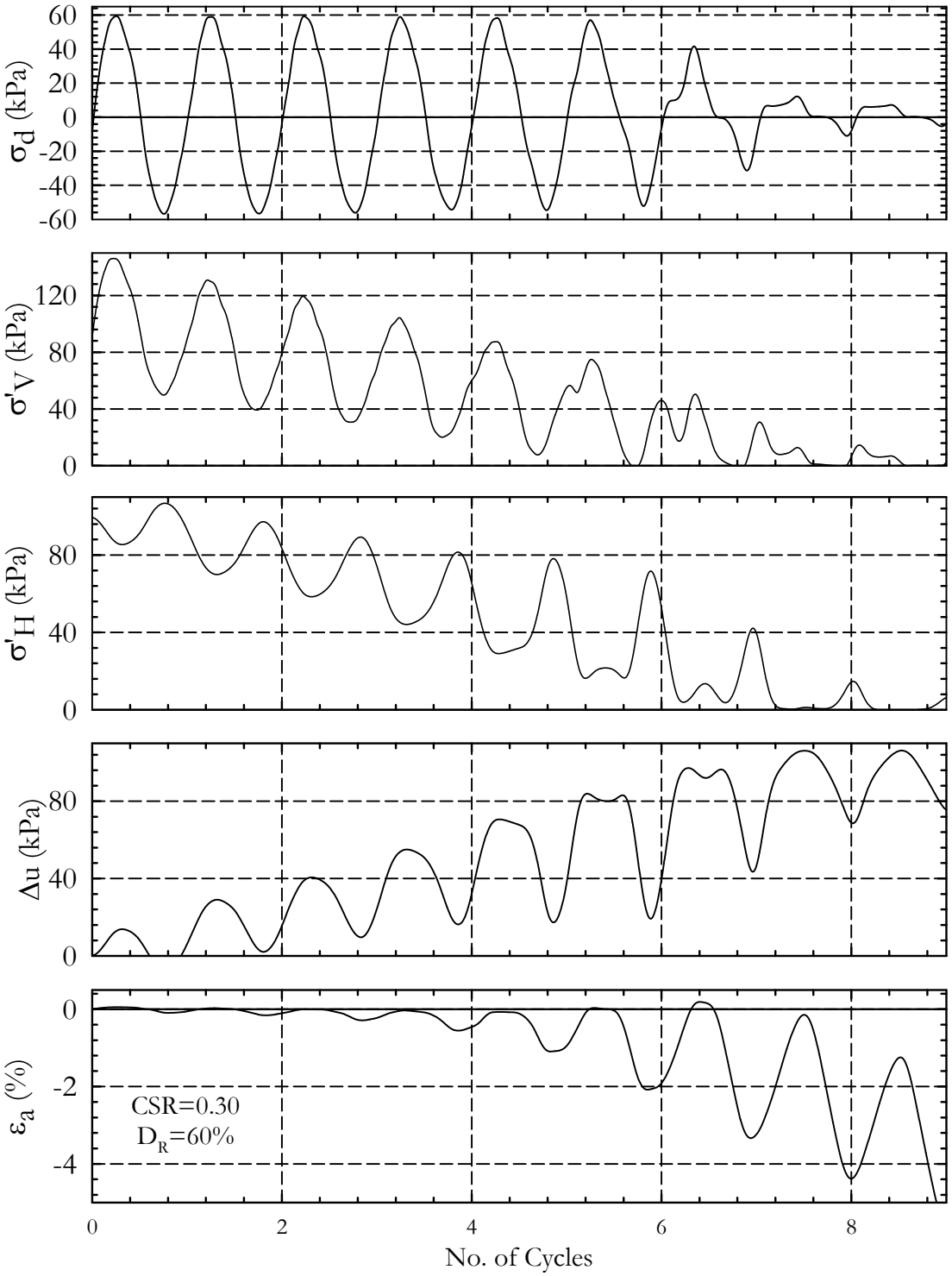

Figure II-36. Cyclic Parameters – Test CTX09

Test No.: CTX10
Test Ref.: 20080114_Cyclic01_D60_CSR35
$D_{R(FINAL)}$: 60% (56.6%)
e: 0.983
σ'_{3CON}: 100 kPa
CSR: 0.35

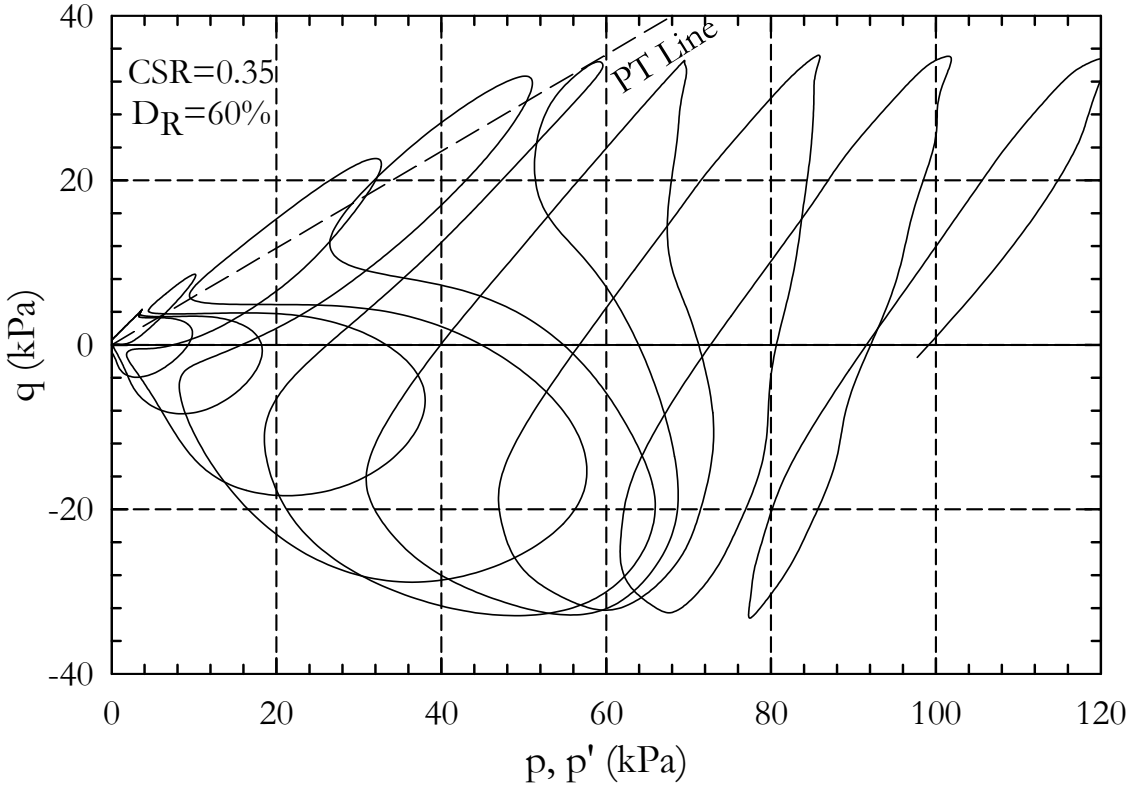

Figure II-37. Stress Path – CTX10

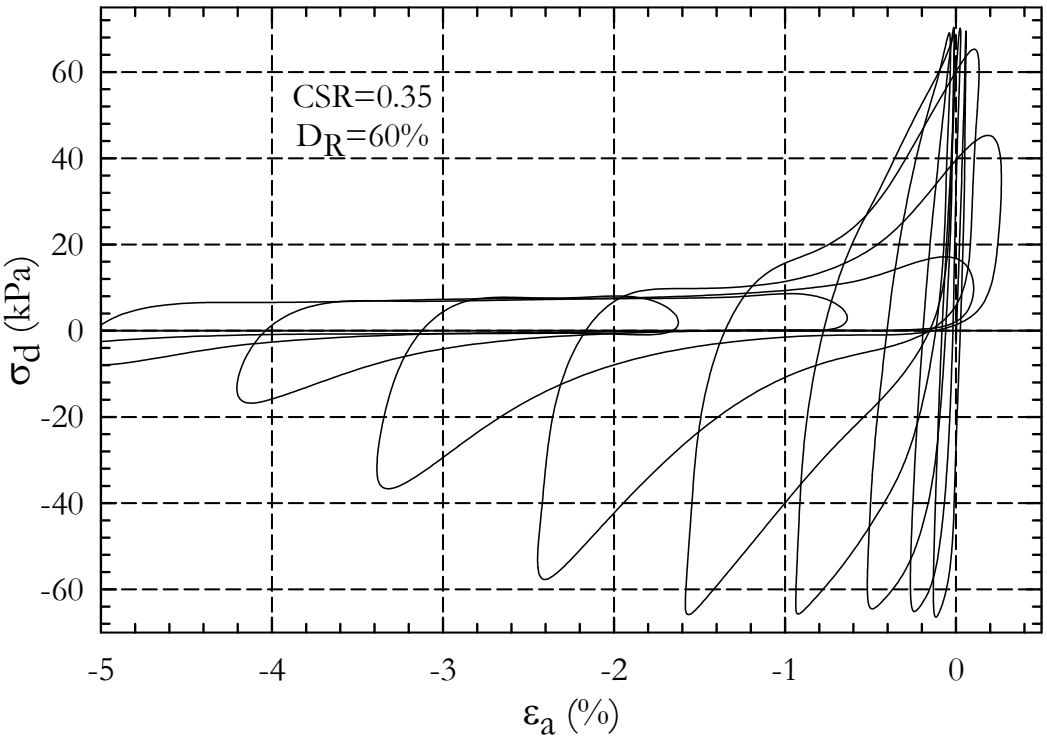

Figure II-38. Strain vs. Deviator stress– Test CTX10

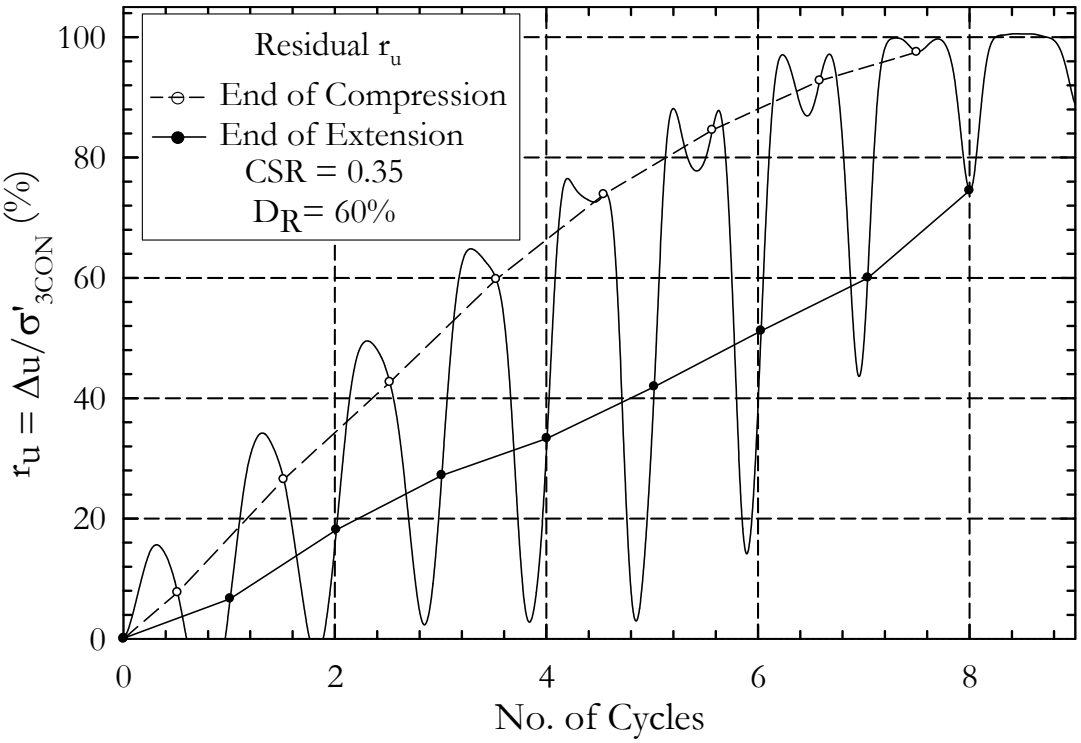

Figure II-39. Pore Pressure Ratio with Residual Pore Pressure – Test CTX10

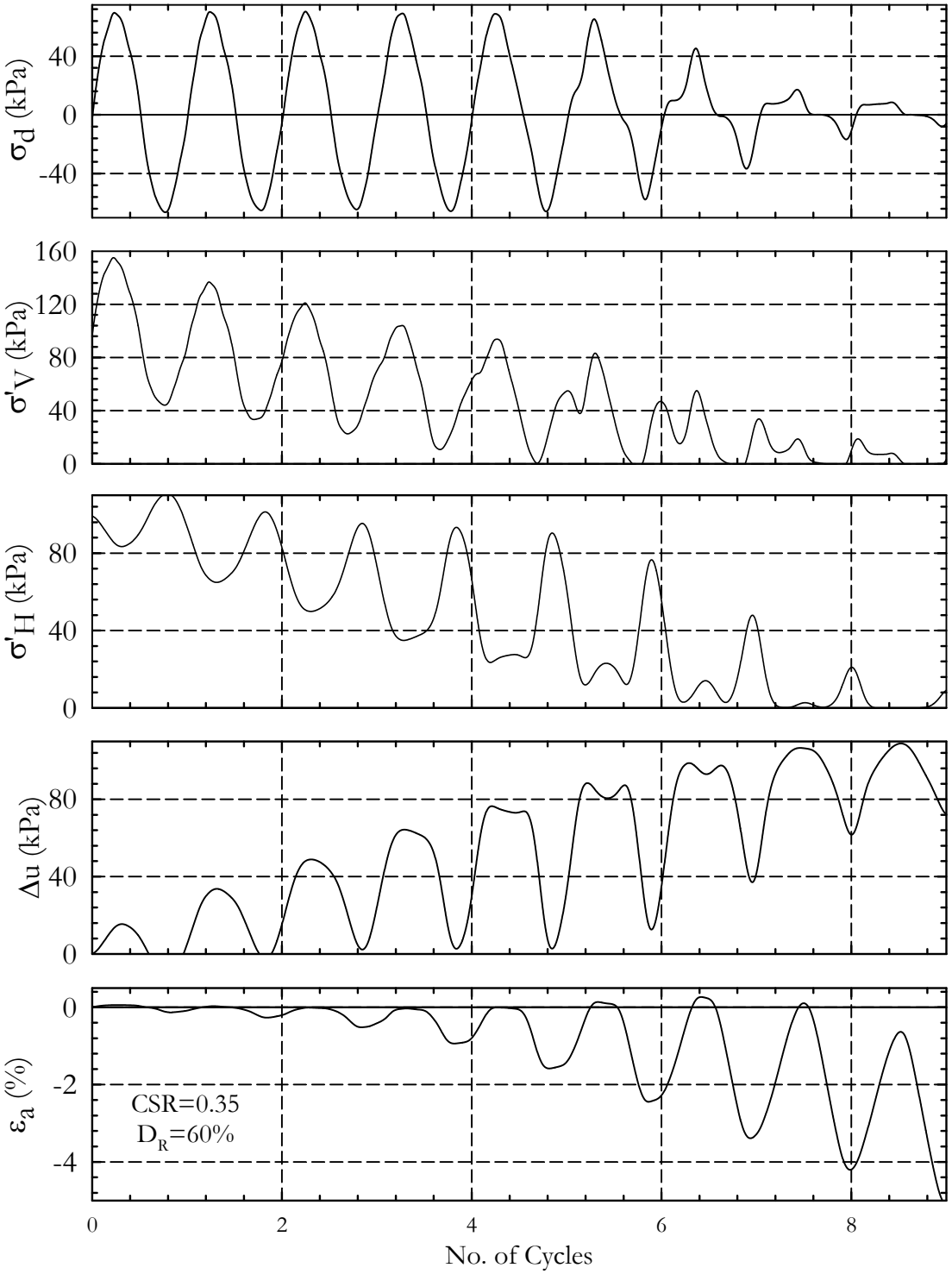

Figure II-40. Cyclic Parameters – Test CTX10

Test No.: CTX11
Test Ref.: 20080115_Cyclic01_D60_CSR32
$D_{R(FINAL)}$: 60% (56.8%)
e: 0.982
σ'_{3CON}: 100 kPa
CSR: 0.32

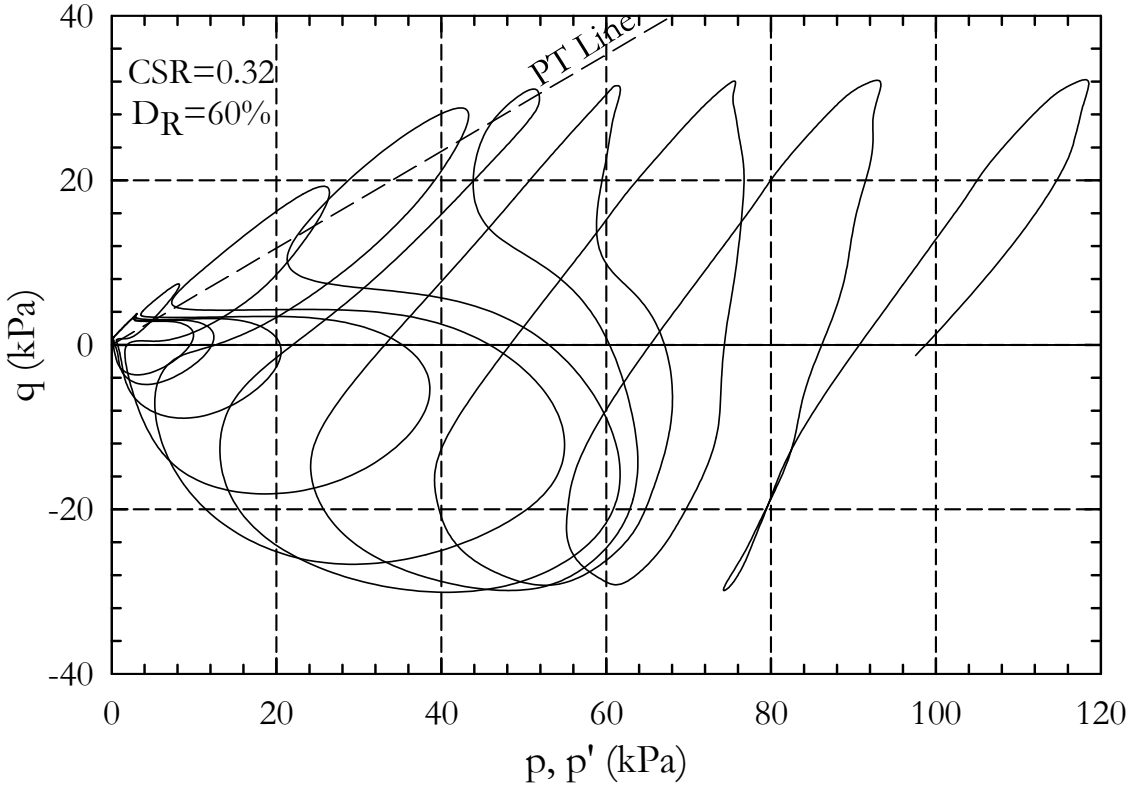

Figure II-41. Stress Path – CTX11

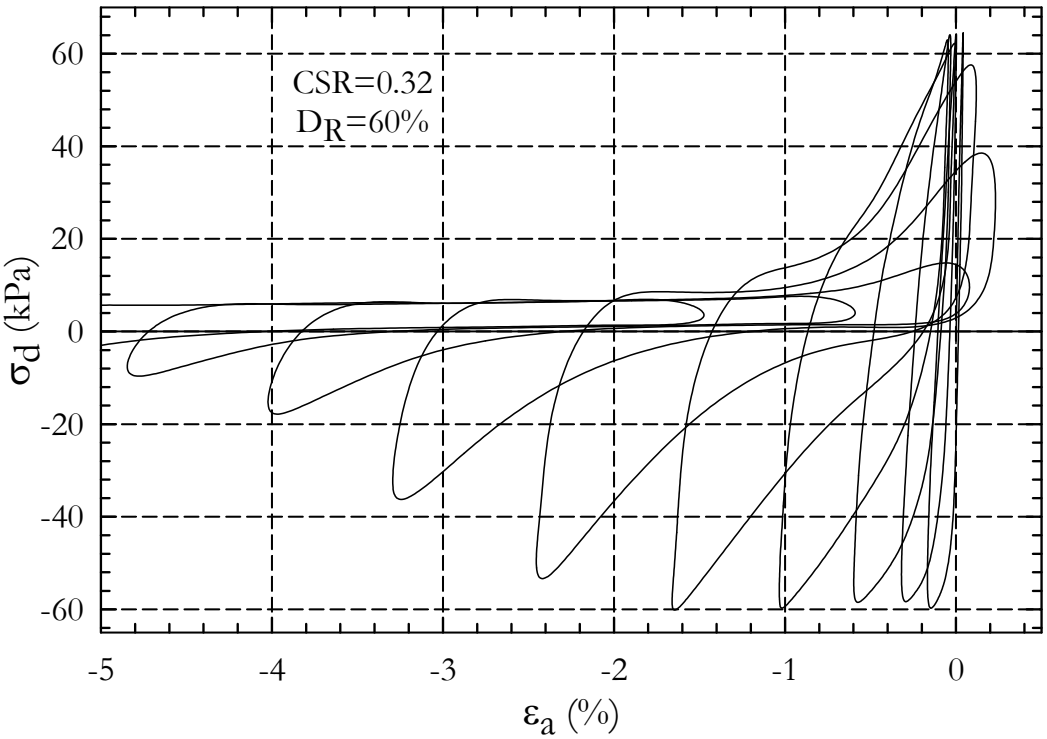

Figure II-42. Strain vs. Deviator stress– Test CTX11

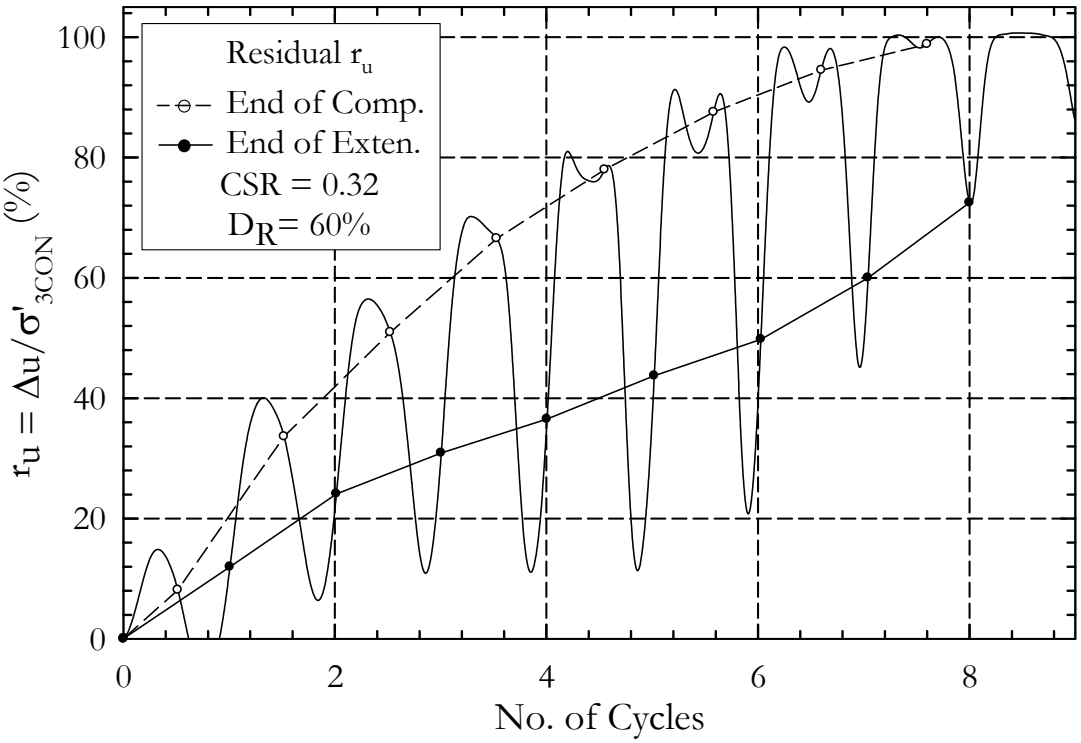

Figure II-43. Pore Pressure Ratio with Residual Pore Pressure – Test CTX11

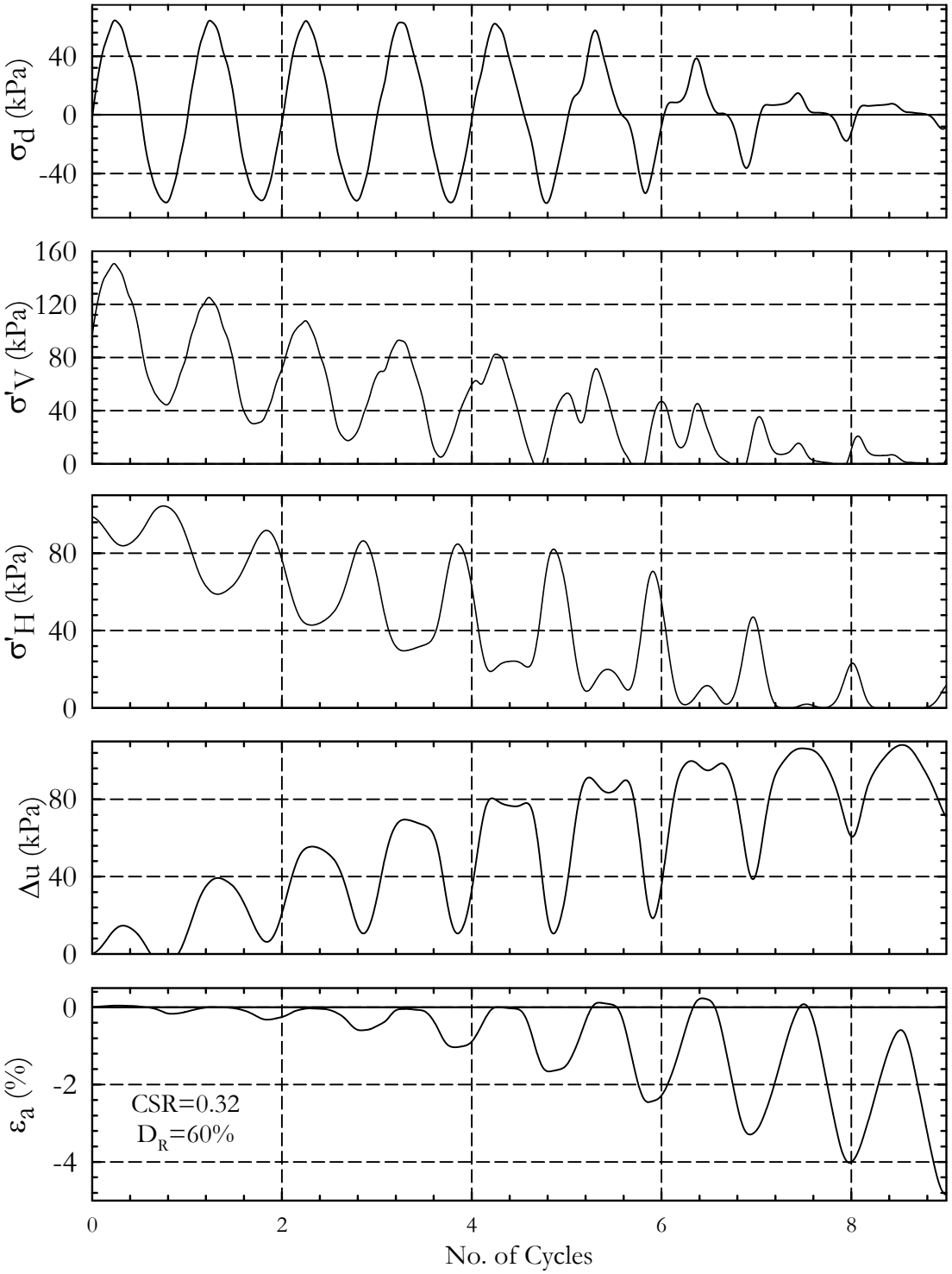

Figure II-44. Cyclic Parameters – Test CTX11

Test No.: CTX12
Test Ref.: 20080116_Cyclic01_D60_CSR30
$D_{R(FINAL)}$: 60% (57.8%)
e: 0.978
σ'_{3CON}: 100 kPa
CSR: 0.30

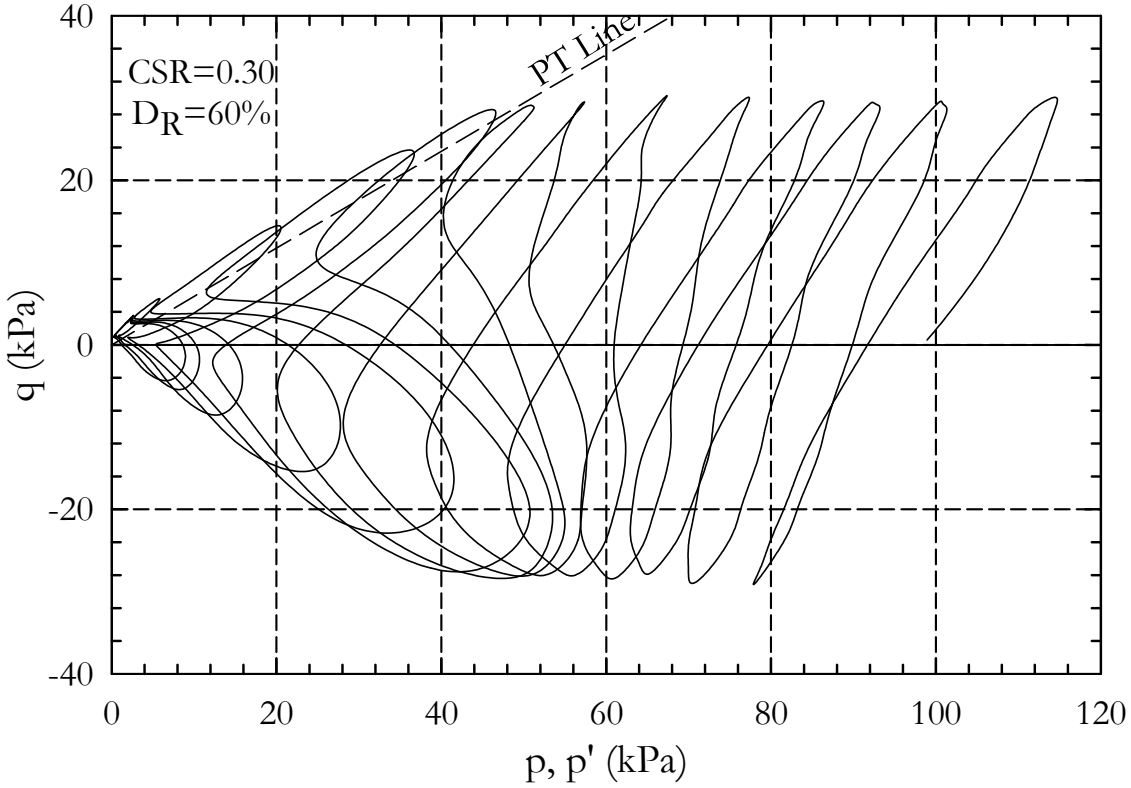

Figure II-45. Stress Path – CTX12

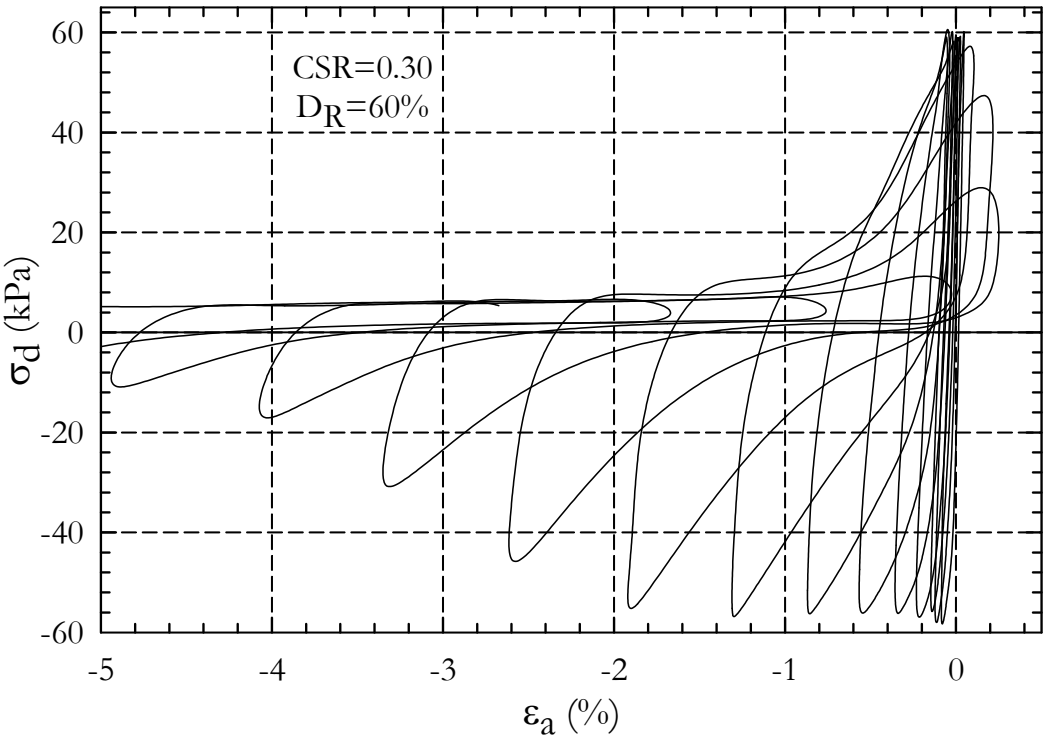

Figure II-46. Strain vs. Deviator stress– Test CTX12

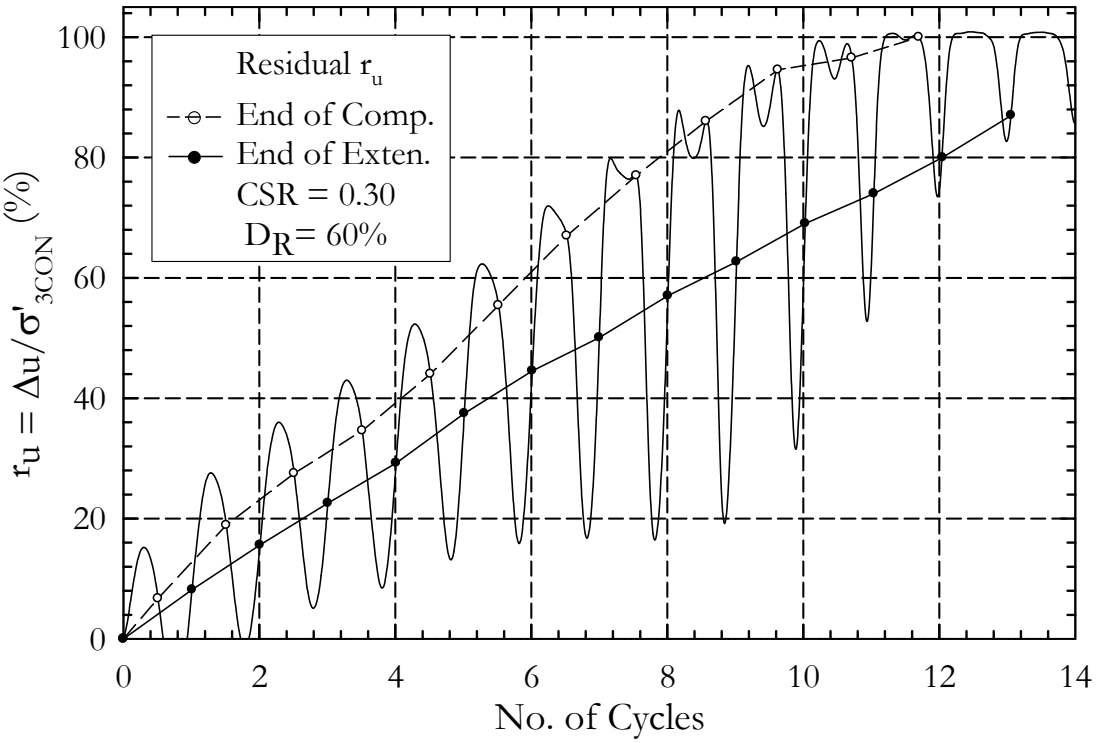

Figure II-47. Pore Pressure Ratio with Residual Pore Pressure – Test CTX12

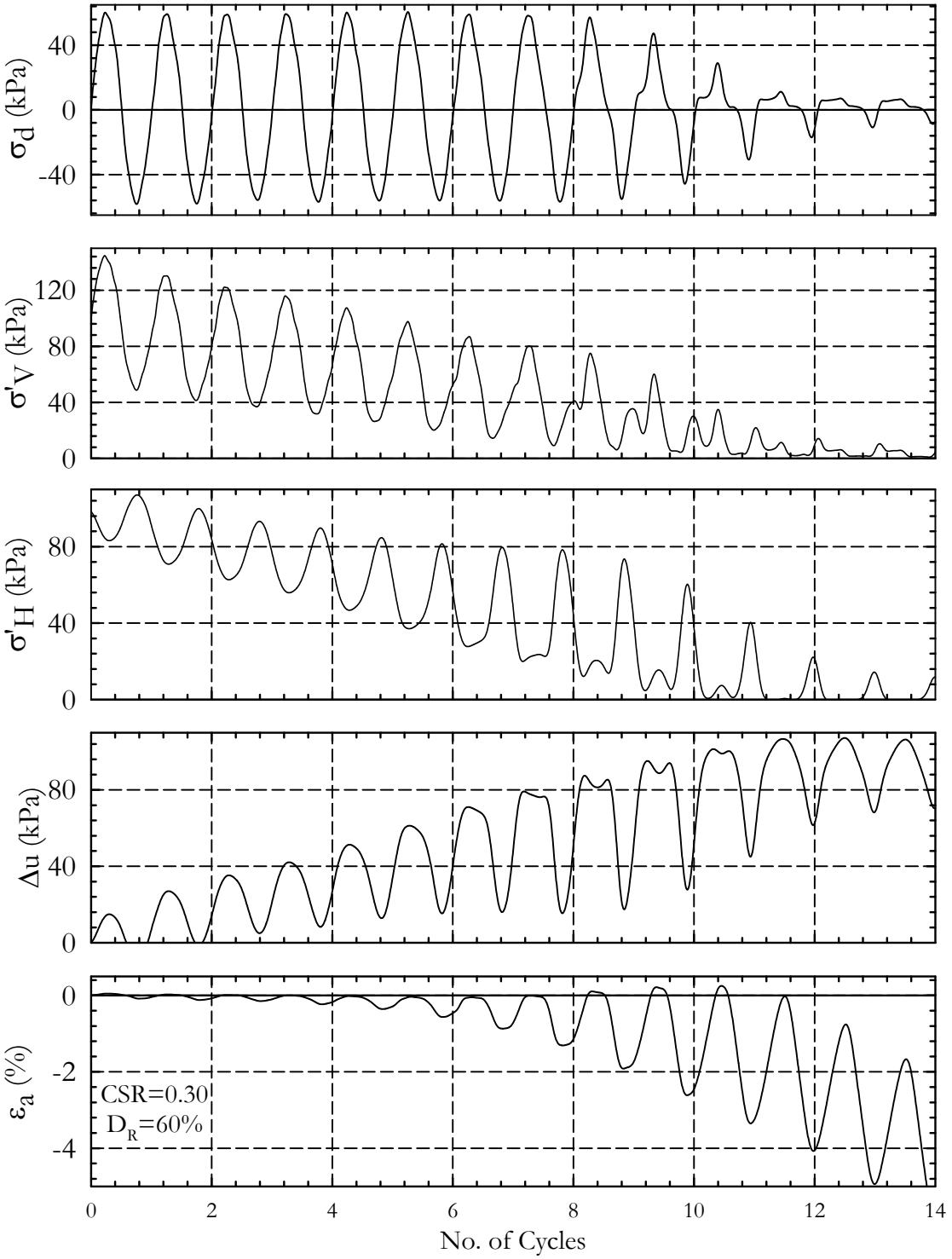

Figure II-48. Cyclic Parameters – Test CTX12

Test No.: CTX13
Test Ref.: 20080110_Cyclic01_D60_CSR25
$D_{R(FINAL)}$: 60% (58.9%)
e: 0.974
σ'_{3CON}: 100 kPa
CSR: 0.25

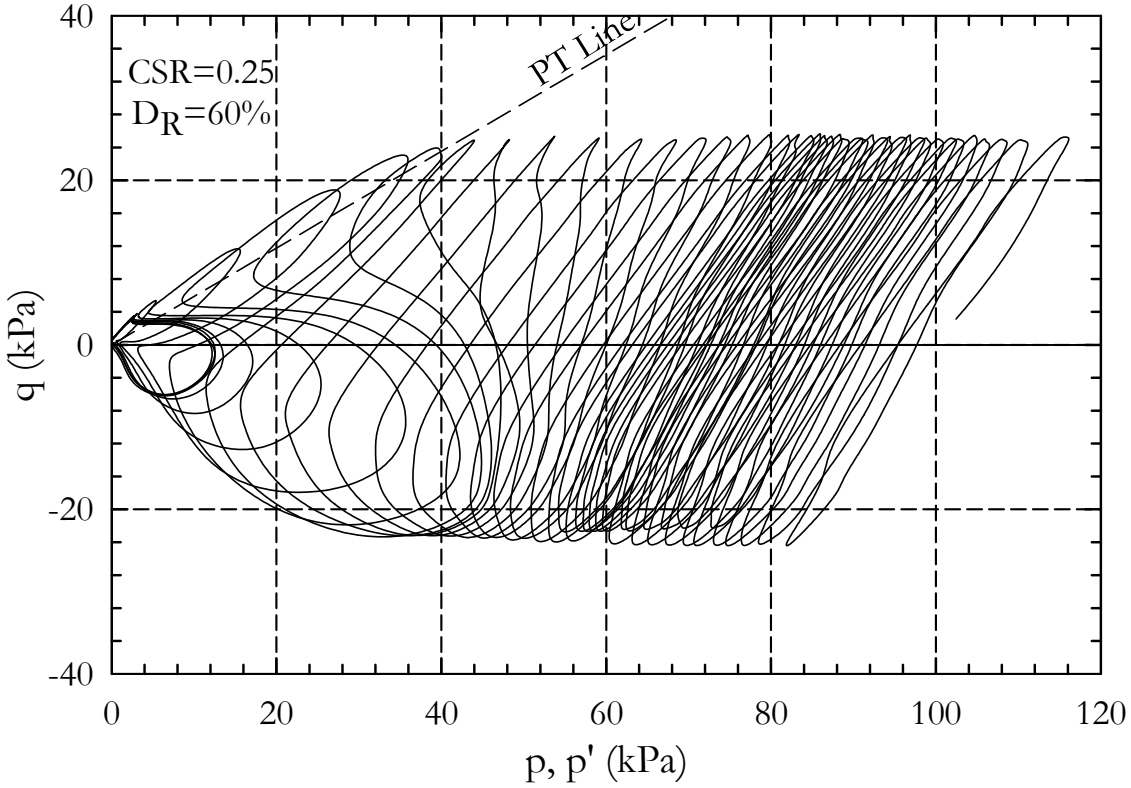

Figure II-49. Stress Path – CTX13

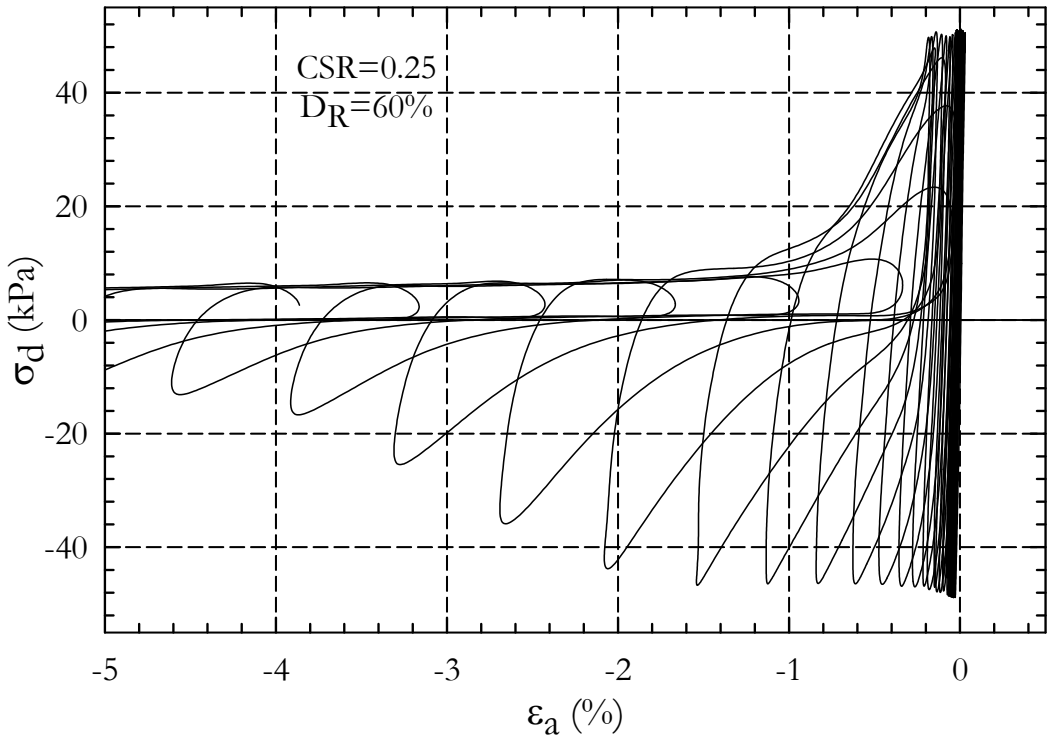

Figure II-50. Strain vs. Deviator stress– Test CTX13

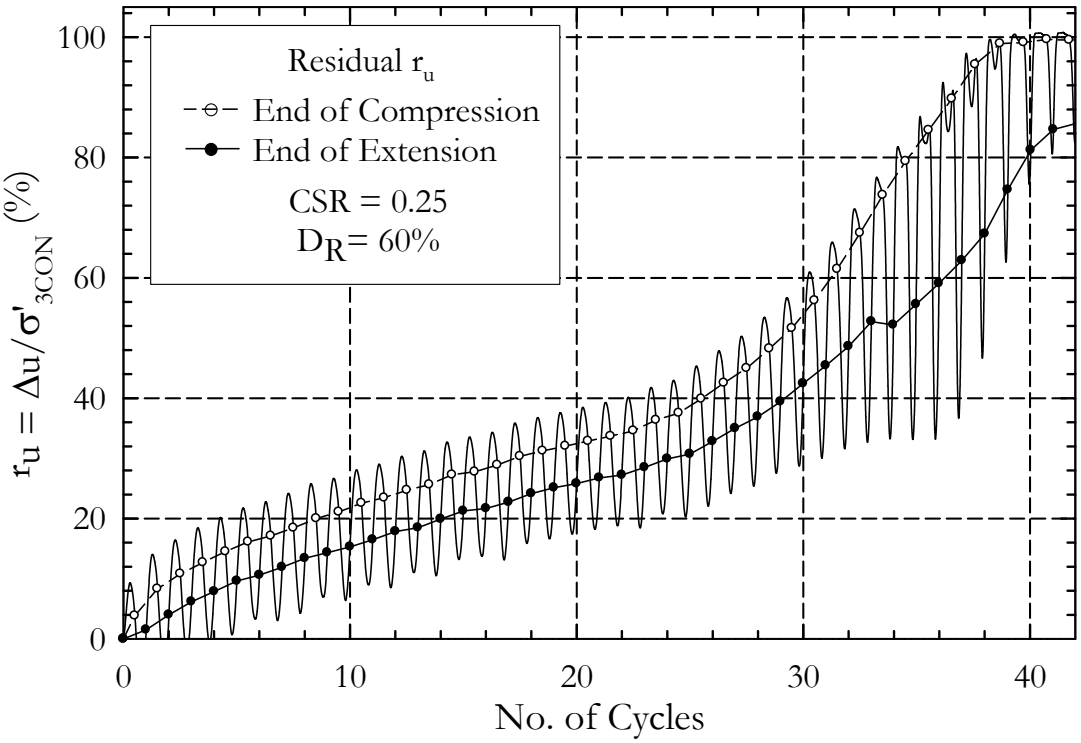

Figure II-51. Pore Pressure Ratio with Residual Pore Pressure – Test CTX13

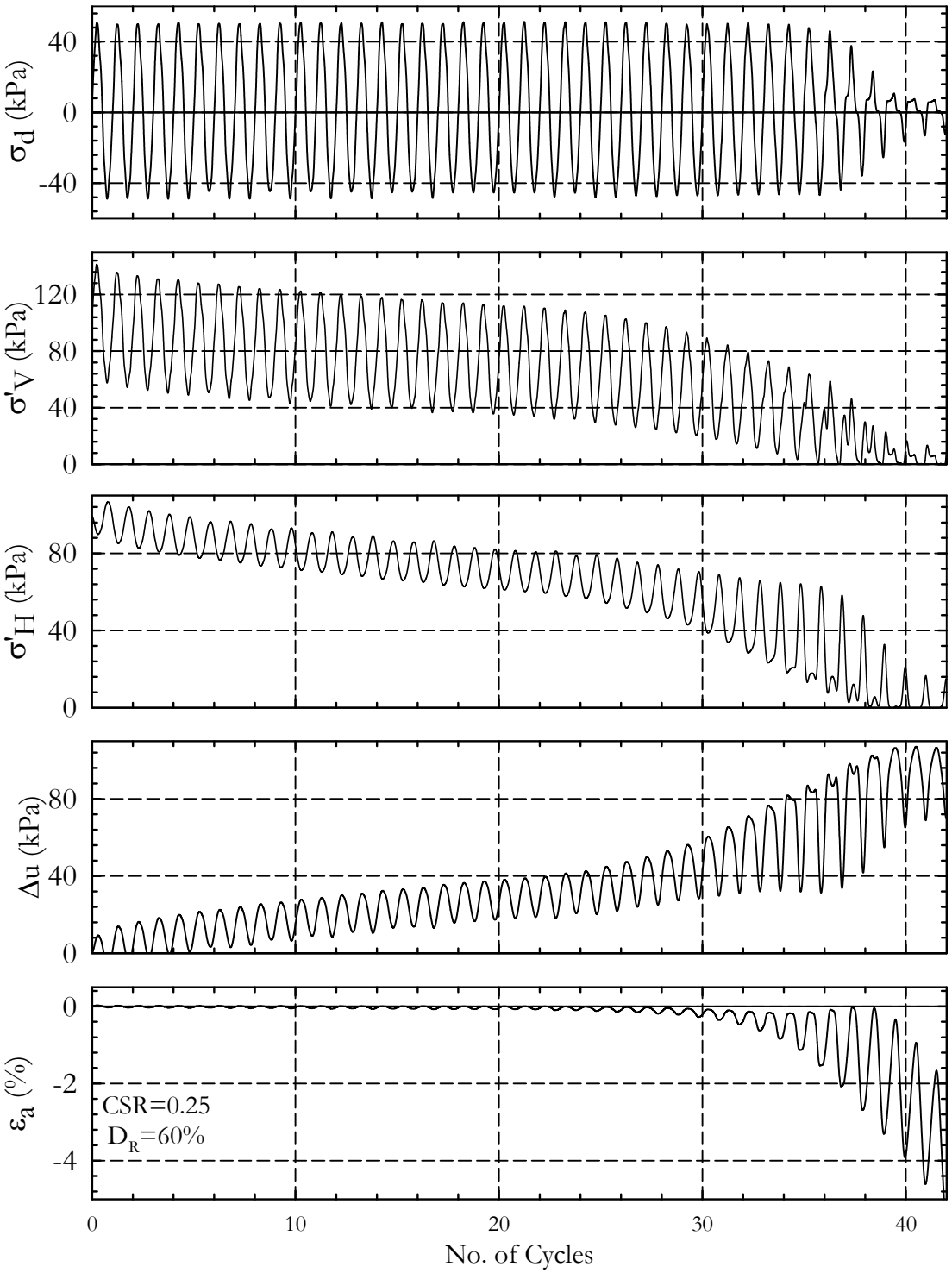

Figure II-52. Cyclic Parameters – Test CTX13

APPENDIX III CYCLIC DATA REDUCTION

Introduction

The basic reduction of the cyclic data is exactly the same as the reduction of the monotonic data. A deviator stress is determined, excess pore-pressure and effective stress is calculated. An additional step in reduction is necessary for the cyclic test results. This step in reduction consists of refinements to make the data presentable for interpretation. Three refinements are made to the results; (1) filtering, (2) applying a phase shift to the cell and sample pressures, and (3) adjusting the offsets or zeros for the sample pressure, cell pressures, and vertical load. The following sections describe in detail how each refinement is made and the justification for making them.

Filtering

Filtering is the act of taking the raw data and altering it to make it more presentable and interpretable. This issue has arisen because the raw load data collected, by the cyclic system is very irregular. The data shows that the load is not applied in a consistent sine way. Some of this can be attributed to noise in the system. Figure III-1 shows a several cycles of the raw load data. The pattern of irregularity is quite consistent from cycle to cycle. To considere these regularizes noise would be wrong because each spike or peak is defined by a steady series of data points and not an unsteady signal. Further more an almost identical pattern is found in the raw displacement data, Figure III-2. This behavior is most likely due to the combination of friction in the system and servo control. The fact that this irregular

loading is occurring can not be ignored. While it is important to keep this in mind; valid results can still be obtained from this data.

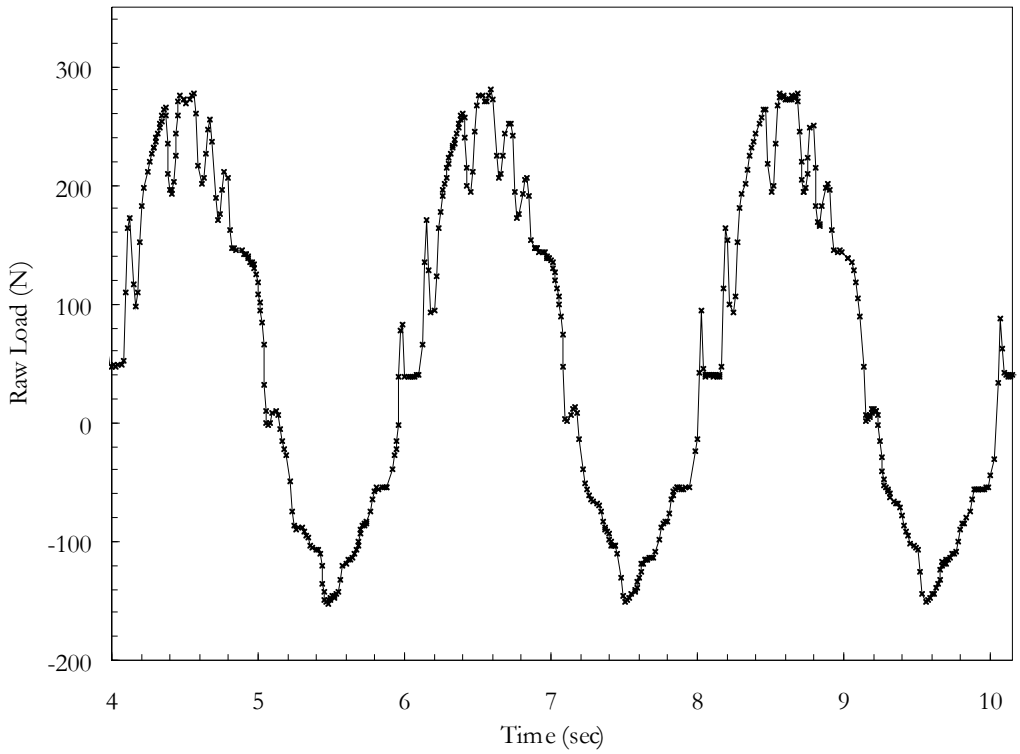

Figure III-1. Typical raw load data

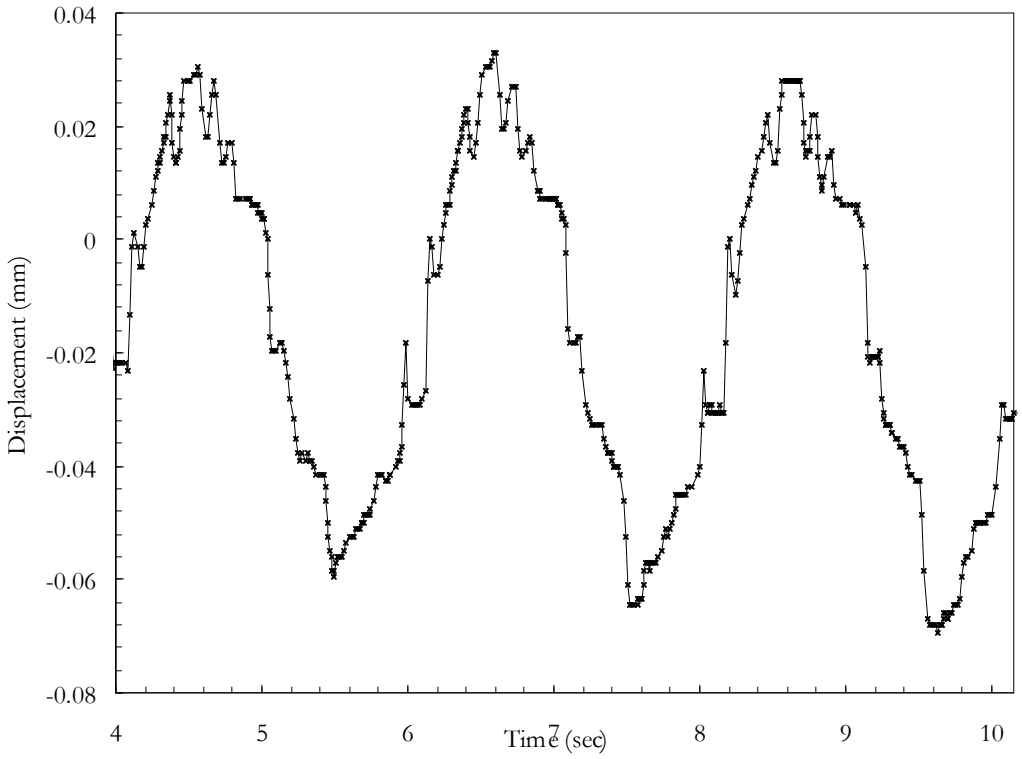

Figure III-2. Typical raw displacement data prior to liquefaction

The Geocomp software (cyclic5.exe) has two methods of retrieving data. Reduced data can be retrieved by going to the 'Report' menu and selecting 'Table'. The software uses a filtering algorithm on this data. The details of this algorithm are not proved in the Goecomp literature, and are a 'Black Box' process. Fully reduced data (σ_d, σ_V', ε_A, Δu…) are provided in the 'Table'. Raw data, that has not been reduced or filtered, can be retrieved by using an 'Engineering Dump' under the 'File' menu.

Several methods can be used to filter the data. By identifying the irregular frequencies, typically higher, they can be subtractedout. A simpler method using a spline curve fitting algorithm seems to be more effective. All reduced cyclic data presented has been filtered

using the spline curve fitting algorithm in MatLab called "SMOOTH." After filtering the data presented Figure III-1 there is significantly difference, see Figure III-3.

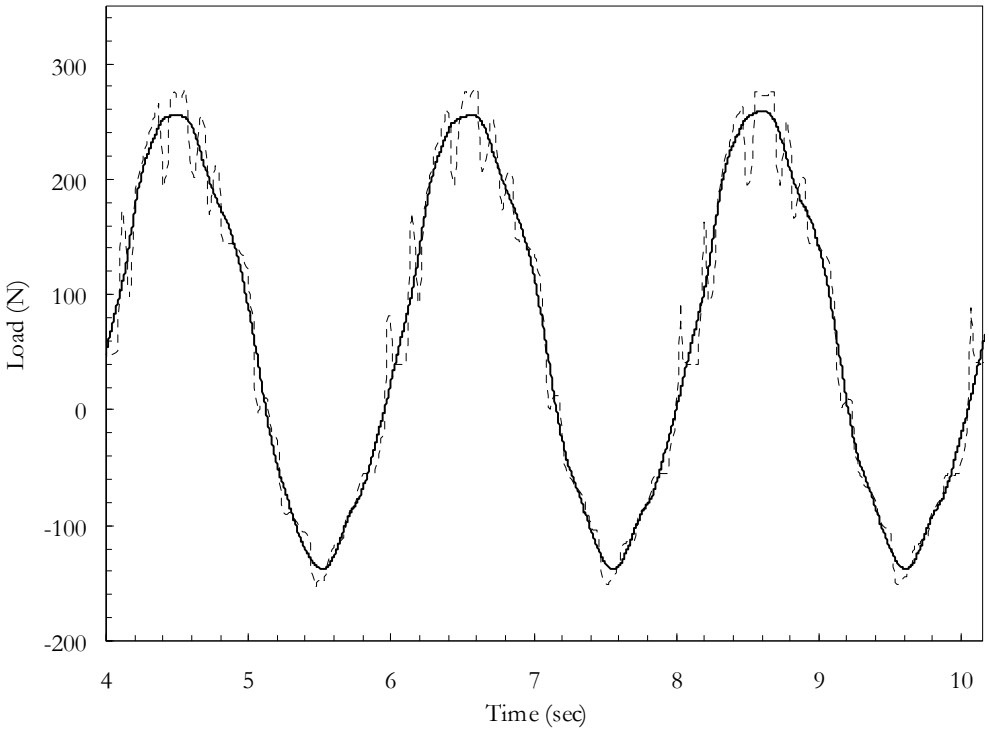

Figure III-3. Filtered load data presented with raw data

Phase Shift of Cell and Sample Pressure

At the time of peak deviator stress, a corresponding peak sample pressure should be expected. Some lag may be anticipated due to the finite incompressibility of the system. A considerable lag was found after careful review of the data as shown in Figure III-4. This results in a phase difference between the vertical load wave and the sample pressure wave. The cell pressure seems to be in phase with the sample pressure, and the displacement seems to be in phase with the deviator stress. At this point in time the author has no explanation as to what causes this lag.

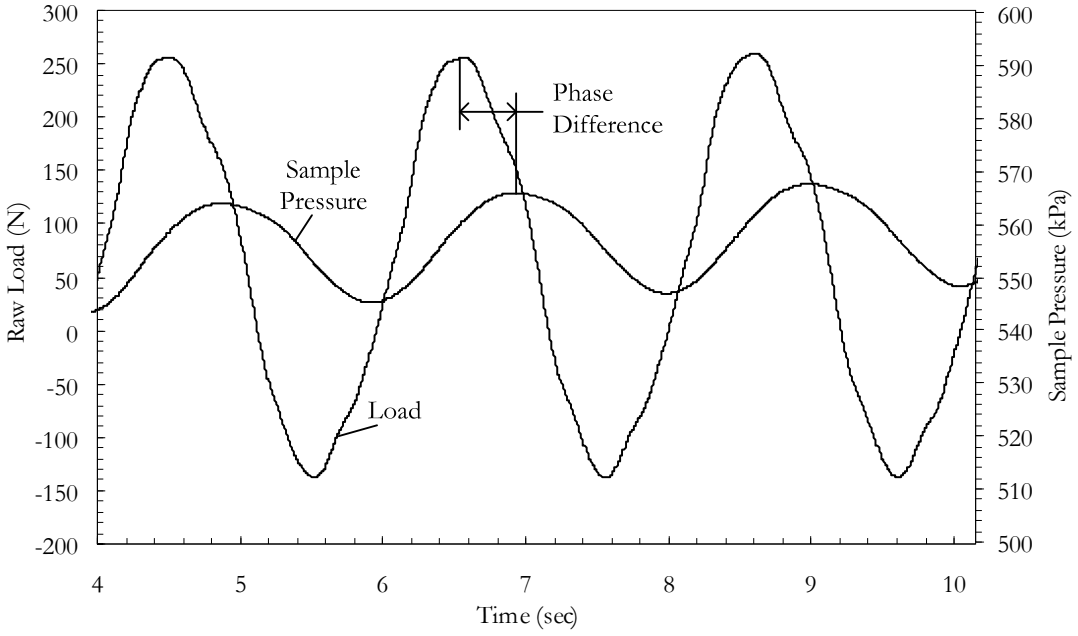

Figure III-4. Phase Difference in load and sample pressure data

The question arises as to weather this lag is actually physically occurring or if there is a delay in acquisition and reporting of these data. After careful review of many tests that this lag seems, in the opinion of the author, to be a problem in the data acquisition system. There is some physical lag occurring, but this seems to be small. In defense of this there are several points: (1) The lag is consistent from test to test even where the load frequency is varied. (2) There is a period of time at the start of the test where there is no change in sample pressure which corresponds to the phase difference. (3) By correcting the phase difference in the data, the soil behavior follows accepted theory. In the uncorrected results consist of sustained stress states beyond the failure envelops, including negative effective vertical stresses.

If the cell and sample pressure data is shifted so that the peak in deviator stress occurs concurrently with the peak in sample pressure there are significant changes in the calculated effective stress path. The local minimum deviator stress, negative, is matched with a local minimum in sample pressure. This matching creates an elevated effective stress state. When the stress path of a soil, sheared under undrained conditions, hits the failure line it with either run up (dilative) or down (contractive) the failure envelope. The stress path will never cross it or maintain a negative mean effective normal stress value. The soil behavior is much more reasonable after the adjustment is made to the phases of the cell and sample pressures. Figure III-5 shows how markedly different the stress path is with and without the phase shift.

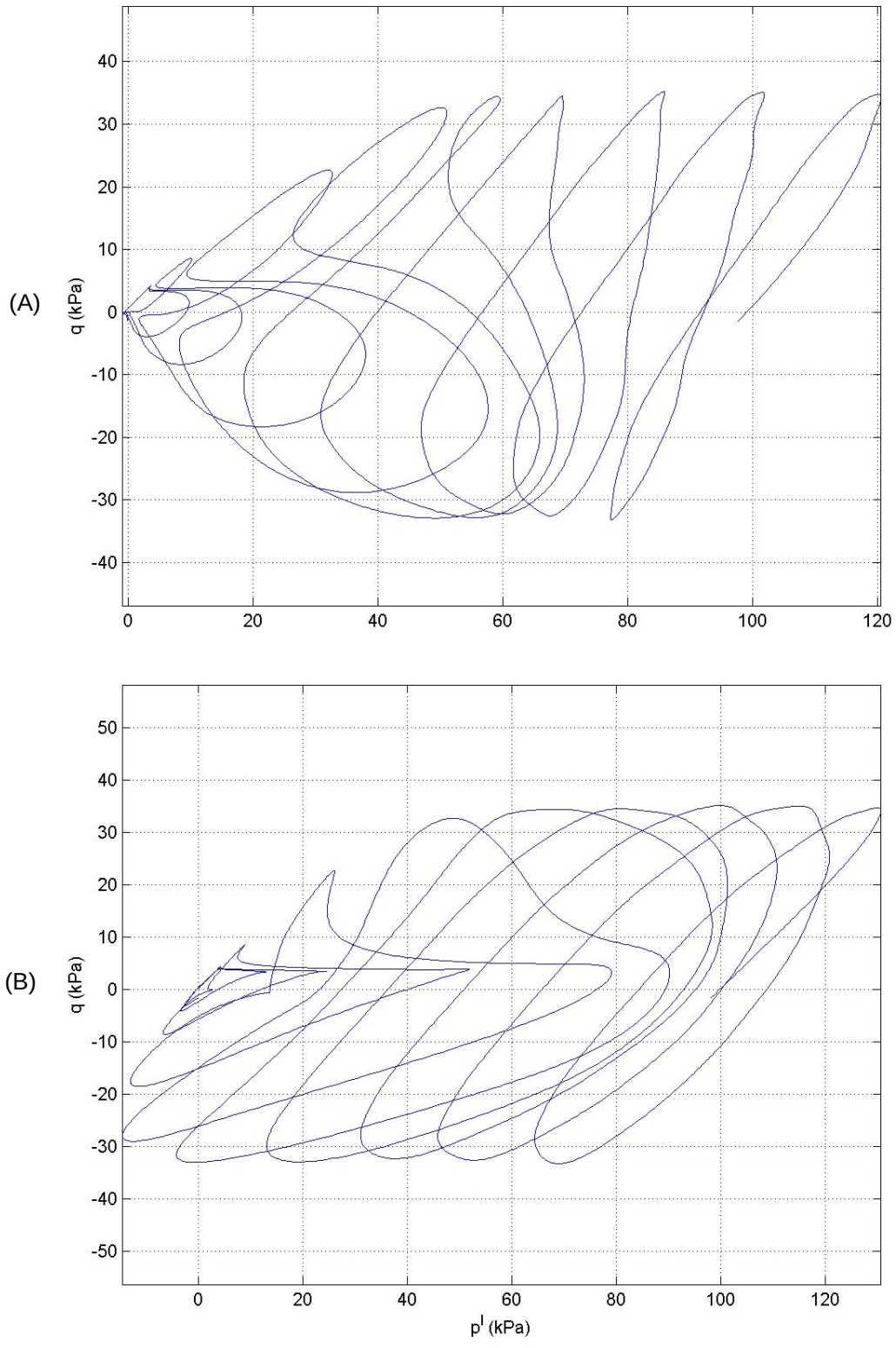

Figure III-5. Stress Path for corrected (A) and uncorrected (B) phase difference

Offset Adjustment

In Monotonic testing the offset, or zero, is a value that is routinely adjusted after the completion of the test. These values are relatively arbitrary and heavily affected by external circumstances such as friction and hydrostatic pressures. In using the Geocomp Cyclic Triaxial System establishing reliable offsets are especially difficult. This system is essentially a static triaxial system with several extra parts part added to perform cyclic loading. The static system does not have the load application or measurement capabilities needed for cyclic testing. For this reason, and several others, the designers essentially added four extra transducers and another method of applying a vertical load. Therefore, the control and measurement of the cyclic phase of the test is totally separate from the static phases. It becomes difficult to maintain consistency in offsets between these two sets of transducers. In other words, the zero for one set of transducers is not be exactly the same as the other.

By looking at the data and understanding what pressures should be associated with certain conditions offsets can be corrected and accounted for. By looking at the behavior after full liquefaction has occurred there are certain conditions that are known. In reality, following liquefaction the integrity of the triaxial test brakes down. The cell pressure can not be held constant, and high strains, coupled with low sample strength need to sustain the load, create problems in the application of the load. But the system is still measuring pressures, load and displacement. Therefore some useful data exists as long as the circumstances are accounted for.

Firstly, if after liquefaction the soil is assumed to be a fluid. The pressure of this fluid, the sample, would be the same as the pressure of the cell fluid. The soil structure is not sustaining any of the confining pressure. Rather, the pore water is sustaining this stress, effective stress is zero. By making this assumption, the cell and sample pressure offsets can be adjusted to so that the cell and sample pressures are equal during this liquefied state. In setting the offsets for the external cell and sample pressure transducers a consistent error is introduced. The zero is set without accounting for hydrostatic pressure causing an error as much as 5 kPa. A review of the difference between the measured pressure at the end of the consolidation phase and the beginning of the cyclic phase is also checked. This check, for the most part, justifies the changes to the sample and cell pressure offset.

Secondly, the vertical load offset is very hard to get exact. In monotonic testing this has little impact because these tests are performed under strain controlled conditions. Also the applied loads are significantly larger than in cyclic testing. A zero can be established by reviewing the data following the test. For cyclic tests this adjustment can also be made. After liquefaction the effective stress path should settle at zero. Liquefied soil strength and membrane strength will effect this, but generally a zero can be established. Proper zeroing of the load prior to testing is extremely difficult, because it is a function of several external forces; the most significant being friction. Exactly how to quantify and account for friction during a cyclic triaxial test is not established. What is known is that soil in a liquefied state will not sustain a significant shear stress; therefore, deviator stress following liquefaction will generally settle at zero. By changing the offset of the deviator stress the 'point of the arrow created by the stress path running up or down the failure envelops can be shifted along a 45°

line to lie at the origin. For all tests included in this study, this error in the initial load offset is small. Because these tests are stress controlled the system will apply positive and negative deviator stresses base on the offset initially provided. This adjustment to the offset will illuminate an asymmetrically applied deviator stress.

Summary

Three types of refinements have been performed on the data. (1) Filtering, (2) Applying a phase shift to the cell and sample pressures, and (3) Adjusting the offsets or zeros for the sample pressure, cell pressures, and vertical load. While Filtering does miss represent the applied loads it is necessary to the understanding and interpretation of the results. The phase difference observed in the data is significant. The observed lag is not physically occurring, and a shift in the phase of the cell and sample pressure is justified. The extent to which the lag is corrected is somewhat arbitrary. Adjustments to offsets are routine in all testing. Determining zeros exactly prior to performing the tests are for the most part impossible. By understanding soil behavior and post liquefaction test conditions small changes to these offsets are fully justified.